SCATTERING BETHE ANSATZ APPROACH

by

SUNG-PO CHAO

A Dissertation submitted to the

Graduate School-New Brunswick

Rutgers, The State University of New Jersey

In partial fulfillment of the requirements

For the degree of

Doctor of Philosophy

Graduate Program in Physics and Astronomy

Written under the direction of

Professor Natan Andrei

And approved by

_____

_____

_____

_____

_____

New Brunswick, New Jersey

October, 2010

ABSTRACT OF THE DISSERTATION

Scattering Bethe Ansatz approach

By SUNG-PO CHAO

Dissertation Director:

Professor Natan Andrei

We derive the transport properties of a quantum impurity system, often realized as a quantum dot, subject to a source-drain bias voltage at zero temperature and magnetic field. Using the Scattering Bethe Anstaz(SBA), a generalization of the traditional Thermodynamic Bethe Ansatz(TBA) to open systems out of equilibrium, we derive some transport results for the small quantum dot, described by Anderson impurity Hamiltonian. Exact dot occupation out of equilibrium and the nonlinear conductance are obtained by introducing phenomenological spin- and charge-fluctuation distribution functions in the computation of the current. The current and dot occupation as a function of voltage are evaluated numerically. We also vary the gate voltage and study the transition from the mixed valence to the Kondo regime in the presence of a non-equilibrium current. For the larger quantum dot the Interacting Resonance Level Model is used to describe the strog correlation problem in this system. We show some current vs voltage results and compare with other theoretical results. We conclude with the difficulties we encountered by using this method and suggest some future extensions related to this SBA approach.

Acknowledgements

I am immensely thankful to Professor Natan Andrei for his support, guidance, patience, and teaching during my graduate study at Rutgers University. Most of what I know about Bethe Ansatz, I learned from him.

I would like to thank my wife, Yu-Ju, who gives me so much love and happiness and always encourages me to pursue my interests.

I am grateful to my parents, King-Long Chao and Bao-Ping Lee, who have continuously support my interests in studying physics. I would also like to thank my brother and sisters-in-law, Iou-Ling Chao, Yu-Mei Huang, and Yu-Wei Yang for their support and encouragements.

Thanks to my friends and office mates, Chuck-Hou Yee, Rebecca Flint, Kshitij Wagh, Deepak Iyer, Marianna Maltseva, Eran Lebanon, Wu-Yen Chuang, Sinisa Coh, Senia Katalinic, Anindya Roy, Ming-Tsung Ho, Chien-Lang Hsueh, Lucia Palova, Kasturi Basu, Hyowon Park, Carl-Johan Eklund, for their various help and discussions. Especially thanks to Chuck who has been a great help in developing programs for our problems.

Many thanks to the faculties at Rutgers, Professors David Vanderbilt, Piers Coleman, Premala Chandra, Kristian Haule, Lev Ioffee, Willem Kloet, Gabriel Kotliar, Sang-Wook Cheong, Michael Gershenson, Duiliu Emanuel Diaconescu, Arthur Kosowsky, Jack Hughes, for their teachings and numerous valuable discussions.

I would also like to thank Guillaume Palacios, Carlos Bolech, Andres Jerez, and Pankaj Mehta who had collaborated with me during Rutgers. Especially thanks to Guillaume for helping me clarify the ideas and improving my writings in our article.

Last but not least, I would like to thank lab staffs, Gabe Alba and Lu-Shu Chang, who had helped me prepare for the undergraduate teaching.

Table of Contents

List of Tables

List of Figures

Chapter 1

Introduction on Quantum impurity problem

This chapter is an introduction to the problems of quantum impurities out of equilibrium. It serves as the major motivation for Scattering Bethe Ansatz approach on out of equilibrium quantum impurity problems which we are going to mention in the next chapter. We briefly discuss experimental results on a single quantum dot, starting with linear response to finite bias, discussing the Kondo physics in this electric transport measurement at low temperature, and ending with the experiments for a larger quantum dot (well) which exhibiting physics of Fermi Edge Singularity. We explain why nonequilibrium quantum impurity problems are theoretically challenging and summarize the various theoretical attempts to tackle the problem thus far.

1.1 Overview of Quantum impurity problem

The past few years have witnessed a spectacular progress in the fabrication and exploration of nanostructures giving experimentalists unprecedented control over the microscopic parameters governing the physics of these systems. The quantum fluctuations play an important role in determining the physical properties of these nano devices and different structures of the devices also display many different aspects of physics. Apart from the practical applications such as solid-state quantum computing, light emitting (quantum dot LED or diode laser), photovoltaic devices, biology ect., the nano devices also provide a rich array of experimental tools for physicists to verify some physical ideas with great control and precision which are difficult to achieve in bulk systems. For the bulk samples most of the physical properties of the materials are fixed as the samples are made and only coarse signatures can be pulled out from the measurements. Another advantage of the nano devices is that we can study the local site out of equilibrium which is not doable in the traditional bulk materials.

In this thesis the term "quantum impurity" means some type of nanostructure. The nanostructure is connected with the leads through some tunneling junctions and thus we treat the nanostructure as the impurity part of the Hamiltonian describing the leads and the nanostructure. The nanostructures could be zero dimensional, such as quantum dot devices, or one dimensional, such as quantum wire made by carbon nanotube or a collection of quantum dots or wires. The quantum

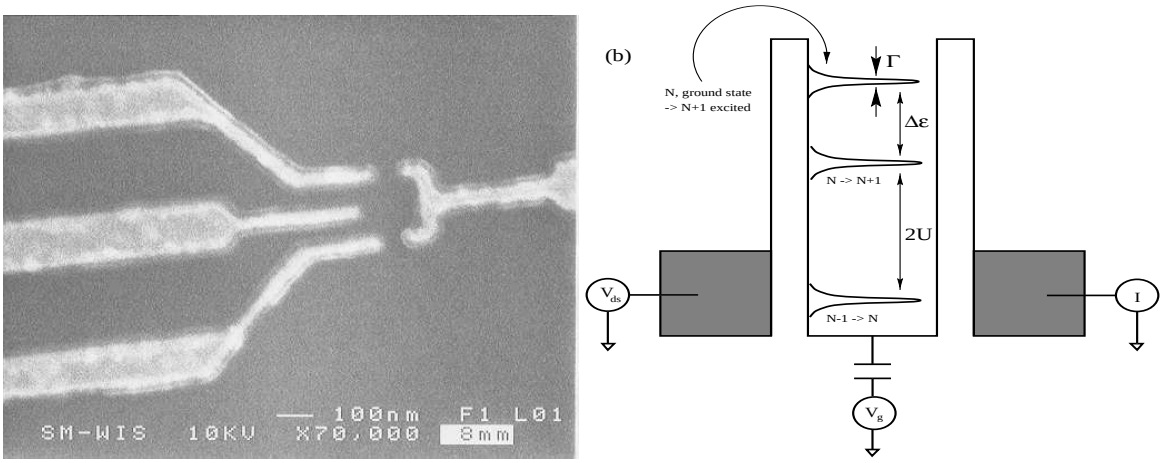

Figure 1.1: Left: Scanning electron microscope image of the lateral quantum dot. The left top and bottom electrodes control the tunneling strengths and left center electrode provide gate voltage on the dot. Top and bottom regions are the source drain part of the two dimensional electron gases which are connected with external source drain electrodes not shown in the picture. Right: Schematic diagram of the relevant energy scale: charging energy U, level spacing δE, tunneling strength Γ. Dot level can be tuned by gate voltage V_g. Both pictures are taken from Ref.[5]

dot devices confine a small droplet of electron liquid or a few electrons within a finite region of space, typically around $10^2 nm$ to μm in length. There are basically three type of these single dot devices[1]: Lateral, vertical and carbon nanotube quantum dots. In the thesis we concentrate our discussion on transport property of the lateral quantum dot, starting with the small size mesoscopic quantum dot.

1.1.1 Small size single quantum dot: Kondo effect

Scanning electron microscope image of small size lateral quantum dot is shown in Fig.1.1. The transport properties through a small size (with diameter around 100 nm) single quantum dot at low temperature, at which strong correlations between dot electrons and itinerant electrons from the leads taking place, is the subject of Chap 3 to Chap 4 of this thesis.

The dot is attached by tunneling junctions to massive electrodes to allow electronic transport across the system. The conductance of such a device is determined by the number of the electrons on the dot, which in turn is controlled by the gate voltage capacitively connected with the dot. Denote Γ as the energy scale related to the electrons tunneling between the dot and the leads, ϵ_d as one of the dot level, $U \simeq \frac{e^2}{2C}$ the charging energy or Coulomb repulsion associated with the energy required to add/remove an electron on the dot with C the total capacitance on the dot, and δE the

mean level spacing on the dot. In the mesoscopic dot we mention in this thesis $\delta E \ll U$ ($\frac{U}{\delta E} \sim 10$ in the experiment[5]) thus we can neglect this energy difference. This simplified picture is depicted in the right figure of Fig.1.1. For more general discussions on the quantum dot systems we refer the reader to the theoretical review article by M. Pustilinik and L. Glazman[2] and experimental review article by M. Grobis et al.[1].

Temperature plays an important role in determining the tunneling strength Γ. For high temperature Γ is lager than the discrete levels in the dot and thus the information of the energy levels within the dot is washed out. As we lower the temperature Γ becomes smaller than the level spacing within the dot and we may begin to see the individual discrete energy levels by performing linear response measurement with different gate voltage. This linear response experiment is done by applying a voltage of a few microvolts between the leads connected with the dot and measuring the current that flows through the droplet as a function of the gate voltage V_g on the dot. For such low applied voltage, current varies linearly with voltage, and the zero bias conductance can be measured[5, 4]. The zero bias conductance vs gate voltage measured by D. Goldhaber-Gordon et al. is shown in Fig.1.2. This can be understood in the following way: When some dot level ϵ_d, which is capacitively controlled by V_g, crosses the equilibrium Fermi surface ϵ_F (in linear response measurement chemical potential from both leads are roughly equal $\mu_1 \simeq \mu_2 = \mu$, and the equilibrium chemical potential determines the Fermi energy of the leads system: $e\mu = \epsilon_F$) a conduction channel is formed and thus the conductance becomes maximum as the level ϵ_d is completely aligned with Fermi surface μ. By tunning the level to $|\epsilon_d - \epsilon_F| > \Gamma$ there will be no available channels to tunnel through the dot. As a result, the conductance decreases on both side of the peak around some gate voltage V_g. This is the so called Coulomb blockade regime.

At even lower temperatures, if there were odd number of electrons on the dot, the spin or magnetic moment of the dot electrons tends to be screened by the delocalized electrons from the leads. This screening occurs through subtle many body correlations, extensively studied since J. Kondo discussed them in 1964 by perturbation theory[3, 61]. This same correlations produce anomalies in the resistivity, susceptibility, and many other properties of bulk magnetic alloys. We digress for a moment to mention two important models related to this Kondo effect. The Kondo effect was first reported in the electrical resistivity measurement of Au done in 1930s, where de Hass et al. found resistance minimum at temperature around 3.7 K, below which the resistance actually increased. This behavior was soon confirmed experimentally to be connected with magnetic impurities such as

Fe or Co within the bulk metals. Theoretical advance in magnetic impurities came in 1964 by J. Kondo's computation on the resistivity where he did third order perturbation in the coupling J of the s-d exchange model, nowadays also named Kondo model. This model's Hamiltonian is given by

$$H = \sum_{k\sigma} \epsilon_k c^\dagger_{k\sigma} c_{k\sigma} + \sum_{kk'ab} J_{k,k'} \vec{S} \cdot c^\dagger_{ka} \vec{\sigma}_{ab} c_{k'b} \tag{1.1}$$

Here $c_{k\sigma}$ is the electron annihilation operator with spin index σ and energy ϵ_k. $\vec{S}$ is the impurity spin. This model can be deduced from Anderson model in the local moment regime ($\epsilon_d << \epsilon_F$ and $\epsilon_d + U >> \epsilon_F$) when the occupation number of impurity electron is fixed at one. The Anderson model was proposed by P. W. Anderson in 1961. It describes the resonance associated with the impurity states and a short range interaction U between the impurity electrons. The Hamiltonian of the Anderson model is given by

$$H = \sum_{\sigma} \epsilon_d d^\dagger_\sigma d_\sigma + U d^\dagger_\uparrow d_\uparrow d^\dagger_\downarrow d_\downarrow + \sum_{k\sigma} \epsilon_k c^\dagger_{k\sigma} c_{k\sigma} + \sum_{k\sigma} (t_k d^\dagger_\sigma c_{k\sigma} + t^*_k c^\dagger_{k\sigma} d_\sigma) \tag{1.2}$$

Here again $c_{k\sigma}$ is the electron annihilation operator with spin index σ and d_σ is the impurity electron annihilation operator with spin index σ. The two-lead version of the Anderson impurity model is the standard model to describe the physics of single quantum dot system as shown in Fig.1.1. For tunneling around the Fermi surface the tunneling amplitude $t_k \simeq t_{k_F}$ is roughly a constant independent of k. We can then relate Γ to t_{k_F} by $\Gamma \simeq |t_{k_F}|^2 2\pi\rho(k_F)$ and linearize the energy spectrum around $k = k_F$, k_F being the Fermi momentum and $\rho(k_F)$ being the itinerant electron density around the Fermi surface. Under these condition the Hamiltonian shown in Eq.(1.2) is integrable and we may write down the Bethe Ansatz wavefunctions as the eigenstates of this Hamiltonian. More details are given in Chap. 3.

Now we come back to the discussion of the Kondo effect in the quantum dot system. As we have mentioned above, the screening effect on the impurity spin only occurs when the system's temperature is lowered below a certain scale, often called the Kondo temperature T_k. The screening enhances the interactions between impurity electrons and delocalized electrons, therefore increasing the resistivity of the bulk sample. The same mechanism in fact increases the conductance of the quantum dot as the enhancement of the interaction produces a sharp (width proportional to T_k) density of states fixed at the Fermi surface. Thus even if the impurity level ϵ_d is far below the Fermi

surface the dot can still have finite conductance. In the case of zero temperature in this Kondo regime the conductance of the dot reaches a maximum value $\frac{2e^2}{h}$, the so called unitary limit in the Landauer transport approach. This has been observed in experiments by W. G. van der Wiel et al.[9]. This screening effect on the impurity spin occurs when there is an odd number of electrons in the impurity. When there is an even number of electrons there is no bare spin to be compensated. Lowering the temperature just means decreasing the effective tunneling strength Γ and thus the conductance in the even valley of electrons decreases as temperature decreases. Even/odd valley here means the valley in linear response conductance vs gate voltage plot when number of electrons on the dot is even/odd. The corresponding experimental plots are shown in Fig.(1.2).

The experiment can also be performed by fixing the initial chemical potentials of the leads on the center of the odd valley, where the Kondo effect is most prominent, and turning on the source drain voltage to produce a current flowing through the dot. By measuring the current vs source drain voltage we may obtain nonlinear differential conductance vs source drain voltage. Both equilibrium and out of equilibrium measurement by W. G. van der Wiel et al.[9] are shown in Fig.1.3. Major features of the nonlinear conductance show a peak structure nearby zero voltage with width around $k_B T_k$, the so called zero bias anomaly, and a broad side peak with width scaled as Γ centered around renormalized impurity level ϵ_d. The overall feature is similar to the impurity density of state as a function of energy[27] since the zero temperature out of equilibrium conductance is related to out of equilibrium density of state on the dot in the case of two leads Anderson model[19]. Our theoretical results have provided qualitative agreements with the experiments, both in and out of equilibrium. The comparison of nonlinear conductance with one of the experiments[10] is shown in Chap. 3. Our approach, Phenomenological Scattering Bethe Ansatz method (pSBA), though not starting from first principle, does capture the main physics related to zero temperature charge transport of this Kondo quantum dot system.

Further experimental designs and setups are used to measure the dephasing mechanism due to nonequilibrium current, the extent of Kondo screening cloud, out of equilibrium density of states, time evolution of the Kondo cloud, to name a few. The holy grail for research on the Kondo effect is to know whether it is possible to measure and control the Kondo cloud [3], which is the crucial question in applying quantum dot to quantum computing.

1.1.2 Large size single quantum dot: Fermi-edge singularity

We now switch gears to consider the interesting case of a larger dot (with diameter a few μm). In this case the spin fluctuations are less important compared with the Coulomb repulsion between electrons from the dot and the leads. This leads to singular behavior in the transmitted current when dot level is aligned with the higher chemical potential lead. The idea, proposed by K. A. Matveev and A. I. Larkin[11] in 1992, is that the electron tunneling in these resonant tunneling devices (RTD)[12] is accompanied by the formation of a positively charged hole bound to the impurity. The Coulomb interaction of electrons with the hole leads to power-law singularities in the transition rate, analogous to those arising in the problem of x-ray-absorption edges in metals[11]. Thus this anomalous behavior in tunneling current is named Fermi-edge singularity (FES). They manifest themselves in I-V characteristic as

$$I \propto (V - V_{th})^{-\alpha}\theta(V - V_{th})$$

where V_{th} is related to the difference between dot level ϵ_d and higher end of the Fermi energy. α is related to many body interactions.

This singularity around the threshold is smeared out when $e|V - V_{th}| \geq \Gamma$. The power law decay in current as a function of voltage nearby the threshold voltage was confirmed experimentally by A. K. Geim et al.[12] in 1993. Recently it was also reported by M. Ruth et al.[14] that without using high magnetic field they can also get FES in their tunneling current. By rescaling their data with effective temperature $k_B T^* \simeq \sqrt{k_B T^2 + \Gamma^2}$[13] they obtained universal behavior for current vs voltage. Their device, a type of self assembled vertical quantum dot, and the universality curve are shown in Fig.(1.4)

The physics of FES in the resonant tunneling devices can be captured by the Interacting Resonant Level Model (IRLM). The Hamiltonian of two leads IRLM is

$$H = \epsilon_d d^\dagger d + \sum_{k,k',a} U d^\dagger d c^\dagger_{ka} c_{k'a} + \sum_{ka} \epsilon_k c^\dagger_{ka} c_{ka} + \sum_{ka} (t_k d^\dagger c_{ka} + t^*_k c^\dagger_{ka} d) \tag{1.3}$$

Here $a = 1, 2$ refers to the lead indices. The pioneering work of Scattering Bethe Ansatz approach by P. Mehta and N. Andrei[16, 15] is in fact started with this IRLM. In Chap. 5 we reexamine their results on this IRLM and extend the formulation to energies higher than impurity level ϵ_d.

We also compare with other theoretical results with our numerical results in Chap. 5. Possible extension of the Scattering Bethe Ansatz approach to other system such as quantum wire or multi leads connections is addressed in Chap 6 based on extension of this two leads IRLM.

1.2 Theoretical efforts and challenges

A number of theoretical approaches to the Kondo model[36, 33, 34] or the Anderson impurity model [17–19, 29, 20, 22] in the quantum dot systems have been developed based on the Keldyish perturbation approach. These approaches can obtain features in the strong coupling Kondo regime, when $eV_{sd} \ll k_B T_k$, or in the weak Kondo regime when $eV_{sd} \gg k_B T_k$. Most of the numerical and analytical approaches used to tackle strong correlation problems, such as $\frac{1}{N}$ expansion, boundary conformal field theory, renormalization group (RG), numerical RG, time-dependent density matrix renormalization group(t-DMRG), Non-crossing approximations, etc. are being developed for nonequilibrium quantum impurity system. Some benchmarks in nonequilibrium IRLM have been achieved by E. Boulat et al.[38, 39] but the *exact* analytic approach is limited at some particular value of interaction.

Similarly, there exists *exact* solutions at the Toulouse limit for Kondo quantum dot. At this limit the nonequilibrium Kondo model can be solved *exactly* by Hershfield Y-operator approach[32]. This method relies on calculating the nonequilibrium density matrix using a resummation of perturbation theory and its complexity makes it technically difficult. Thus, despite the numerous valiant efforts, no real theoretical approach exists that can describe the above experiments in the regimes of interest[15].

The bulk of this thesis is dedicated to presenting the Scattering Bethe Ansatz approach[16] to nonequilibrium quantum impurity physics. The idea of this method is to construct *exact* many body scattering eigenstates of the full Hamiltonian and fix the energy distribution from the asymptotic boundary conditions. Thus in principle this is *ab initio* approach to solve this type of nonequilibrium quantum. However the application of this approach leads to some problems and we have not yet succeeded in finding the solutions to these problems. We developed some phenomenological ideas to get around these difficulties. The *exact* SBA approach, however, is still under development and far from complete.

1.3 Summary of the thesis

In this chapter we have briefly introduced the experimental setup of quantum impurity systems. The main physical quantity we are interested in is the zero temperature steady state transport through these quantum impurity systems. From the transport measurement we can extract the information about the many body interactions among the delocalized electrons from the leads and the electrons from the impurities. Strong correlation problems such as Kondo effect and Fermi-edge singularities can be observed and measured with great accuracy in quantum dots, wells, or wires.

The main tool we tackle the problems of steady state transport through quantum impurity is the Scattering Bethe Ansatz (SBA) approach[16]. We introduced the general ideas and procedures of SBA and compare it with traditional Bethe Ansatz (TBA) in Chap. 2.

In Chap 3. we apply this SBA method to two leads finite U Anderson impurity model, the two leads version of Eq.(1.2). We proved the equivalence of TBA and SBA in equilibrium dot occupation. We find that the direct computation by this method when taking the system out of equilibrium in the bound state cases leads to problems contradicting the steady state assumptions. A phenomenological approach, named phenomenological Scattering Bethe Ansatz (pSBA), is proposed to circumvent this difficulty. The numerical results of this pSBA are shown and compared with known experimental results and theories. Exact results of dot occupation and Friedel sum rule are compared with pSBA results in equilibrium. Universality in nonlinear conductance vs voltage scaled by Kondo temperature T_k, expected from Fermi liquid picture in strong coupling and weak coupling regime, are shown in our numerical results.

In Chap 4. we apply the pSBA method to infinite U Anderson impurity model, the $U \to \infty$ limit of the finite U case. We showed by direct calculations how to connect finite U and infinite U results in Bethe Ansatz bases. Numerical results for conductance and dot occupation vs voltage are shown. Similar universality curves are shown for conductance vs rescaled voltage. In the end of this chapter we discuss some preliminary work on the two leads Kondo model (or two leads version of s-d model shown in Eq.(1.1)) and connect it with the infinite U Anderson model.

In Chap 5. we step from smaller quantum dot devices into larger quantum dot devices or quantum well devices. We extend the formulations of SBA on the two leads IRLM from real Bethe momenta to complex (bound state) Bethe momenta. We redo the numerical computation and examine the condition of dot occupation in equilibrium. We find qualitative agreement between our results with

expected FES behaviors.

Chap 6. is about some possible extension of the current frame work. In the discussion from Chap. 3 to Chap. 5 the computations are done with zero temperature and zero field. We set up the free energy formulation of finite temperature and finite field in infinite U Anderson model, proving the ground state configurations at zero temperature and zero field limit. Different geometry such as three leads connections or quantum wire devices are also discussed. Possible application to time dependent problems is briefly mentioned in the end.

Chap 7. gives a summary of the accomplishments of this SBA approach, discusses the problems encountered in bound states, and states how we plan to proceed in the near future.

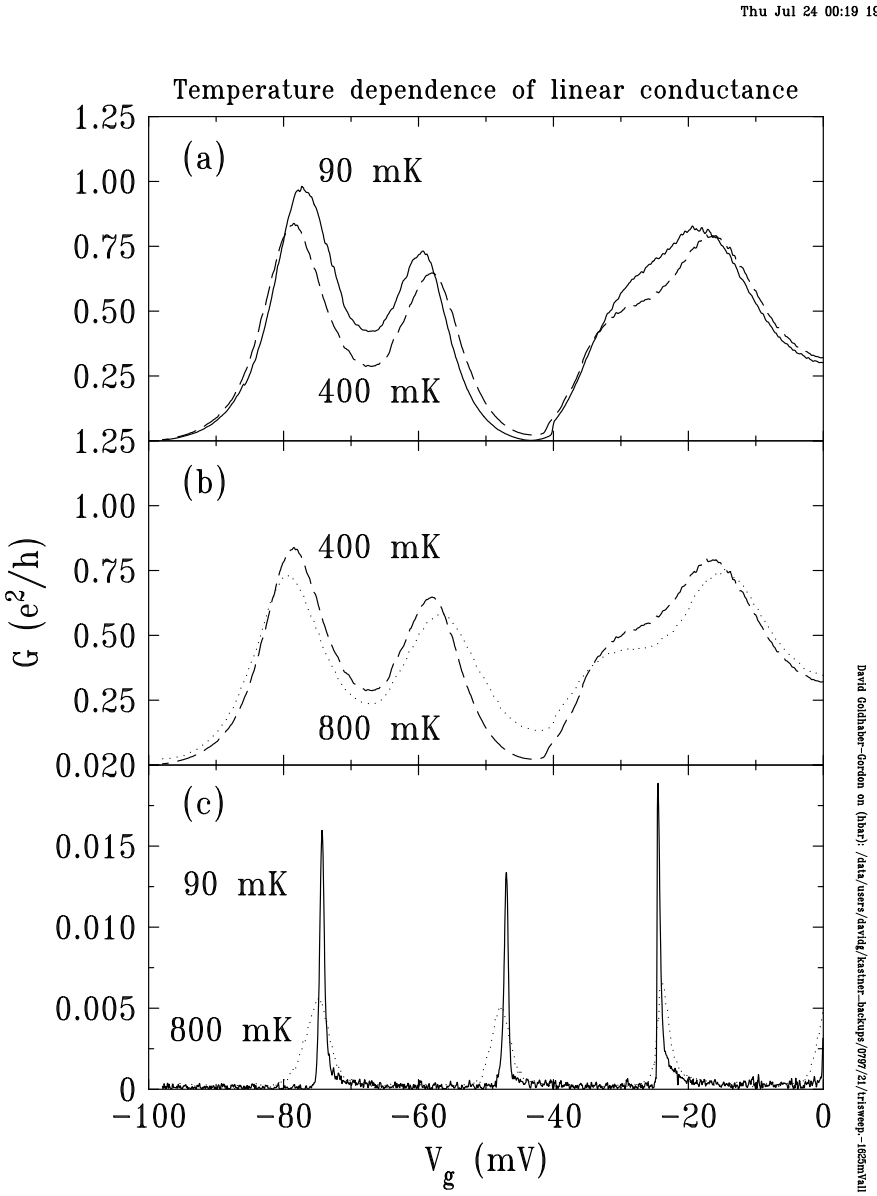

Figure 1.2: Temperature dependence of zero-bias conductance G through two different spatial states on the quantum dot. (a) Paired peaks corresponding to the two spin states for each spatial state become better resolved with increasing temperature from 90mK (full line) to 400mK (dashed). The intra-pair valleys become deeper and the peaks become narrower. (b) From 400mK (dashed line) to 800mK (dotted) the paired peaks near $V_g \sim 270$mV broaden. The peaks near $V_g \sim 225$mV are still becoming better resolved even at 800 mK, as they have larger Γ and hence larger T_K. (c) When Γ is reduced (as illustrated by shorter and narrower peaks), U increases relative to δE, so peak pairing is no longer evident. Because the Kondo phenomenon is suppressed, peaks become narrower as temperature is decreased at all T down to our base temperature of 90 mK. Full line is for 90 mK, dotted line for 800 mK. Figs and captions taken from Ref.[5]

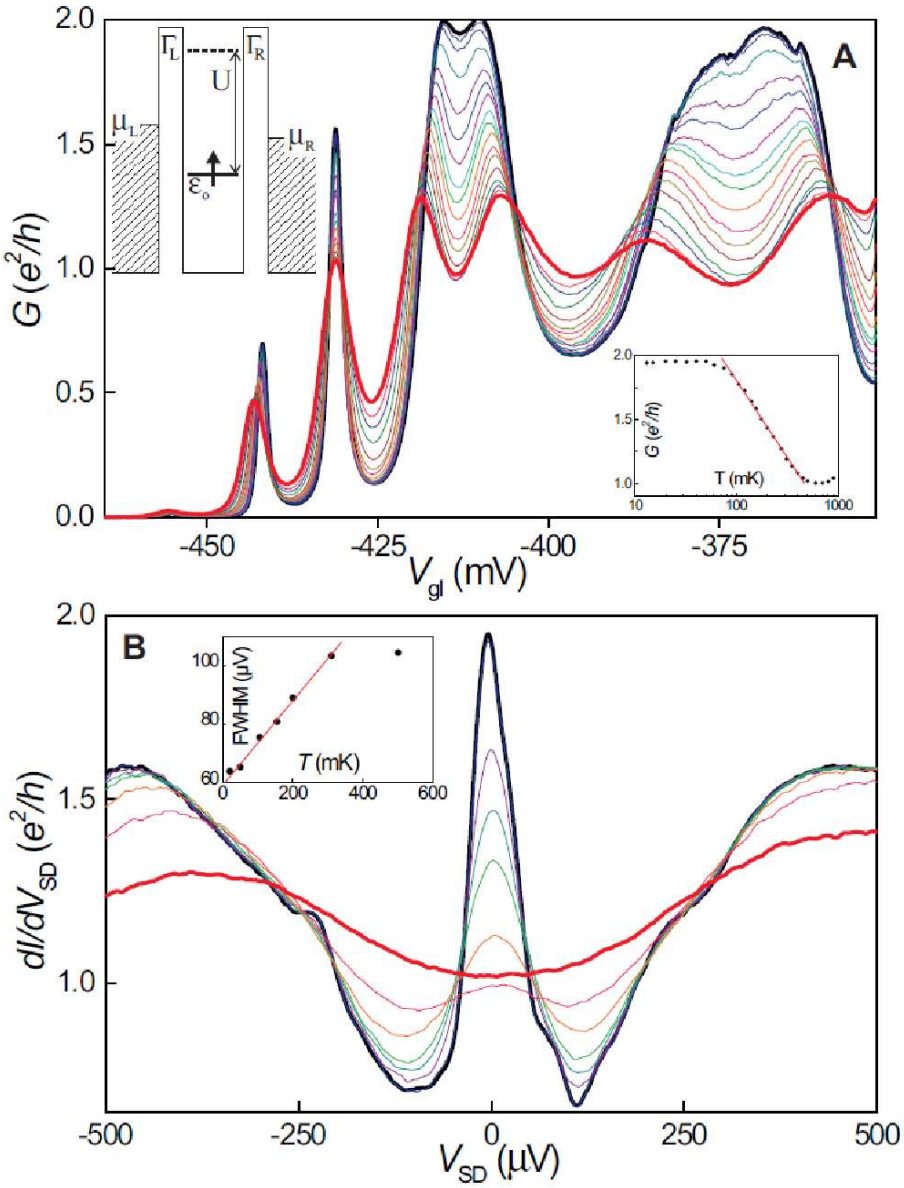

Figure 1.3: (A) Coulomb oscillations in G versus V_{gl} at $B = 0.4$ T for different temperatures. $T = 15$ mK (thick black trace) up to 800 mK (thick red trace). V_{gr} is fixed at -448 mV. The lower-right inset highlights the logarithmic T-dependence between ∼90 and ∼500 mK for $V_{gl} = -413$ mV. The upper-left inset explains the symbols used in the text with $\Gamma = \Gamma_L + \Gamma_R$. Note that ϵ_d is negative and measured from the Fermi level in the leads at equilibrium. (B) Differential conductance, $\frac{dI}{dV_{sd}}$, versus dc bias voltage between source and drain contacts, V_{sd}, for $T = 15$ mK (thick black trace) up to 900 mK (thick red trace), also at $V_{gl} = -413$ mV and $B = 0.4$ T. The left inset shows that the width of the zero-bias peak, measured from the full-width-at-half-maximum (FWHM) increases linearly with T. The red line indicates a slope of 1.7 k_B/e, where k_B is the Boltzmann constant. At 15 mK the FWHM = 64 μV and it starts to saturate around 300 mK. Figs and captions taken from Ref.[9]

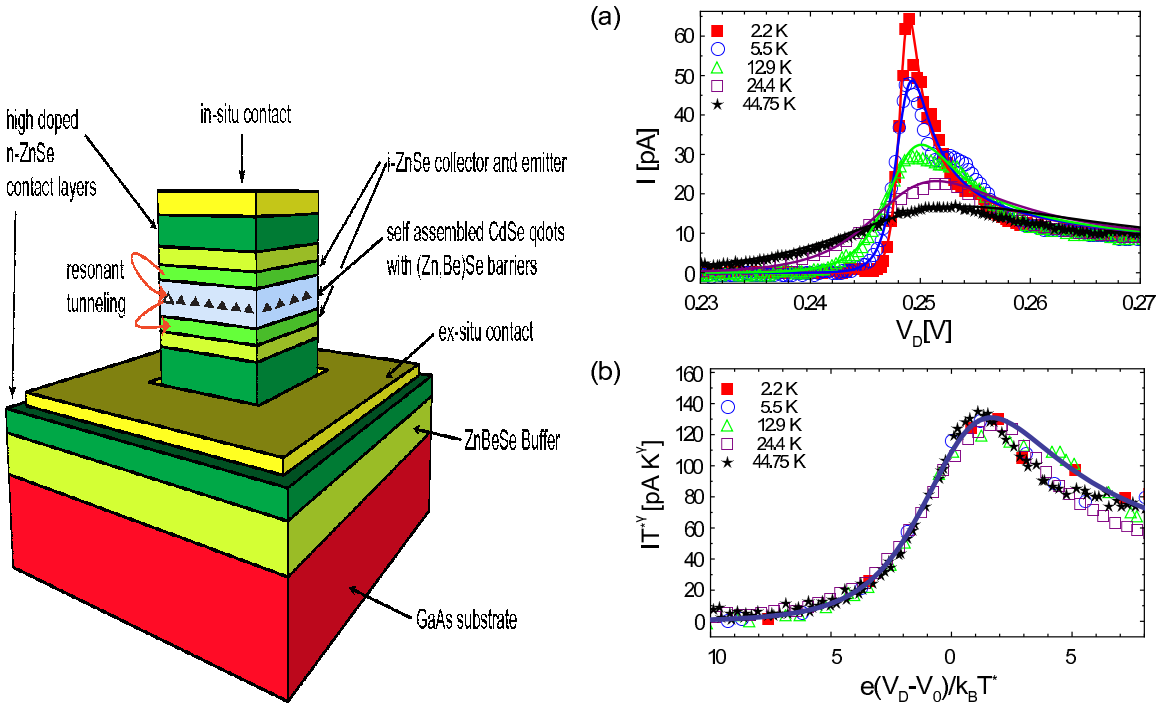

Figure 1.4: Left: Device layout and layer structure. Self assembled quantum dots which are embedded in the (Zn,Be)Se tunnel barrier provide the resonant state for the tunneling transport mechanism. Right: (a) (color online) $I(V_D)$ characteristics for various temperatures up to 45 K and at zero magnetic field. Symbols are the experimental data. The colored line for each dataset represents a fit to equation in Ref.[13] for each temperature. (b) Rescaling both axes collapses the datasets for all temperatures on a single scaling curve. The solid line is a fit to the rescaled equation in Ref.[13] which is now independent of the effective temperature T^*. Captions and pictures are from Ref.[14]

Chapter 2

Introduction of Scattering Bethe Ansatz approach

2.1 Introduction on methods on nonequilibrium quantum impurity

The physical phenomena we want to describe in this thesis is the transport measurement on quantum impurity system (dot or wire) as introduced in the previous chapter. The problem is intrinsically time dependent. As we couple the leads with the dot the current would start from zero immediately before the coupling and eventually reach a steady state current after certain amount of transient time. The steady state means the expectation value of current does not change with time and it is a non-equilibrium steady state as we need to keep up the voltage difference to maintain this current. The physics of how the system goes from initial zero current to the steady state current is a very interesting problem in non-equilibrium physics and is one of the future extension we want to achieve with the Scattering Bethe Ansatz (SBA) approach (see Chap 6). It has also been studied by various numerical methods such as real time numerical renormalization group, time dependent density matrix renormalization group (t-dMRG), time-dependent non-crossing approximation etc to name a few. The primary work in this thesis is to concentrate on the steady state part assuming steady state can be achieved in this system.

The current measured in experiment is in fact the steady state current (A measurement done with pulsed voltage was done by T. Fujisawa et al.[35] in 2000 to measure the transient time scale related to spin relaxation time in quantum dot system. Typically the time scale they obtained in this measurement is around μs. Thus for usual direct current measurement the current obtained is already in the steady state.). How one reaches the steady state for this quantum impurity system from theoretical point of view is still an interesting open question. B. Doyon and N. Andrei[36] had used Keldyshi perturbation approach to show order by order that this steady state can be achieved in Kondo model by taking the size of the leads to be infinite before taking the initial time (the time to couple the leads with the dot) to minus infinity. Another condition is the leads are described by Fermi distributions. The quantum impurity models we describe in this thesis have some special limit related to Kondo model. Based on this connection we assume the steady state can also be

achieved in these models. More rigorous proof on this argument is required though.

One way to describe the steady state problem related to transport measurement is to use scattering eigenstates. To construct the scattering eigenstates of the quantum impurity models in general is quite a formidable task due to the strong correlation between particles and the complication of scattering mechanism which may or may not conserve number of particles. For a special subset of quantum-impurity models, the full Hamiltonian is integrable and the multi particles scattering eigenstates can be explicitly constructed by Bethe Ansatz method. Bethe Ansatz is a way to write down *exact* many particles eigenstates in the product form of single particle eigenstates and two particles scattering matrices. This form of solution, strictly speaking, can only be applied in one (spatial) dimensional system as extra dimensions will result in three or more particles scattering event at one spacetime. In low energy regime the physics can be treated as if it were one dimensional problem and we may use this Ansatz to obtain the *exact* multi particles eigenstates.

The way we use to judge whether the Hamiltonian is integrable or not is to write down its two particles scattering eigenstate. We can assume the two particles eigenstate takes the product form of two single particle's eigenstates with the two particles' S-matrix determined by the interaction. If the two particles S-matrix obtained satisfied the Yang-Baxter equations, which are some consistency equations for exchanging particles, then we say the Hamiltonian is integrable and the many particles' eigenstate can be written as the product form of single particle's eigenstates and many two particles S-matrices determined by the interaction between any two of the particles. The physical reason behind this approach is that in one dimensional system the interactions among particles always occur pairwise. Quite often we are interested in the *universality* region which does not depend on particular energy spectra of the system. In this region the energy can be linearized and only s-wave scattering is needed to be taken into account in the scattering eigenstate construction. Higher order of scattering channels such as p or d-wave in general could be included but sometimes it would break the integrability of the model. Thus we confine ourself in the simpler case where the Hamiltonian is integrable and we can write down the multi particles scattering eigenstate by Bethe Ansatz approach.

There are two main differences between SBA and traditional Bethe Ansatz (TBA). One is in the boundary condition of the eigenstates. As we have stated in the discussion of reaching steady state from time dependent picture we need to require the size of the leads to be infinite from the beginning. The scattering eigenstate constructed has *open* boundary rather than the *closed* boundary (periodic

	SBA	TBA
System	Infinite	Finite
Boundary condition	asymptotic (open)	periodic
Wavefunctions	used explicitly	not used
Thermodynamics	difficult	difficult
Scattering Properties	possible	not possible
Nonequilibrium Generalization	Yes	No

Table 2.1: Summary of differences between the Scattering Bethe Ansatz (SBA) and Traditional Bethe Ansatz (TBA). Table is modified from Ref.[15].

boundary condition) in the eigenstate of equilibrium system. The energy spectrum of this scattering eigenstate is determined by the incoming state (asymptotic boundary condition) , or the initial state in the time dependent picture. The other major difference is that we use explicitly the wavefunctions to compute matrix elements of various physical quantity. From these matrix element computation we then compute expectation value of the physical quantity. In TBA the thermodynamical quantities are derived by taking various derivative on the free energy and the wavefunctions are not used explicitly. The comparison between SBA and TBA is summarized in Table.2.1.

In the following we give an overview of SBA and its application on some general quantum impurity model without going into any particular Hamiltonian. The specific application of SBA for two leads finite U Anderson model, infinite U Anderson model, Kondo model (some preliminary results), and interacting resonance level model(IRLM) will be shown in later chapters.

2.2 General introduction of Scattering Bethe Ansatz

The bulk of this thesis is to use Scattering Bethe Ansatz approach to compute transport property of quantum impurity system. Here we give a brief overview of this approach. Imagine we turn on the coupling H_{int} between the leads and impurity adiabatically in the infinite past at $t = -\infty$

$$H = H_0 + e^{\eta t} H_{int}$$

Here H_0 describes the leads Hamiltonian or the system in the initial state. At $t = -\infty$ the quantum impurity is decoupled from the electron baths and the system is described by an eigenstate of H_0 which we denote as $|\Phi\rangle$. At later times, the baths and the quantum impurity are coupled adiabatically and at later time the eigenstate of the system $\Psi(t)\rangle$ is described by time evolving state $|\Phi\rangle$ with

time evolution operator $U(t, -\infty)$

$$|\Psi(t)\rangle = U(t, -\infty)|\Phi\rangle = T\{\int_{-\infty}^{t'} e^{iH(t')dt'}\}|\Phi\rangle$$

From Gellman-Low theorem we can take the limit $\eta \to 0$ and see that $|\Psi(t=0)\rangle \to |\Psi\rangle_s$ is an eigenstate of the full Hamiltonian H. The state $|\Psi\rangle_s$ is in close analogy to the scattering state in ordinary quantum mechanics describing scattering of a wave-packet by localized, spherically symmetric potential. The formal structure of this scattering state is given by solving Lippman-Schwinger equation

$$|\Psi\rangle_s = |\Phi\rangle + \frac{1}{E - H_0 \pm i\eta} H_{int}|\Psi\rangle_s$$

We construct the scattering eigenstate $|\Psi\rangle_s$ with asymptotic boundary condition $|\Phi\rangle$ to describe the solution of the full Hamiltonian under the assumption that the steady state can be achieved. Note that this asymptotic boundary condition $|\phi\rangle$ in time independent picture of steady state corresponds to the initial condition in time dependent picture.

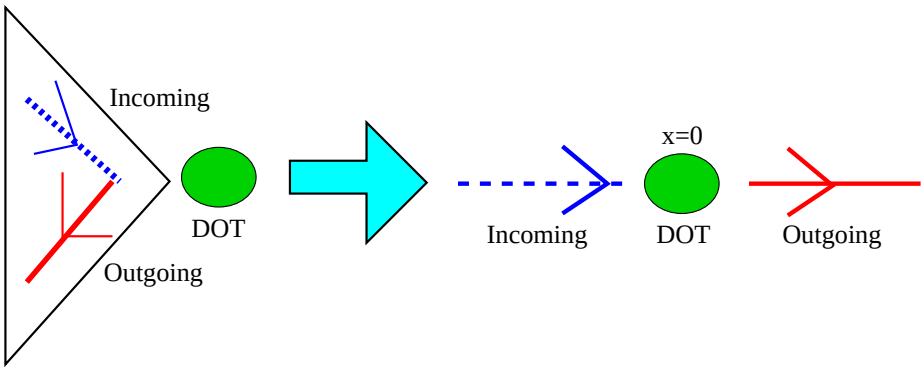

Figure 2.1: We work in a chiral-electron picture where the leads have been unfolded. The incoming particles correspond to $x < 0$ and the reflected outgoing particles, $x > 0$ in the case of quantum dot system. Figure and caption taken from P. Mehta's thesis[15]

For the models we are going to describe in this thesis we further assume the energy spectra of the leads are linear. For mathematical convenience we further unfold these linear spectra into right movers only. The first step is to say that the physics we are interested in is nearby the Fermi surface of the leads and we are interested in the universality behavior nearby this regime. Thus we can

expand the quadratic spectra around Fermi surface and get linearized spectra as

$$\epsilon(k) = \frac{k^2 - k_F^2}{2m} \simeq \frac{k_F}{m}(k - k_F)$$

In our convention the Fermi velocity $\frac{k_F}{m} = 1$ and $\hbar = e = 1$ which we can put them back when needed. Since we are interested in low energy physics, we keep only the modes where $|k - k_F| < D$. We define right and left movers by

$$\psi_{R,L}(r) = \int_{-D}^{D} dk e^{\pm ikr} \psi(k + k_F)$$

In terms of left and right movers, the Hamiltonian can be written as

$$H = H_0 + H_{int} = -i \int_{-\infty}^{0} dr \{\psi_R^\dagger \partial \psi_R - \psi_L^\dagger \partial \psi_L\}$$

Use the fact that $\psi_R(0) = \psi_L(0)$ and $\psi_R(r) = \psi_L(-r)$ for the electron operators we may unfold this linear spectra to right movers only for mathematical convenience. Thus the general Hamiltonian describing some quantum impurity system (dot(s), wire, or interferometer etc.) can be written as

$$H = H_0 + H_{int} \tag{2.1}$$

$$H_0 = \sum_{i,\alpha_i} \int_{-\infty}^{\infty} dx \psi_{i\alpha_i}^\dagger(x) \partial \psi_{i\alpha_i}(x) \tag{2.2}$$

We put back the indices for leads and other degrees of freedom. Here i refers to the lead index and α refers to spin and other degrees of freedom such as levels splitting due to crystal field. H_{int} could be of any form at the moment but is required to be confined in a small (compared with the size of the leads) physical region such as a quantum dot or quantum wire. The pictorial description of this unfolding process is plotted in Fig.(2.1). In this unfolded picture the incoming state are in the $x < 0$ region and the outgoing state are in the $x > 0$ region. The quantum dot is sitting at $x = 0$ in this coordinate.

2.2.1 The Bethe Ansatz basis and the Fock basis

To construct scattering eigenstates for integrable quantum models, the Bethe-Ansatz wavefunction exploits the large degeneracy of the *linearized* free electron gas shown in Eq.(2.2. We shall show that

the Bethe Ansatz basis is the correct basis to be chosen in the non-interacting free electron problem described by H_0 when the interaction H_{int} is turned on. The simplest example is to look at two particles solution. Consider the first quantized version of H_0 (obtained by acting the Hamiltonian H_0 on some two particles state $|p_1+q, p_2-q\rangle$). In the two particles sector, the first quantized H_0 is just given by $H_0 = \partial_{x_1} + \partial_{x_2}$. Notice that any wavefunction of the form

$$|p_1+q, p_2-q\rangle = \int dx A^q_{\alpha_1\alpha_2} e^{i(p_1+q)x_1 + i(p_2-q)x_2} \psi^\dagger_{\alpha_1}(x_1)\psi^\dagger_{\alpha_2}(x_2)|0\rangle$$

is an eigenfunction of H_0 with energy $E = p_1 + p_2$. Since q can take on any value, there are an infinite number of such states. Any linear combination of eigenfunctions of the above form is also an eigenfunction of the H_0 with energy E. This argument can be easily generalized to N particles solution of the form

$$|N\rangle = \int (\prod_{j=1}^{N} dx_j e^{ip_j x_j}) \prod_{i<j} f_{\alpha_i\alpha_j}(x_i - x_j)\psi^\dagger_{\alpha_i}(x_i)|0\rangle \tag{2.3}$$

which is an N particles eigenstate of H_0 and N is the total number of particles from the leads ($N = N_1 + N_2$ for two leads Hamiltonian). Now let us get back to two particles solution of the *full* Hamiltonian H. What we find is that the solution takes the following form

$$\begin{aligned} |k_i, k_j\rangle &= \int dx_i dx_j e^{i(k_i x_i + k_j x_j)}(\theta(x_i - x_j) + S_{ij}\theta(x_j - x_i)) \\ &\times \sum_{\alpha_i,\alpha_j} A_{\alpha_i\alpha_j} f_{\alpha_i}(x_i) f_{\alpha_j}(x_j)\tilde{\psi}^\dagger_{\alpha_i}(x_i)\tilde{\psi}^\dagger_{\alpha_j}(x_j)|0\rangle \end{aligned} \tag{2.4}$$

Here $f_{\alpha_j}(x_j)$ refers to some functions determined by single particle solution of the Hamiltonian H and it carries the information of phase shift (contained in H_{int} part) across the impurity. $\tilde{\psi}^\dagger_{\alpha_j}(x_j)$ represents leads creation operator $\psi^\dagger_{\alpha_j}(x_j)$ when x_j is away from interacting region ($x_j > 0$ or $x_j < 0$, assuming H_{int} occurs at $x_j = 0$ only for quantum dot system. For quantum wire it could be $|x_j| > \frac{l}{2}$ with l being the length of the wire.) and represents dot/wire particle when x_j is within the interacting region. The two particles S-matrix S_{ij} is determined by H_{int} and thus model dependent. For H with $SU(2)$ symmetry in spin space for example, the general structure of S_{ij} can be written as

$$S_{ij} = \frac{(\beta(k_i) - \beta(k_j))\hat{I}_{ij} - i\hat{P}_{ij}}{\beta(k_i) - \beta(k_j) - i}.$$

Here $\hat{I}_{ij}$ is the identity operator and $\hat{P}_{ij} = \frac{1}{2}(\hat{I}_{ij} + \hat{\sigma}_i \cdot \hat{\sigma}_j)$ is the spin exchnage operator between particle i and j. In the asymptotic region ($x_j \ll 0$) the operators $\tilde{\psi}^\dagger_{\alpha_i}(x_i)$ become $\psi^\dagger_{\alpha_i}(x_i)$ and $f_{\alpha_j}(x_j)$ reduces to $\theta(-x_j)$ times some constant. The two particles eigenstate shown in Eq.(2.4) becomes

$$\begin{aligned} |k_i, k_j\rangle|_{x\ll 0} &= \int dx_i dx_j e^{i(k_i x_i + k_j x_j)}(\theta(x_i - x_j) + S_{ij}\theta(x_j - x_i)) \\ &\times \sum_{\alpha_i,\alpha_j} A_{\alpha_i\alpha_j}\theta(-x_i)\theta(-x_j)\psi^\dagger_{\alpha_i}(x_i)\psi^\dagger_{\alpha_j}(x_j)|0\rangle \end{aligned} \tag{2.5}$$

By acting H_0 on Eq.(2.5) it is easy to see that $H_0|k_i, k_j\rangle|_{x\ll 0} = (k_i + k_j)|k_i, k_j\rangle|_{x\ll 0}$ and confirm that this is indeed an eigenstate of the free Hamiltonian H_0 in the asymptotic region. The Fock basis, the simplest basis for solution of free Hamiltonian H_0, can be viewed as a special solution of this two particles solution by choosing $S_{ij} = 1$. The interaction in the full Hamiltonian H breaks the degeneracy in the linear spectra and picks out a particular form of tow particles S-matrix. This is the same idea as doing perturbation theory for a highly degenerate system where we need to choose a particular linear combination when the interaction is turned on.

2.2.2 Scattering eigenstates in the Bethe Ansatz form

Now let us summarize the previous discussion and generalize the discussion to multi particles from two particles solution. The first stage of the SBA is to construct eigenstates of this general Hamiltonian such that far away from the quantum-impurity, the eigenstate for the incoming particles reduce to an eigenstate of the free electrons Hamiltonian H_0. Another requirement is that we can identify the leads indices of the incoming particles from this scattering eigenstate. As discussed previously, the incoming particles are those to the left of the impurity ($x < 0$) and the outgoing scattered particles are those to the right of the impurity ($x > 0$). The SBA constructs eigenstates of the Hamiltonian by using Bethe Ansatz approach. This approach utilizes the integrability of the Hamiltonian H to divide multi particles scattering events into sets of two particles scattering events characterized by the two particles S matrices. The integrability of the Hamiltonian H is confirmed by self consistency conditions on the two particles S-matrices known as the Yang Baxter Equations. These conditions ensure all multi particles interactions can be *consistently* broken up into pairwise interactions and the multi particles wavefunction can be written in the Bethe Ansatz form.

As we have stated in the steady state conditions the quantum impurity need to be coupled to non

interacting electrons. Quite often this is a valid assumption as well since the leads itinerant electrons can screen out effectively any interactions from the quantum impurity due to the smallness of the impurity part. We further assume that total number of particles is conserved in the Hamiltonian H and thus fixed number of particles can be used to construct an eigenstate. Wavefunctions of Bethe Ansatz divide the configuration space into $N!$ regions according to the ordering of the particles on the infinite line. Each such region is labeled by a permutation Q in the symmetric group of degree N. The general wavefunction of Bethe Ansatz form can be written as

$$|BA, \{k_j\}\rangle = \int \prod_j dx_j e^{\sum_j k_j x_j} \sum_Q S^Q A_{\alpha_1 \ldots \alpha_N}(Q)\theta(x_Q) \prod_{j=1}^{N} f_{\alpha_j}(x_j)\tilde{\psi}^\dagger_{\alpha_j}(x_j)|0\rangle \tag{2.6}$$

with $\theta(x_Q) = \theta(x_{Q(1)} < x_{Q(2)} \ldots x_{Q(N)} < x_{Q(0)})$ and Q runs over all $N!$ permutations. $A_{\alpha_1 \ldots \alpha_N}(Q)$ represents the amplitude for the wavefunctions in some defined by permutation Q which incorporates spin or other physical degrees of freedom. The two particles solution is written in Eq.(2.4) as an example. In the asymptotic region ($x_j \ll 0$) Eq.(2.6) reduces to

$$|BA, \{k_j\}\rangle|_{x_j \ll 0} = \int \prod_j dx_j e^{\sum_j k_j x_j} \sum_Q S^Q A_{\alpha_1 \ldots \alpha_N}(Q)\theta(x_Q) \prod_{j=1}^{N} \psi^\dagger_{\alpha_j}(x_j)|0\rangle \tag{2.7}$$

which is an eigenstate of the free Hamiltonian H_0 with eigenvalue $E = \sum_j k_j$. This is due to the fact that $A_{\alpha_1 \ldots \alpha_N}(Q)\theta(x_Q)$ takes the product form of $\theta(x_{Q(i)} - x_{Q(j)})$ between particles i and j and this form does not affect the energy of the linear spectrum. Thus far the distribution of $\{k_j\}$ is arbitrary. The next step is to find the distribution of $\{k_j\}$ such that in this asymptotic region Eq.(2.7) describes the energy distribution in the form of the free Fermi seas of the leads.

2.2.3 Imposing asymptotic boundary conditions

To simplify the discussion let us first concentrate on zero temperature case. The leads in zero temperature are described by two Fermi seas filled from lowest available levels to their respective Fermi energy. Fig.2.2 shows one of the leads condition. The description of these Fermi seas is straightforward for Fock bases (S_{ij} or S^Q equals to one): It starts filling the integers corresponding to lowest energy level and from there fills up all the available integers up to the integers corresponding to some Fermi level. This can be achieved in the asymptotic region in th Fock basis. By imposing the periodic boundary condition in the asymptotic region which means applying the periodic boundary

condition for plane wave solution in the Fock basis,

$$e^{ik_jL} = 1 \rightarrow k_jL = 2\pi n_j \rightarrow k_j = \frac{2\pi n_j}{L} \tag{2.8}$$

with L being the size of the leads to be taken to infinity in thermodynamic limit and n_j some integer. The procedure to find energy distribution in the Bethe basis is quite similar to the Fock basis in zero temperature case. Since at zero temperature we need to fill up all available particles state (i.e. no hole state in zero temperature problem), we shall also apply periodic boundary condition in the asymptotic region and require that all integers n_j are filled. The periodic boundary condition in the asymptotic region gives

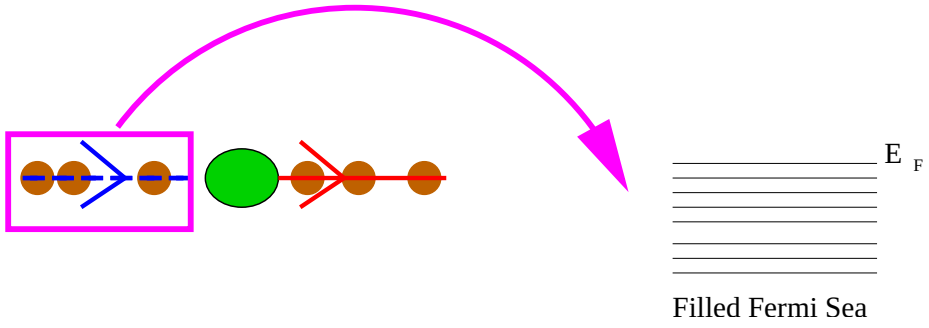

Figure 2.2: Pictorial representation of fixing energy eigenvalue by the asymptotic boundary condition. The incoming states correspond to the initial states described by filled Fermi sea at zero temperature and zero field. Figure taken from P. Mehta's thesis[15]

$$e^{ik_jL}A_{\alpha_1\ldots\alpha_N} = S^{jj-1}\ldots S^{j1}S^{jN}\ldots S^{jj+1}A_{\alpha_1\ldots\alpha_N} \tag{2.9}$$

To solve Eq.(2.10) usually requires the Quantum inverse scattering method. For spinless system such as IRLM the two particle S-matrices are some $U(1)$ phases, denoted as $S_{ij} = e^{i\Phi(k_i,k_j)}$, and Eq.(2.10) can be simplified as

$$e^{ik_jL} = \prod_{i\neq j}^{N} e^{i\Phi(k_j,k_i)} \rightarrow k_j = \frac{2\pi n_j}{L} + \frac{1}{L}\sum_{i\neq j}^{N}\Phi(k_j,k_i) \tag{2.10}$$

In taking the limit $L \rightarrow \infty$ the discrete energy levels can be viewed as continuous spectra as the energy level difference is of order $\frac{1}{L}$ which is approaching to zero as $L \rightarrow \infty$. For the one lead (traditional Bethe Ansatz) we may define the single lead Bethe momenta density (In fact the term Bethe momentum here actually refers to the energy eigenvalue. The momentum is not conserved in

an impurity model which breaks translational invariance. In literature, however, it is widely called as Bethe momentum and we also take this convention.)

$$\rho(p) = \frac{1}{L}\frac{dn}{dp}$$

by taking the continuous limit of Eq.(2.10) and obtain

$$\rho(p) = \frac{1}{2\pi} - \frac{1}{2\pi}\int dk \frac{\partial \Phi(p,k)}{\partial p}\rho(k)dk$$

the case of multi leads is to put in the information of leads indices back in Bethe momenta k and will be illustrated in specific models shown in the later chapters.

2.2.4 Computing with Scattering States

Once we obtain the energy distribution from the asymptotic condition the next thing to do is to compute the expectation value of some physical operator $\hat{O}$ with respect to the scattering eigenstates by using Eq.(2.6)

$$\langle \hat{O} \rangle = \frac{\langle BA, \{p_j\}|\hat{O}|BA, \{k_j\}\rangle}{\langle BA, \{p_j\}|BA, \{k_j\}\rangle} \tag{2.11}$$

Essentially this type of computation is to obtain the matrix element of the physical operator $\hat{O}$ in the vector space of the Bethe basis. To carry out this calculation in general is quite complicated. The simplification comes from the fact that we work directly with infinite system. Technically, this means that in the infinite systems we can retain terms of order $\frac{1}{L}$ and ignore terms of order higher than $\frac{1}{L^2}$. Under this approximation the orthogonality between different Bethe momenta state is valid. The expectation value of two such wavefunctions $\langle BA, \{p_j\}|BA, \{k_j\}\rangle$ is given by(suppressing the internal index α_j for notational brevity)

$$\sum_{Q,\tilde{Q}} \int d\vec{x} d\vec{y}\, e^{i\sum_j (k_j x_j - p_j y_j)} \theta(x_Q)\theta(y_{\tilde{Q}}) A(Q)A(\tilde{Q}) \langle 0| \prod_{s=1}^{N} f(y_s)\psi(y_s) \prod_{j=1}^{N} f^*(x_j)\psi^\dagger(x_j)|0\rangle \tag{2.12}$$

The impurity part of particles operators does not contribute to overall normalization factor in this $L \to \infty$ limit. The fermion operators just give rise to a Slater determinant which gives

$$\sum_{Q,\tilde{Q},S} (-1)^{sgn(S)} \int d\vec{x} d\vec{y}\, e^{i\sum_j (k_j x_j - p_j y_j)} \theta(x_Q)\theta(y_{\tilde{Q}}) A(Q)A(\tilde{Q}) \prod_{j=1}^{N} f^*(x_{S(j)}) f(y_j) \delta(x_{S(j)} - y_j) \quad (2.13)$$

where S is a permutation of the N particles. Integrating over $\vec{y}$, we have

$$\begin{aligned} \langle BA, \{p_j\} | BA, \{k_j\} \rangle &= \sum_{Q,S} (-1)^{sgn(S)} \int d\vec{x}\, e^{i\sum_j (k_j x_j - p_j x_{S(j)})} \theta(x_Q) A(Q) A(QS^{-1}) |f(x_j)|^2 \\ &= \sum_{Q,\tilde{Q},S} (-1)^{sgn(S)} \int d\vec{x}\, e^{i\sum_j (k_j - p_{S^{-1}(j)}) x_j} \theta(x_Q) A(Q) A(QS^{-1}) |f(x_j)|^2 \end{aligned} \quad (2.14)$$

$|f(x_j)|^2$ usually leads to some constant as a function of x_j. Thus, we see that this expression is just the norm of plane waves integrated over a region $\theta(x_Q)$. As is usual we regularize plane waves by first taking L which is then taken to infinity at the end of the calculation.

$$\lim_{L\to\infty} \int_{-L}^{0} dx e^{i(k_j - p_j)x_j} \theta(x_1 < x_2 \ldots < x_N). \quad (2.15)$$

The integration taken from $L \to$ directly gives essentially the same results[71]. It is straightforward to show that the leading order contribution in L to this integral is just $L^N/N!$ which occurs only if the two Bethe-Ansatz momenta are identical $\{k_j\} = \{p_j\}$ (or $k_j^+ + k_l^- = p_j^+ + p_l^-$ in the case of complex momenta, see Appendix for details). This is simply saying that plane waves are orthogonal even on a region $\theta(x_Q)$ for an infinite system. Thus for an infinite size system we can ignore all terms in Eq.(2.14) where the $k_j \neq p_{S^{-1}(j)}$ for all j. This leads to great technical simplifications as we only need to keep $S = 1$ terms in Eq.(2.14). Similar simplifications occur when computing the matrix element of an operator $\hat{O}$ between the Bethe Ansatz wavefunctions. Assuming the operator $\hat{O}$ is related to impurity part the computation of $\langle BA, \{p_j\} | \hat{O} | BA, \{p_j\} \rangle$ leads to

$$\langle BA, \{p_j\} | \hat{O} | BA, \{k_j\} \rangle = O_1 L^{N-1} + O_2 L^{N-2} + \ldots$$

The expectation value Eq.(2.11) is then in the form of $O_1 \frac{1}{L} + O_2 \frac{1}{L^2} + \ldots$. For an infinite size system we can take the leading order term O_1 and ignore the rest of the higher order terms.

Notice that in the SBA the information of nonequilibrium is not built into the Hamiltonian H.

Rather, the nonequilibrium is characterized by different number of particles incoming from different leads or, in the other words, the information is carried by the asymptotic boundary conditions on the wavefunctions. The number of particles from lead i is controlled by the chemical potential μ_i in the free energy F, given by

$$\frac{F}{L} = \frac{1}{L}\sum_i E_i - \mu_i N_i$$

with

$$\frac{E_i}{L} = \int_D^{B_i} dp\, p\, \rho_i(p)$$

and

$$\frac{N_i}{L} = \int_D^{B_i} dp\, \rho_i(p)$$

in the case of IRLM at zero temperature and zero magnetic field case.

2.2.5 Extension to finite temperature and finite magnetic field

So far we have only discussed the case of zero temperature. The case for finite temperature and/or finite magnetic field can also be generalized from this zero temperature free energy

$$\frac{F}{L} = \frac{1}{L}\sum_i E_i - \mu_i N_i - T_i S_i - m_i h_i$$

where T_i and h_i are temperature and magnetic field in the lead i. S_i and m_i denote entropy and magnetization of the lead i. The explicit calculation of this free energy without magnetic field for infinite U Anderson model is shown in chapter 6 where minimization of this free energy is used to prove the ground state configuration close to zero temperature. A complication in the Bethe bases is that the entropy and magnetic moment terms cannot always be distinguished by the leads labels. This is shown in the infinite U Anderson case when the quantum inverse scattering method is applied to solve the eigenvalue problem. Thus it remains to be questionable whether we can use this SBA approach to find thermal current induced by different temperature within the leads.

Apart from this problem of identifying the entropy and magnetic moment by the leads in the

SBA method, the main difficulty in obtaining the finite temperature solution is very similar to the TBA. At finite temperature we need to consider all possible solutions of the energy eigenvalue. Some of the eigenvalues could be complex solutions with some regular poles structure predicted by string hypothesis, and some of the complex pairs do not have string type of solutions like the case of IRLM with Bethe momenta higher than impurity level. Even if the string hypothesis were valid, as is the case for Anderson model and Kondo model, the analytic solution involve infinite sets of integral equations which are not easily carried out in practical calculations. The complexity of matrix element computation, however, is similar to the complexity encountered in the case of complex solution in finite U or infinite U Anderson model. Higher order of complex pairs basically have the same type of matrix element evaluation methods. Thus we conclude that the level of difficulty for TBA and SBA at finite temperature in Tab.2.1 to be the same.

2.3 Summary of the SBA

Here we use a flow chart shown in the last page of this chapter to summarize the procedures of the SBA method. The first step is to see if the system can reach steady state after certain transient time. In most of the experimental DC measurements this condition is almost always valid. The theoretical treatment for this problem, however, is much more involved and not easy to prove the existence of steady state. This thesis is based on the proof of existence of steady state shown by B. Doyon and N. Andrei[36] in the two leads Kondo model. We say that the models we use in this thesis have the limiting form of two leads Kondo model thus we can assume there are also steady state existing for our models. Further proof regarding this assumption is still needed.

To solve the steady state problem we solve the scattering eigenstates of the full Hamiltonian. The method we use to find the N particles eigenstates is the Bethe Ansatz approach. This approach requires the two particles S-matrices satisfying Yang-Baxter equations as the consistency conditions to construct many particles wavefunctions. The major difference of the SBA and the traditional Bethe Anatz is that the scattering eigenstates are constructed directly on infinite line (open boundary) rather than in a closed system.

Once we have the eigenstates the next thing to do is to fix the energy distribution by the asymptotic boundary condition in the incoming region. For zero temperature and zero field, which is the main line of this thesis work, the leads are in their respective ground state. For finite temperature

or finite field the leads states are described by some thermal distribution which we have to resort to finite temperature Bethe Ansatz approach to include all possible excitation states weighted by Boltzman distributions in the Hamiltonian.

Given the eigenstates with proper energy distribution we can then carry out the expectation value of the physical quantity we are interested in. For this part of computation it involves matrix element evaluations of the operators describing the corresponding physical quantity. It has been successfully applied in the case of real Bethe momenta k, while in the case of complex momenta or bound state solution we have not got physically reasonable results as it leads to non steady state problem. This is discussed in more details as we begin to apply this model in finite U Anderson model shown in next chapter. We circumvent this difficulty by applying phenomenological ideas to describe the transport related to the bound states. It is still not how to overcome this difficulty and hinders the practical application of this scattering approach in Bethe Ansatz.

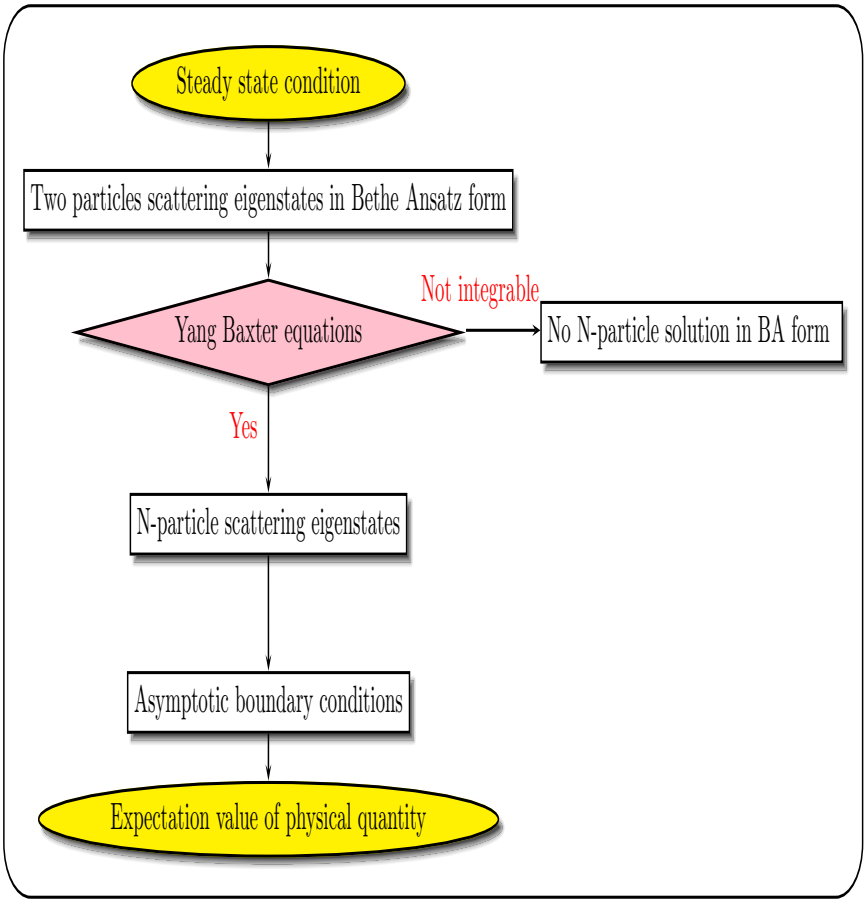
Steady state condition
Two particles scattering eigenstates in Bethe Ansatz form
Yang Baxter equations
Not integrable
No N-particle solution in BA form
Yes
N-particle scattering eigenstates
Asymptotic boundary conditions
Expectation value of physical quantity

Chapter 3

Two leads Finite U Anderson impurity model

3.1 Introduction on Finite U Anderson model

Nano-structures, beyond their practical applications, display an array of emergent phenomena stemming from their reduced dimensionality which enhances quantum fluctuations and strong correlations. Often, experiments are carried out under non-equilibrium conditions, with currents passing through the structures. The measurements are performed over a wide range of parameters, such as temperature and applied bias, allowing experimental exploration of the interplay between non-equilibrium dynamics and strong correlation physics [5, 7, 6, 8–10]. A canonical example is the non-equilibrium Kondo effect observed in a quantum dot attached to two leads held at different chemical potentials μ_i. The voltage difference $V = \mu_1 - \mu_2$ induces a non-equilibrium current $I(V)$ through the dot, interfering with and eventually destroying the Kondo effect as the voltage is increased.

In this chapter we develop a *phenomenological* approach, based on an exact method, the Scattering Bethe Ansatz (SBA), recently developed by P. Mehta and N. Andrei[16], a non-perturbative implementation of the Keldysh formalism to construct the current-carrying, *open-system* scattering eigenstates for the two-lead nonequilibrium Anderson impurity model, the standard model to describe the system[17–20, 25, 21, 26, 22–24, 27–31]. The basic idea of SBA is to construct scattering eigenstate of the full Hamiltonian defined directly on the infinite line and match the incoming states by two Fermi seas describing the initial state of the leads. The non-equilibrium steady state transport properties of the system are then expressed as expectation values of the current or dot occupation operators in these eigenstates. This program has been implemented for the Interacting Resonance Level Model (IRLM), a spinless interacting model, described in Ref.[16] where the zero temperature results for current and dot occupation $\langle \hat{n}_d \rangle$ for all bias voltages are shown in chapter 5.

Carrying out the program for the non-equilibrium Anderson model we find difficulties in the direct application of the SBA approach due to the fact that the ground state in the Bethe basis consists of bound pairs of quasi-particles, leading to problems in the computation of the scattering

phase shifts for the quasi-particles with complex momenta. This problem is not present in the IRLM when the Bethe momenta are below the impurity level and no bound states can be formed. We circumvent this difficulty by means of the following argument: The transport property computed in the IRLM is related to the single particle phase shift across the impurity in the Bethe basis. Based on the same idea we develop a phenomenological approach to describe the transport property in the Anderson impurity model. We identify two types of possible phase shifts across impurity, which we refer to as "spin-fluctuation" and "charge-fluctuation" types to label two phenomenological phase shifts akin to the fundamental excitations described in the traditional Bethe Ansatz in this model. The phenomenological Ansatz is checked against exact results on the dot occupation in equilibrium and the Friedel sum rule[40, 41], in the linear response regime. Subsequently, we discuss our results for the out of equilibrium current, conductance and dot occupation. The scaling relations for the conductance, predicted from the Fermi liquid picture of the problem at strong and weak coupling, are also discussed.

We start with the construction of scattering eigenstates of the full Hamiltonian. The (unfolded) 2-lead Anderson impurity Hamiltonian reads,

$$\hat{H} = \sum_{i=1,2} \int dx\, \psi^{\dagger}_{i\sigma}(x)(-i\partial_x)\psi_{i\sigma}(x) + \epsilon_d d^{\dagger}_{\sigma} d_{\sigma} + t_i(\psi^{\dagger}_{i\sigma}(0)d_{\sigma} + d^{\dagger}_{\sigma}\psi_{i\sigma}(0)) + U\, d^{\dagger}_{\uparrow} d_{\uparrow} d^{\dagger}_{\downarrow} d_{\downarrow} \qquad (3.1)$$

where summation over the spin indices σ is implied. The fields $\psi_{i\sigma}(x)$ describe chiral, right-moving electrons from lead i, U is the on-site Coulomb repulsion between electrons on the dot, t_i is the coupling between the dot and the lead i, and ϵ_d is the gate voltage. We have set the Fermi velocity $v_F = 1$.

3.2 The Scattering Bethe Ansatz approach

The model's equilibrium properties have been studied in great detail via the traditional Thermodynamic Bethe Ansatz (TBA)[46, 47]. The SBA exploits in a new way the integrability of the Anderson Model to construct current-carrying scattering eigenstates on the open line. There are two main requirements: One is the construction of scattering eigenstates with the number of electrons in each lead conserved prior to scattering off the impurity. Another is the asymptotic boundary condition: that the wave function of the incoming electrons, i.e. in the region ($x \ll 0$), tend to that of two

free Fermi seas far from the impurity [16]. All information about the external bias applied to the system is encoded in the boundary condition by appropriately choosing the chemical potential of the incoming Fermi seas. As in all Bethe-Ansatz constructions, the full multi-particle wavefunction is constructed from single particle eigenstates (now on the infinite open line) and the appropriate two-particle S-matrices.

3.2.1 Scattering state construction

We first rewrite Eq. (3.1) in the even-odd basis as

$$\begin{aligned}
\hat{H} &= \hat{H}_e + \hat{H}_o \\
\hat{H}_e &= \sum_\sigma \int dx\, \psi^\dagger_{e\sigma}(x)(-i\partial_x)\psi_{e\sigma}(x) + \epsilon_d d^\dagger_\sigma d_\sigma + \; t(\psi^\dagger_{e\sigma}(0)d_\sigma + d^\dagger_\sigma \psi_{e\sigma}(0)) + U d^\dagger_\uparrow d_\uparrow d^\dagger_\downarrow d_\downarrow \\
\hat{H}_o &= \sum_\sigma \int dx\, \psi^\dagger_{o\sigma}(x)(-i\partial_x)\psi_{o\sigma}(x)
\end{aligned}$$

With

$$\begin{aligned}
\psi_{e\sigma}(x) &= \frac{t_1\psi_{1\sigma}(x) + t_2\psi_{2\sigma}(x)}{\sqrt{t_1^2+t_2^2}} \\
\psi_{o\sigma}(x) &= \frac{t_2\psi_{1\sigma}(x) - t_1\psi_{2\sigma}(x)}{\sqrt{t_1^2+t_2^2}}
\end{aligned}$$

and $t = \sqrt{t_1^2+t_2^2}$. In what follows we consider the case $t_1 = t_2 = \frac{t}{\sqrt{2}}$ for simplicity and we shall discuss the $t_1 \neq t_2$ case in the discussion for IRLM. We show from single particle to two particles solution and show the integrability in the following three sections.

single particle solution

The single particle solution for even and odd basis is: $|e, p\sigma\rangle = \int dx\, (e^{ipx} g_p(x)\psi^\dagger_{e\sigma}(x) + e_p\delta(x)d^\dagger_\sigma)|0\rangle$ and $|o, p\sigma\rangle = \int dx\, e^{ipx} h_p(x)\psi^\dagger_{o\sigma}(x)|0\rangle$, with $|0\rangle$ the vacuum state and $g_p(x)$, $h_p(x)$, e_p independent of spin and given by

$$\begin{aligned}
&g_p(x) = \theta(-x) + e^{i\delta_p}\theta(x) + s_{ep}\,\theta(x)\theta(-x)\ , \\
&h_p(x) = \theta(-x) + \theta(x) + s_{op}\,\theta(x)\theta(-x)\ , \\
&e_p = \frac{t(1 + e^{i\delta_p} + s_{ep}/2)}{2(p-\epsilon_d)}\ .
\end{aligned} \tag{3.2}$$

Here $\delta_p \equiv 2\tan^{-1}(\frac{\Gamma}{\epsilon_d - p})$ is the single particle scattering phase shift of the electrons off the impurity with $\Gamma \equiv \frac{t^2}{2}$ being the width of the resonance level. We adopted a symmetric regularization scheme $\theta(\pm x)\delta(x) = \frac{1}{2}\delta(x)$ and imposed $|p| \leq D$, D being the bandwidth cut-off [49]. The $s(x) = \theta(x)\theta(-x)$ term is a local constant ($\partial_x s(x) = 0$) in this scheme and it is included in the odd channel function to allow the same two particle S-matrices, Eq.(3.20), in all channels[50]. The $\theta(x)\theta(-x)$ term in the even channel wave function is introduced in order to modify the single particle phase shift across the impurity. The choice of s_{op} and s_{ep} will be addressed later. In the lead basis, $|i, p\sigma\rangle$, the single-particle scattering eigenstates with the incoming particle incident from lead i, can be restored by taking a proper linear combination of even-odd states. For example, $|1, p\sigma\rangle = \frac{1}{\sqrt{2}}(|e, p\sigma\rangle + |o, p\sigma\rangle)$ is written as

$$|1, p\sigma\rangle = \int dx\, e^{ipx}\Big\{[\theta(-x)+\frac{1}{2}(e^{i\delta_p}+1)\theta(x)]\psi^\dagger_{1\sigma}(x)+\frac{1}{2}(e^{i\delta_p}-1)\theta(x)\psi^\dagger_{2\sigma}(x)+e_p d^\dagger_\sigma \delta(x)+s^\dagger_{1p\sigma}(x)\Big\}|0\rangle \tag{3.3}$$

with $|2, p\sigma\rangle = \frac{1}{\sqrt{2}}(|e, p\sigma\rangle - |o, p\sigma\rangle)$ and $s^\dagger_{ip\sigma}(x)$ related to the $\theta(x)\theta(-x)$ terms. These states have a single incoming particle ($x < 0$) from lead i, that is reflected back into lead i with amplitude, $R_p = (e^{i\delta_p} + 1)/2$ and transmitted to the opposite lead with amplitude $T_p = (e^{i\delta_p} - 1)/2$. Similar single particle states are discussed in Ref. [16].

From two particles solution to multi particles solution

The multi-particle Bethe-Ansatz wave-function is constructed by means of the two-particle S-matrix, $\mathrm{S}(p, k)$, describing the scattering of two electrons with momenta p and k. The two-particles solution in spin singlet state takes the following form

$$|ik, \uparrow; jp, \downarrow\rangle = \int dx_1 dx_2 A\{e^{i(kx_1+px_2)} Z_{kp}(x_1 - x_2)\alpha^\dagger_{ik,\uparrow}(x_1)\alpha^\dagger_{jp,\downarrow}(x_2)\}|0\rangle$$

Here $\int dx e^{ik_i x}\alpha^\dagger_{ik_i,a_i}(x_i) = |ik_i, a_i\rangle$ with a multiplication factor $\tilde{Z}_{kp}(0) \equiv \frac{k+p-2\epsilon_d}{k+p-U-2\epsilon_d} Z_{kp}(0)$ multiplied on the $d^\dagger_\uparrow d^\dagger_\downarrow$ term in two particles eigenstate. The explicit form for this two particles case is written in Eq. (3.58) with the derivation given by the following: For the two particles solution we follow similar construction in P B Wiegmann and A M Tsvelick's work[46] and the Scattering Bethe Ansatz approach developed by P. Mehta and N. Andrei[16]. Since Eq.(3.1) is rotational invariant

the spin quantum number is conserved. We show the solution with both particles with spin singlet incoming from lead 1 as an example in the following. Spin quantum number in z direction S_z is a good quantum number and we can write the two particle solution of $S_z = 0$ state as:

$$|\Psi\rangle = \{\int dx_1 dx_2 \{Ag(x_1,x_2)\psi^\dagger_{e\uparrow}(x_1)\psi^\dagger_{e\downarrow}(x_2) + Ch(x_1,x_2)\psi^\dagger_{o\uparrow}(x_1)\psi^\dagger_{o\downarrow}(x_2) + Bj(x_1,x_2)(\psi^\dagger_{e\uparrow}(x_1)\psi^\dagger_{o\downarrow}(x_2)$$
$$-\psi^\dagger_{e\downarrow}(x_1)\psi^\dagger_{o\uparrow}(x_2))\} + \int dx(Ae(x)(\psi^\dagger_{e\uparrow}(x)d^\dagger_\downarrow - \psi^\dagger_{e\downarrow}(x)d^\dagger_\uparrow) + Bo(x)(\psi^\dagger_{o\uparrow}(x)d^\dagger_\downarrow - \psi^\dagger_{o\downarrow}(x)d^\dagger_\uparrow)) + Amd^\dagger_\uparrow d^\dagger_\downarrow\}|0\rangle$$

Here A, B, C are arbitrary constants to be determined later. To satisfy $\hat{H}|\Psi\rangle = E|\Psi\rangle = (k+p)|\Psi\rangle$ we have:

$$[-i(\partial_{x_1} + \partial_{x_2}) - E]g(x_1,x_2) + t[\delta(x_1)e(x_2) + \delta(x_2)e(x_1)] = 0 \tag{3.4}$$

$$[-i(\partial_{x_1} + \partial_{x_2}) - E]h(x_1,x_2) = 0 \tag{3.5}$$

$$[-i(\partial_{x_1} + \partial_{x_2}) - E]j(x_1,x_2) + t[\delta(x_1)o(x_2)] = 0 \tag{3.6}$$

$$(-i\partial_x - E + \epsilon_d)e(x) + tg(0,x) + t\delta(x)m = 0 \tag{3.7}$$

$$(-i\partial_x - E + \epsilon_d)o(x) + tj(0,x) = 0 \tag{3.8}$$

$$(U + 2\epsilon_d)m + 2te(0) = Em \tag{3.9}$$

For $U = 0$ the model becomes non-interacting and the two particles solution becomes direct product of two one particle solutions.

$$|\Psi\rangle = |\psi_{k\uparrow}\rangle \otimes |\psi_{p\downarrow}\rangle + |\psi_{p\uparrow}\rangle \otimes |\psi_{k\downarrow}\rangle$$
$$= \int dx_1 dx_2 \{(g_k(x_1)\psi^\dagger_{e\uparrow}(x_1) + h_k(x_1)\psi^\dagger_{o\uparrow}(x_1) + e_k d^\dagger_\uparrow \delta(x_1))(g_p(x_2)\psi^\dagger_{e\downarrow}(x_2) + h_p(x_2)\psi^\dagger_{o\downarrow}(x_2) + e_p d^\dagger_\downarrow \delta(x_2))$$
$$+(g_p(x_1)\psi^\dagger_{e\uparrow}(x_1) + h_p(x_1)\psi^\dagger_{o\uparrow}(x_1) + e_p d^\dagger_\uparrow \delta(x_1))(g_k(x_2)\psi^\dagger_{e\downarrow}(x_2) + h_k(x_2)\psi^\dagger_{o\downarrow}(x_2) + e_k d^\dagger_\downarrow \delta(x_2))\}|0\rangle$$

Therefore at $U = 0$ we have:

$$g(x_1, x_2) = g_k(x_1)g_p(x_2) + g_k(x_2)g_p(x_1)$$

$$h(x_1, x_2) = h_k(x_1)h_p(x_2) + h_k(x_2)h_p(x_1)$$

$$j(x_1, x_2) = g_k(x_1)h_p(x_2) + h_k(x_2)g_p(x_1)$$

$$e(x) = e_k g_p(x) + e_p g_k(x)$$

$$o(x) = e_k h_p(x) + e_p h_k(x)$$

$$m = 2e_p e_k$$

Now for $U \neq 0$ we shall derive the solution of this form

$$g(x_1, x_2) = Z_{kp}(x_1 - x_2)g_k(x_1)g_p(x_2) + Z_{kp}(x_2 - x_1)g_k(x_2)g_p(x_1) \tag{3.10}$$

Plug Eq.(3.10) into Eq.(3.4) we get

$$e(x) = Z_{kp}(-x)g_p(x)e_k + Z_{kp}(x)g_k(x)e_p \tag{3.11}$$

Plugging above two results into Eq.(3.7) into Eq.(3.9) we get for $m = 2\tilde{Z}_{kp}(0)e_k e_p$ we have:

$$(-i\partial_x Z_{kp}(-x))g_p(x)e_k + (-i\partial_x Z_{kp}(x))g_k(x)e_p - tZ_{kp}(-x)e_p\delta(x)e_k$$

$$-tZ_{kp}(x)e_k\delta(x)e_p + 2tZ^*_{kp}(0)e_k e_p = 0 \tag{3.12}$$

$$2\tilde{Z}_{kp}(0)e_k e_p = \frac{2t(Z_{kp}(0)g_p(0)e_k + Z_{kp}(0)g_k(0)e_p)}{p + k - U - 2\epsilon_d} \tag{3.13}$$

Now take $Z_{kp}(x) = e^{-i\phi_{kp}}\theta(-x) + e^{i\phi_{kp}}\theta(x)$ we get $\tan(\phi_{kp}) = \frac{-Ut^2}{(k-p)(p+k-U-2\epsilon_d)}$ and $\tilde{Z}_{kp}(0) = \frac{k+p-2\epsilon_d}{k+p-U-2\epsilon_d}Z_{kp}(0)$. Define $\Gamma \equiv \frac{t^2}{2}$ and $B(k) \equiv k(k - 2\epsilon_d - U)$ as in Ref. [47] we can rewrite $\tan(\phi_{kp}) = \frac{-2U\Gamma}{(B(k)-B(p))}$.

From Eq.(3.5) we can write $h(x_1, x_2)$ as:

$$h(x_1, x_2) = Z^{oo}_{kp}(x_1 - x_2)h_k(x_1)h_p(x_2) + Z^{oo}_{kp}(x_2 - x_1)h_k(x_2)h_p(x_1)$$

with arbitrary $Z^{oo}_{kp}(x_1 - x_2)$. Now write $j(x_1, x_2)$ as:

$$j(x_1, x_2) = Z^{eo}_{kp}(x_1 - x_2)g_k(x_1)h_p(x_2) + Z^{eo}_{kp}(x_2 - x_1)h_k(x_2)g_p(x_1)$$

again with $Z^{eo}_{kp}(x_1 - x_2)$ undetermined. Plug Eq.(3.14) into Eq.(3.6) we get $o(x)$ is written as:

$$o(x) = Z^{eo}_{kp}(-x)h_p(x)e_k + Z^{eo}_{kp}(x)h_k(x)e_p \tag{3.14}$$

Now if we choose $Z^{eo}_{kp}(x_1 - x_2) = Z_{kp}(x_1 - x_2)$ and plug Eq.(3.14) and Eq.(3.14) into Eq.(3.8) we get:

$$\begin{aligned}&(-k + \epsilon_d)Z_{kp}(-x)h_p(x)e_k + (-p + \epsilon_d)Z_{kp}(x)h_k(x)e_p + t(Z_{kp}(-x)h_p(x)g_k(0) + Z_{kp}(x)h_k(x)g_p(0))\\ &+(-i)(\partial_x Z_{kp}(-x))h_p(x)e_k + (-i)(\partial_x Z_{kp}(x))h_k(x)e_p = -2\sin(\phi_{kp})(h_p(0)e_k - h_k(0)e_p) = 0\end{aligned} \tag{3.15}$$

To satisfy Eq.(3.15) we can set $h_p(0) = 0$ for arbitrary p. This can be done by choosing $s_{op} = -4$ in Eq.(4.2). Now since $Z^{oo}_{kp}(x_1 - x_2)$ is arbitrary we can choose $Z^{oo}_{kp}(x_1 - x_2) = Z_{kp}(x_1 - x_2)$. Also from Eq.(3.13) we have

$$\tilde{Z}_{kp}(0) = \frac{p + k - 2\epsilon_d}{p + k - U - 2\epsilon_d} Z_{kp}(0) \tag{3.16}$$

Since the Hamiltonian in Eq.(3.1) has rotational invariance the general form of scattering matrix for particles with momentum k, p and spins σ_1, σ_2 is given by:

$$S^{\sigma_1' \sigma_2'}_{\sigma_1 \sigma_2}(k, p) = b(k, p) + c(k, p)\hat{P}_{12} \tag{3.17}$$

where $\hat{P}_{12} = \frac{1}{2}(1 \cdot 1 + \vec{\sigma_1} \cdot \vec{\sigma_2})$ is the permutation operator in spins. For antiparallel spins (singlet state) as shown above $\hat{P}_{12} = -1$ thus we have:

$$b(k, p) - c(k, p) = \frac{Z_{kp}(x > 0)}{Z_{kp}(x < 0)} = \frac{B(k) - B(p) - i2U\Gamma}{B(k) - B(p) + i2U\Gamma} \tag{3.18}$$

For the triplet state ($\hat{P}_{12} = 1$) the interaction term with the impurity is absent and the particles

passing through each other without changing their phase

$$b(k,p) + c(k,p) = 1 \tag{3.19}$$

Thus from Eq.(3.18) and Eq.(3.19) we get the two particle S-matrix as:

$$\hat{S}(k,p) = \frac{(B(k) - B(p))\mathrm{I}_{\tau,\tau'} + i2U\Gamma\mathrm{P}_{\tau,\tau'}}{B(k) - B(p) + i2U\Gamma} \tag{3.20}$$

In general we denote the $\hat{S}(k_i,k_j)$ as $\mathrm{S}^{a_i a_i^{'}}_{a_j a_j^{'}}(k_i,k_j)$ with a_i denotes the spin index before the scattering and $a_i^{'}$ the spin index after the scattering. These matrices satisfy the Yang-Baxter equations

$$\begin{aligned}
&\mathrm{S}^{a_1 a_1^{'}}_{a_2 a_2^{'}}(k_1,k_2)\mathrm{S}^{a_1 a_1^{'}}_{a_3 a_3^{'}}(k_1,k_3)\mathrm{S}^{a_2 a_2^{'}}_{a_3 a_3^{'}}(k_2,k_3) \\
&= \mathrm{S}^{a_2 a_2^{'}}_{a_3 a_3^{'}}(k_2,k_3)\mathrm{S}^{a_1 a_1^{'}}_{a_3 a_3^{'}}(k_1,k_3)\mathrm{S}^{a_1 a_1^{'}}_{a_2 a_2^{'}}(k_1,k_2)
\end{aligned}$$

Thus the integrability of two leads with Anderson type dot system is similar to the integrability of one lead Anderson model.

The choice of identical two particles S-matrices (by choosing $s_{op} = -4$; the choice of s_{ep} will be discussed later and does not affect the result here) enables us to construct the scattering state labeled by lead indices by choosing appropriate A, B, C in this even-odd basis. For example, if both particles are coming from lead 1, we shall choose $(A,B,C) = A_0(\frac{t_2^2}{t_2^2}, \frac{-t^2}{t_1 t_2}, \frac{t_2^2}{t_1^2})$ such that the amplitude of incoming state from lead 2 is zero (A_0 being an overall renormalization constant). We can therefore label the eigenstate by the incoming state from lead i and/or lead j. Without this s_{op} term we cannot write back from even-odd basis to lead indices basis in this two leads Anderson model and similarly in IRLM in Ref. [16].

Since the S-matrix is the same for all even-odd combinations the S-matrix does not depend on the lead index i, and the number of electrons in a lead, N_i, can change only at the impurity site. This circumstance allows us to construct the fully-interacting eigenstates of our Hamiltonian characterized by the incoming quantum numbers, N_1 and N_2 the numbers of incident electrons from lead 1 and 2 respectively. These quantum numbers are subsequently determined by the chemical potentials μ_1 and μ_2. This leads us to the topic of fixing these momenta distribution by imposing the asymptotic boundary condition in the next section.

3.2.2 Choosing the momenta distribution by the asymptotic boundary conditions

To complete the construction of the SBA current-carrying, scattering eigenstate, $|\Psi, \mu_i\rangle$, we must still choose the "Bethe-Ansatz momenta" $\{p_l\}_{l=1}^{N_1+N_2}$ of the single particles states to ensure that the incoming particles look like two Fermi seas in the region $x < 0$. This requirement translates into a set of "free-field" SBA equations for the Bethe-Ansatz momenta-density of the particles from the two leads [16]. The argument is as follows: Away from the impurity $|i, p\sigma\rangle$ reduces to $\psi^\dagger_{i\sigma}(x)$ with the inter-particle S-matrix Eq. (3.20) present. Thus the scattering eigenstates describing non-interacting electrons are in the Bethe basis rather than in the Fock basis of plane waves.

The existence of many bases for the free electron is due to their linear spectrum which leads to degeneracy of the energy eigenvalues. The wave function

$$e^{ip_1x_1+ip_2x_2}[\theta(x_1-x_2) + \mathrm{S}\theta(x_2-x_1)]A$$

is an eigenstate of the *free* Hamiltonian for any choice of S with, in particular, S = 1 defining the Fock basis and S given in Eq. (3.20) defining the Bethe basis. The Bethe basis is the correct "zero order" choice of a basis in the degenerate energy space required in order to turn on the interactions. We proceed to describe the leads (two free Fermi seas) in this basis.

We consider the system at zero temperature and zero magnetic field in this paper. To describe the two Fermi seas on the leads translates to a set of Bethe Ansatz equations whose solution in this case consists of complex conjugate pairs: $p^{\pm}(\lambda) = x(\lambda) \mp iy(\lambda)$ in the λ-parametrization [47, 46, 48] with

$$x(\lambda) = \epsilon_d + \frac{U}{2} - \Big(\frac{\lambda + (\epsilon_d + \frac{U}{2})^2 + ((\lambda + (\epsilon_d + \frac{U}{2})^2)^2 + U^2\Gamma^2)^{1/2}}{2}\Big)^{1/2} \tag{3.21}$$

$$y(\lambda) = \Big(\frac{-(\lambda + (\epsilon_d + \frac{U}{2})^2) + ((\lambda + (\epsilon_d + \frac{U}{2})^2)^2 + U^2\Gamma^2)^{1/2}}{2}\Big)^{1/2}. \tag{3.22}$$

We may simplify this expression by defining $\tilde{\epsilon}_d = \epsilon_d + U/2$ to get

$$\begin{aligned} x(\lambda) &= \tilde{\epsilon}_d - \sqrt{\frac{\lambda + \tilde{\epsilon}_d^2 + \sqrt{(\lambda + \tilde{\epsilon}_d^2)^2 + U^2\Gamma^2}}{2}} \\ y(\lambda) &= \sqrt{\frac{-(\lambda + \tilde{\epsilon}_d^2) + \sqrt{(\lambda + \tilde{\epsilon}_d^2)^2 + U^2\Gamma^2}}{2}}. \end{aligned}$$

Each member of a pair can be either in lead 1 or in lead 2, since the S-matrix is unity in the lead space. There are, therefore, two possible configurations for these bounded pairs. One possible way of forming bounded pairs is described by four types of complex solutions whose densities we denote $\sigma_{ij}(\lambda)$ with $\{ij\} = \{11, 12, 21, 22\}$ indicating the incoming electrons from lead i and lead j. The other possibility, which is perhaps more intuitive in comparing with the free electron in the Fock basis, is to include only $\{ij\} = \{11, 22\}$. These two types of states give the same results when evaluating the expectation value of the dot occupation in equilibrium. However when we turn on the bias voltage, the results obtained from a 4-bound states description show some charge fluctuations even way below the impurity level which is not expected from the non-interacting ($U \to 0$) theory (shown in Appendix A). Thus we shall focus on the 2-bound states description in the following discussion.

Derivation for momenta distribution for 2-bound states

The momenta distribution can be derived from imposing boundary condition in the free leads (incoming state) region and the value of momenta is connected with spin rapidity λ by using the quantum inverse scattering method. The Bethe Ansatz equation solved with periodic condition at lead region with total number of particles N ($N = N_1 + N_2$ as sum of particle number from lead 1 and 2) and the total spin projection S ($S = S_1 + S_2 = N/2 - M$ with $M = M_1 + M_2$ as number of down spin particles) is given by

$$e^{ik_j^l L} = \prod_{\alpha=1}^{M} \frac{B(k_j^l) - \lambda_\alpha + iU\Gamma}{B(k_j^l) - \lambda_\alpha - iU\Gamma} \tag{3.23}$$

$$\prod_{l=R,L} \prod_{j=1}^{N_l} \frac{B(k_j^l) - \lambda_\alpha - iU\Gamma}{B(k_j^l) - \lambda_\alpha + iU\Gamma} = \prod_{\beta \neq \alpha}^{M} \frac{\lambda_\alpha - \lambda_\beta + i2U\Gamma}{\lambda_\alpha - \lambda_\beta - i2U\Gamma} \tag{3.24}$$

with total energy $E = E_1 + E_2$ and $E_l = \sum_j k_j^l$ indicating the energy of the electrons within the lead l at zero temperature.

The spectrum of Eq.(3.23,3.24) for one lead case has been analyzed by N. Kawakami and A. Okiji [47] where they found that the ground state at zero temperature is composed of real λ_i and complex k_j^l in the thermodynamic limit for $U > 0$. The same situation also occurs in the special limit where $U \to \infty$ where P. Schlottmann [65] has done also in the one lead case. The proof for two leads ground state is similar to the one lead case and is shown explicitly for the finite temperature

calculation for the infinite U case in Chapter 6.

As has been mentioned above in the ground state all λ_i are real (and distinct) and k_j^l form bound state for $j = 1, .., 2M$ with bound state momenta given by the poles or zeros in the S-matrix defined in Eq.(3.20)

$$B(k_j^{l\pm}) = \lambda_j \pm iU\Gamma = B(k^{l\pm}(\lambda_j)) = B(x(\lambda_j) \pm iy(\lambda_j)) + \gamma^{\pm}(\lambda_j) \tag{3.25}$$

where $\gamma^{\pm} = O(exp(-L))$ and from Eq.(3.25) we have

$$x(\lambda) = \epsilon_d + \frac{U}{2} - (\frac{\lambda + (\epsilon_d + \frac{U}{2})^2 + ((\lambda + (\epsilon_d + \frac{U}{2})^2)^2 + U^2\Gamma^2)^{1/2}}{2})^{1/2}$$
$$y(\lambda) = (\frac{-(\lambda + (\epsilon_d + \frac{U}{2})^2) + ((\lambda + (\epsilon_d + \frac{U}{2})^2)^2 + U^2\Gamma^2)^{1/2}}{2})^{1/2}$$

Note that the bound state can be formed from four possible configurations for $B_2 < \lambda_\alpha < \infty$ which we denote bound state from lead i and lead j quasi momenta denoted as λ_α^{ij}. The bound state between $B_1 < \lambda_\alpha < B_2$ can only be formed by quasi momenta both coming from lead 1. Below we surpass the index of lead in λ and put back the index dependence in the end for simplification. Inserting Eq.(3.25) into Eq.(3.23,3.24) we get

$$e^{ik_\alpha^+ L} = \prod_{\beta=1}^{M} \frac{\lambda_\alpha - \lambda_\beta + i2U\Gamma}{\lambda_\alpha - \lambda_\beta + \gamma_\alpha^+} \tag{3.26}$$

$$e^{ik_\alpha^- L} = \prod_{\beta=1}^{M} \frac{\lambda_\alpha - \lambda_\beta + \gamma_\alpha^-}{\lambda_\alpha - \lambda_\beta - i2U\Gamma} \tag{3.27}$$

$$\prod_{\beta=1}^{M} \frac{\lambda_\beta - \lambda_\alpha + \gamma_\beta^+}{\lambda_\beta - \lambda_\alpha + \gamma_\beta^-} = 1 \tag{3.28}$$

Thus for $L \to \infty$ from multiplication of Eq.(3.26) and Eq.(3.27) we have

$$e^{2ix(\lambda_\alpha)L} = \prod_{\beta} \frac{\lambda_\alpha - \lambda_\beta + i2U\Gamma}{\lambda_\alpha - \lambda_\beta - i2U\Gamma} \tag{3.29}$$

Taking the logarithm of Eq.(3.29) we have:

$$2\pi J_\alpha = -2x(\lambda_\alpha)L - \sum_{\beta} (2\theta_2(\frac{\lambda_\alpha - \lambda_\beta}{2U\Gamma}) + \pi) \tag{3.30}$$

with $\theta_n(x) \equiv \tan^{-1}(2x/n)$ and J_α some integers. We can extend the definition of J_α to include integers or half integers and rewrite Eq.(3.30) as

$$\frac{\pi}{L}J_\alpha = -x(\lambda_\alpha) - \frac{1}{L}\sum_\beta \theta_2(\frac{\lambda_\alpha - \lambda_\beta}{2U\Gamma}) \tag{3.31}$$

Now let us put back the dependence in lead indices. Note that there is one one correspondence between λ_α and J_α from Eq.(3.31) and by the method of quantum inverse scattering we have the constraint of all λ_α being different. Thus λ_α^{ij} is uniquely determined by one J_α. For notational simplification we relabel $\{ij\} = \{11, 22\}$ as $\{l\} = \{1, 2\}$. Now define $\sum_{ij}\sigma(\lambda_\alpha^{ij}) = \frac{1}{L}\frac{dJ_\alpha}{d\lambda_\alpha} \equiv \sum_l \sigma^{(l)}(\lambda_\alpha)$ and using $\partial_x\theta_n(x) = \frac{2/n}{1+(2x/n)^2}$ we can write Eq.(3.31) in continuous form (by taking $L \to \infty$ and differentiate Eq.(3.31) with respect to λ) as the following two regions. For $B_2 < \lambda < \infty$ we have all particle state labeled by different l as

$$\begin{aligned}\sum_{l=1}^{2}\sigma^{(l)}(\lambda) &= \frac{-1}{\pi}\frac{dx(\lambda)}{d\lambda} - \frac{1}{\pi}\int_{B_2}^{\infty} d\lambda'\sigma^{(2)}(\lambda')\frac{2U\Gamma}{(2U\Gamma)^2 + (\lambda-\lambda')^2} \\ &- \frac{1}{\pi}\int_{B_1}^{\infty} d\lambda'\sigma^{(1)}(\lambda')\frac{2U\Gamma}{(2U\Gamma)^2 + (\lambda-\lambda')^2}\end{aligned} \tag{3.32}$$

For $B_1 < \lambda < B_2$ we can introduce hole state for distribution of $\sigma^{(2)}(\lambda)$. Denote hole state as $\tilde{\sigma}^{(l)}(\lambda)$ we get

$$\begin{aligned}\sigma^{(1)}(\lambda) + \tilde{\sigma}^{(l)}(\lambda) &= \frac{-1}{\pi}\frac{dx(\lambda)}{d\lambda} - \frac{1}{\pi}\int_{B_2}^{\infty} d\lambda'\sigma^{(2)}(\lambda')\frac{2U\Gamma}{(2U\Gamma)^2 + (\lambda-\lambda')^2} \\ &- \frac{1}{\pi}\int_{B_1}^{\infty} d\lambda'\sigma^{(1)}(\lambda')\frac{2U\Gamma}{(2U\Gamma)^2 + (\lambda-\lambda')^2}\end{aligned} \tag{3.33}$$

Since $\tilde{\sigma}^{(l)}(\lambda)$ obeys the same equation as $\sigma^{(1)}(\lambda)$ as seen from Eq.(3.33) and structure of Eq.(3.33) is the same as Eq.(3.32) (apart from different region in λ) we may combine Eq.(3.32) and Eq.(3.33) together to get

$$\begin{aligned}2\sigma(\lambda) &= \frac{-1}{\pi}\frac{dx(\lambda)}{d\lambda} - \frac{1}{\pi}\int_{B_2}^{\infty} d\lambda' 2\sigma(\lambda')\frac{2U\Gamma}{(2U\Gamma)^2 + (\lambda-\lambda')^2} \\ &- \frac{1}{\pi}\int_{B_1}^{B_2} d\lambda'\sigma(\lambda')\frac{2U\Gamma}{(2U\Gamma)^2 + (\lambda-\lambda')^2}\end{aligned} \tag{3.34}$$

with $B_1 < \lambda < \infty$. From Eq.(3.26) we get $\frac{dx(\lambda)}{d\lambda}$ as

$$\frac{dx(\lambda)}{d\lambda} = -\left(\frac{1 + \frac{(\lambda+\frac{1}{4}(U+2\epsilon_d)^2)}{\sqrt{U^2\Gamma^2+(\frac{1}{4}(U+2\epsilon_d)^2+\lambda)^2}}}{2\sqrt{2}\sqrt{\frac{1}{4}(U+2\epsilon_d)^2+\lambda+\sqrt{U^2\Gamma^2+(\frac{1}{4}(U+2\epsilon_d)^2+\lambda)^2}}}\right) \tag{3.35}$$

Thus to describe in the Bethe basis the two leads as two Fermi seas filled up to μ_1 and μ_2, respectively, these densities must satisfy the SBA equations,

$$2\sigma_i(\lambda) = -\frac{1}{\pi}\frac{\mathrm{d}x(\lambda)}{\mathrm{d}\lambda}\theta(\lambda - B_i) - \sum_{j=1,2}\int_{B_j}^{\infty}\mathrm{d}\lambda'\ K(\lambda-\lambda')\sigma_j(\lambda') \tag{3.36}$$

with

$$K(\lambda) = \frac{1}{\pi}\frac{2U\Gamma}{(2U\Gamma)^2+\lambda^2}$$

.

Each density is defined on a domain extending from B_i to the cutoff D - to be sent to infinity. The B_i play the role of chemical potentials for the Bethe-Ansatz momenta and are determined from the physical chemical potentials of the two leads, μ_i, by minimizing the *charge free energy*,

$$F = \sum_i (E_i - \mu_i N_i) = 2\sum_i \int_{B_i}^{\infty}\mathrm{d}\lambda\,(x(\lambda)-\mu_i)\sigma_i(\lambda) \tag{3.37}$$

with σ_1 the lead 1 particle density and σ_2 the lead 2 particle density. Note that σ_1 and σ_2 obeys the same integral equation Eq. (3.36) with different boundary ($\sigma_1(\lambda)$ with $\lambda \subset (B_1, \infty)$ and $\sigma_2(\lambda)$ with $\lambda \subset (B_2, \infty)$). The connection between μ_i and B_i are shown explicitly in the following discussion.

Minimization of charge free energy

The free energy of the system at zero temperature is given by

$$F = F_1 + F_2 = \int_{B_1}^{\infty} 2(x(\lambda)-\mu_1)\sigma^{(1)}(\lambda)d\lambda + \int_{B_2}^{\infty} 2(x(\lambda)-\mu_2)\sigma^{(2)}(\lambda)d\lambda \tag{3.38}$$

where μ_1 and μ_2 are chemical potential of the system. The condition of minimization is given by $\frac{\partial F}{\partial B_1} = 0$ and $\frac{\partial F}{\partial B_2} = 0$. From Eq.(3.38) we get

$$\frac{\partial F}{\partial B_1} = 0 = -(x(B_1) - \mu_1)2\sigma^{(1)}(B_1) + \int_{B_1}^{\infty}(x(\lambda) - \mu_1)\frac{\partial 2\sigma^{(1)}}{\partial B_1} + \int_{B_2}^{\infty}(x(\lambda) - \mu_2)\frac{\partial 2\sigma^{(2)}}{\partial B_1}$$
$$\frac{\partial F}{\partial B_2} = 0 = -(x(B_2) - \mu_2)2\sigma^{(2)}(B_2) + \int_{B_1}^{\infty}(x(\lambda) - \mu_1)\frac{\partial 2\sigma^{(1)}}{\partial B_2} + \int_{B_2}^{\infty}(x(\lambda) - \mu_2)\frac{\partial 2\sigma^{(2)}}{\partial B_2}$$

Now we simplify the notation by noticing that both $\sigma^{(1)}(\lambda)$ and $\sigma^{(2)}(\lambda)$ obeys Eq.(3.34) so we have $\frac{\partial\sigma^{(1)}(\lambda)}{\partial B_i} = \frac{\partial\sigma^{(2)}(\lambda)}{\partial B_i} = \frac{\partial\sigma(\lambda)}{\partial B_i}$ and also by definition $\sigma^{(1)}(B_1) = \sigma(B_1)$, $\sigma^{(2)}(B_2) = \sigma(B_2)$. Thus above equations are simplified as:

$$\begin{aligned} 0 &= -(x(B_1) - \mu_1)2\sigma(B_1) + \int_{B_2}^{\infty}(2x(\lambda) - \mu_1 - \mu_2)\frac{\partial 2\sigma}{\partial B_1} + \int_{B_1}^{B_2}(x(\lambda) - \mu_1)\frac{\partial 2\sigma}{\partial B_1} \\ 0 &= -(x(B_2) - \mu_2)2\sigma(B_2) + \int_{B_2}^{\infty}(2x(\lambda) - \mu_1 - \mu_2)\frac{\partial 2\sigma}{\partial B_2} + \int_{B_1}^{B_2}(x(\lambda) - \mu_1)\frac{\partial 2\sigma}{\partial B_2} \end{aligned} \tag{3.39}$$

From Eq.(3.34) we have $\frac{\partial\sigma}{\partial B_i}$ as:

$$\begin{aligned} \frac{\partial 2\sigma(\lambda)}{\partial B_1} &= -\frac{1}{\pi}\int_{B_2}^{\infty}\frac{\partial 2\sigma}{\partial B_1}\frac{2U\Gamma}{(2U\Gamma)^2 + (\lambda - \lambda')^2}d\lambda' - \frac{1}{\pi}\int_{B_1}^{B_2}\frac{\partial\sigma}{\partial B_1}\frac{2U\Gamma}{(2U\Gamma)^2 + (\lambda - \lambda')^2} \\ &+ \frac{1}{\pi}\sigma(B_1)\frac{2U\Gamma}{(2U\Gamma)^2 + (\lambda - B_1)^2} \\ \frac{\partial 2\sigma(\lambda)}{\partial B_2} &= -\frac{1}{\pi}\int_{B_2}^{\infty}\frac{\partial 2\sigma}{\partial B_2}\frac{2U\Gamma}{(2U\Gamma)^2 + (\lambda - \lambda')^2}d\lambda' - \frac{1}{\pi}\int_{B_1}^{B_2}\frac{\partial\sigma}{\partial B_2}\frac{2U\Gamma}{(2U\Gamma)^2 + (\lambda - \lambda')^2} \\ &+ \frac{1}{\pi}\sigma(B_2)\frac{2U\Gamma}{(2U\Gamma)^2 + (\lambda - B_2)^2} \end{aligned} \tag{3.40}$$

These formulas can be simplified by dividing the first line in both Eq.(3.39) and Eq.(3.40) by $2\sigma(B_1)$ and those of second line by $2\sigma(B_2)$. Define $f(\lambda, B_i) \equiv \frac{\partial 2\sigma(\lambda)}{\partial B_i}\frac{1}{2\sigma(B_i)}$ and follow Eq.(3.39) and Eq.(3.40) we have

$$\begin{aligned} (x(B_1) - \mu_1) &= \int_{B_1}^{\infty}(x(\lambda) - \mu_1)f(\lambda, B_1) + \int_{B_2}^{\infty}(x(\lambda) - \mu_2)f(\lambda, B_1) \\ (x(B_2) - \mu_2) &= \int_{B_1}^{\infty}(x(\lambda) - \mu_1)f(\lambda, B_2) + \int_{B_2}^{\infty}(x(\lambda) - \mu_2)f(\lambda, B_2) \end{aligned} \tag{3.41}$$

with $f(\lambda, B_i)$ given by:

$$\begin{aligned} f(\lambda, B_i) &= -\frac{1}{2\pi}\int_{B_1}^{\infty} f(\lambda', B_i)\frac{2U\Gamma}{(2U\Gamma)^2+(\lambda-\lambda')^2} - \frac{1}{2\pi}\int_{B_2}^{\infty} f(\lambda', B_i)\frac{2U\Gamma}{(2U\Gamma)^2+(\lambda-\lambda')^2} \\ &+ \frac{1}{2\pi}\frac{2U\Gamma}{(2U\Gamma)^2+(\lambda-B_i)^2} \end{aligned} \tag{3.42}$$

It is unclear how to solve these coupled integral equations exactly. The practical way to solve these equations is to use numerical methods to solve Eq.(3.42) and plugging back the results to Eq.(3.41) to find the corresponding (μ_1, μ_2) from arbitrary choice of (B_1, B_2). Now let us define the following parameters and write chemical potential μ_1 and μ_2 explicitly:

$$\begin{aligned} A &\equiv \int_{B_1}^{\infty} f(\lambda, B_1) \\ B &\equiv \int_{B_2}^{\infty} f(\lambda, B_1) \\ G &\equiv \int_{B_1}^{\infty} x(\lambda) f(\lambda, B_1) + \int_{B_2}^{\infty} x(\lambda) f(\lambda, B_1) \\ C &\equiv \int_{B_1}^{\infty} f(\lambda, B_2) \\ D &\equiv \int_{B_2}^{\infty} f(\lambda, B_2) \\ F &\equiv \int_{B_1}^{\infty} x(\lambda) f(\lambda, B_2) + \int_{B_2}^{\infty} x(\lambda) f(\lambda, B_2) \end{aligned} \tag{3.43}$$

Using these definitions and solve Eq.(3.41) we have:

$$\begin{aligned} \mu_1 &= \frac{(F - x(B_2))B + (x(B_1) - G)(D-1)}{(D-1)(1-A) + BC} \\ \mu_2 &= \frac{(x(B_1) - G)(-C) + (x(B_2) - F)(A-1)}{(D-1)(1-A) + BC} \\ \Rightarrow V &= \mu_1 - \mu_2 = \frac{(A+B-1)(F - x(B_2)) + (C+D-1)(x(B_1) - G)}{(D-1)(1-A) + BC} \end{aligned} \tag{3.44}$$

For the numerical analysis of nonequilibrium situation we may keep dot level ϵ_d fixed at certain value and change μ_1 and μ_2. Here we choose μ_1 to be fixed with some (B_1, B_2) and then find the corresponding μ_2 for the sake of simplicity in numerical process. In this way we may plot the $I - V$ curves and find the nonequilibrium differential conductance.

Now let us consider the special case of equilibrium and quasi-equilibrium. In equilibrium we have $B_1 = B_2$ which leads to the solution of $\mu_1 = \mu_2$ from Eq.(3.38) to Eq.(3.40). The equations

decoupled when $B_1 = B_2 \equiv B$ and we may define the dressed energy $\epsilon(\lambda)$ for the single quasi-particle excitation as:

$$\epsilon(\lambda) = (x(\lambda) - \mu) - \frac{1}{\pi}\int_B^\infty \frac{2U\Gamma}{(2U\Gamma)^2 + (\lambda - \lambda')^2}\epsilon(\lambda') \tag{3.45}$$

This definition can be obtained by iteration of Eq.(3.40) on Eq.(3.39) in $B_1 = B_2 = B$ case with a factor of two in the driving term removed as we are discussing a single quasi-particle rather than a bounded pair of quasi-particles. In the case of quasi-equilibrium we can take $B_1 \simeq B_2$ and from Eq.(3.45) we have the voltage difference as (by taking the difference of Eq(3.45) nearby $B_1 = B_2 = B$ and take $\delta_B \to 0$):

$$eV_{12} = \mu_1 - \mu_2 = 2\epsilon'(B)\delta_B \simeq \delta_B(-2x'(B) - \frac{1}{\pi}\int_B^\infty \frac{2U\Gamma}{(2U\Gamma)^2 + (\lambda - \lambda')^2}2\epsilon'(\lambda')) \tag{3.46}$$

Notice that in the Fock space we may define voltage difference as the energy difference due to different number of particles:

$$V = \frac{2\pi}{e}(\frac{N_1 - N_2}{L}) = \frac{4\pi}{e}\int_{B_1}^{B_2}\sigma(\lambda)d\lambda \tag{3.47}$$

Nearby equilibrium we can take $B_1 \simeq B_2$ or $B_2 = B_1 + \delta_B$ with $\delta_B \to 0$. Comparing Eq.(3.46) with Eq.(3.34) we have $2\epsilon'(B) = 4\pi\sigma(B)$ or the voltage difference $V_{12} \simeq 4\pi\sigma(B)\delta_B$ as given in Eq.(3.47). To find this quasi-equilibrium boundary B we have to solve Eq.(3.45) with $\epsilon(B) = 0$. The equation is written as

$$\begin{aligned}
\epsilon(B) &= (x(B) - 0) - \frac{1}{\pi}\int_B^\infty \frac{2U\Gamma}{(2U\Gamma)^2 + (B - \lambda')^2}\epsilon(\lambda') = 0 \\
&= (\epsilon_d + \frac{U}{2} - (\frac{B + (\epsilon_d + \frac{U}{2})^2 + ((B + (\epsilon_d + \frac{U}{2})^2 + U^2\Gamma^2)^{1/2}}{2})^{1/2}) \\
&- \frac{1}{\pi}\int_B^\infty \frac{2U\Gamma}{(2U\Gamma)^2 + (B - \lambda')^2}\epsilon(\lambda')
\end{aligned} \tag{3.48}$$

Determination of equilibrium Bethe boundary B for $\mu = 0$

There are two ways to solve Eq.(3.48). One way is to use Weiner Hopf method to obtain exact result. The second approach is to use numerical approach suggested by G. Palacios[68]. First let us discuss the computation by using Weiner Hopf method.

Define $\epsilon^{\pm}(\lambda) \equiv \epsilon(\lambda)\theta(\pm\lambda \mp B)$ and $h(\lambda - \lambda') \equiv -\frac{1}{\pi}\frac{2U\Gamma}{(2U\Gamma)^2+(\lambda-\lambda')^2}$. Using the convention of Fourier transform as

$$f(\omega) = \int_{-\infty}^{\infty} f(t)e^{i\omega t}dt$$

Thus we have the Fourier transform of $h(\lambda-\lambda')$ as $h(\omega) = -e^{2U\Gamma|\omega|}$. Now write $\epsilon^{\pm}(\lambda) = \epsilon(\lambda)\theta(\pm\lambda\mp B)$ then we can rewrite Eq.(3.68) in Fourier transformed form as

$$\epsilon^{+}(\omega) + \epsilon^{-}(\omega) = 2x(\omega) + h(\omega)\epsilon^{+}(\omega)$$

Next we connect the integration kernel term with lower and upper plane by rewriting $(1 - h(\omega)) \equiv \frac{1}{G^{+}(\omega)G^{-}(\omega)}$. The functions $G^{\pm}(\omega)$ are [46]:

$$G^{-}(\omega) = G^{+}(-\omega) = \sqrt{2\pi}(\frac{i2U\Gamma\omega + 0}{2\pi e})^{\frac{i\omega 2U\Gamma}{2\pi}}/\Gamma(\frac{1}{2} + \frac{i\omega 2U\Gamma}{2\pi}) \tag{3.49}$$

Thus we have $\epsilon^{+}(\omega)$ as

$$\begin{aligned} &\epsilon^{+}(\omega) = G^{+}(\omega)\frac{e^{i\omega B}}{2\pi i}\int d\omega' \frac{1}{\omega' - \omega - i\delta} 2x(\omega')G^{-}(\omega')e^{-i\omega' B} \\ &\rightarrow \epsilon^{+}(\lambda) = \frac{1}{2\pi}\int_{-\infty}^{\infty} e^{-i\omega\lambda}\epsilon^{+}(\omega)d\omega \end{aligned} \tag{3.50}$$

First let us compute $x(\omega) = \int_{-\infty}^{\infty} x(\lambda)e^{i\omega\lambda}d\lambda$:

$$x(\omega) = 2\pi\delta(\omega)(\epsilon_d + \frac{U}{2}) + e^{-i\omega(\epsilon_d+\frac{U}{2})^2}\sqrt{2\pi}\frac{(|\omega| - i\omega)(\cosh(U\Gamma\omega) - \sinh(U\Gamma\omega))}{4|\omega|^{5/2}}$$

Plugging this back to Eq.(3.50) we have

$$\begin{aligned} \epsilon^{+}(\lambda) &= 2(\epsilon_d + \frac{U}{2}) + 5\sqrt{\frac{2U\Gamma}{\pi}}(-1)^{1/4}(-i\zeta(-\frac{1}{2}, \frac{3}{4} + i\frac{\lambda + (\epsilon_d + \frac{U}{2})^2}{4U\Gamma}) + \zeta(-\frac{1}{2}, \frac{3}{4} - i\frac{\lambda + (\epsilon_d + \frac{U}{2})^2}{4U\Gamma}) \\ &- \zeta(-\frac{1}{2}, \frac{1}{4} + i\frac{\lambda + (\epsilon_d + \frac{U}{2})^2}{4U\Gamma}) + i\zeta(-\frac{1}{2}, -\frac{1}{4} - i\frac{\lambda + (\epsilon_d + \frac{U}{2})^2}{4U\Gamma}) \end{aligned} \tag{3.51}$$

with $\zeta(s, a)$ defined as the generalized Riemann zeta function.

The following trick in numerical computation can also solve this equilibrium boundary B. Let

us define a new parameter $\bar{\lambda} \equiv \lambda + (\epsilon_d + \frac{U}{2})^2$ then we can rewrite Eq.(3.48) as

$$\epsilon(\bar{\lambda}) = (\epsilon_d + \frac{U}{2} - \sqrt{\frac{\bar{\lambda} + \sqrt{\bar{\lambda}^2 + (U\Gamma)^2}}{2}}) - \frac{1}{\pi}\int_{\bar{B}}^{\bar{D}} \frac{2U\Gamma}{(2U\Gamma)^2 + (\bar{\lambda} - \bar{\lambda}')^2}\epsilon(\bar{\lambda}') \tag{3.52}$$

Since the Eq.(3.52) is a linear equation we can separate the driving term and $\epsilon(\bar{\lambda})$ into two parts by $\epsilon(\bar{\lambda}) \equiv \epsilon_d\epsilon_1(\bar{\lambda}) + \epsilon_2(\bar{\lambda})$ with the new parameters defined by:

$$\epsilon_1(\bar{\lambda}) = 1 - \frac{1}{\pi}\int_{\bar{B}}^{\infty} \frac{2U\Gamma}{(2U\Gamma)^2 + (\bar{\lambda} - \bar{\lambda}')^2}\epsilon_1(\bar{\lambda}')$$
$$\epsilon_2(\bar{\lambda}) = (\frac{U}{2} - \sqrt{\frac{\bar{\lambda} + \sqrt{\bar{\lambda}^2 + (U\Gamma)^2}}{2}}) - \frac{1}{\pi}\int_{\bar{B}}^{\infty} \frac{2U\Gamma}{(2U\Gamma)^2 + (\bar{\lambda} - \bar{\lambda}')^2}\epsilon_2(\bar{\lambda}')$$

We choose the boundary $\bar{B}$ satisfying $\epsilon(\bar{B}) = 0 = \epsilon_d\epsilon_1(\bar{B}) + \epsilon_2(\bar{B})$. So we can find the relationship between $\bar{B} = B + (\epsilon_d + \frac{U}{2})^2$ and ϵ_d as $\epsilon_d = -\frac{\epsilon_2(\bar{B})}{\epsilon_1(\bar{B})}$. We will use this relation in the discussion of equilibrium property such as dot occupation as a function of impurity level ϵ_d and the linear response conductance given by the Friedel sum rule.

3.3 Expectation value of current and dot occupation: SBA to pSBA

Solving the SBA equations subject to the minimization of the charge free energy fully determines the current-carrying eigenstate, $|\Psi, \mu_i\rangle$ and allows for calculation of physical quantities by evaluating expectation value of the corresponding operators. In the following we shall discuss our results from equilibrium cases to non-equilibrium ones, starting with the expression for various expectation value of physical quantities.

For $\mu_1 = \mu_2$ all B_i are equal to some equilibrium boundary B fixed by the choice of μ_i. The dot occupation is given by the expectation value $\sum_\sigma \langle\Psi, \mu_i|d_\sigma^\dagger d_\sigma|\Psi, \mu_i\rangle$. Taking the limit $L \to \infty$ (L being the size of the lead) one can express n_d as an integral over the density of λ and some matrix element $\nu(\lambda) \simeq \frac{\langle p^+(\lambda)p^-(\lambda)|\sum_\sigma d_\sigma^\dagger d_\sigma|p^+(\lambda)p^-(\lambda)\rangle}{\langle p^+(\lambda)p^-(\lambda)|p^+(\lambda)p^-(\lambda)\rangle}$ taken to order $\frac{1}{L}$. Here we address the different choice of s_{ep} (with $s_{op} = -4$ fixed to have the same S-matrix in all channels) which gives rise to different forms of $\nu(\lambda)$. We shall first discuss $s_{ep} = 0$ and show it reproduces the *exact* result for the dot occupation in equilibrium. While in checking the condition for out-of-equilibrium it fails. Thus we propose $s_{ep} \neq 0$ schemes to circumvent this difficulty and check our proposed scheme against the *exact* equilibrium answer in the second part of the discussion. The nonzero choices of

s_{ep} introduces two types of single particle phase shifts which we introduce *phenomenologically* their respective distribution function. Thus we call the later approach as phenomenological SBA (pSBA). The numerical results in out of equilibrium regime are all done with this pSBA approach.

3.3.1 SBA result with $s_{ep} = 0$: Its success in equilibrium and problem in out of equilibrium

We choose $s_{ep} = 0$ as in the case of the 1-lead Anderson impurity model. Denote $\nu(\lambda) = \nu^{SBA}(\lambda)$ in this choice. The dot occupation expectation value in equilibrium is given by

$$n_d = \frac{\langle \Psi, \mu_1 = \mu_2 | \sum_\sigma \hat{d}_\sigma^\dagger \hat{d}_\sigma | \Psi, \mu_1 = \mu_2 \rangle}{\langle \Psi, \mu_1 = \mu_2 | \Psi, \mu_1 = \mu_2 \rangle} = 2 \int_B^\infty d\lambda \, \sigma(\lambda) \nu^{SBA}(\lambda) \tag{3.53}$$

where the factor 2 in front of the integral accounts for the spin degeneracy. The matrix element of the operator $d_\sigma^\dagger d_\sigma$ in the SBA state is given by

$$\nu^{SBA}(\lambda) = \frac{2\Gamma}{\tilde{x}^2(\lambda) + \tilde{y}_+^2(\lambda)} + \frac{16 y(\lambda) \Gamma^2}{[\tilde{x}^2(\lambda) + \tilde{y}_-^2(\lambda)][\tilde{x}^2(\lambda) + \tilde{y}_+^2(\lambda)]} \left(\frac{\tilde{x}(\lambda)}{2\tilde{x}(\lambda) - U} \right)^2 .$$

where we introduced, for simplified notations, the functions $\tilde{x}(\lambda) = x(\lambda) - \epsilon_d$ and $\tilde{y}_\pm(\lambda) = y(\lambda) \pm \Gamma$.

Eq.(3.53) can be proved to be exact by comparing with the traditional Bethe Ansatz where $\langle \sum_\sigma d_\sigma^\dagger d_\sigma \rangle = 2 \int_B^\infty d\lambda \, \sigma_{\rm imp}(\lambda)$ with impurity density $\sigma_{\rm imp}(\lambda)$ given by

$$\sigma_{\rm imp}(\lambda) = \frac{\delta_{p^+} + \delta_{p^-}}{2\pi} - \int_B^\infty d\lambda' \, K(\lambda - \lambda') \sigma_{\rm imp}(\lambda') \tag{3.54}$$

By comparing Eq.(3.54) and Eq.(3.36) in equilibrium ($\sigma_i(\lambda) = \sigma_b(\lambda)$ describing bulk quasi-particle density when $B_1 = B_2 = B$.) we get

$$\int_B^\infty d\lambda \, \sigma_{\rm imp}(\lambda) \left(\frac{-1}{\pi} \frac{dx(\lambda)}{d\lambda} \right) = 2 \int_B^\infty d\lambda \, \sigma_b(\lambda) \left(\frac{\delta_{p^+} + \delta_{p^-}}{2\pi} \right) \tag{3.55}$$

by noting that the integration kernel $K(\lambda - \lambda')$ is symmetric in λ and λ'. Since the equality is true

for arbitrary B we can also rewrite Eq.(3.55) as

$$\int_B^\infty d\lambda\,\sigma_{\rm imp}(\lambda) = 2\int_B^\infty d\lambda\,\sigma_b(\lambda)\begin{pmatrix}\delta_{p^+}+\delta_{p^-}\\ -2\frac{dx(\lambda)}{d\lambda}\end{pmatrix} \equiv 2\int_B^\infty d\lambda\,\sigma_b(\lambda)\nu^{TBA}(\lambda)$$

and the resulting $\nu^{TBA}(\lambda)$ is given by

$$\nu^{TBA}(\lambda) = \frac{-\tilde{x}(\lambda)\frac{y'(\lambda)}{x'(\lambda)} - \tilde{y}_-(\lambda)}{\tilde{x}^2(\lambda)+\tilde{y}_+^2(\lambda)} + \frac{\tilde{x}(\lambda)\frac{y'(\lambda)}{x'(\lambda)} + \tilde{y}_+(\lambda)}{\tilde{x}^2(\lambda)+\tilde{y}_+^2(\lambda)} \tag{3.56}$$

Now let us show the computation for $\nu^{SBA}(\lambda)$. First we write one particle state of Eq.(3.1) in even channel (with $s_{ek}=0$ for the moment) as

$$\begin{aligned}|k,\sigma\rangle &= \int e^{ikx}\alpha^\dagger_{ek,\sigma}(x)dx|0\rangle \\ &= \int e^{ikx}\{(\bar{\theta}+A_k\theta)\psi^\dagger_{e\sigma}+B_k d^\dagger_\sigma\delta(x)\}dx|0\rangle\end{aligned} \tag{3.57}$$

Solving $\hat{H}|k,\sigma\rangle = k|k,\sigma\rangle$ we get

$$\begin{aligned}-i(-1+A_k)+B_k t &= 0\\ \epsilon_d B_k + t\frac{1+A_k}{2} &= kB_k\end{aligned}$$

Thus we get $A_k = \frac{k-\epsilon_d - i\frac{t^2}{2}}{k-\epsilon_d+i\frac{t^2}{2}}$ and $B_k = \frac{t}{k-\epsilon_d+i\frac{t^2}{2}}$. We may also define $g_k(x) = e^{ipx}(\bar{\theta}+A_k\theta)$ and $e_k = B_k$ to have easier comparison with Wiegmann and Tsvelick's work[46]. The two particles state is obtained by constructing product of two $\alpha^\dagger_{ep,\sigma}(x)$ particles state with appropriate two particles S-matrix expressed in $Z_{k^+k^-}(x_1-x_2)$.

In principle we shall use $|\Psi,N_1,N_2\rangle$ as the many body state to compute expectation value. However the simplification here, similar to the case of IRLM in Ref.[16], is that different λ (corresponding to different $p(\lambda)$) are orthogonal to each other in $L\to\infty$ limit. Thus the many body expectation value can be obtained via two body computation and the rest just get canceled by normalization factor. We shall demonstrate the explicit computation for two particles in the following.

Denote $|\Psi\rangle$ as the two particles solution. We may write spin singlet state as

$$\begin{aligned}
|\Psi\rangle &= \int dx_1 dx_2 \mathcal{A}\left\{e^{i(kx_1+px_2)} Z_{kp}(x_1-x_2)\alpha^\dagger_{ek,\uparrow}(x_1)\alpha^\dagger_{ep,\downarrow}(x_2)\right\}|0\rangle \\
&= \int dx_1 dx_2 \Big\{ Z_{kp}(x_1-x_2)\{g_k(x_1)g_p(x_2)\psi^\dagger_\uparrow(x_1)\psi^\dagger_{e\downarrow}(x_2) + g_k(x_1)e_p\psi^\dagger_\uparrow(x_1)d^\dagger_\downarrow\delta(x_2) \\
&\quad + e_k g_p(x_2)d^\dagger_\uparrow\delta(x_1)\psi^\dagger_\downarrow(x_2) + e_k e_p d^\dagger_\uparrow d^\dagger_\downarrow\delta(x_1)\delta(x_2)\} - Z_{kp}(x_2-x_1)\{g_k(x_2)g_p(x_1)\psi^\dagger_{e\downarrow}(x_2)\psi^\dagger_{e\uparrow}(x_1) \\
&\quad + g_k(x_2)e_p\psi^\dagger_{e\downarrow}(x_2)d^\dagger_\uparrow\delta(x_1) + e_k g_p(x_1)d^\dagger_\downarrow\delta(x_2)\psi^\dagger_{e\uparrow}(x_1) + e_k e_p d^\dagger_\downarrow d^\dagger_\uparrow\delta(x_1)\delta(x_2)\}\Big\}|0\rangle \\
&= \Big\{\int dx_1 dx_2 [Z_{kp}(x_1-x_2)g_k(x_1)g_p(x_2) + Z_{kp}(x_2-x_1)g_k(x_2)g_p(x_1)]\psi^\dagger_{e\uparrow}(x_1)\psi^\dagger_{e\downarrow}(x_2) \\
&\quad + \int dx [Z_{kp}(x)g_k(x)e_p + Z_{kp}(-x)g_p(x)e_k](\psi^\dagger_{e\uparrow}(x)d^\dagger_\downarrow - \psi^\dagger_{e\downarrow}(x)d^\dagger_\uparrow) + 2e_k e_p\tilde{Z}_{kp}(0)d^\dagger_\downarrow d^\dagger_\uparrow\Big\}|0\rangle
\end{aligned}$$

With $\mathcal{A}$ denoting anti-symmetrization and $\tilde{Z}_{kp}(0) = \frac{k+p-2\epsilon_d}{k+p-U-2\epsilon_d} Z_{kp}(0)$.

Solving $\hat{H}|k,\sigma;p,-\sigma\rangle = (k+p)|k,\sigma;p,-\sigma\rangle$ we obtain

$$Z_{kp}(x_1-x_2) = \theta(x_1-x_2) + \frac{(k-p)(k+p-2\epsilon_d-U) - iUt^2}{(k-p)(k+p-2\epsilon_d-U)+iUt^2}\theta(x_2-x_1)$$

For the case of bound state the two particle S-matrix is given by $Z_{k^+k^-}(x_1-x_2) = \theta(x_1-x_2) \equiv \theta^x_{12}$. The normalization factor and matrix element of dot occupation given by the even channel two particles wavefunction are

$$\begin{aligned}
\langle\Psi|\Psi\rangle &= \int dy_1 dy_2 \int dx_1 dx_2 (\theta^y_{12} g_{k^+}(y_1)g_{k^-}(y_2) + \theta^y_{21} g_{k^+}(y_2)g_{k^-}(y_1))^* \\
&\quad \times(\theta^x_{12} g_{k^+}(x_1)g_{k^-}(x_2) + \theta^x_{21} g_{k^+}(x_2)g_{k^-}(x_1))\delta(x_1-y_1)\delta(x_2-y_2) \\
&\quad +2\int dy \int dx [\theta(y)g_{k^+}(y)e_{k^-} + \theta(-y)g_{k^-}(y)e_{k^+}]^*[\theta(x)g_{k^+}(x)e_{k^-} + \theta(-x)g_{k^-}(x)e_{k^+}]\delta(x-y) \\
&\quad +4(e_{k^+}e_{k^-}\tilde{Z}_{k^+k^-}(0))^*(e_{k^+}e_{k^-}\tilde{Z}_{k^+k^-}(0)) \\
\sum_\sigma \langle\Psi|\hat{d}^\dagger_\sigma\hat{d}_\sigma|\Psi\rangle &= 2\int dy \int dx [\theta(y)g_{k^+}(y)e_{k^-} + \theta(-y)g_{k^-}(y)e_{k^+}]^*[\theta(x)g_{k^+}(x)e_{k^-} + \theta(-x)g_{k^-}(x)e_{k^+}]\delta(x-y) \\
&\quad +8(e_{k^+}e_{k^-}\tilde{Z}_{k^+k^-}(0))^*(e_{k^+}e_{k^-}\tilde{Z}_{k^+k^-}(0)) \\
&= 2\left\{\int dx [\theta(x)|g_{k^+}(x)e_{k^-}|^2 + \theta(-x)|g_{k^-}(x)e_{k^+}|^2] + 4|e_{k^+}e_{k^-}\tilde{Z}_{k^+k^-}(0)|^2\right\}
\end{aligned}$$

Note that the even channel bound state can be written as sum over bound state of $\{11,12,21,22\}$ (4 strings type) or $\{11,22\}$ (2 strings type) with the same real part of energy $k = x(\lambda)$. This can be viewed as the consistency counting from Fock basis to Bethe basis as electrons in lead 1 and lead 2

has 4 fold degeneracies in its initial state (2 different spins in each lead). Also note that

$$\begin{aligned}
\int dx_1 dx_2\ \theta_{12}^x |g_{k^+}(x_1) g_{k^-}(x_2)|^2 &= \int dx_1 dx_2 |e^{i(k^+ x_1 + k^- x_2)}(\bar{\theta}_1 + \theta_1 A_{k^+})(\bar{\theta}_2 + \theta_2 A_{k^-})|^2 \theta_{12} \\
&= \int dx_1 dx_2\ e^{-2\xi_k (x_1 - x_2)} |\bar{\theta}_1 \bar{\theta}_2 \theta_{12} + \theta_1 \bar{\theta}_2 \theta_{12} A_{k^+} + \theta_1 \theta_2 \theta_{12} A_{k^+} A_{k^-}|^2 \\
&= \left(\frac{L}{2\xi_k} - \frac{1 - e^{-2\xi_k L}}{(2\xi_k)^2} \right) \left(1 + |A_{k^+} A_{k^-}|^2 \right) + \left(\frac{1 - e^{-2\xi_k L}}{2\xi_k} \right)^2 |A_{k^+}|^2 \\
\int dx\, \theta(x) |g_{k^+}(x) e_{k^-}|^2 &= \int dx\, \theta(x) |e^{i(k + i\xi_k)x} (\theta(-x) + A_{k^+} \theta(x)) e_{k^-}|^2 = \int_0^L dx\, e^{-2\xi_k x} |A_{k^+} e_{k^-}|^2 \\
&= \frac{1}{2\xi_k} \left| \frac{k - \epsilon_d + i\xi_k - i\Gamma}{k - \epsilon_d + i\xi_k + i\Gamma} \frac{t}{k - \epsilon_d - i\xi_k + i\Gamma} \right|^2 = \frac{1}{2\xi_k} \left| \frac{t}{k - \epsilon_d + i\xi_k + i\Gamma} \right|^2 \\
\int dx\, \theta(-x) |g_{k^-}(x) e_{k^+}|^2 &= \int dx\, \theta(-x) |e^{i(k - i\xi_k)x} (\theta(-x) + A_{k^-} \theta(x)) e_{k^+}|^2 = \int_{-L}^0 dx\, e^{2\xi_k x} |A_{k^-} e_{k^+}|^2 \\
&= \frac{1}{2\xi_k} \left| \frac{t}{k - \epsilon_d + i\xi_k + i\Gamma} \right|^2
\end{aligned}$$

with $\tilde{Z}_{k^+k^-}(0) = \frac{2(k-\epsilon_d)}{2(k-\epsilon_d)-U} Z_{k^+k^-}(0)$ and $Z_{k^+k^-}(0) = \frac{1}{2}$ based on our regularization scheme. By expressing $k = x(\lambda)$ and $\xi_k = y(\lambda)$ and taking $L \to \infty$ thus preserving $\frac{1}{L}$ terms only we get

$$\begin{aligned}
\frac{\langle \Psi | \sum_\sigma \hat{d}_\sigma^\dagger \hat{d}_\sigma | \Psi \rangle}{\langle \Psi | \Psi \rangle} &= \frac{1}{L} \nu^{SBA}(\lambda) \qquad (3.58) \\
&= \frac{1}{L} \left\{ \frac{2\Gamma}{\tilde{x}^2(\lambda) + \tilde{y}_+^2(\lambda)} + \frac{16 y(\lambda) \Gamma^2}{(\tilde{x}^2(\lambda) + \tilde{y}_-^2(\lambda))(\tilde{x}^2(\lambda) + \tilde{y}_+^2(\lambda))} \left(\frac{\tilde{x}(\lambda)}{2\tilde{x}(\lambda) - U} \right)^2 \right\} .
\end{aligned}$$

By expressing $\nu^{TBA}(\lambda)$ and $\nu^{SBA}(\lambda)$ in λ explicitly we see that $\nu^{TBA}(\lambda) = \nu^{SBA}(\lambda)$. Since $\langle \sum_\sigma d_\sigma^\dagger d_\sigma \rangle = 2 \int_B^\infty d\lambda \sigma_{imp}(\lambda)$ in TBA we have proved that the expectation value evaluated by the state we constructed is exact and the equivalence of SBA and TBA in equilibrium in this two-lead Anderson model. This observation that the SBA and TBA results for n_d agree in equilibrium shows the connection between the dot occupation and the dressed phase shift across the impurity. It also proves unambiguously that the approximation $L \to \infty$ we made in obtaining the matrix element and therefore the orthogonality between different λ states for dot occupation computation are valid.

To describe the out-of-equilibrium state we first check if the steady state condition $\frac{d\langle \hat{n_d} \rangle}{dt} = 0$ (or equivalently, $\frac{d\langle \hat{N}_1 + \hat{N}_2 \rangle}{dt} = 0$) is satisfied in this basis. As mentioned earlier these scattering states are formed by bounded quasi-particles with complex momenta and therefore the single particle phase across the impurity is not well defined in the sense that $|e^{i\delta_{p^\pm}}| \neq 1$. This problem begins to surface

as we set out to evaluate transport expectation value and renders

$$\frac{d\langle \hat{n_d} \rangle}{dt} = \int_{B_{11}}^{B_{22}} d\lambda \sigma_b(\lambda)\Delta(\lambda) \neq 0 \tag{3.59}$$

with

$$\Delta(\lambda) = \frac{y^2(\lambda)\Gamma^2}{[\tilde{x}^2(\lambda)+\tilde{y}_-^2(\lambda)][\tilde{x}^2(\lambda)+\tilde{y}_+^2(\lambda)]} \ .$$

Thus it appears that using this basis the steady state condition is not observed. This problem does not appear when the momenta are real as in the IRLM case[16].

3.3.2 SBA phenomenology (pSBA) : Choosing $s_{ep} \neq 0$

To remedy this problem we redefine the single particle phase shifts across the impurity, in analogy to the results for the IRLM[16], through the choice of nonzero s_{ep} in Eq.(4.2). With a suitable choice of s_{ep} we may restore a well defined single particle phase $|e^{i\tilde{\delta}_p^{\pm}}| = 1$ with $\tilde{\delta}_p^{\pm}$ denoting this new phase. The way we judge whether we make the correct choice for the new phases $\tilde{\delta}_p^{\pm}$ is to compare the dot occupation n_d in equilibrium before and after the redefined phase. The explicit form of s_{ep} and phase $\tilde{\delta}_p^{\pm}$ will be motivated below but first we shall show that a single redefined phase is not sufficient to satisfy the constraint of dot occupation comparison.

Again the choice of new phases is constrained by the requirement that we shall obtain the same result for $\langle \sum_\sigma d_\sigma^\dagger d_\sigma \rangle$ as given by $\nu^{SBA}(\lambda)$ in equilibrium. Based on this constraint it can be shown explicitly that a single well defined phase (in the sense of $|e^{i\tilde{\delta}_p}| = 1$) is not sufficient to reproduce the equilibrium $\nu^{SBA}(\lambda)$ as following: The new dot amplitude $\tilde{e}_{p^+}$ and $\tilde{e}_{p^-}$ have to satisfy

$$\begin{aligned} |\tilde{e}_{p^+}|^2 + |\tilde{e}_{p^-}|^2 &= \frac{4\Gamma}{\tilde{x}^2(\lambda)+\tilde{y}_+^2(\lambda))} \ , \\ |\tilde{e}_{p^+}|^2 |\tilde{e}_{p^-}|^2 &= \frac{4\Gamma^2}{[\tilde{x}^2(\lambda)+\tilde{y}_+^2(\lambda)][\tilde{x}^2(\lambda)+\tilde{y}_-^2(\lambda)]} \ . \end{aligned}$$

As both $|\tilde{e}_{p^+}|^2$ and $|\tilde{e}_{p^-}|^2$ are positive we see that a single redefined phase cannot satisfy the above constraints simultaneously. Therefore we have to choose at least two sets of redefined phases $\tilde{\delta}_{p^\pm}^i$ (with $i = s, h$ denoting spin-fluctuation or charge-fluctuation to be addressed later) and, along with them, some distribution functions f^i to set the weight for these phases.

To motivate the idea of searching the correct phase shifts we shall come back to the derivation of

dot occupation in traditional Bethe Ansatz (TBA) picture. In TBA the total energy of the system is described by energy of the leads electrons and energy shifts from the impurity,

$$E = \sum_j p_j = \sum_j \left(\frac{2\pi n_j}{L} + \frac{1}{L}\delta_j \right) \tag{3.60}$$

Based on Feynman-Hellman theorem, which is applicable in equilibrium (closed) system, we have

$$\langle \hat{n}_d \rangle = \frac{\partial E}{\partial \epsilon_d} = \frac{1}{L}\sum_j \frac{\partial \delta_j}{\partial \epsilon_d} = \frac{1}{L}\sum_j \frac{\partial(\delta_{p_j^+} + \delta_{p_j^-})}{\partial \epsilon_d} \tag{3.61}$$

The result for Eq.(3.61) agrees with those obtained from Eq.(3.55) and can be viewed as a third approach to obtain the expectation value of the dot occupation. The key observation here is that this quantity is related to the *bare* phase shift $\delta_{p^+} + \delta_{p^-}$ and therefore the redefined phases must be proportional to this quantity. Among them there are two likely candidates with redefined phase shift given by $\delta_{p^+} + \delta_{p^-}$, describing the tunneling of a bounded pair, and $\frac{\delta_{p^+} + \delta_{p^-}}{2}$, describing the tunneling of a single quasi-particle. In a sense this is the echo for the elementary excitations above the Fermi surface in the Bethe basis characterized by N. Kawakami and A. Okiji[51] as charge-fluctuation excitation, which describes bounded pair quasi-particles excitation, and spin-fluctuation excitation, which describes one quasi-particle excitation. Another similar picture is the spin-fluctuation and charge-fluctuation two fluids picture proposed by D. Lee et al[52] albeit in a different context. We identify the phase defined by

$$\tilde{\delta}_{p^-} = \tilde{\delta}_{p^+} = \frac{\delta_{p^+} + \delta_{p^-}}{2} \equiv \tilde{\delta}_p^s$$

(with $s_{ep^\pm} \equiv s^s_{ep^\pm} = \frac{2}{\Gamma}(i(p^\pm - \epsilon_d) - \Gamma)(e^{i(\frac{\delta_{p^+} + \delta_{p^-}}{2})} - 1))$ as spin-fluctuation phase shift and

$$\tilde{\delta}_{p^-} = \tilde{\delta}_{p^+} = \delta_{p^+} + \delta_{p^-} \equiv \tilde{\delta}_p^h$$

(with $s_{ep^\pm} \equiv s^h_{ep^\pm} = \frac{2}{\Gamma}(i(p^\pm - \epsilon_d) - \Gamma)(e^{i(\delta_{p^+} + \delta_{p^-})} - 1))$ as charge-fluctuation phase shift.

The out-of-equilibrium current is evaluated by the expectation value of current operator $\hat{I}$ with $\langle \hat{I} \rangle$ defined by

$$\langle \hat{I} \rangle = \frac{-\sqrt{2}iet}{\hbar} \langle \sum_\sigma ((\psi^\dagger_{1\sigma}(0^\pm) - \psi^\dagger_{2\sigma}(0^\pm))d_\sigma - h.c.) \rangle \tag{3.62}$$

in the state $|\Psi, \mu_i\rangle$. Notice that $\psi^\dagger_{i\sigma}(0^\pm) \equiv \lim_{\epsilon \to 0}(\psi^\dagger_{i\sigma}(-\epsilon) + \psi^\dagger_{i\sigma}(+\epsilon))/2$ is introduced in transport

related quantity to be consistent with our regularization scheme which introduces another local discontinuity in odd channel at impurity site.

From Eq.(3.62) and the expression for the phases $\tilde{\delta}_p^s$ and $\tilde{\delta}_p^h$ we have the expression for current as

$$I(\mu_1,\mu_2) = \langle \Psi, \mu_1, \mu_2 | \hat{I} | \Psi, \mu_1, \mu_2 \rangle = \frac{2e}{\hbar} \int_{B_1}^{B_2} \mathrm{d}\lambda \; \sigma_b(\lambda)(f_s(\lambda) J^s(\lambda) + f_h(\lambda) J^h(\lambda)) \tag{3.63}$$

The corresponding spin-fluctuation and charge-fluctuation matrix element of the current operator, denoted as $J^s(\lambda)$ and $J^h(\lambda)$, are given by

$$J^s(\lambda) = 1 + \frac{\mathrm{sgn}(\tilde{x}(\lambda))(\tilde{x}^2(\lambda) + y(\lambda)^2 - \Gamma^2)}{\sqrt{(\tilde{x}^2(\lambda) + y^2(\lambda) - \Gamma^2)^2 + 4\Gamma^2 \tilde{x}^2(\lambda)}} \tag{3.64}$$

$$J^h(\lambda) = \frac{2\Gamma^2 \tilde{x}^2(\lambda)}{(\tilde{x}^2(\lambda) + \Gamma^2)^2 - 2y^2(\lambda)(\Gamma^2 - \tilde{x}^2(\lambda)) + y^4(\lambda)}. \tag{3.65}$$

Here $\mathrm{sgn}(x) = \frac{x}{|x|}$ is the sign function. It is introduced in order to pick up the correct branch when taking the square root in denominator of Eq.(3.64). This way we ensure that $J^s(\lambda)$ has the proper limit when U is sent to infinity (cf Chap 4). Other than the motivations mentioned above for identifying spin and charge fluctuation phase shifts the functional forms of $J^s(\lambda)$ and $J^h(\lambda)$ as a function of bare energy $x(\lambda)$ can also be used to identify these two type of phase shifts (See Fig.4.4 in Chap.4 for infinite U Anderson model, the finite U is similar).

Next we shall choose the appropriate weight for each type of phase shift. So far we have not yet been able to deduce the form of these weight functions $f_s(\lambda)$ and $f_h(\lambda)$ and we introduce them *phenomenologically*. Let us define *phenomenological* spin-fluctuation and charge-fluctuation weight functions as

$$f_s(\varepsilon(\lambda)) = \frac{D_s(\varepsilon(\lambda))}{D_s(\varepsilon(\lambda)) + D_h(\varepsilon(\lambda))} \tag{3.66}$$

and

$$f_h(\varepsilon(\lambda)) = \frac{D_h(\varepsilon(\lambda))}{D_s(\varepsilon(\lambda)) + D_h(\varepsilon(\lambda))} \; . \tag{3.67}$$

Here $D_s(\varepsilon(\lambda))$ is the spin-fluctuation density of state, $D_h(\varepsilon(\lambda))$ is the charge-fluctuation density of state as defined in Ref.[51], and $\varepsilon(\lambda)$ is the corresponding dressed energy i.e. the energy required to produce these spin- and charge-fluctuation excitations above the Fermi level. Their functional forms are plotted in Fig.(3.1). Here dressed energy refers to the sum of the bare energy of adding/removing

one bound state, as in charge fluctuation, or single quasi particle, as in spin fluctuation, and the energy shift from other quasi particles due to this change. The equation that solves a single quasi-particle's dressed energy $\varepsilon(\lambda)$ reads[53]

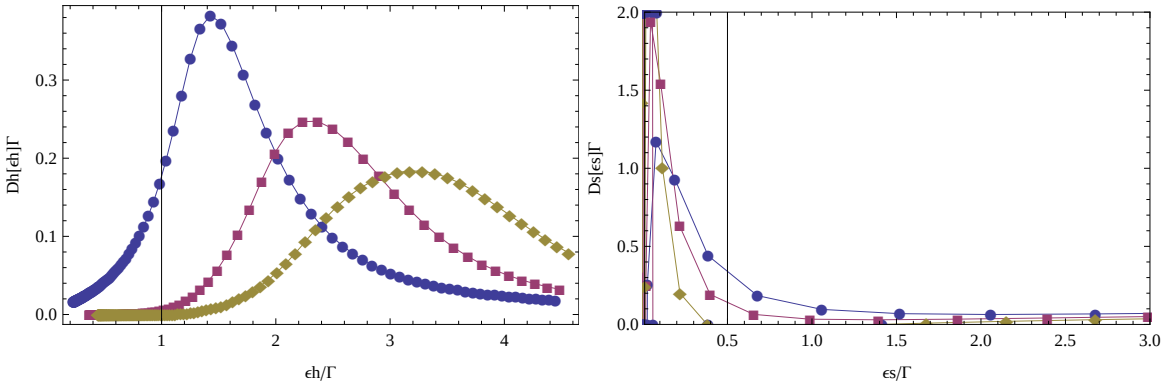

Figure 3.1: Left: Holon density of state vs holon dressed energy for $\frac{U}{\Gamma} = 2, 4, 6$ (blue, purple, brown) with $\epsilon_d = -\frac{U}{2}$. Right: Spinon density of state vs spinon dressed energy for $\frac{U}{\Gamma} = 4, 6, 8$ (blue, purple, brown) with $\epsilon_d = -\frac{U}{2}$.

$$\varepsilon(\lambda) = (x(\lambda) - \mu) - \int_B^\infty \mathrm{d}\lambda' \, K(\lambda - \lambda')\varepsilon(\lambda') \,. \tag{3.68}$$

We wish to compare at this point our approach to the one taken by Konik et al[42, 43]. The authors' Landauer approach is based on an ensemble of renormalized excitations, the holons and spinons, and the conductance is expressed in terms of their phase shift crossing the impurity. However, the leads are built of bare electrons and thus the difficult problem arises of how to construct a bare electron out of renormalized excitations in order to be able to impose the voltage boundary condition. The basic approximation adopted,*electron* $\approx$ *antiholon* + *spinon*, is valid only when the electron is on the Fermi surface (see N. Andrei[54]), and the approach is valid therefore only for small momenta. In contrast we construct the eigenstates of the Hamiltonian directly in terms of the bare electron field and can therefore impose the asymptotic boundary condition that the wave function tend to a product of two free Fermi seas composed of bare electrons. While we do not have a mathematically rigorous derivation of the weight functions we introduced, the validity of the scattering formalism is not restricted to any energy window other than energy cutoff.

3.4 pSBA: In and Out of Equilibrium

In the following section we focus on the numerical results of pSBA, both in and out of equilibrium. First we check the consistency in equilibrium by comparing pSBA with SBA/TBA. We find overall quantitative agreement between the two except some mismatch in the mixed valence region. We then perform the computation for finite voltage and see that the obtained results agree with the scaling relation in Kondo region. The obtained current and dot occupation out of equilibrium are compared with other theoretical results.

3.4.1 Results for equilibrium and linear response

In the numerical computation, for the practical purpose, we assumed Kondo limit ($U = -2\epsilon_d$, $\frac{U}{\Gamma} \gg 1$) form of the spin-fluctuation and charge-fluctuation distributions, i.e.

$$D_s(\varepsilon(\lambda)) \simeq \frac{1}{\pi}\frac{T_k}{\varepsilon^2(\lambda)+T_k^2} \tag{3.69}$$

and

$$D_h(\varepsilon(\lambda)) \simeq \frac{1}{\sqrt{2U\Gamma}}\frac{\Gamma^2}{(\varepsilon(\lambda)+\epsilon_d)^2+\Gamma^2} \tag{3.70}$$

with T_k being the Kondo scale derived in Ref. [51] as

$$T_k = \frac{\sqrt{2U\Gamma}}{\pi} e^{\pi \frac{\epsilon_d(\epsilon_d+U)+\Gamma^2}{2U\Gamma}} \ . \tag{3.71}$$

We also take $\varepsilon(\lambda) \simeq x(B) - x(\lambda)$ for numerical convenience with B denoting the Bethe momenta given by $\mu_1 = \mu_2 = 0$. The dot occupation $\langle \sum_\sigma d_\sigma^\dagger d_\sigma \rangle$ evaluated by these new phases is given by

$$\langle \sum_\sigma d_\sigma^\dagger d_\sigma \rangle = 2\left(\int_{B1}^{\infty} d\lambda\, \sigma_b(\lambda)(\nu^s(\lambda) f_s(\lambda) + \nu^h(\lambda) f_h(\lambda)) + \int_{B_2}^{\infty} d\lambda\, \sigma_b(\lambda)(\nu^s(\lambda) f_s(\lambda) + \nu^h(\lambda) f_h(\lambda)) \right) \tag{3.72}$$

with $\nu^s(\lambda)$ and $\nu^h(\lambda)$ given as

$$\begin{aligned} \nu^s(\lambda) = \frac{1}{\Gamma}\Bigg[1 - \frac{(\tilde{x}^2(\lambda)+y(\lambda)^2-\Gamma^2)}{\sqrt{(\tilde{x}^2(\lambda)+y^2(\lambda)-\Gamma^2)^2+4\Gamma^2\tilde{x}^2(\lambda)}}\Bigg] \\ \times \Bigg[1 + 8y(\lambda)\frac{1}{\Gamma}\left(1 - \frac{(\tilde{x}^2(\lambda)+y(\lambda)^2-\Gamma^2)}{\sqrt{(\tilde{x}^2(\lambda)+y^2(\lambda)-\Gamma^2)^2+4\Gamma^2\tilde{x}^2(\lambda)}}\right)\left(\frac{\tilde{x}(\lambda)}{2\tilde{x}(\lambda)-U}\right)^2\Bigg] \end{aligned} \tag{3.73}$$

$$\nu^h(\lambda) = \left[\frac{2\Gamma\tilde{x}^2(\lambda)}{(\tilde{x}^2(\lambda)+\Gamma^2)^2 - 2y^2(\lambda)(\Gamma^2-\tilde{x}^2(\lambda)) + y^4(\lambda)}\right] \times \left[1 + \frac{36y(\lambda)\Gamma\tilde{x}^2(\lambda)}{(\tilde{x}^2(\lambda)+\Gamma^2)^2 - 2y^2(\lambda)(\Gamma^2-\tilde{x}^2(\lambda)) + y^4(\lambda)} \left(\frac{\tilde{x}(\lambda)}{2\tilde{x}(\lambda)-U}\right)^2\right] \quad (3.74)$$

respectively. We may check whether this choice of *phenomenological distribution functions* satisfy the condition in equilibrium that

$$\langle \sum_\sigma d_\sigma^\dagger d_\sigma \rangle = 4\int_B^\infty d\lambda\, \sigma_b(\lambda)\nu^{SBA}(\lambda) = 4\left(\int_B^\infty d\lambda\, \sigma_b(\lambda)(\nu^s(\lambda)f_s(\lambda) + \nu^h(\lambda)f_h(\lambda))\right) . \quad (3.75)$$

We can see from the Left of Fig.3.2 that the comparison between the phenomenological and the exact result for the dot occupation in equilibrium is good deep into the Kondo regime ($\epsilon_d \simeq -\frac{U}{2}$) and far away from it ($\epsilon_d \gg 0$) but is worse when we are in mixed valence region ($\epsilon_d \simeq 0$). This discrepancy, due in part to the approximations we made for $D_s(\varepsilon)$ and $D_h(\varepsilon)$, may go away if we took more realistic form of $D_s(\varepsilon(\lambda))$ and $D_h(\varepsilon(\lambda))$ also in mixed valence regime as suggested in Fig.3.2. However the numerical procedure is much more complicated there. We confine ourself to this simpler limit in our phenomenological approach.

Another check on our result in equilibrium is to find the linear response conductance through our formulation and compare with the exact linear result given by the Friedel sum rule[40, 41]. The Friedel sum rule, which relates the equilibrium dot occupation to the phase shift experienced by electrons crossing the dot, is related to zero voltage conductance by $\frac{dI}{dV}|_{V=0} = 2\sin^2(\pi\langle\hat{n}_d\rangle/2)$. The zero bias conductance in our construction can be analyzed easily[55] by noting that at low-voltage $eV = \mu_1 - \mu_2 \simeq \frac{2\pi}{L}(N_1 - N_2) = 4\pi\int_{B_1}^{B_2}\sigma_b(\lambda)d\lambda$. By taking $B_2 \simeq B_1 = B$ in the expression for the current across the impurity Eq. (3.63) we get the zero bias conductance expressed as

$$\frac{dI}{dV}\Big|_{V=0} = \frac{e^2}{h}\left[f_s(B)J^s(B) + f_h(B)J^h(B)\right] \quad (3.76)$$

Here $B = B(\mu, \epsilon_d, \Gamma, U)$ is determined by $\mu_1 = \mu_2 = 0$. The comparison between Friedel sum rule (FSR) result and the conductance given by Eq. (3.76) (denoted as (pSBA)) is shown at the Bottom of Fig. 3.2. It displays the consequence of the equilibrium Kondo effect in the quantum dot set up: due to the formation of the Kondo peak attached to the Fermi level the Coulomb blockade is lifted and a unitary conductance is reached for a range of gate voltages ϵ_d around $-U/2$. Again we see that the comparison is good for large U/Γ but poorer in mixed valence regime for smaller U/Γ,

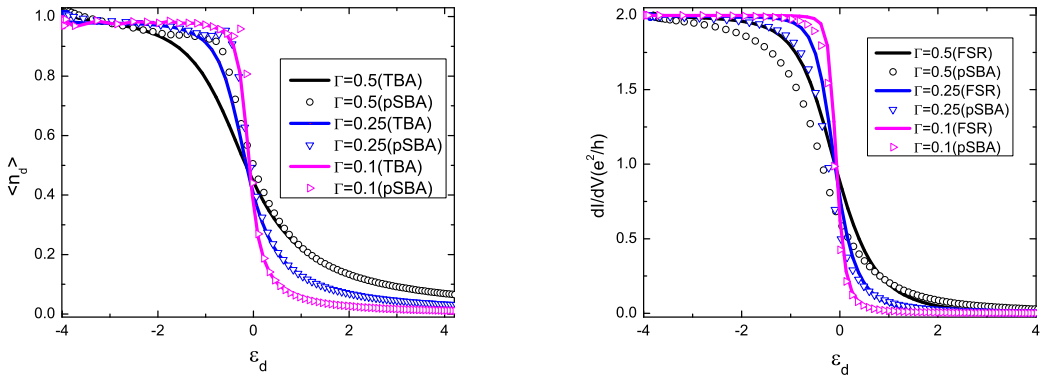

Figure 3.2: Left: $\langle \hat{n_d} \rangle$ as a function of ϵ_d from the exact result (dotted line) and from Eq. (3.75) (solid line). Right: The differential conductance in the linear-response regime, as a function of ϵ_d from the phenomenological Scattering Bethe Ansatz (pSBA) and exact linear response conductance from Friedel sum rule (FSR) for $\Gamma = 0.5$, 0.25, 0.1, and $U = 8$.

which is consistent with the observation we made when evaluating $\langle \hat{n}_d \rangle$ as shown in top figure of Fig. 3.2. Having checked our results in equilibrium we shall go on to compute the current and the dot occupation in the out-of-equilibrium regime.

3.4.2 Results Out-Of-Equilibrium

Now let us begin to investigate the current and dot occupation change as we turn on the voltage. We start with the discussion on current vs voltage for various regime. The current vs voltage is plotted in the inset of figure of Fig. 3.3 for different values of U and at the symmetric point $\epsilon_d = -U/2$. Note that we use an asymmetric bias voltage when solving numerically the integral equations originating from Eq. (3.36) with constraint of minimizing the charge free energy Eq. (3.38): Namely we fix $\mu_1 \simeq 0$ (around $10^{-3} - 10^{-5}$) and lower μ_2. Therefore, a direct confrontation between the results obtained from real-time simulations of the Anderson model out-of-equilibrium [27, 30, 26] is difficult but the main features of our calculation match the predicted results: a linear behavior of the I-V characteristics at low-voltage, the slope being obtained from the FSR (2 in units of e^2/h at the symmetric point), and a non-monotonic behavior at higher voltage, the so-called non-linear regime. In particular, our calculations show clearly that the current will decrease as U/Γ is increased which is in agreement with other numerical approaches (e.g. cf Fig. 2 of Ref.[27] for a comparison).

The plots of the differential conductance vs source drain voltage for different dot levels, ϵ_d, tunneling strengths Γ and interaction strengths U are shown in Fig.3.3 and Fig.3.5. Two major

features emerge from these plots: 1) A narrow peak around zero bias reaching maximal value of $2e^2/h$ (the unitary limit) for values of the gate voltage close to the symmetric point ($\epsilon_d \simeq -U/2$). 2) A broader peak developing at finite bias. The first peak is a non-perturbative effect identified as the many body Kondo peak, characteristic of strong spin fluctuations in the system. But the broad peak is due to renormalized charge fluctuations around the impurity level. Notice the two features merge as the gate voltage, ϵ_d is raised from the Kondo regime, $\epsilon_d = -U/2$, to the mixed valence regime, $\epsilon_d = 0$, with the Kondo effect disappearing. As a function of the bias the various curves describing the Kondo peak for different values of the parameters can be collapsed onto a single universal function $\mathrm{d}I/\mathrm{d}V = \mathrm{d}I/\mathrm{d}V(V/T_k^*)$ as shown in Fig. 3.4. Here T_k^* is defined as

$$T_k^* = c_1 \frac{\sqrt{2U\Gamma}}{\pi} e^{\frac{\epsilon_d(\epsilon_d+U)+\Gamma^2}{2U\Gamma}} \tag{3.77}$$

with $c_1 = 0.002$. The energy scale T_k^* was extracted from the numerics by requiring that the function $\mathrm{d}I/\mathrm{d}V(V/T_k^*)$ decreases to half its maximal value when $V \simeq T_k^*$. The expression for T_k^* as given by Eq.(3.77) differs from the thermodynamic T_k as defined in Eq. (3.71). The difference of prefactor in the exponential is certainly related to the unusual choice of regularization scheme in the SBA [49]. The other possible implication for this different formulation for the Kondo scale is also addressed later when we discuss the experiment done by L. Kouwenhoven et al[9].

The small voltage behavior for differential conductance in symmetric case, i.e. $\epsilon_d \simeq -\frac{U}{2}$, is expected to be [23, 20]

$$\frac{dI}{dV}\Big|_{V \ll T_k^*} \simeq \frac{2e^2}{h}\left(1 - \alpha_V \left(\frac{V}{T_k^*}\right)^2\right)$$

and allows us to identify the constant α_V from the quadratic deviation from $2e^2/h$. The quadratic fit of the universal curve around $V \simeq 0$, as shown in Fig.3.4, gives $\alpha_V \simeq 1$. It is also expected for $T_k^* \ll V \ll \frac{U}{2}$ that the tail of the peak decays logarithmically [20] as

$$\frac{dI}{dV} \sim \frac{2e^2}{h} \frac{1}{\ln^2(\frac{V}{T_k^*})} \ .$$

The latter behavior is observed (see inset of Fig.3.4) in the regime $\frac{U}{\Gamma} \gg 1$ for $10^2 < \frac{V}{T_k^*} < 10^4$ with

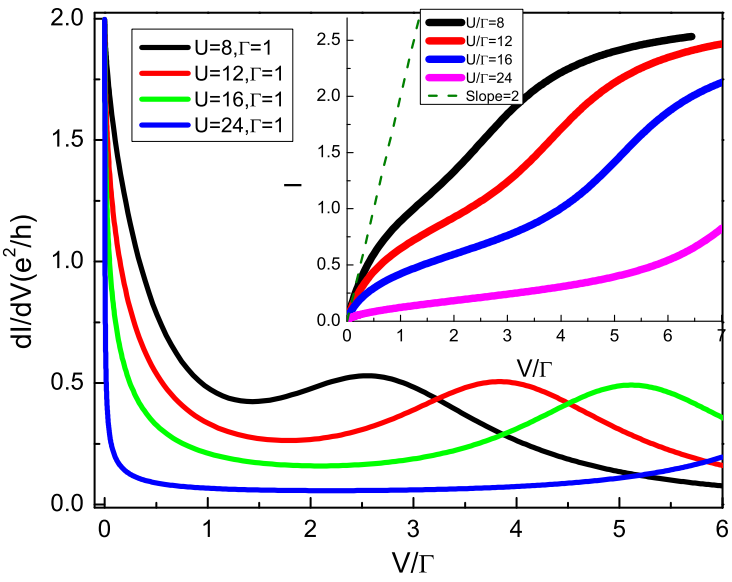

Figure 3.3: dI/dV vs V/Γ for $\Gamma = 1$, $\epsilon_d = -U/2$, and various U. Inset: Steady state current vs voltage curves for $\Gamma = 1$, $\epsilon_d = -U/2$, and various U. Dashed line is a line with constant conductance $\frac{2e^2}{h}$ plotted for comparison.

the logarithmic function given by

$$\frac{dI}{dV} = \frac{e^2}{h}\left[f\left(\frac{U}{\Gamma}\right) + \frac{c_2}{\ln^2(\frac{V}{T_k^*})}\right]$$

with the parameter $c_2 = 0.055$. Here $f(\frac{U}{\Gamma})$ is simply a constant (in V) shift. As suggested from the bottom plot of Fig.3.4 (see also Fig.4.6 for the infinite U case) the charge fluctuation side peak does not fall into the same scaling relation but the strong correlations shift the center of the side peak closer to $V = 0$ (see Fig.3.3 and Fig.3.5). In other words the position of the resonance in the dI/dV curve naively expected around $V = |\epsilon_d|$ is renormalized[58] by the presence of interactions. In the inset of Fig.3.5 we show the logarithm of the voltage obtained at half width half maximum (HWHM) of the zero voltage peak and compare it with

$$\ln T_k^* = \frac{\epsilon_d(\epsilon_d + U) + \Gamma^2}{2U\Gamma} + \ln\left(c_1\frac{\sqrt{2U\Gamma}}{\pi}\right)$$

(after subtracting the constant $\ln c_1$). What is important and *universal* is that both quantities ($\ln V_{\mathrm{HWHM}}$ and $\ln T_k^*$) exhibit a quadratic behavior in the gate voltage ϵ_d. Similar results had been

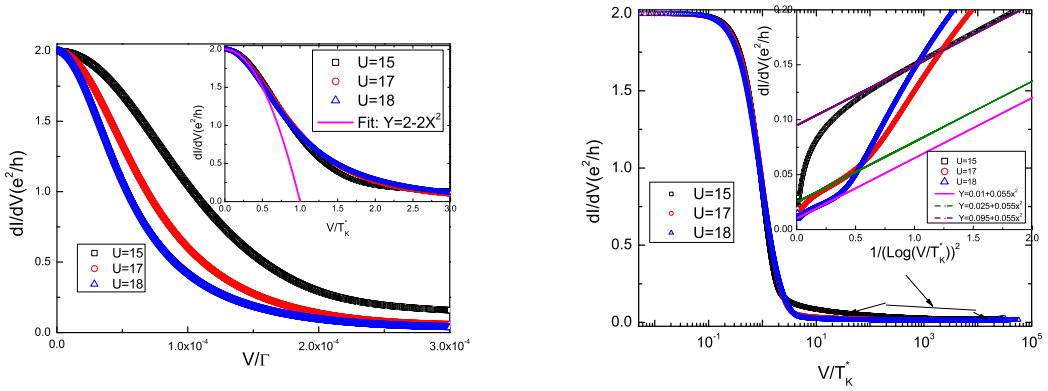

Figure 3.4: Left: Zoomed in picture of the differential conductance vs voltage nearby zero voltage. Inset shows the universality in conductance vs voltage scaled by T_k^* when $\frac{V}{T_k^*} \leq 1$. The quadratic behavior occurs for $\frac{V}{T_k^*} < 0.5$ as indicated by the fitted curve. Right: Differential conductance vs voltage scaled by T_k^* nearby the Kondo peak structure. Inset shows the logarithmic behavior when $\frac{V}{T_k^*} \gg 1$. $\Gamma = 0.5$ for all these data sets.

found experimentally by L. Kouwenhoven et al[9] when they compare the full width half maximum of dI/dV (from which they obtain a Kondo scale T_{k_1} at finite voltage) with the temperature dependence of the linear response differential conductance (from which another Kondo scale T_{k_2} is extracted). It is suggested from our numerical results that both $\ln T_{k_2}$ (in analogy with our T_k) and $\ln T_{k_1}$ (which is our T_k^*) follows similar quadratic behavior in ϵ_d but differ in their curvatures by a factor of π. In Ref.[9] the curvatures of the quadratic behavior differ by a factor of around 2 (see Fig.3B in Ref.[9]) which is attributed to dephasing of spin fluctuations at finite voltage.

Notice that in all the numerical data shown for current vs voltage we have chosen $\frac{U}{\Gamma} \geq 8$ to explore the scaling relation in the Kondo regime. Another reason is that our *phenomenological distribution functions* introduced to control the relative weight for spin- and charge-fluctuation contributions work is much better in the large $\frac{U}{\Gamma}$ regime (cf. Fig. 3.2).

Next let us study the change in the dot occupation as a function of the voltage. The extension of the computation of the dot occupation out of equilibrium is straightforward. Suppose we find the correct distribution functions $f_s(\lambda)$ and $f_h(\lambda)$ then we have $\nu^{SBA}(\lambda) = \nu^s(\lambda)f_s(\lambda) + \nu^h(\lambda)f_h(\lambda)$. Under this assumption $\nu^{SBA}(\lambda)$ retains its form in and out-of-equilibrium and the general expression

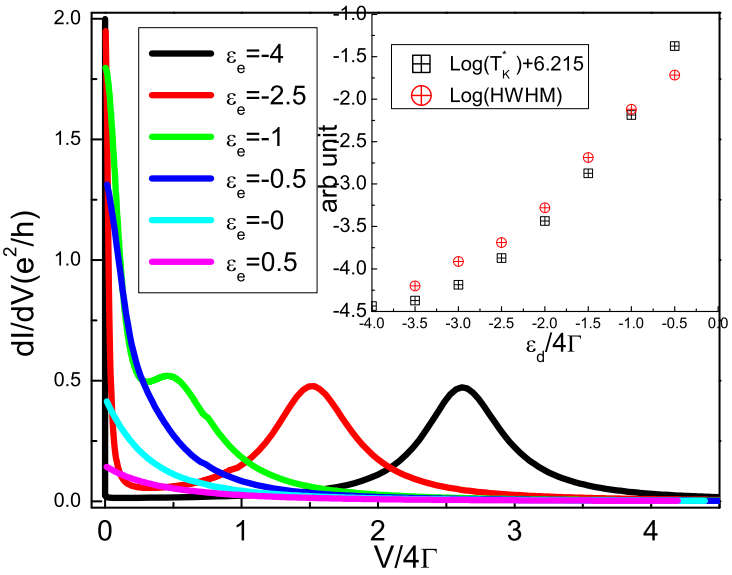

Figure 3.5: dI/dV vs $V/4\Gamma$ for $U = 8$, $\Gamma = 0.25$ and various ϵ_d from Kondo ($\epsilon_d = -4$) to mixed valence regime ($\epsilon_d \simeq 0$). Inset: Comparison of $\ln(T_k^*) - \ln(c_1)$ and $\ln(V_{HWHM})$ as a function of impurity level ϵ_d. Here V_{HWHM} is the voltage difference estimated at half value of differential conductance at zero voltage. The constant shift $-\ln(c_1)$ is chosen to give the best fit in the data away from $\epsilon_d = -\frac{U}{2}$.

for $\langle \hat{n}_d \rangle$ is

$$n_d(\mu_1, \mu_2) = \langle \Psi, \mu_1, \mu_2 | \hat{n}_d | \Psi, \mu_1, \mu_2 \rangle \tag{3.78}$$
$$= 2\left(\int_{B_1}^{\infty} \mathrm{d}\lambda \; \sigma_b(\lambda) \nu^{SBA}(\lambda) + \int_{B_2}^{\infty} \mathrm{d}\lambda \; \sigma_b(\lambda) \nu^{SBA}(\lambda) \right)$$

As the form for $\nu^{SBA}(\lambda)$ is proved to be *exact* in equilibrium, we shall regard Eq.(3.78) as an *exact* result for $\langle \hat{n_d} \rangle$ in and out of equilibrium and valid in all different range of U, ϵ_d, Γ. In the numerical results shown hereafter we shall use this *exact* expression, Eq.(3.78), for matrix element of dot occupation rather than Eq.(3.75). We adopt the same voltage drive scheme by fixing μ_1 and lowering μ_2.

By using this *exact* result we do not need to confine ourself for large $\frac{U}{\Gamma}$. The case for different $\frac{U}{\Gamma}$ with $\epsilon_d = -\frac{U}{2}$ and for $U = 8, \Gamma = 0.25$ with different ϵ_d are shown in Fig.3.6 and Fig. 3.7. The main features of these plots are a relatively slow decrease of the dot occupation at low voltage followed by an abrupt drop of $\langle n_d \rangle$. The decrease of $\langle n_d \rangle$ takes place within a range of voltage of the order

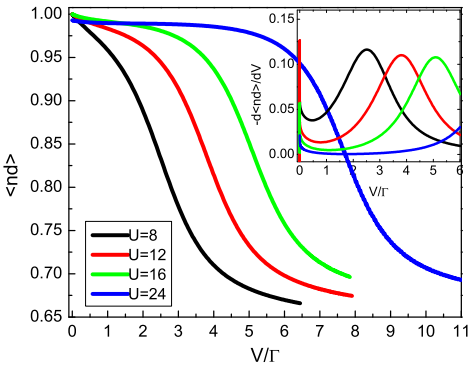

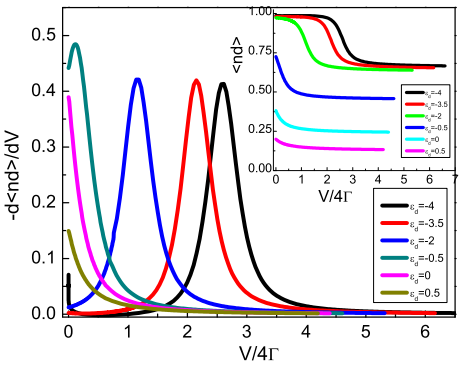

Figure 3.6: Left figure: $\langle \hat{n_d} \rangle$ vs V/Γ for different U with $\epsilon_d = -\frac{U}{2}$ and $\Gamma = 1$ case. Inset: The corresponding nonequilibrium charge susceptibility. A small peak shows up nearby $V = 0$ for all these curves.

Figure 3.7: Right figure: $-\frac{d\langle \hat{n}_d \rangle}{dV}$ vs $V/4\Gamma$ for $\Gamma = 0.25$, $U = 8$, and various ϵ_d from Kondo to mixed valence regime. We see that the small peak nearby $V = 0$ only appears when $\epsilon_d \to -\frac{U}{2}$. Inset: The corresponding $\langle \hat{n_d} \rangle$ vs $V/4\Gamma$.

of Γ. Then as we increase the voltage further another plateau develops. Note that, as expected, the bigger U is the higher the voltage needed to drive the system out of the $\langle n_d \rangle = 1$ plateau. In a sense the charge fluctuations are strongly frozen at large U and it costs more energy to excite them. The voltage where the abrupt drop in $\langle n_d \rangle$ occurs corresponds to the energy scale at which the "charge fluctuation peak" was observed in the conductance plots. This can be seen by comparing the position of the broader peak in Fig.3.5 with that of the abrupt dot occupation drop in Fig.3.7.

Similar to the differential conductance we may define the *nonequilibrium charge susceptibility* as

$$\chi_c(V)|_{\epsilon_d} = -\frac{\partial \langle \hat{n_d} \rangle}{\partial V}$$

that we obtain by taking a numerical derivative of the dot occupation data with respect to the voltage. In the case of $U = -\epsilon_d/2$ there are two features as can be seen from the inset of Fig.3.6 and main figure of Fig.3.7. Nearby $V \simeq 0$ we see a first small peak arising with width and height decreasing with increasing $\frac{U}{\Gamma}$. We identify this peak as a small remnant of the charge fluctuations in the Kondo regime. This statement is confirmed by noticing that this peak goes away as $\frac{U}{\Gamma}$ increases, vanishing when $U \to \infty$ as shown in Section III where the infinite U Anderson model is discussed. The second peak is located at the same voltage as the charge fluctuation peak observed in the conductance plots and is therefore associated to the response of the renormalized impurity level to

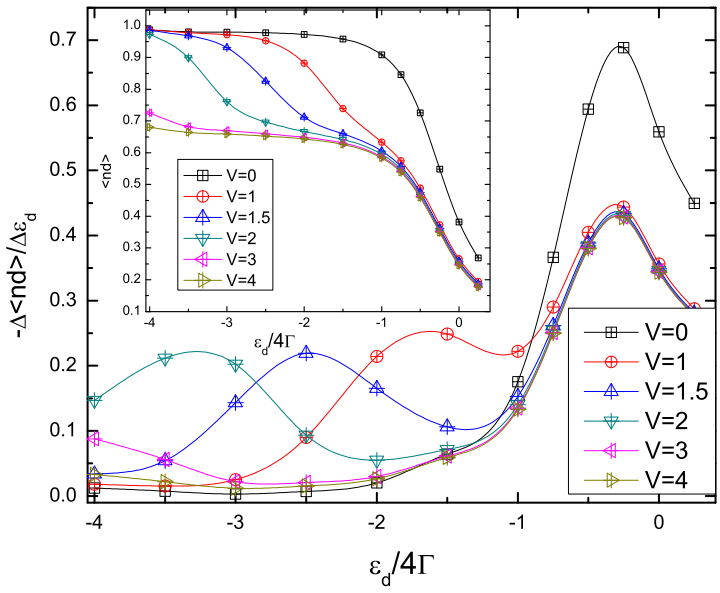

Figure 3.8: $-\frac{\Delta\langle\hat{n}_d\rangle}{\Delta\epsilon_d}$ for various fixed voltages as a function of ϵ_d for $\Gamma = 0.25$, $U = 8$. Inset shows $\langle\hat{n}_d\rangle$ vs ϵ_d for various fixed voltage.

the charge susceptibility. This can be seen when comparing Fig.3.5 and Fig.3.7.

Another interesting quantity, the usual *charge susceptibility*, defined by $\chi_c(\epsilon_d)|_V = -\frac{\partial\langle\hat{n_d}\rangle}{\partial\epsilon_d}$, can also be qualitatively described. In Fig.3.8 we plot $-\frac{\Delta\langle\hat{n_d}\rangle}{\Delta\epsilon_d}$ as a function of ϵ_d as we only have a few points in fixed ϵ_d for finite voltage. Notice that $\chi_c(\epsilon_d)|_V$ tends to be an universal curve in large voltage, indicating charge on the dot remains at some constant value in the steady state with large voltage. This constant value at large voltage, as pointed out by C. J. Bolech, is around 0.65 for $\epsilon_d = -\frac{U}{2}$ case. In preparing this article we noticed that a similar computation, adopting the same asymmetric voltage drive protocol as we have here, is carried out by R. V. Roermund et al[28] for the dot occupation out of equilibrium by using equation of motion method. We do get a similar value for the dot occupation at large voltage. This value is different from the dot occupation value $n_d \simeq 0.5$ at large voltage when the interaction U is turned off as shown in Fig.4.5. This difference might have to do with the 0.7 structure observed in quantum point contact[8] in high temperature (temperature is high compared with the Kondo scale but still small compared with phonon modes or electronic level) and zero magnetic field as the linear response conductance given by $n_d = 0.65$ by using Friedel sum rule is around 0.73. In a sense the voltage seems to play a similar role to the temperature on the way it influences the dot occupation. Further connection between these two behaviors could be

clarified by computing the decoherence factor as in Ref. [28]. This decoherence factor is related to the dot correlation function out of equilibrium which can be computed in three-lead setup[63] by using our approach.

3.5 Comparison with other theoretical and experimental results

In most of the other theoretical approaches[25, 26, 42, 43, 28, 29, 27] the symmetric voltage drive ($\mu_1 = -\mu_2$) is usually assumed to preserve particle-hole symmetry in symmetric case ($\epsilon_d = -\frac{U}{2}$). It is thus difficult for us to make any definite comparison with other theoretical results. The qualitative feature, as shown by the black curves in Fig.3.9 done by D. Matsumoto[29] by using perturbation expansion in U at strong coupling fixed point, is similar to our results in the sense that the height of the charge fluctuation side peak and width are almost the same. The major differences are in the shape of Kondo peak and the position of the charge fluctuation side peak. A clear signature of renormalized dot level ϵ_d as hinted in renormalization computation[59, 58] is clearly seen in our result. The shape of Kondo resonance nearby zero voltage deviates from its quadratic behavior expected from Fermi liquid picture at smaller voltage in our case as is expected for asymmetric voltage drive[22, 24].

We can also compare our results with experiments. As shown in the inset of Fig.3.10 is the $\frac{dI}{dV}$ vs V measured in Co ion transistor by J. Park et al. [10]. We rescaled the differential conductance and superimposed our numerical results on the data graph. The measurement was done by using an asymmetric drive of the voltage (by keeping $\mu_1 = 0$ and changing μ_2 to be larger or smaller than zero) and thus there is an asymmetry in the differential conductance as a function of voltage as illustrated in the data curve. In our numerics we only compute the scenario for $\mu_1 = 0$ and lowering μ_2 (only for $V > 0$ region of Fig.3.10). The $V < 0$ region is plotted by just a reflection with respect to the $V = 0$ axis which illustrates the case of $\mu_2 = 0$ and lowering μ_1. To compare with the correct voltage setup on the $V < 0$ side as in experiment will involve computations within a different parametrization for bare the Bethe momenta which is beyond our current scope. The comparison on the $V > 0$ region shows good agreement between our theory and experimental result. The discrepancy on the width of the charge fluctuation side peak could be due to the vibron mode[60]. To describe these type of transistors we shall start with the Anderson-Holstein Hamiltonian. We are currently exploring the possibility of solving this model by the Bethe Ansatz approach.

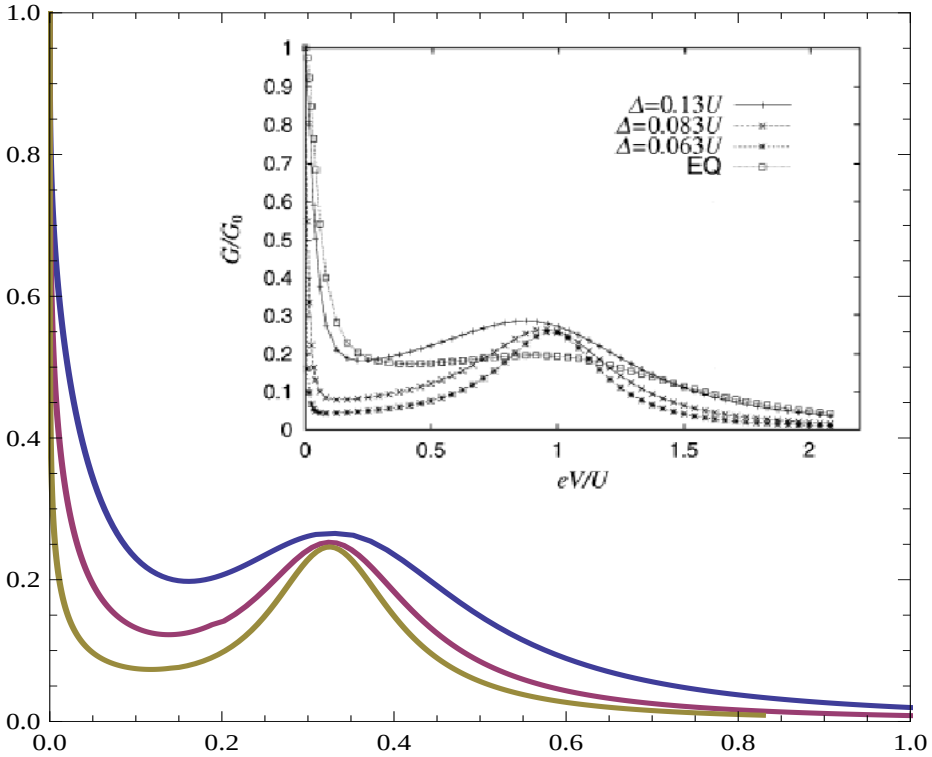

Figure 3.9: Comparison of our theory with perturbation expansion in U done by D. Matsumoto on dI/dV (y-axis in unit of $2e^2/h$) vs V/U (x-axis). Our data (Blue, purple, and brown lines correspond to $\frac{\Gamma}{U} = 0.13, 0.083, 0.063$ respectively. Δ shown in inset is Γ in our notation. EQ in the inset is conductance computed by equilibrium density of state which is not relevant to our discussion here.) is shown as the main figure and Fig.8 in Ref [29] is shown in the inset. In Ref [29] the voltage is driven symmetrically, i.e. $\mu_1 = -\mu_2$, rendering the factor of two difference in the voltage (i.e. $\frac{V}{U} = 0.5$ in our case corresponds to $\frac{eV}{U} = 1$ in the inset. $e = 1$ in our convention.) in comparing our result with that in Ref [29].

3.6 Concluding Remarks

In this chapter we have explicitly computed the non-equilibrium transport properties in the Anderson model for all voltages using the Scattering Bethe Ansatz. In the case of equilibrium we have also shown the equivalence of traditional Bethe Ansatz and Scattering Bethe Ansatz by evaluating dot occupation in equilibrium. For the expression of current we have introduced *phenomenological distribution functions* to set the weight for spin-fluctuation and charge-fluctuation contributions to the current. The result shows correct scaling relation in Kondo regime as well as satisfying the Friedel sum rule for linear response for large $\frac{U}{\Gamma}$.

Other interesting quantities, such as the *nonequilibrium charge susceptibility* or the usual charge susceptibility, are computed numerically via *exact* expression for dot occupation as a function of voltage and impurity level. We believe this is the first report of an *exact* computation of the dot

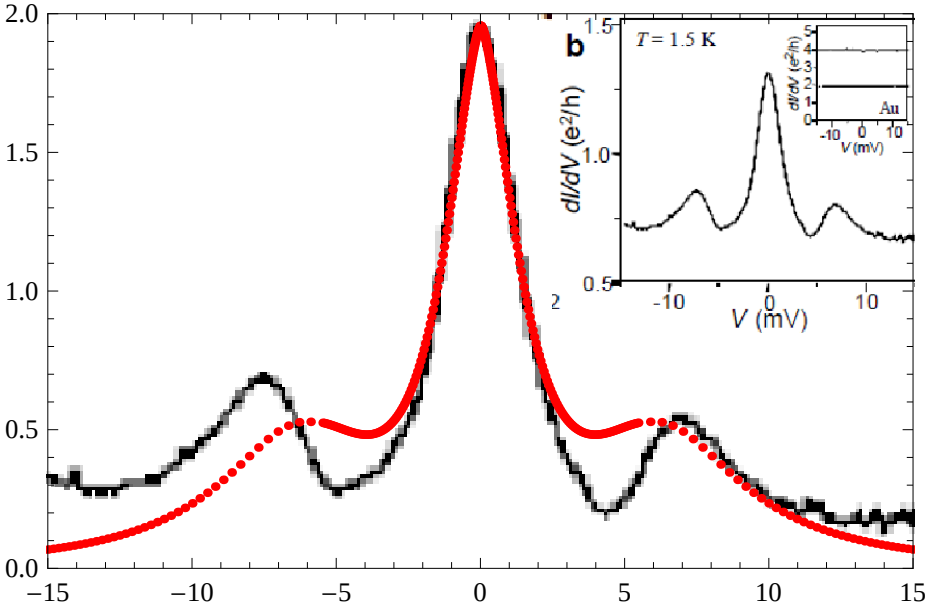

Figure 3.10: Comparison of theory with experiment of dI/dV (y-axis in unit of e^2/h) vs V (x-axis in unit of mV). Inset is the original data graph published in Ref. [10]. The red dots are given by our theory for $\frac{U}{\Gamma} = 8$ with voltage rescaled to fit with original data in unit of mV. The value of differential conductance (experiment data in black line) is rescaled from $(0.6, 1.3)$ to $(0, 2)$ in unit of $\frac{e^2}{h}$.

occupation out-of-equilibrium and it may have interesting application in quantum computing as we understand more the dephasing mechanism. We have also compared our results with perturbation calculation and experimental measurement of nonlinear differential conductance of a quantum dot.

The major difficulty we encounter by using SBA comes from the single particle phase shift for complex momenta which leads to a breakdown of steady state condition when out of equilibrium. One possible issue resulting in this is the local discontinuity at odd channel s_{op}, the choice we made to enable us to construct a scattering state with fixed particles from lead 1 and lead 2. It can be proved that without this choice we cannot write down fixed number of particles incoming from each lead[50] in this Anderson impurity model and similarly for IRLM. The other issue in the study for Anderson model is whether we shall include all possible bound states in the ground state construction. From the mathematical structure we shall choose 4 type of bound states but the results from charge susceptibility seems to suggest 2 type of bound states is the correct choice. To check whether this is in general correct we plan to come back to study the whole spectrum, which include bound state when Bethe energy higher than impurity level, of IRLM as this model bares structure similarity to the Anderson model described in this article. Following the SBA on

IRLM[16] there are lots of numerical approach and different exact methods[38] developed for this model and detailed comparison for different approaches is desired for better understanding its physics and scaling relation. By learning how to deal with complex momenta in this model we may also find the rule which may lead us to the *exact* expression for current in this Anderson impurity model.

Chapter 4

Two leads Infinite U Anderson model and Kondo model

4.1 Infinite U Anderson model

In the limit of $\frac{U}{\Gamma} \to \infty$ the finite U two-lead Anderson impurity Hamiltonian becomes the two-lead infinite U Anderson model. The latter model is closely related, via the Schrieffer-Wolff transformation[61], to the notorious Kondo model, a model of spin coupled to a Fermi liquid bath. The reason for that is simple: since $U \to \infty$ the charge fluctuations are essentially frozen out and only the spin fluctuations dominate the low-energy physics. We shall come back to this discussion in the latter part of this chapter. The Hamiltonian for infinite U Anderson model is given by

$$\hat{H} = \sum_{i=1,2} \int dx\, \psi^{\dagger}_{i\sigma}(x)(-i\partial_x)\psi_{i\sigma}(x) + \epsilon_d d^{\dagger}_{\sigma} d_{\sigma} + t_i(\psi^{\dagger}_{i\sigma}(0) b^{\dagger} d_{\sigma} + d^{\dagger}_{\sigma} b \psi_{i\sigma}(0)) \tag{4.1}$$

Here the bosonic operator b is introduced to conserve $b^{\dagger}b + \sum_{\sigma} d^{\dagger}_{\sigma} d_{\sigma} = 1$ and by applying the slave boson technique we project out the phase space of double occupancy occurring in finite U case.

4.1.1 Scattering state construction

We first rewrite Eq.(4.1) in the even-odd basis as

$$\begin{aligned}
\hat{H} &= \hat{H}_e + \hat{H}_o \\
\hat{H}_e &= \sum_{\sigma} \int dx\, \psi^{\dagger}_{e\sigma}(x)(-i\partial_x)\psi_{e\sigma}(x) + \epsilon_d d^{\dagger}_{\sigma} d_{\sigma} + \; t(\psi^{\dagger}_{e\sigma}(0) b^{\dagger} d_{\sigma} + d^{\dagger}_{\sigma} b \psi_{e\sigma}(0)) \\
\hat{H}_o &= \sum_{\sigma} \int dx\, \psi^{\dagger}_{o\sigma}(x)(-i\partial_x)\psi_{o\sigma}(x)
\end{aligned}$$

With

$$\begin{aligned}
\psi_{e\sigma}(x) &= \frac{t_1\psi_{1\sigma}(x) + t_2\psi_{2\sigma}(x)}{\sqrt{t_1^2 + t_2^2}} \\
\psi_{o\sigma}(x) &= \frac{t_2\psi_{1\sigma}(x) - t_1\psi_{2\sigma}(x)}{\sqrt{t_1^2 + t_2^2}}
\end{aligned}$$

and $t = \sqrt{t_1^2 + t_2^2}$. In what follows we again consider the case $t_1 = t_2 = \frac{t}{\sqrt{2}}$ for simplicity and defer the discussion for the $t_1 \neq t_2$ case in the IRLM. We show from single particle to two particles solution and show the integrability in the following sections.

single particle solution

The single particle solution for even and odd basis is: $|e, p\sigma\rangle = \int dx\, (e^{ipx} g_p(x)\psi^\dagger_{e\sigma}(x) + e_p \delta(x) d^\dagger_\sigma b)|0\rangle$ and $|o, p\sigma\rangle = \int dx\, e^{ipx} h_p(x)\psi^\dagger_{o\sigma}(x)|0\rangle$, with $|0\rangle$ the vacuum state and $g_p(x)$, $h_p(x)$, e_p independent of spin and given by

$$\begin{aligned} g_p(x) &= \theta(-x) + e^{i\delta_p}\theta(x) + s_{ep}\,\theta(x)\theta(-x)\ , \\ h_p(x) &= \theta(-x) + \theta(x) + s_{op}\,\theta(x)\theta(-x)\ , \\ e_p &= \frac{t(1 + e^{i\delta_p} + s_{ep}/2)}{2(p - \epsilon_d)}\ . \end{aligned} \tag{4.2}$$

Here $\delta_p \equiv 2\tan^{-1}(\frac{\Gamma}{\epsilon_d - p})$ is the single particle scattering phase shift of the electrons off the impurity with $\Gamma \equiv \frac{t^2}{2}$ being the width of the resonance level. We adopted a symmetric regularization scheme $\theta(\pm x)\delta(x) = \frac{1}{2}\delta(x)$ and imposed $|p| \leq D$, D being the bandwidth cut-off [49]. The $s(x) = \theta(x)\theta(-x)$ term is a local constant ($\partial_x s(x) = 0$) in this scheme and it is included in the odd channel function to allow the same two particle S-matrices, Eq.(4.19), in all channels[50]. The $\theta(x)\theta(-x)$ term in the even channel wave function is introduced in order to modify the single particle phase shift across the impurity. The choice of s_{op} and s_{ep} will be addressed later. In the lead basis, $|i, p\sigma\rangle$, the single-particle scattering eigenstates with the incoming particle incident from lead i, can be restored by taking a proper linear combination of even-odd states. For example, $|1, p\sigma\rangle = \frac{1}{\sqrt{2}}(|e, p\sigma\rangle + |o, p\sigma\rangle)$ is written as

$$|1, p\sigma\rangle = \int dx\, e^{ipx}\Big\{[\theta(-x) + \frac{1}{2}(e^{i\delta_p}+1)\theta(x)]\psi^\dagger_{1\sigma}(x) + \frac{1}{2}(e^{i\delta_p}-1)\theta(x)\psi^\dagger_{2\sigma}(x) + e_p d^\dagger_\sigma b\delta(x) + s^\dagger_{1p\sigma}(x)\Big\}|0\rangle \tag{4.3}$$

with $|2, p\sigma\rangle = \frac{1}{\sqrt{2}}(|e, p\sigma\rangle - |o, p\sigma\rangle)$ and $s^\dagger_{ip\sigma}(x)$ related to the $\theta(x)\theta(-x)$ terms. These states have a single incoming particle ($x < 0$) from lead i, that is reflected back into lead i with amplitude, $R_p = (e^{i\delta_p} + 1)/2$ and transmitted to the opposite lead with amplitude $T_p = (e^{i\delta_p} - 1)/2$. Similar single particle states are discussed in the finite U Anderson model.

From two particles solution to multi particles solution

The multi-particle Bethe-Ansatz wave-function is constructed by means of the two-particle S-matrix, $S(p,k)$, describing the scattering of two electrons with momenta p and k. The two-particles solution in spin singlet state takes the following form

$$|ik,\uparrow;jp,\downarrow\rangle = \int dx_1 dx_2 A\{e^{i(kx_1+px_2)} Z_{kp}(x_1-x_2)\alpha^\dagger_{ik,\uparrow}(x_1)\alpha^\dagger_{jp,\downarrow}(x_2)\}|0\rangle$$

Here $\int dx e^{ik_i x}\alpha^\dagger_{ik_i,a_i}(x_i) = |ik_i,a_i\rangle$ with the exception that there is no $d^\dagger_\uparrow d^\dagger_\downarrow b b^\dagger$ term due to Pauli exclusion. The explicit form for this two particles case is derived in the following. For the two particles solution we follow similar construction in P Scholotman's work[65] and the Scattering Bethe Ansatz approach developed by P. Mehta and N. Andrei[16]. Since Eq.(4.1) is rotational invariant the spin quantum number is conserved. We show the solution with both particles with spin singlet incoming from lead 1 as an example in the following. Spin quantum number in z direction S_z is a good quantum number and we can write the two particle solution of $S_z = 0$ state as:

$$|\Psi\rangle = \{\int dx_1 dx_2 \{Ag(x_1,x_2)\psi^\dagger_{e\uparrow}(x_1)\psi^\dagger_{e\downarrow}(x_2) + Ch(x_1,x_2)\psi^\dagger_{o\uparrow}(x_1)\psi^\dagger_{o\downarrow}(x_2) + Bj(x_1,x_2)(\psi^\dagger_{e\uparrow}(x_1)\psi^\dagger_{o\downarrow}(x_2)$$
$$-\psi^\dagger_{e\downarrow}(x_1)\psi^\dagger_{o\uparrow}(x_2))\} + \int dx (Ae(x)(\psi^\dagger_{e\uparrow}(x)d^\dagger_\downarrow - \psi^\dagger_{e\downarrow}(x)d^\dagger_\uparrow)b + Bo(x)(\psi^\dagger_{o\uparrow}(x)d^\dagger_\downarrow - \psi^\dagger_{o\downarrow}(x)d^\dagger_\uparrow))b\}|0\rangle$$

Here A, B, C are arbitrary constants to be determined later. To satisfy $\hat{H}|\Psi\rangle = E|\Psi\rangle = (k+p)|\Psi\rangle$ we have:

$$[-i(\partial_{x_1}+\partial_{x_2}) - E]g(x_1,x_2) + t[\delta(x_1)e(x_2) + \delta(x_2)e(x_1)] = 0 \tag{4.4}$$

$$[-i(\partial_{x_1}+\partial_{x_2}) - E]h(x_1,x_2) = 0 \tag{4.5}$$

$$[-i(\partial_{x_1}+\partial_{x_2}) - E]j(x_1,x_2) + t[\delta(x_1)o(x_2)] = 0 \tag{4.6}$$

$$(-i\partial_x - E + \epsilon_d)e(x) + tg(0,x) = 0 \tag{4.7}$$

$$(-i\partial_x - E + \epsilon_d)o(x) + tj(0,x) = 0 \tag{4.8}$$

We derive the solution of this form

$$g(x_1,x_2) = Z_{kp}(x_1-x_2)g_k(x_1)g_p(x_2) + Z_{kp}(x_2-x_1)g_k(x_2)g_p(x_1) \tag{4.9}$$

Plug Eq.(4.9) into Eq.(4.4) we get

$$e(x) = Z_{kp}(-x)g_p(x)e_k + Z_{kp}(x)g_k(x)e_p \tag{4.10}$$

Plugging above two results into Eq.(4.7) we get

$$(-i\partial_x Z_{kp}(-x))g_p(x)e_k + (-i\partial_x Z_{kp}(x))g_k(x)e_p - tZ_{kp}(-x)e_p\delta(x)e_k - tZ_{kp}(x)e_k\delta(x)e_p = 0 \tag{4.11}$$

Now take $Z_{kp}(x) = e^{-i\phi_{kp}}\theta(-x) + e^{i\phi_{kp}}\theta(x)$ we get

$$\tan(\phi_{kp}) = \frac{t^2}{k-p}.$$

From Eq.(4.5) we can write $h(x_1, x_2)$ as:

$$h(x_1, x_2) = Z^{oo}_{kp}(x_1 - x_2)h_k(x_1)h_p(x_2) + Z^{oo}_{kp}(x_2 - x_1)h_k(x_2)h_p(x_1) \tag{4.12}$$

with arbitrary $Z^{oo}_{kp}(x_1 - x_2)$. Now write $j(x_1, x_2)$ as:

$$j(x_1, x_2) = Z^{eo}_{kp}(x_1 - x_2)g_k(x_1)h_p(x_2) + Z^{eo}_{kp}(x_2 - x_1)h_k(x_2)g_p(x_1) \tag{4.13}$$

again with $Z^{eo}_{kp}(x_1 - x_2)$ undetermined. Plug Eq.(4.13) into Eq.(4.6) we get $o(x)$ is written as:

$$o(x) = Z^{eo}_{kp}(-x)h_p(x)e_k + Z^{eo}_{kp}(x)h_k(x)e_p \tag{4.14}$$

Now if we choose $Z^{eo}_{kp}(x_1 - x_2) = Z_{kp}(x_1 - x_2)$ and plug Eq.(4.13) and Eq.(4.14) into Eq.(4.8) we get:

$$\begin{aligned}&(-k + \epsilon_d)Z_{kp}(-x)h_p(x)e_k + (-p + \epsilon_d)Z_{kp}(x)h_k(x)e_p + t(Z_{kp}(-x)h_p(x)g_k(0) + Z_{kp}(x)h_k(x)g_p(0))\\ &+(-i)(\partial_x Z_{kp}(-x))h_p(x)e_k + (-i)(\partial_x Z_{kp}(x))h_k(x)e_p = -2\sin(\phi_{kp})(h_p(0)e_k - h_k(0)e_p) = 0\end{aligned} \tag{4.15}$$

To satisfy Eq.(4.15) we can set $h_p(0) = 0$ for arbitrary p. This can be done by choosing $s_{op} = -4$ in Eq.(4.3). Now since $Z^{oo}_{kp}(x_1 - x_2)$ is arbitrary we can choose $Z^{oo}_{kp}(x_1 - x_2) = Z_{kp}(x_1 - x_2)$. Since the Hamiltonian in Eq.(4.1) has rotational invariance the general form of scattering matrix for particles

with momentum k, p and spins σ_1, σ_2 is given by:

$$S^{\sigma_1^{'}\sigma_2^{'}}_{\sigma_1\sigma_2}(k,p) = b(k,p) + c(k,p)\hat{P}_{12} \tag{4.16}$$

where $\hat{P}_{12} = \frac{1}{2}(1 \cdot 1 + \vec{\sigma_1} \cdot \vec{\sigma_2})$ is the permutation operator in spins. For antiparallel spins (singlet state) as shown above $\hat{P}_{12} = -1$. Denote $\Gamma = \frac{t^2}{2}$ we have:

$$b(k,p) - c(k,p) = \frac{Z_{kp}(x>0)}{Z_{kp}(x<0)} = \frac{k-p-i2\Gamma}{k-p+i2\Gamma} \tag{4.17}$$

For the triplet state ($\hat{P}_{12} = 1$) the interaction term with the impurity is absent and the particles passing through each other without changing their phase

$$b(k,p) + c(k,p) = 1 \tag{4.18}$$

Thus from Eq.(4.17) and Eq.(4.18) we get the two particle S-matrix as:

$$\hat{S}(k,p) = \frac{(k-p)\mathrm{I}_{\tau,\tau'} + i2\Gamma\mathrm{P}_{\tau,\tau'}}{(k-p)+i2\Gamma} \tag{4.19}$$

In general we denote the $\hat{S}(k_i,k_j)$ as $\mathrm{S}^{a_i a_i^{'}}_{a_j a_j^{'}}(k_i,k_j)$ with a_i denotes the spin index before the scattering and $a_i^{'}$ the spin index after the scattering. These matrices satisfy the Yang-Baxter equations

$$\begin{aligned}&\mathrm{S}^{a_1 a_1^{'}}_{a_2 a_2^{'}}(k_1,k_2)\mathrm{S}^{a_1 a_1^{'}}_{a_3 a_3^{'}}(k_1,k_3)\mathrm{S}^{a_2 a_2^{'}}_{a_3 a_3^{'}}(k_2,k_3)\\ &= \mathrm{S}^{a_2 a_2^{'}}_{a_3 a_3^{'}}(k_2,k_3)\mathrm{S}^{a_1 a_1^{'}}_{a_3 a_3^{'}}(k_1,k_3)\mathrm{S}^{a_1 a_1^{'}}_{a_2 a_2^{'}}(k_1,k_2)\end{aligned}$$

Thus the integrability of two leads with infinite U Anderson type dot system is similar to the integrability of one lead infinite U Anderson model.

The choice of identical two particles S-matrices (by choosing $s_{op} = -4$; the choice of s_{ep} will be discussed later and does not affect the result here) enables us to construct the scattering state labeled by lead indices by choosing appropriate A, B, C in this even-odd basis. For example, if both particles are coming from lead 1, we shall choose $(A,B,C) = A_0(\frac{t^2}{t_2^2}, \frac{-t^2}{t_1 t_2}, \frac{t^2}{t_1^2})$ such that the amplitude of incoming state from lead 2 is zero (A_0 being an overall renormalization constant). We can therefore label the eigenstate by the incoming state from lead i and/or lead j. Without this

s_{op} term we cannot write back from even-odd basis to lead indices basis in this two leads infinite U Anderson model.

Since the S-matrix is the same for all even-odd combinations the S-matrix does not depend on the lead index i, and the number of electrons in a lead, N_i, can change only at the impurity site. This circumstance allows us to construct the fully-interacting eigenstates of our Hamiltonian characterized by the incoming quantum numbers, N_1 and N_2 the numbers of incident electrons from lead 1 and 2 respectively. These quantum numbers are subsequently determined by the chemical potentials μ_1 and μ_2. This leads us to the topic of fixing these momenta distribution by imposing the asymptotic boundary condition in the next section.

4.2 Asymptotic boundary condition: Distribution of Bethe momenta

The corresponding Bethe momenta distribution function for the infinite U Anderson model is given by

$$2\sigma(\Lambda) = \frac{1}{\pi} - \int_{-\infty}^{B_2} d\Lambda' K(\Lambda - \Lambda')\sigma(\Lambda') - \int_{-\infty}^{B_1} d\Lambda' K(\Lambda - \Lambda')\sigma(\Lambda') \tag{4.20}$$

with $K(\Lambda) = \frac{1}{\pi}\frac{2\Gamma}{(2\Gamma)^2+(\Lambda-\Lambda')^2}$.

Eq. (4.20) can be derived directly following the same procedures as in the finite U Anderson model by taking $U \to \infty$. We shall sketch the derivation of this equation in the following.

The two particle S-matrix derived by solving two particles scattering eigenstate takes the form

$$\hat{S}(k,p) = \frac{k - p - i\hat{P}t^2}{k - p - it^2} \tag{4.21}$$

By using quantum inverse scattering method we solve the eigenstate of quasi particle momenta and spin rapidity by

$$e^{ik_j^l L} = \prod_{\alpha=1}^{M} \frac{k_j^l - \Lambda_\alpha - i\frac{t^2}{2}}{k_j^l - \Lambda_\alpha + i\frac{t^2}{2}} \tag{4.22}$$

$$\prod_{l=R,L}\prod_{j=1}^{N_l} \frac{k_j^l - \Lambda_\alpha + i\frac{t^2}{2}}{k_j^l - \Lambda_\alpha - i\frac{t^2}{2}} = \prod_{\beta\neq\alpha}^{M} \frac{\Lambda_\alpha - \Lambda_\beta - it^2}{\Lambda_\alpha - \Lambda_\beta + it^2} \tag{4.23}$$

The ground state is composed by real Λ_i and complex k_j^l with bound state momenta given by

$k^{\pm} = \Lambda \pm it^2/2$ obtained by taking poles or zeros of Eq.(4.21). For two leads with different number of particles (due to different chemical potentials) where total energy is given by $\sum_{jl} k_j^l = \sum_{\alpha=1}^{M} 2\Lambda_\alpha$ with $S = \frac{N}{2} - M = 0$ we shall find the appropriate distribution function for the bound state momenta which describes two free electron baths. With that in mind let us first write down the Eq.(4.22,4.23) for bound state infinite U case:

$$e^{ik_\alpha^+ L} = \prod_{\beta=1}^{M} \frac{\Lambda_\alpha - \Lambda_\beta + \gamma_\alpha^+}{\Lambda_\alpha - \Lambda_\beta + it^2} \tag{4.24}$$

$$e^{ik_\alpha^- L} = \prod_{\beta=1}^{M} \frac{\Lambda_\alpha - \Lambda_\beta - it^2}{\Lambda_\alpha - \Lambda_\beta + \gamma_\alpha^-} \tag{4.25}$$

$$\prod_{\beta=1}^{M} \frac{\Lambda_\beta - \Lambda_\alpha + \gamma_\beta^+}{\Lambda_\beta - \Lambda_\alpha + \gamma_\beta^-} = 1 \tag{4.26}$$

Thus multiplication of Eq.(4.24) and Eq.(4.25) gives rise to

$$e^{2i\Lambda_\alpha} = \prod_{\beta=1}^{M} \frac{\Lambda_\alpha - \Lambda_\beta - it^2}{\Lambda_\alpha - \Lambda_\beta + it^2} \tag{4.27}$$

Taking the logarithm of Eq.(4.27) and denoting $\Gamma = \frac{t^2}{2}$ we have:

$$2\pi J_\alpha = -2\Lambda_\alpha L + \sum_\beta (2\theta_2(\frac{\Lambda_\alpha - \Lambda_\beta}{2\Gamma}) + \pi) \tag{4.28}$$

Now take the thermodynamic limit and follow the same argument as the finite U case we have the continuous form of infinite U Anderson model as

$$2\sigma(\Lambda) = \frac{1}{\pi} + \frac{1}{\pi}\int_{-\infty}^{B_2} d\Lambda' 2\sigma(\Lambda') \frac{2\Gamma}{(2\Gamma)^2 + (\Lambda - \Lambda')^2} + \frac{1}{\pi}\int_{B_2}^{B_1} d\Lambda' \sigma(\Lambda') \frac{2\Gamma}{(2\Gamma)^2 + (\Lambda - \Lambda')^2} \tag{4.29}$$

Solving this Fredholm equation can give us the Λ distribution.

It can also be derived from the finite U result, Eq. (3.36), by taking the large U limit ($U \gg \epsilon_d$,

$U \gg \Gamma$):

$$\begin{aligned}
\frac{x(\lambda)}{U} &\rightarrow \frac{1}{2} - \sqrt{\frac{\frac{\lambda}{U^2}+\frac{1}{4}+\sqrt{(\frac{\lambda}{U^2}+\frac{1}{4})^2+\frac{\Gamma^2}{U^2}}}{2}} \\
&\rightarrow \frac{1}{2} - \sqrt{\frac{\frac{\lambda}{U^2}+\frac{1}{4}+|\frac{\lambda}{U^2}+\frac{1}{4}|}{2}} \\
&\rightarrow \frac{1}{2} - \frac{1}{2}(1+\frac{2\lambda}{U^2}+\ldots) \rightarrow -\frac{\lambda}{U^2} = \frac{\Lambda}{U}
\end{aligned} \tag{4.30}$$

$$\begin{aligned}
\frac{y(\lambda)}{U} &\rightarrow \sqrt{\frac{-(\frac{\lambda}{U^2}+\frac{1}{4})+((\frac{\lambda}{U^2}+\frac{1}{4})^2+\frac{\Gamma^2}{U^2})^{1/2}}{2}} \\
&\rightarrow \sqrt{\frac{(\frac{\lambda}{U^2}+\frac{1}{4})(-1+(1+\frac{(\frac{\Gamma}{U})^2}{(\frac{\lambda}{U^2}+\frac{1}{4})^2})^{1/2})}{2}} \\
&\rightarrow \left(\frac{1}{4}\frac{(\frac{\Gamma}{U})^2}{\frac{1}{4}}\right)^{1/2} + \mathcal{O}(U^{-2}) \simeq \frac{\Gamma}{U}
\end{aligned} \tag{4.31}$$

with $\Lambda \equiv -\frac{\lambda}{U}$.

4.3 Dot occupation and current: pSBA

Similar procedures as in evaluating dot occupation for finite U Anderson model give the matrix element $\nu_\infty^{SBA}(\Lambda)$ for the dot occupation in the infinite U Anderson model in equilibrium to be

$$\nu_\infty^{SBA}(\Lambda) = \frac{2\Gamma}{(\Lambda-\epsilon_d)^2+(2\Gamma)^2} \ . \tag{4.32}$$

In going to the out-of-equilibrium regime ($\mu_1 \neq \mu_2$) we follow the same phenomenological method (pSBA) as for the finite U case. The result for the spin-fluctuation and charge-fluctuation contributions to the dot occupation are given by

$$\begin{aligned}
\nu_\infty^s(\Lambda) &= \frac{1}{\Gamma}\left(1 - \frac{\epsilon_d-\Lambda}{\sqrt{(\epsilon_d-\Lambda)^2+4\Gamma^2}}\right) \\
\nu_\infty^h(\Lambda) &= \frac{2\Gamma}{(\Lambda-\epsilon_d)^2+(2\Gamma)^2} \ .
\end{aligned} \tag{4.33}$$

Note that in this case it seems to suffice the equilibrium dot occupation condition by just choosing the charge fluctuation part. This part alone, however, misses the Kondo physics which shall always occur when the dot level is below the Fermi surface in equilibrium regime. In what follows we assume

the necessity of introducing both spin and charge fluctuation part by its analogy with finite U case.

4.3.1 Dot occupation in equilibrium

We check the consistency with the exact result for the dot occupation in equilibrium, namely

$$\begin{aligned}\langle\sum_{\sigma} d_{\sigma}^{\dagger} d_{\sigma}\rangle &= 4\int_{D}^{B} d\Lambda\ \sigma_b(\Lambda)\nu_{\infty}^{SBA}(\Lambda) \\ &= 4\int_{D}^{B} d\Lambda\ \sigma_b(\Lambda)(\nu_{\infty}^{s}(\Lambda)f_s^{\infty}(\Lambda) + \nu_{\infty}^{h}(\Lambda)f_h^{\infty}(\Lambda))\ .\end{aligned}$$

Here D is related to the bandwidth and B is determined by the equilibrium Fermi energy $\mu_1 = \mu_2 = 0$. $f_s^{\infty}(\Lambda) = \frac{D_s^{\infty}(\Lambda)}{D_s^{\infty}(\Lambda)+D_h^{\infty}(\Lambda)}$ and $f_h^{\infty}(\Lambda) = \frac{D_h^{\infty}(\Lambda)}{D_s^{\infty}(\Lambda)+D_h^{\infty}(\Lambda)}$. $D_s^{\infty}(\Lambda)$, the spinon density, and $D_h^{\infty}(\Lambda)$, the holon density, are expressed as

$$D_s^{\infty}(\Lambda) = \frac{T_k^{\infty}/\pi}{(\Lambda - B)^2 + (T_k^{\infty})^2} \tag{4.34}$$

$$D_h^{\infty}(\Lambda) = \frac{2\Gamma}{(\Lambda - B - \epsilon_d)^2 + (2\Gamma)^2}. \tag{4.35}$$

Here the Kondo scale T_k^{∞} used in $f_s(\Lambda)$ takes the form[62]

$$T_k^{\infty} = \frac{\sqrt{10|D|\Gamma}}{\pi} e^{-\pi\frac{|\epsilon_d|}{\Gamma}}\ .$$

Here we digress from the main topic and discuss the spinon and holon density in the infinite Anderson U model.

Discussion on spinon and holon density

Following the idea of N. Kawakami and Okiji in Ref.[47] we carry out the computation for spinon and holon density and their respective excitation energy in the following. First let us compute the spinon and holon excitation energy and compare them with the dressed energy of a bounded pair derived from iterations of *charge free energy*.

The spinon energy is given by the sum of the bare energy of adding/removing ($\pm$ for k value) a single quasi-particle with Bethe momenta k and the back flow energy from other electrons within the bath due to this change:

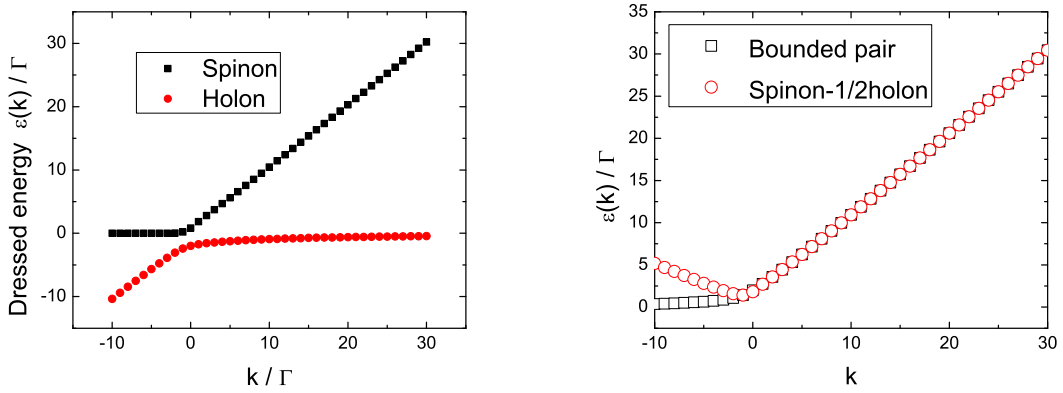

Figure 4.1: Left: $\epsilon_s(k)$ vs k (black square) and $\epsilon_h(k)$ vs k (red circle). The symbol in the main text for bare energy is Λ_0 but changed to k for convenience. $\frac{D}{\Gamma} = -100$ and $\frac{\epsilon_d}{\Gamma} = -5$. Right: $\epsilon(k)$ vs k (black empty square) and $\epsilon_s(k) - 0.5\epsilon_h(k)$ vs k (red empty circle) with same sets of parameters.

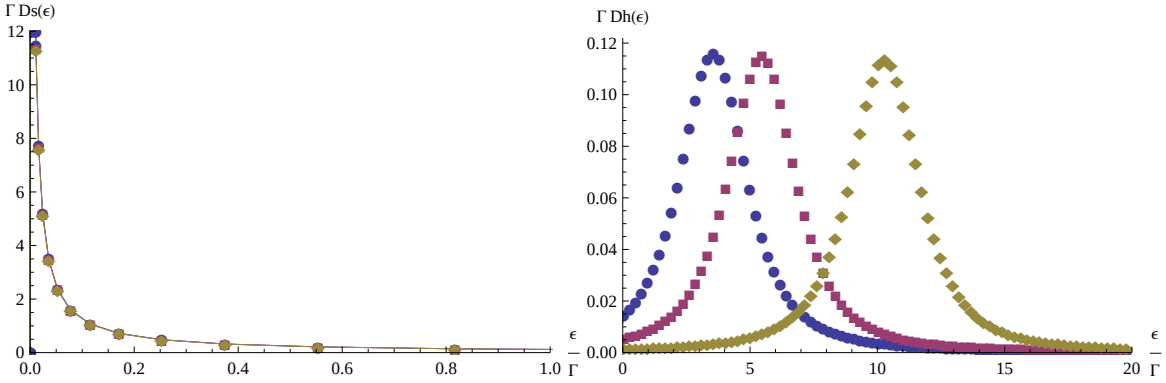

Figure 4.2: Left: $\Gamma D_s(\epsilon)$ vs $\frac{\epsilon}{\Gamma}$ with $\frac{D}{\Gamma} = -100$ and $\frac{\epsilon_d}{\Gamma} = -3, -5, -10$ (blue,purple,brown lines). Right:$\Gamma D_h(\epsilon)$ vs $\frac{\epsilon}{\Gamma}$ with $\frac{D}{\Gamma} = -100$ and $\frac{\epsilon_d}{\Gamma} = -3, -5, -10$ (blue,purple,brown dots). Equilibrium chemical potential is chosen at zero.

$$\epsilon_s(k) = \pm k + \int_D^B 2\sigma_b^s(\Lambda, k)\Lambda d\Lambda \tag{4.36}$$

with back flow density for spinon $\sigma_b^s(\Lambda, k)$ given by

$$\sigma_b^s(\Lambda, k) = \frac{\pm 1}{\pi} \frac{(\Gamma/2)^2}{(\Lambda - k)^2 + (\Gamma/2)^2} - \int_D^B \sigma_b^s(\Lambda', k) K(\Lambda, \Lambda') d\Lambda'. \tag{4.37}$$

The holon energy is given by the sum of the bare energy of adding/removing a pair of quasi-particles with Bethe momenta $2\Lambda_0$ (coming from bare energy of a bounded pair of $k^{\pm} = \Lambda_0 \pm i\Gamma$) and the

back flow energy from other electrons within the bath due to this change:

$$\epsilon_h(\Lambda_0) = \pm 2\Lambda_0 + \int_D^B 2\sigma_b^h(\Lambda, \Lambda_0)\Lambda d\Lambda \tag{4.38}$$

with back flow density for holon $\sigma_b^h(\Lambda, \Lambda_0)$ given by

$$\sigma_b^h(\Lambda, \Lambda_0) = \mp(\delta(\Lambda - \Lambda_0) + \frac{1}{\pi}\frac{\Gamma^2}{(\Lambda - \Lambda_0)^2 + \Gamma^2}) - \int_D^B \sigma_b^h(\Lambda', \Lambda_0)K(\Lambda, \Lambda')d\Lambda'. \tag{4.39}$$

In the left figure of Fig.(4.1) both spinon and holon dressed energy are plotted as a function of bare energy above/below the equilibrium Fermi surface. The equilibrium Fermi surface in bare Bethe momenta is chosen at $B = 0$ and the lower bound is set at $\frac{D}{\Gamma} = -100$. The impurity level is fixed at $\frac{\epsilon_d}{\Gamma} = -5$. From this plot we can see that for bare energy higher than the impurity level the dominant fluctuation is in the spinon sector. For bare energy less than the impurity level the dominant fluctuation is in the holon sector.

Another interesting thing to compare is the dressed energy for adding/removing one electron in the incoming state. The dressed energy for adding/removing one electron from a pair in singlet state (the groud state is formed by many singlet states) is given by

$$\epsilon(k) = k - 2\int_D^B \epsilon(\Lambda)K(\Lambda, k)d\Lambda \tag{4.40}$$

which is derived from iterating the bare energy in the expression for the *charge free energy*. From the right figure of Fig.(4.1) we can see that this dressed energy is roughly equaled to dressed energy of spinon minus half of the dressed energy of holon. In the other words this provide a numerical evidence for the assumption that *electron* $\simeq$ *spinon+half of antiholon* above the Fermi surface. This assumption seems to work better for infinite U Anderon model than the finite U Anderson model.

The density of state for spinon and holon, denoted as $D_s^\infty(\epsilon_s)$ and $D_h^\infty(\epsilon_h)$ respectively, are defined by

$$D_s^\infty(\epsilon_s) = \frac{\delta J_0}{\delta \epsilon_s} = \frac{\frac{\delta J_0}{\delta k}}{\frac{\delta \epsilon_s}{\delta k}}$$

and

$$D_s^\infty(\epsilon_h) = \frac{\delta I_0}{\delta \epsilon_h} = \frac{\frac{\delta I_0}{\delta k}}{\frac{\delta \epsilon_h}{\delta k}}$$

. Here J_0 and I_0 represent the integers corresponding to the added/removed bare momenta k in

the case of spinon and holon excitation. These density of state as a function of respective dressed energy are shown in Fig.4.2. From the left figure of Fig.4.2 the spinon density essentially diverges at $\epsilon \simeq 0$ and the numerical results at Fermi surface is not very precise. We may, however, try to approximate this spinon density of state by a simple form as in Eq.(4.35) with Kondo scale T_k^∞ given by thermodynamic scaling relation which gives a rough estimate of the width of the divering peaks nearby equilibrium Fermi surface. By the same token we may approximate the holon density of state by Eq.(4.35). The right figure of Fig.4.2 actually shows the anti-holon density of state as the energy axis in the plot has been flipped, but we call it holon density based on the convention in the literature. The main feature of this holon density of state is that it has a Lorentzian-like structure nearby $\epsilon \simeq \epsilon_d$ with a width controlled by Γ. Notice that the height of holon density is scaled up by a factor of π in the Eq.(4.35) compared with the numerical results shown in the right figure of Fig.4.2.

The idea of the pSBA is to take both spin-fluctuation and charge-fluctuation into consideration when dicussing the phase shift of electrons through the impurity. Thus the distribution functions $f_s(\epsilon)$ and $f_h(\epsilon)$ are intrdocued to account for the weight in each part. We have also made further approximations by assuming the bare energy is sufficient good to approximate the bare energy, or $\Lambda \simeq \epsilon(\Lambda)$, for practical numerical computation. We check the validity of these assumptions by comparing our pSBA results in equilibrium with the exact dot occupation evaluated by TBA in the following subsection.

4.3.2 Consistency check in equilibrium

The results for the dot occupation and Friedel sum rule check in the infinite U case are shown in Fig.4.3. Again we see a nice match between our phenomenological approach and the exact result for $|\frac{\epsilon_d}{\Gamma}| \neq 0$ and some mismatch in the mixed valence region $|\frac{\epsilon_d}{\Gamma}| \simeq 0$. This is consistent with the results for finite U.

The corresponding spin and charge fluctuation matrix element for current, $J^s_\infty(\Lambda)$ and $J^h_\infty(\Lambda)$, are given by

$$\begin{aligned} J^s_\infty(\Lambda) &= 1 - \frac{\epsilon_d - \Lambda}{\sqrt{(\epsilon_d - \Lambda)^2 + 4\Gamma^2}} \\ J^h_\infty(\Lambda) &= \frac{2\Gamma^2}{(\Lambda - \epsilon_d)^2 + (2\Gamma)^2} \end{aligned} \tag{4.41}$$

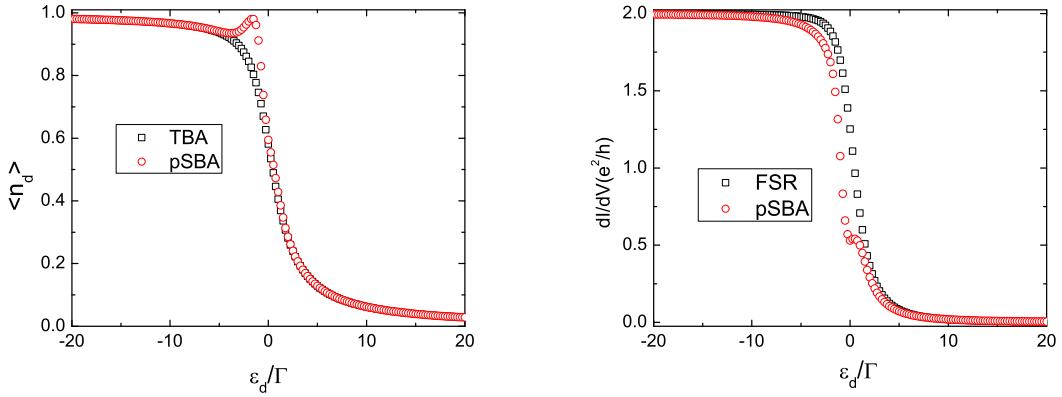

Figure 4.3: Left: $\langle \hat{n}_d \rangle$ vs $\frac{\epsilon_d}{\Gamma}$ for exact TBA result and pSBA. Right: Linear response conductance $dI/dV|_{V\to 0}$ vs $\frac{\epsilon_d}{\Gamma}$ for exact result (FSR) and pSBA in the infinite U Anderson model. $\frac{D}{\Gamma} = -100$. Similar to the case of finite U the comparison nearby mixed valence region ($\epsilon_d \simeq 0$) is poorer.

The current expectation value is given by

$$\langle \hat{I} \rangle = \frac{2e}{\hbar} \int_{B_2}^{B_1} d\Lambda \sigma(\Lambda) (J^s_\infty(\Lambda) f^\infty_s(\Lambda) + J^h_\infty(\Lambda) f^\infty_h(\Lambda))$$

where B_1 and B_2 are related to μ_1 and μ_2 by minimizing charge free energy F

$$F = 2 \left(\int_D^{B_1} d\Lambda \, \sigma(\Lambda)(\Lambda - \mu_1) + \int_D^{B_2} d\Lambda \, \sigma(\Lambda)(\Lambda - \mu_2) \right) .$$

Before we proceed to discuss the numerical results for current vs voltage in this infinite U model let us look at the structure of $J^s_\infty(\Lambda)$ and $J^h_\infty(\Lambda)$ as a function of Λ as shown in Fig. 4.4. Λ here represents the bare energy of the quasi-particle and plays the same role as $x(\lambda)$ in the finite U Anderson model. $J^s_\infty(\Lambda)$ alone would reproduce the main feature in the Friedel sum rule for $\epsilon_d \ll 0$. In this region the linear response conductance comes mainly from the spin fluctuations. The left figure of Fig. 4.4 fixes ϵ_d and shows $J^s_\infty(\Lambda)$ vs Λ. We may also fix $\Lambda = 0$ (in the sense of choosing the equilibrium Fermi surface energy at $\Lambda = 0$) and plot $J^s_\infty(\epsilon_d)$ vs ϵ_d as shown in the right figure of Fig. 4.4. In this way we can see that $J^s_\infty(\epsilon_d)$ vs ϵ_d reproduces the overall structure of the linear response conductance from the Kondo region ($\epsilon_d \leq 0$) to the mixed valence regime ($\epsilon_d \simeq 0$). Therefore we identify the phase shift $\frac{\delta_{p^+} + \delta_{p^-}}{2}$, contributing to $J^s_\infty(\Lambda)$, as the phase shift related to spin-fluctuation.

$J^h_\infty(\Lambda)$ gives a Lorentz shape in bare energy scale Λ. This structure is akin to the charge

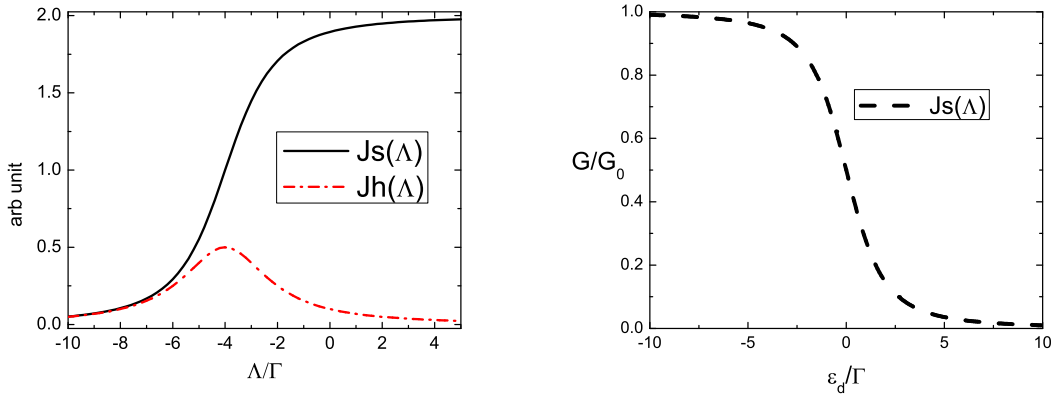

Figure 4.4: Left: $J_s(\Lambda)$ and $J_h(\Lambda)$ vs Bethe momenta Λ (scaled by Γ) in infinite U Anderson model. $\frac{\epsilon_d}{\Gamma} = -4$ in this graph. Similar graph appears for finite U case with x-axis replaced by real part of Bethe momenta $x(\lambda)$. Right: $J_s(\Lambda = 0)$ vs ϵ_d by fixing the chemical potential at $B_1 = B_2 = 0$ and changing ϵ_d. It shows the main feature of Friedel sun rule.

fluctuation side peak with peak position at energy scale around ϵ_d as seen from lower plot of Fig. 4.4. Thus we identify the phase shift $\delta_{p^+} + \delta_{p^-}$, contributing to $J^h_\infty(\Lambda)$, as the phase shift related to charge-fluctuation. These structures also apply to the case of the finite U Anderson model.

4.3.3 Out of equilibrium results

Now let us discuss the out of equilibrium numerical results. The voltage is again driven asymmetrically by fixing $\mu_1 \simeq 0$ and lowering μ_2. The *exact* dot occupation vs voltage for different ϵ_d for infinite U and $U = 0$, $\frac{\epsilon_d}{\Gamma} = -6$ case (black dots) are shown in Fig. 4.5. We see again the dot occupation decreases slowly at low voltage and develops an abrupt drop at a voltage scale corresponding to impurity level ϵ_d. Also notice the apparent difference between the $U = 0$ plot (black dots) and the $U \to \infty$ case (red dots) and for the same value of $\frac{\epsilon_d}{\Gamma}$. For $U \to \infty$, the dot occupation at large voltage is around 0.65 for $\frac{\epsilon_d}{\Gamma} \ll 0$ which is consistent with the result of the finite U case when $\frac{U}{\Gamma}$ is large (cf. Chap 2 section??). In contrast the non-interacting case ($U = 0$) shows that $\langle n_d \rangle \to 0.5$ at large bias. The *phenomenological* current vs voltage and the corresponding differential conductance vs voltage are plotted in the top figure of Fig. 4.6. Again we see the zero bias anomaly and a broad charge fluctuation side peak in the differential conductance vs voltage. The scaling relation of differential conductance vs voltage expected in small voltage region can also be extracted by rescaling

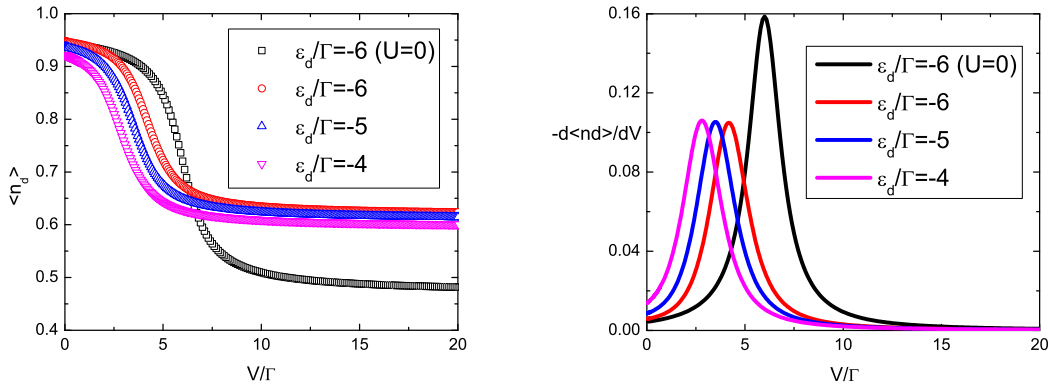

Figure 4.5: Left:$\langle \hat{n}_d \rangle$ vs $\frac{V}{\Gamma}$ in infinite U Anderson model (for Red, Blue, and Purple dots. The Black dots are $U = 0$ case shown for comparison). Right: $-\partial \langle \hat{n}_d \rangle \partial V$ vs $\frac{V}{\Gamma}$ in infinite U Anderson model (for Red, Blue, and Purple lines corresponding to $\frac{\epsilon_d}{\Gamma} = -6, -5, -4$. The Black line is $U = 0$ and $\frac{\epsilon_d}{\Gamma} = -6$ case shown for comparison). $\frac{D}{\Gamma} = -100$ in these graphs.

the voltage by $T_k^{\infty *}$ as shown in bottom figure of Fig. 4.6. Here $T_k^{\infty *}$ is given by

$$T_k^{\infty *} = \frac{\sqrt{10|D|\Gamma}}{\pi} e^{-\pi \frac{|\epsilon_d|}{2\Gamma}} \ .$$

Notice this $T_k^{\infty *}$ differs from T_k^{∞} with a factor of two within the exponent. This factor of two difference represents the difference in the curvature of the parabola as function of ϵ_d (the logarithm of half width at half maximum of the Kondo peak vs ϵ_d shows parabolic curve as in inset of Fig. 3.6 for finite U case). This factor of two ratio bears even closer resemblance to the results shown in Ref. [9]. Note that in bottom figure of Fig. 4.6 the positions of the side peak are different and show no universality in that region. It shows universality for $\frac{V}{T_k^*} \leq 1$.

4.4 Kondo model

For infinite U Anderson model the phase space of doubly occupied state is projected out from the finite U Anderson model. We can represent the mulitparticle eigenstate as ϕ_0 and ϕ_1, characterizing zero dot electron and one dot electron state. If the ground state of the system is described by one dot electron state such as the case of Kondo model, we could express the Schordinger equation in

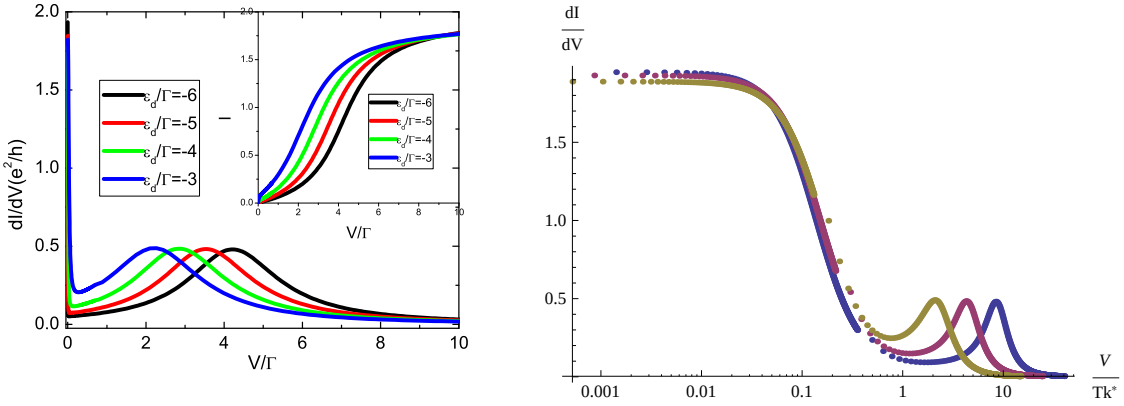

Figure 4.6: Left: $\frac{dI}{dV}$ vs $\frac{V}{\Gamma}$ in infinite U Anderson model. Inset shows the $I-V$ curves for these parameters. $\frac{D}{\Gamma}=-100$ in this graph. Right: $\frac{dI}{dV}$ vs $\frac{V}{T_k^*}$ shows the scaling relation nearby zero voltage for $\frac{\epsilon_d}{\Gamma}=-6,-5,-4$ (Blue, Purple, Brown).

the form

$$\begin{bmatrix} H_{00} & H_{01} \\ H_{10} & H_{11} \end{bmatrix} \begin{bmatrix} \phi_0 \\ \phi_1 \end{bmatrix} = E \begin{bmatrix} \phi_0 \\ \phi_1 \end{bmatrix} \tag{4.42}$$

Here $H_{nn'}=P_nHP_{n'}$ and P_n is a projection operator on to the subspace with dot electron occupation n. For example, $P_0=(1-n_{d,\uparrow})(1-n_{d,\downarrow})$ and $P_1=n_{d,\uparrow}+n_{d,\downarrow}-2n_{d,\uparrow}n_{d,\downarrow}$. Together with the fact that in $n_d=1$ subspace $d_\uparrow^\dagger d_\downarrow$ can be replaced by the spin operator S^+ for spin 1/2 we may express the dot operators by $S^+=d_\uparrow^\dagger d_\downarrow$, $S_-=d_\downarrow^\dagger d_\uparrow$, and $S_z=\frac{1}{2}(n_{d,\uparrow}-n_{d,\downarrow})$ with the constraits $n_{d,\uparrow}+n_{d,\downarrow}=1$ and $n_{d,\uparrow}n_{d,\downarrow}=0$. In this way we obtain the Hamiltonian for two leads Kondo model

$$H=-i\int_{-\infty}^{\infty}dx\sum_{ja}\psi_{ja}^\dagger(x)\partial_x\psi_{ja}(x)+J\hat{S}\cdot((\psi_{1a}^\dagger(0)+\psi_{2a}^\dagger(0))\hat{\sigma}_{ab}(\psi_{1b}(0)+\psi_{2b}(0)) \tag{4.43}$$

with $J=\sum_k\frac{t^2}{\epsilon_k-\epsilon_d}$. This Schrieffer-Wolff transformation for finite U Anderson is written explcitily in A. C. Hewson's book[61]. To solve this Hamiltonian we again transform it to even and odd bases, defined by

$$\psi_{e/o,\sigma}(x)=\frac{\psi_{1,\sigma}(x)+\psi_{2,\sigma}(x)}{\sqrt{2}}$$

Thus the Hamiltonian is decoupled into interacting Hamiltonian in even channel and non-interacting one in odd channel

$$
\begin{aligned}
H &= H_e + H_o \\
H_o &= -i \int_{-\infty}^{\infty} dx \sum_a \psi_{oa}^\dagger(x) \partial_x \psi_{oa}(x) \\
H_e &= -i \int_{-\infty}^{\infty} dx \sum_a \psi_{ea}^\dagger(x) \partial_x \psi_{ea}(x) + 2J\hat{S} \cdot (\psi_{ea}^\dagger(0) \hat{\sigma}_{ab} \psi_{eb}(0))
\end{aligned}
$$

The equilibrium version of this two leads Kondo has been solved by N. Andrei and A. Jerez[66] as a special case (anisotropic 2 channels Kondo model) in their article on anisotropic multichannel Kondo model. To couple the flavors (channels degree of freedom) with spin degree of freedom a curvature term (second oder derivative) is introduced in the kinetic part. This regularization scheme leads to correct counting in the isotropic mulitchanel Kondo model[67].

To construct the scattering eigenstate in lead bases which enables us to compute out of equilibrium state, however, requires the conservation of number of particles from the incoming leads. Thus far we have not yet been successful in finding the regularization scheme (or equivalently, s_{op} in the odd channel in finite U or infinite U Anderson model) to achieve this goal. The trick used in P. Mehta's thesis[15] is not correct as it does not include the regularization scheme in checking the Yang -Baxter equation and the results obtained in there is also incorrect.

In the following we check the consistency condition (Yang-Baxter equation) with an arbitrary chosen two particle S-matrix on the scattered side (denoted as S_R). First we show the S-matrices which satisfy these equations. Then we show that this S-matrix structure does not conserve number of particles from the incoming leads. Thus this Hamiltonian is integrable but we could not obtain out of equilibrium information from there. We also show some of the failed attempts to obtain leads preserving S-matrix in the incoming channel.

4.4.1 Consistency check for two particle S-matrix

The consistency equation for exchanging particles across the impurity is given by $S_{ij(L)} S_{i0} S_{j0} = S_{j0} S_{i0} S_{ij(R)}$ and $S_{jk(L)} S_{lk(L)} S_{jl(L)} = S_{jl(R)} S_{lk(R)} S_{jk(R)}$. Let us check the first condition. Expressing

the electron impurity S-matrix in even-odd basis we have

$$S_{i0} = \begin{bmatrix} S^e_{i0} & 0 & 0 & 0 \\ 0 & S^o_{i0} & 0 & 0 \\ 0 & 0 & S^e_{i0} & 0 \\ 0 & 0 & 0 & S^o_{i0} \end{bmatrix}; S_{j0} = \begin{bmatrix} S^e_{j0} & 0 & 0 & 0 \\ 0 & S^e_{j0} & 0 & 0 \\ 0 & 0 & S^o_{j0} & 0 \\ 0 & 0 & 0 & S^o_{j0} \end{bmatrix} \tag{4.44}$$

The explicit form satisfying $S_{ij(L)}S_{i0}S_{j0} = S_{j0}S_{i0}S_{ij(R)}$ is given by

$$\begin{aligned} S_{ij(L)}S_{i0}S_{j0} &= \begin{bmatrix} S^{ee}_{ij} & 0 & 0 & 0 \\ 0 & S^{oe}_{ij} & 0 & 0 \\ 0 & 0 & S^{eo}_{ij} & 0 \\ 0 & 0 & 0 & S^{oo}_{ij} \end{bmatrix} \begin{bmatrix} S^e_{i0} & 0 & 0 & 0 \\ 0 & S^o_{i0} & 0 & 0 \\ 0 & 0 & S^e_{i0} & 0 \\ 0 & 0 & 0 & S^o_{i0} \end{bmatrix} \begin{bmatrix} S^e_{j0} & 0 & 0 & 0 \\ 0 & S^e_{j0} & 0 & 0 \\ 0 & 0 & S^o_{j0} & 0 \\ 0 & 0 & 0 & S^o_{j0} \end{bmatrix} \\ &= \begin{bmatrix} S^{ee}_{ij}S^e_{i0}S^e_{j0} & 0 & 0 & 0 \\ 0 & S^{oe}_{ij}S^o_{i0}S^e_{j0} & 0 & 0 \\ 0 & 0 & S^{eo}_{ij}S^e_{i0}S^o_{j0} & 0 \\ 0 & 0 & 0 & S^{oo}_{ij}S^o_{i0}S^o_{j0} \end{bmatrix} = \begin{bmatrix} S^e_{j0}S^e_{i0}S^{ee}_{ij} & 0 & 0 & 0 \\ 0 & S^e_{j0}S^o_{i0}S^{oe}_{ij} & 0 & 0 \\ 0 & 0 & S^o_{j0}S^e_{i0}S^{eo}_{ij} & 0 \\ 0 & 0 & 0 & S^o_{j0}S^o_{i0}S^{oo}_{ij} \end{bmatrix} \\ &= \begin{bmatrix} S^e_{j0} & 0 & 0 & 0 \\ 0 & S^e_{j0} & 0 & 0 \\ 0 & 0 & S^o_{j0} & 0 \\ 0 & 0 & 0 & S^o_{j0} \end{bmatrix} \begin{bmatrix} S^e_{i0} & 0 & 0 & 0 \\ 0 & S^o_{i0} & 0 & 0 \\ 0 & 0 & S^e_{i0} & 0 \\ 0 & 0 & 0 & S^o_{i0} \end{bmatrix} \begin{bmatrix} S^{ee}_{ij} & 0 & 0 & 0 \\ 0 & S^{oe}_{ij} & 0 & 0 \\ 0 & 0 & S^{eo}_{ij} & 0 \\ 0 & 0 & 0 & S^{oo}_{ij} \end{bmatrix} = S_{j0}S_{i0}S_{ij(R)} \end{aligned} \tag{4.45}$$

Here electron-electron S-matrix

$$S^{\alpha\beta}_{ij} = \frac{(\lambda_i - \frac{1}{J_\alpha}) - (\lambda_j - \frac{1}{J_\beta}) - i\hat{P}_{ij}}{(\lambda_i - \frac{1}{J_\alpha}) - (\lambda_j - \frac{1}{J_\beta}) - i}$$

and the electron-impurity S-matrix is

$$S^{\alpha}_{i0} = \frac{(\lambda_i - \frac{1}{J_\alpha}) - i\hat{P}_{i0}}{(\lambda_i - \frac{1}{J_\alpha}) - i}$$

with $\hat{P}_{ij}$ representing the spin exchange operator and subindex α or β refers to even or odd here. $\lambda_i = \frac{\tilde{\lambda}_i}{J_i}$ and $\tilde{\lambda}_i = \frac{k_i}{\Lambda}$ with Λ being the cut-off momenta taken to be ∞ in the end of the calculation. In this case $S_{ij(L)} = S_{ij(R)}$ and we shall call this minimum two particle S-matrix. (Minimum in the sense when $J_e = J_o$ it corresponds to two channel Kondo without coupling between flavor and spin.)

Let us first check its form in lead indices basis by rotating back from even-odd to lead indices basis:

$$US_{ij}U^{\dagger} = \frac{1}{4}\begin{pmatrix} 2S_{ij}+S^{eo}_{ij}+S^{oe}_{ij} & S^{oe}_{ij}-S^{eo}_{ij} & S^{eo}_{ij}-S^{oe}_{ij} & 2S_{ij}-S^{eo}_{ij}-S^{oe}_{ij} \\ S^{oe}_{ij}-S^{eo}_{ij} & 2S_{ij}+S^{eo}_{ij}+S^{oe}_{ij} & 2S_{ij}-S^{eo}_{ij}-S^{oe}_{ij} & S^{eo}_{ij}-S^{oe}_{ij} \\ S^{eo}_{ij}-S^{oe}_{ij} & 2S_{ij}-S^{eo}_{ij}-S^{oe}_{ij} & 2S_{ij}+S^{eo}_{ij}+S^{oe}_{ij} & S^{oe}_{ij}-S^{eo}_{ij} \\ 2S_{ij}-S^{eo}_{ij}-S^{oe}_{ij} & S^{eo}_{ij}-S^{oe}_{ij} & S^{oe}_{ij}-S^{eo}_{ij} & 2S_{ij}+S^{eo}_{ij}+S^{oe}_{ij} \end{pmatrix} \tag{4.46}$$

The S_{ij} inside the matrix refers to the case as even-even and odd-odd ($\alpha = \beta$ case) and thus the form is given by $S_{ij} = \frac{\tilde{\lambda}_i - \tilde{\lambda}_j - i\hat{P}_{ij}}{\tilde{\lambda}_i - \tilde{\lambda}_j - i}$. The other relevant terms are given by

$$S^{eo}_{ij} - S^{oe}_{ij} = -\frac{2iJ_eJ_o(\hat{P}_{ij}-1)(J_e-J_o)}{(J_o+J_e(-1+J_o(\lambda_i-\lambda_j-i)))(-J_o+J_e(1+J_o(\lambda_i-\lambda_j-i)))} \tag{4.47}$$

$$S^{eo}_{ij} + S^{oe}_{ij} = \frac{2\left(J_e^2\left(-1+J_o^2(\lambda_i-\lambda_j-i)(-i\hat{P}_{ij}+\lambda_i-\lambda_j)\right)+2J_eJ_o-J_o^2\right)}{(J_o+J_e(-1+J_o(\lambda_i-\lambda_j-i)))(-J_o+J_e(1+J_o(\lambda_i-\lambda_j-i)))} \tag{4.48}$$

Notice that by taking $J_e \gg 1$ and $J_o \gg 1$ the off-diagonal terms reduce to zero in $\frac{1}{J}$ order. Thus to the order of $\frac{1}{J}$ approximation we may have the minimum S-matrix as the lead indices preserving one.

The case we are really interested in is $J_e = 2J$ and $J_o = 0$. This leads to $S^{eo}_{ij} - S^{oe}_{ij} = 0$ and $S^{eo}_{ij} + S^{oe}_{ij} = 2$. This form does not preserve the lead indices.

4.4.2 Possible extension?

Now let us explore more possibility by using arbitrary form of S-matrix on the right hand side. The matrix form relating to consistency condition is given by

$$S_{j0}S_{i0}S_{ij(R)} = \begin{bmatrix} S^e_{j0} & 0 & 0 & 0 \\ 0 & S^e_{j0} & 0 & 0 \\ 0 & 0 & S^o_{j0} & 0 \\ 0 & 0 & 0 & S^o_{j0} \end{bmatrix} \begin{bmatrix} S^e_{i0} & 0 & 0 & 0 \\ 0 & S^o_{i0} & 0 & 0 \\ 0 & 0 & S^e_{i0} & 0 \\ 0 & 0 & 0 & S^o_{i0} \end{bmatrix} \begin{bmatrix} a_{1,1} & a_{1,2} & a_{1,3} & a_{1,4} \\ a_{2,1} & a_{2,2} & a_{2,3} & a_{2,4} \\ a_{3,1} & a_{3,2} & a_{3,3} & a_{3,4} \\ a_{4,1} & a_{4,2} & a_{4,3} & a_{4,4} \end{bmatrix}$$

$$= \begin{bmatrix} S^e_{j0}S^e_{i0}a_{1,1} & S^e_{j0}S^e_{i0}a_{1,2} & S^e_{j0}S^e_{i0}a_{1,3} & S^e_{j0}S^e_{i0}a_{1,4} \\ S^e_{j0}S^o_{i0}a_{2,1} & S^e_{j0}S^o_{i0}a_{2,2} & S^e_{j0}S^o_{i0}a_{2,3} & S^e_{j0}S^o_{i0}a_{2,4} \\ S^o_{j0}S^e_{i0}a_{3,1} & S^o_{j0}S^e_{i0}a_{3,2} & S^o_{j0}S^e_{i0}a_{3,3} & S^o_{j0}S^e_{i0}a_{3,4} \\ S^o_{j0}S^o_{i0}a_{4,1} & S^o_{j0}S^o_{i0}a_{4,2} & S^o_{j0}S^o_{i0}a_{4,3} & S^o_{j0}S^o_{i0}a_{4,4} \end{bmatrix} \quad (4.49)$$

The $a_{m.n}$ here refers to the two particle S-matrix in spin space on the right hand side. The general form which preserving $SU(2)$ symmetry in spin space is given by

$$a_{ij} = \frac{\alpha^R_i - \beta^R_j - i\hat{P}_{ij}}{\gamma^R_{ij}} \quad (4.50)$$

By comparing with the matrix structure in Eq.(4.51) we set $a_{1,2} = a_{1,3} = a_{2,1} = a_{3,1} = a_{4,2} = a_{4,3} = a_{2,4} = a_{3,4} = 0$. However this general structure does not give consistency condition in off-diagonal terms even for arbitrary form of S-matrix (still preserving $SU(2)$) on the left. Also along the diagonal we shall expect $a_{2,2} = a_{3,3}$ while the minimum S-matrix shown in Eq.(**??**) does not have this property. Thus it seems unlikely to have any extension at the moment.

4.4.3 An explicit check on lead conserving form

The general form of two particle S-matrix on the incoming side S_L with conserving lead indices (no channel mixing) can be written in even odd basis as

$$S_{ij(L)} = S_{ij}^{spin}(\frac{1}{2}\{1+\tau_x\otimes\tau_x\}+\frac{b}{2}\{1-\tau_x\otimes\tau_x\}+i\frac{c}{2}\{\tau_z\otimes\tau_z+\tau_y\otimes\tau_y\})$$
$$= 0.5S_{ij}^{spin}\begin{bmatrix} b+ic+1 & 0 & 0 & -b-ic+1 \\ 0 & b-ic+1 & -b+ic+1 & 0 \\ 0 & -b+ic+1 & b-ic+1 & 0 \\ -b-ic+1 & 0 & 0 & b+ic+1 \end{bmatrix} \quad (4.51)$$

In this section we check the general structure following by Eq.(4.51) in the consistency equation with an arbitrary S-matrix satisfying SU(2) symmetry on the right hand side. The S-matrix on the left hand side has structure as

$$S_{ij(L)} = \begin{bmatrix} S_{ij}^1 & 0 & 0 & S_{ij}^3 \\ 0 & S_{ij}^2 & S_{ij}^3 & 0 \\ 0 & S_{ij}^3 & S_{ij}^2 & 0 \\ S_{ij}^3 & 0 & 0 & S_{ij}^1 \end{bmatrix} \quad (4.52)$$

Here $S_{ij}^1 = S_{ij}^{ee} = S_{ij}^{oo}$ is given by the usual S-matrix in spin space. Let $S_{ij}^2 = \frac{(\alpha_L-\beta_L)-i\hat{P}_{ij}}{\alpha_L-\beta_L-i}$ and the corresponding right hand side $S_{ij}^{2(R)} = \frac{(\alpha_L-\beta_L)-i\hat{P}_{ij}+\gamma\hat{P}_{io}+\delta\hat{P}_{jo}+\eta\hat{P}_{io}\hat{P}_{jo}}{N}$ we write down the form of $(2,2)$ component in the consistency equation:

$$\frac{(\alpha_L-\beta_L)-i\hat{P}_{ij}}{\alpha_L-\beta_L-i}\frac{(\tilde{\lambda}_i-\frac{1}{J_o})-i\hat{P}_{i0}}{(\tilde{\lambda}_i-\frac{1}{J_o})-i}\frac{(\tilde{\lambda}_j-\frac{1}{J_e})-i\hat{P}_{j0}}{(\tilde{\lambda}_j-\frac{1}{J_e})-i}$$
$$= \frac{(\tilde{\lambda}_j-\frac{1}{J_e})-i\hat{P}_{j0}}{(\tilde{\lambda}_j-\frac{1}{J_e})-i}\frac{(\tilde{\lambda}_i-\frac{1}{J_o})-i\hat{P}_{i0}}{(\tilde{\lambda}_i-\frac{1}{J_o})-i}\frac{(\alpha_L-\beta_L)-i\hat{P}_{ij}+\gamma\hat{P}_{io}+\delta\hat{P}_{jo}+\eta\hat{P}_{io}\hat{P}_{jo}}{N}$$

Expanding above equation terms by terms we get

$$\text{PPP term}: \quad N = \alpha_L - \beta_L - i$$

$$\text{PP term}: \quad \frac{(\tilde{\lambda}_j - \frac{1}{J_e}) + (\alpha_L - \beta_L)}{(\alpha_L - \beta_L) - i} = \frac{1}{N}\{(\tilde{\lambda}_i - \frac{1}{J_o}) + (\tilde{\lambda}_j - \frac{1}{J_e})\delta + (\tilde{\lambda}_j - \frac{1}{J_e})(\tilde{\lambda}_i - \frac{1}{J_o})\eta\}$$

$$\frac{(\tilde{\lambda}_i - \frac{1}{J_o})}{(\alpha_L - \beta_L) - i} = \frac{1}{N}\{(\tilde{\lambda}_j - \frac{1}{J_e}) + (\alpha_R - \beta_R) + (\tilde{\lambda}_i - \frac{1}{J_o})\gamma\}$$

$$\text{P term} \quad \frac{(\tilde{\lambda}_i - \frac{1}{J_o})(\tilde{\lambda}_j - \frac{1}{J_e})}{(\alpha_L - \beta_L) - i} = \frac{1}{N}\{(\tilde{\lambda}_j - \frac{1}{J_e})(\tilde{\lambda}_i - \frac{1}{J_o})\}$$

$$\frac{(\alpha_L - \beta_L)(\tilde{\lambda}_j - \frac{1}{J_e})}{(\alpha_L - \beta_L) - i} = \frac{1}{N}\{(\tilde{\lambda}_j - \frac{1}{J_e})(\alpha_R - \beta_R) + (\tilde{\lambda}_j - \frac{1}{J_e})(\tilde{\lambda}_i - \frac{1}{J_o})\gamma\}$$

$$\frac{(\alpha_L - \beta_L)(\tilde{\lambda}_i - \frac{1}{J_o})}{(\alpha_L - \beta_L) - i} = \frac{1}{N}\{(\tilde{\lambda}_i - \frac{1}{J_o})(\alpha_R - \beta_R) + (\tilde{\lambda}_j - \frac{1}{J_e})(\tilde{\lambda}_i - \frac{1}{J_o})\delta\}$$

$$\text{1 term} \quad \frac{(\alpha_L - \beta_L)(\tilde{\lambda}_i - \frac{1}{J_o})(\tilde{\lambda}_j - \frac{1}{J_e})}{(\alpha_L - \beta_L) - i} = \frac{1}{N}\{(\tilde{\lambda}_j - \frac{1}{J_e})(\tilde{\lambda}_i - \frac{1}{J_o})(\alpha_R - \beta_R) - i\gamma(\tilde{\lambda}_j - \frac{1}{J_e}) - i\delta(\tilde{\lambda}_i - \frac{1}{J_o})\}$$

The only solution we have is $\gamma = \delta = 0 = \eta$. That is, $S^2_{ij} = S^{oe}_{ij}$ as described in Eq.(4.45). By writing down similar equations in $(3,3)$ component in consistency equation we get $S^2_{ij} = S^{eo}_{ij}$, which is not consistent with the form we would like to have.

Besides from this issue in diagonal term the off diagonal term in two particle S-matrix does not seem to work even in this generalized form of S-matrix as you can see from PPP term and P_{ij} term. For example, the $(2,3)$ component for PPP term is

$$(\alpha_L - \beta_L - i)(\tilde{\lambda}_i - \frac{1}{J_o} - i)(\tilde{\lambda}_j - \frac{1}{J_e} - i) = (\tilde{\lambda}_j - \frac{1}{J_o} - i)(\tilde{\lambda}_i - \frac{1}{J_e} - i)N$$

While the case for P_{ij} term we have

$$\frac{(\tilde{\lambda}_i - \frac{1}{J_o})(\tilde{\lambda}_j - \frac{1}{J_e})}{(\alpha_L - \beta_L - i)(\tilde{\lambda}_i - \frac{1}{J_o} - i)(\tilde{\lambda}_j - \frac{1}{J_e} - i)} = \frac{(\tilde{\lambda}_j - \frac{1}{J_e})(\tilde{\lambda}_i - \frac{1}{J_o})}{(\tilde{\lambda}_j - \frac{1}{J_o} - i)(\tilde{\lambda}_i - \frac{1}{J_e} - i)N}$$

Thus this general structure does not help us extend the two particle S-matrix into off diagonal form.

Chapter 5

Two leads Interacting Resonance Level Model

5.1 Introduction

Two leads Interacting Resonant Level model can be used to describe tunneling current through the resonant tunneling devices (RTD). These devices, often grown by molecular beam epitaxy, can be viewed as larger quantum dots or quantum wells. This model is also the first example of SBA by P. Mehta and N. Andrei[16, 15] and the interesting results from their work kindled numerous theoretical work[37, 38, 72] on this model. Here we reexamine their work, redo the numerics, and show the formulation for Bethe momenta higher than impurity level. We compare the real momenta case with the other theoretical results.

5.2 Two leads Interacting resonant level model

The Hamiltonian for Interacting Resonant level model is:

$$H_{IRLM} = \epsilon_d d^\dagger d + \sum_{i=1,2} -i \int dx \psi_i^\dagger(x) \partial \psi_i(x) + t_i \delta(x)(\psi_i^\dagger(0) d + h.c.) + U \psi_i^\dagger(0) \psi_i(0) d^\dagger d \qquad (5.1)$$

We can shift to even and odd basis defined by: $\psi_e(x) = \frac{t1\psi_1(x)+t_2\psi_2(x)}{\sqrt{t_1^2+t_2^2}}$ and $\psi_o(x) = \frac{t2\psi_1(x)-t_1\psi_2(x)}{\sqrt{t_1^2+t_2^2}}$ thus the above Hamiltonian becomes:

$$\begin{aligned} H &= H_e + H_0 \\ H_e &= -i \int dx \psi_e^\dagger(x) \partial \psi_e(x) + U \psi_e^\dagger(0) \psi_e(0) d^\dagger d + t \delta(x)(\psi_e^\dagger(0) d + h.c.) + \epsilon_d d^\dagger d \\ H_o &= -i \int dx \psi_o^\dagger(x) \partial \psi_o(x) + U \psi_o^\dagger(0) \psi_o(0) d^\dagger d \end{aligned}$$

with $t = \sqrt{t_1^2 + t_2^2}$. In this even-odd bases there is no coupling terms between the odd bath electrons and the dot electrons. This decoupling helps

5.2.1 single particle solution

The most general single particle solution for even and odd basis is:

$$\begin{aligned} |e,p\rangle &= (\int dx g_p(x)\psi_e^\dagger(x) + e_p d^\dagger)|0\rangle \\ |o,p\rangle &= \int dx h_p(x)\psi_o^\dagger(x)|0\rangle \end{aligned}$$

Substituting into above Hamiltonian equations we get the one particle Schordinger equations:

$$\begin{aligned} &-i\partial g_p(x) + te_p\delta(x) = pg_p(x) \\ &tg_p(0) = (p-\epsilon_d)e_p \\ &-i\partial h_p(x) = ph_p(x) \end{aligned}$$

We take the ansatz:

$$\begin{aligned} g_p(x) &= e^{ipx}[a\theta(-x) + b\theta(x)] \\ h_p(x) &= ce^{ipx}(x \neq 0) \\ h_p(x) &= de^{ipx}(x = 0) \end{aligned}$$

Plugging into above Schordinger equations and using $\delta(x)\theta(\pm x) = \frac{1}{2}\delta(x)$ we get:

$$\frac{b}{a} = \frac{i + \frac{t^2}{2(p-\epsilon_d)}}{i - \frac{t^2}{2(p-\epsilon_d)}} \equiv e^{i\delta_p} \tag{5.2}$$

with $\delta_p = -2\tan^{-1}\frac{t^2}{2(p-\epsilon_d)}$. d is chosen to satisfy $h_p(0) = d = g_p(0) = \frac{a(1+e^{i\delta_p})}{2}$ and $c = a$. Take the case of $t_1 = t_2$ to simplify the discussion in the following. By choosing these sets of parameter we may write the incoming state from lead 1 as

$$\begin{aligned} |1p\rangle &= \frac{1}{\sqrt{2}}(|e,p\rangle + |o,p\rangle) = \int dx e^{ipx}\alpha_{1p}^\dagger(x)|0\rangle \\ &= \frac{a}{\sqrt{2}}\int dx e^{ipx}\{(\theta(-x) + \frac{e^{i\delta_p}+1}{2}\theta(x))\psi_1^\dagger(x) + \frac{e^{i\delta_p}-1}{2}\theta(x)\psi_2^\dagger(x) + \frac{2\Gamma/t}{(p-\epsilon_d)+i\Gamma}\delta(x)d^\dagger\}|0\rangle \\ &= \frac{a}{\sqrt{2}}\int dx e^{ipx}\{(\theta(-x) + R_p\theta(x))\psi_1^\dagger(x) + T_p\theta(x)\psi_2^\dagger(x) + \frac{2\Gamma/t}{(p-\epsilon_d)+i\Gamma}\delta(x)d^\dagger\}|0\rangle \end{aligned}$$

with $\Gamma = \frac{t^2}{2}$ and a an overall normalization constant. $T_p = \frac{e^{i\delta_p}-1}{2}$ as transmission amplitude and $R_p = \frac{e^{i\delta_p}+1}{2}$ as reflection amplitude. $\alpha^\dagger_{ip}(x)$ is a compact notation indicating the incoming state from lead i with Bethe momenta p. The incoming state from lead 2 can also be constructed in this way by writing

$$|2p\rangle = \frac{1}{\sqrt{2}}(|e,p\rangle - |o,p\rangle) = \int dx e^{ipx}\alpha^\dagger_{2p}(x)|0\rangle$$

The purpose of choosing discontinuous $h_p(0)$ is to make the two particle S-matrix identical in all different channels and this prescription is essentially the same as inserting $s_{op}\theta(x)\theta(-x)$ in the odd sector as prescribed in finite U and infinite U Anderson model in previous two chapters. Next we study this IRLM scattering eigenstate from two particles to multi particles through the check of consistency conditions.

5.2.2 From two particles to multi particles solution

Here we start with the computation for two particles solution. The most general two particles solution has the form:

$$\begin{aligned}|ip,jk\rangle = &\int\int dx_1 dx_2 (Ag(x_1,x_2)\psi^\dagger_e(x_1)\psi^\dagger_e(x_2) + Ch(x_1,x_2)\psi^\dagger_o(x_1)\psi^\dagger_o(x_2)\\ &+Bj(x_1,x_2)\psi^\dagger_o(x_1)\psi^\dagger_o(x_2))|0\rangle + \int dx\,(Ae(x)\psi^\dagger_e(x)d^\dagger + Bf(x)\psi^\dagger_0(x)d^\dagger)|0\rangle\end{aligned}$$

with A, B, and C arbitrary constants to be determined by the incoming state i and j with Bethe momenta p and k. The Schrondinger equations for this system are:

$$(-i\partial_{x_1} - i\partial_{x_2} - E)g(x_1,x_2) - \frac{t}{2}[\delta(x_1)e(x_2) - \delta(x_2)e(x_1)] = 0 \tag{5.3}$$

$$(-i\partial_{x_1} - i\partial_{x_2} - E)h(x_1,x_2) = 0 \tag{5.4}$$

$$(-i\partial_{x_1} - i\partial_{x_2} - E)j(x_1,x_2) - t\delta(x_1)f(x_2) = 0 \tag{5.5}$$

$$(-i\partial_x - E + \epsilon_d)f(x) - tj(0,x) + U\delta(x)f(x) = 0 \tag{5.6}$$

$$(-i\partial_x - E + \epsilon_d)e(x) - 2tg(0,x) + U\delta(x)e(x) = 0 \tag{5.7}$$

We take this form of two particles solution

$$2!g(x_1,x_2) = g_p(x_1)g_k(x_2)Z(x_1-x_2) - g_p(x_2)g_k(x_1)Z(x_2-x_1) \tag{5.8}$$

with $Z(x)$ an arbitrary function. Plugging this form into Eq.(5.3) gives a form for $e(x)$

$$e(x) = -e_p g_k(x) Z(-x) + e_k g_p(x) Z(x) \tag{5.9}$$

We also assume

$$j(x_1, x_2) = g_p(x_1) h_k(x_2) Y(x_1 - x_2) - g_k(x_1) h_p(x_2) \tilde{Y}(x_2 - x_1) \tag{5.10}$$

with $Y(x)$ and $\tilde{Y}(x)$. Plugging this into Eq.(5.5) one has

$$f(x) = -e_p h_k(x) Y(-x) + e_k h_p(x) \tilde{Y}(x) \tag{5.11}$$

Finally, one takes

$$2! h(x_1, x_2) = h_p(x_1) h_k(x_2) W(x_1 - x_2) - h_p(x_2) h_k(x_1) W(x_2 - x_1) \tag{5.12}$$

Plugging the form of $e(x)$ and $f(x)$ into Eq.(5.7) and Eq.(5.6) respectively yields

$$i[e_p g_k(x) \partial_x Z(-x) - e_k g_p(x) \partial_x Z(x)] = U \delta(x) [e_p g_k(x) Z(-x) + e_k g_p(x) Z(x)] \tag{5.13}$$

$$i[e_p h_k(x) \partial_x Y(-x) - e_k h_p(x) \partial_x \tilde{Y}(x)] = U \delta(x) [e_p h_k(x) Y(-x) + e_k h_p(x) \tilde{Y}(x)] \tag{5.14}$$

Consider first the Eq.(5.13). We take the ansatz that $Z(x) = C\theta(-x) + D\theta(x)$. Then, we get

$$\begin{aligned} \frac{D}{C} &= \frac{i[e_p g_k(0) + e_k g_p(0)] - \frac{U}{2}[e_p g_k(0) - e_k g_p(0)]}{i[e_p g_k(0) + e_k g_p(0)] + \frac{U}{2}[e_p g_k(0) - e_k g_p(0)]} \\ \frac{D}{C} &= \frac{i + \frac{U}{2} \frac{p-k}{k+p-2\epsilon_d}}{i - \frac{U}{2} \frac{p-k}{k+p-2\epsilon_d}} \equiv e^{2i\Phi(p,k)} \end{aligned} \tag{5.15}$$

where $\Phi(p,k) \equiv \tan^{-1}(\frac{\frac{U}{2}(p-k)}{p+k-2\epsilon_d})$. To get from the first to the second equation we have used the relationship Eq.(5.2) between $g_p(0)$ and e_p. Thus, the S-matrix between even flavored particles is simply $S_{ee} = e^{2i\Phi(p,k)}$. From this we get that

$$Z(x) = e^{i\Phi(p,k)\mathrm{sgn}x} \tag{5.16}$$

We now make the assumption that $Y(x) = \tilde{Y}(x)$. We do an analogous calculation for Eq.(5.14) and taking the ansatz $Y(x) = A\theta(-x) + B\theta(x)$ to get the equations

$$\begin{aligned} \frac{B}{A} &= \frac{i[e_p h_k(0) + e_k h_p(0)] - \frac{U}{2}[e_p h_k(0) - e_k h_p(0)]}{i[e_p h_k(0) + e_k h_p(0)] + \frac{U}{2}[e_p h_k(0) - e_k h_p(0)]} \\ \rightarrow \frac{B}{A} &= \frac{i + \frac{U}{2}\frac{p-k}{k+p-2\epsilon_d}}{i - \frac{U}{2}\frac{p-k}{k+p-2\epsilon_d}} = e^{2i\Phi(p,k)} \end{aligned} \tag{5.17}$$

In the last step in Eq.(5.17) we have used the condition of $h_p(0) = g_p(0)$ by inserting a local discontinuity at $h_p(0)$. This gives the S-matrix between the even and odd particles as the same form as even and even particles S-matrix. Hence, we get that:

$$Y(x) = e^{i\Phi(p,k)\mathrm{sgnx}} \tag{5.18}$$

Note that $W(x)$ is arbitrary and we can write it the same as $Y(x)$. Since all the S-matrices are $U(1)$ phases the Yang-Baxter equation is trivially satisfied. Thus, the explicit form of the two particle wave function is just Eq.(5.3) with $e(x)$ and $f(x)$ given by Eq.(5.9) and Eq.(5.11) and $g(x_1, x_2)$, $h(x_1 x_2)$, $j(x_1, x_2)$ given by Eq.(5.8), Eq.(5.12) and Eq.(5.10) respectively.

Now we construct the two particle scattering eigenstates. Let us fix some notation. Denote the two particle state with particles only coming from lead 1 (or 2) as $|1p, 1k\rangle$ (or $|2p, 2k\rangle$). Explicitly, this means that in the scattering state $|1p, 1k\rangle$, the wavefunction amplitude disappears when there is a particle of flavor 2 to the left of the impurity. As such it will be helpful to rewrite Eq.(5.3) in the 1, 2 basis. This gives

$$\begin{aligned} |1p, 1k\rangle = \int dx_1\, dx_2\ & [\mathrm{A\,g(x_1, x_2) + B\,j(x_1, x_2) + C\,h(x_1, x_2)}]\, \psi_1^\dagger(x_1)\psi_1^\dagger(x_2) \\ & + [\mathrm{A\,g(x_1, x_2) - B\,j(x_1, x_2) + C\,h(x_1, x_2)}]\, \psi_2^\dagger(x_1)\psi_2^\dagger(x_2) \\ & + [2\mathrm{A\,g(x_1, x_2) - B\ (j(x_1, x_2) + j(x_2, x_1)) + 2C\,g(x_1, x_2)}]\, \psi_1^\dagger(x_1)\psi_2^\dagger(x_2) \\ & + \int dx\, [\mathrm{Ae(x) + Cf(x)}]\, \psi_1^\dagger(x) + [\mathrm{Ae(x) - Cf(x)}]\, \psi_2^\dagger(x)|0\rangle \end{aligned} \tag{5.19}$$

We write down the explicit form of each of the above components:

$$\begin{aligned}
g(x_1,x_2) &= e^{i(px_1+kx_2)}\left[\theta(-x_1)+e^{i\delta_p}\theta(x_1)\right]\left[\theta(-x_2)+e^{i\delta_k}\theta(x_2)\right]e^{i\Phi(p,k)\mathrm{sgn}(x_1-x_2)}-(x_1\leftrightarrow x_2)\\
h(x_1,x_2) &= e^{i(px_1+kx_2)}e^{i\Phi(p,k)\mathrm{sgn}(x_1-x_2)}-(x_1\leftrightarrow x_2)\\
j(x_1,x_2) &= e^{i(px_1+kx_2)}\left[\theta(-x_1)+e^{i\delta_p}\theta(x_1)\right]e^{i\Phi(p,k)\mathrm{sgn}(x_1-x_2)}\\
&- e^{i(kx_1+px_2)}\left[\theta(-x_1)+e^{i\delta_k}\theta(x_1)\right]e^{i\Phi(p,k)\mathrm{sgn}(x_2-x_1)}
\end{aligned}\tag{5.20}$$

Now we use these forms in Eq.(5.19) and require that the amplitude vanishes when any particle in the incoming region is in lead 2. This yields

$$\begin{aligned}
&[2\mathrm{A}\,\mathrm{g}(x_1,x_2)-\mathrm{B}\,(\mathrm{j}(x_1,x_2)+\mathrm{j}(x_2,x_1))+2\mathrm{C}\,\mathrm{g}(x_1,x_2)]=0 \qquad x_2<0\\
&\left[\mathrm{A}\,\mathrm{g}(x_1,x_2)-\frac{\mathrm{B}}{2}\,(\mathrm{j}(x_1,x_2)-\mathrm{j}(x_2,x_1))+\mathrm{C}\,\mathrm{h}(x_1,x_2)\right]=0 \qquad x_1<0\\
&\left[\mathrm{A}\,\mathrm{g}(x_1,x_2)-\frac{\mathrm{B}}{2}\,(\mathrm{j}(x_1,x_2)-\mathrm{j}(x_2,x_1))+\mathrm{C}\,\mathrm{h}(x_1,x_2)\right]=0 \qquad x_1<0
\end{aligned}\tag{5.21}$$

Solving these sets of equations give $(A,B,C)=A_0(1,1,1)$. Similar computation can also give scattering state of $|ip,jk\rangle$ with $(i,j)\subset(1,2)$. Since the consistency equations (Yang-Baxter equations) are satisfied trivially in this case we can write down the multi particles scattering eigenstate $|\Psi,N_1,N_2\rangle$ as

$$|\Psi,N_1,N_2\rangle=\int\prod_j dx_j e^{ip_jx_j}e^{\sum_{s<t}i\Phi(p_s,p_t)\mathrm{sgn}(x_s-x_t)}\prod_{u=1}^{N_1}\alpha^\dagger_{1p_u}(x_u)\prod_{v=N_1+1}^{N_2}\alpha^\dagger_{2p_v}(x_v)|0\rangle \tag{5.22}$$

Notice that the compact form shown in Eq.(5.22) is only valid if the two particle S-matrix is a simple phase. For solutions involving spin degree of freedom the multi particles solution does not have this compact form.

The next step is to determine these particles' Bethe momenta distribution which describes the incoming two Fermi seas.

5.2.3 Determining Bethe momenta by asymptotic boundary condition

To analyze the structure of the eigenvalues of these scattering eigenstates we again look for poles (or zeros) structure of two particle S-matrix. Denoting $\beta_i=k_i-\epsilon_d$ and $c=\frac{U}{2}$ we have the two particle

S-matrix as

$$S_{12} = \frac{\beta_1 + \beta_2 - ic(\beta_1 - \beta_2)}{\beta_1 + \beta_2 + ic(\beta_1 - \beta_2)} \tag{5.23}$$

Eq.(5.23) has a pole at $\beta_1+\beta_2+ic(\beta_1-\beta_2) = 0$ with complex solution for β_i. Let $\beta_{1/2} = \beta_{+/-} = k \pm i\xi$ with $\xi > 0$ by our convention we have

$$(k + i\xi) + (k - i\xi) + ic((k + i\xi) - (k - i\xi)) = 0 = 2k - 2c\xi.$$

Thus for $c > 0$ we have bound state solution if $\beta_i > 0$ and for $c < 0$ we only have real β_i solution. Further investigation on the pole structure given by the bound state for $c > 1$ case implies more type of complex solution which does not located at the locale assumed by string hypothesis[69, 70]. We focus our discussion on $c < 1$ or $U < 2$ in the rest of this chapter.

As stated above we have two regions we need to consider for repulsive interaction ($U > 0$): For $p < \epsilon_d$ all Bethe momenta are real. For $p > \epsilon_d$ Bethe momenta could have real or complex. Again the complex solution or bound state solution does not correspond to physical (measurable) bound state here. It is just a solution from the pole structure of two particle S-matrix. First lets discuss the case for $p < \epsilon_d$.

Two leads with real Bethe momenta: $p < \epsilon_d$ regime

Eq.(5.22) reduces to the following form describing the incoming states in the asymptotic region ($x \ll 0$):

$$|\Psi, N_1, N_2\rangle|_{x_i \ll 0} \to \int \prod_j dx_j e^{ip_j x_j} e^{\sum_{s<t} i\Phi(p_s,p_t)\mathrm{sgn}(\mathrm{x_s}-\mathrm{x_t})} \prod_{u=1}^{N_1} \psi^\dagger_{1p_u}(x_u) \prod_{v=N_1+1}^{N_2} \psi^\dagger_{2p_v}(x_v)|0\rangle \tag{5.24}$$

To describe the two Fermi seas with chemical potentials μ_1 and μ_2 we apply periodic conditions (by assuming the lead with size L and then take $L \to \infty$) on the Bethe momenta to get

$$e^{ip_j L} = e^{i\sum_{i\neq j}\Phi(p_j,p_i)} \Longrightarrow p_j = \frac{1}{L}\sum_{i\neq j}\Phi(p_j, p_i) + \frac{2\pi n_j}{L} \tag{5.25}$$

We may check these momenta do describe Fermi seas of the two leads by summing all momenta

$$\sum_j p_j = \sum_{j=1}^{N_1+N_2} \frac{2\pi n_j}{L} = \sum_{j=1}^{N_1} \frac{2\pi n_j}{L} + \sum_{j=N_1+1}^{N_1+N_2} \frac{2\pi n_j}{L}$$

as $\sum_j \sum_{i\neq j} \Phi(p_j, p_i) = 0$ due to the antisymmetric nature of the two particles scattering phase shift $\Phi(p_j, p_i) = -\Phi(p_i, p_j)$. Unlike the case for finite U Anderson model or infinite U Anderson model there is no exclusion of identical Bethe momenta in different leads[71]. We shall argue, however, that similar constraint of exclusion in the backflow part of the Eq.(5.25) also exists which renders the continuous version of Eq.(5.25) taking the form:

$$\begin{aligned} \rho_i(p) &= \frac{\theta(B_i - p)}{2\pi} - \int_D^{B_1} K(p,k)\rho_1(k)dk - \int_D^{B_2} K(p,k)\rho_2(k)dk \\ K(p,k) &= \frac{U}{2\pi} \frac{(k-\epsilon_d)}{(p+k-2\epsilon_d)^2 + \frac{U^2}{4}(p-k)^2} = \frac{1}{4\pi} \frac{\partial \Phi(p,k)}{\partial p} \end{aligned} \tag{5.26}$$

Here $\rho_i(p_j) = \frac{1}{L}\frac{dn_j}{dp_j}$ represents the Bethe momenta density in lead i and B_i is the upper bound of the integral which represents the Bethe momenta at the Fermi surface. D is the lower bound of the linearized spectrum. We will come back to discuss Eq.(5.26) in more details in analyzing equilibrium dot occupation for IRLM. Now we continue to discuss the regime of complex momenta, or $p > \epsilon_d$ case, in the following subsection.

Two leads with complex Bethe momenta: $p > \epsilon_d$ regime

For the bare Bethe momenta $p > \epsilon_d$ there could be complex solutions above this impurity level based on the poles (or zeros) structure of the two particles S-matrices. Let us assume that the solutions above ϵ_d are all complex or bound state solutions and position ϵ_d between the two Fermi surface of the two lead system (say $B_2^0 < \epsilon_d < B_1^0$). In this case we have:

$$\begin{aligned} p_j L &= 2\pi N_j + i\sum_l \ln(S_{uu}(p_j, p_l)) + i\sum_l \ln(S_{ub}(p_j, \bar{k_l})) \\ 2\bar{k_j} L &= 2\pi \bar{M_j} + i\sum_l \ln(S_{bb}(\bar{k_j}, \bar{k_l})) + i\sum_l \ln(S_{bu}(\bar{k_j}, p_l)) \end{aligned} \tag{5.27}$$

where $\bar{k_j}$ is defined as the real part of the complex momentum. Note that the summation for real momenta include both lead 1 and lead 2. The S-matrices are defined as:

$$S_{uu}(k,p) = \frac{(k+p-2\epsilon_d) - i\frac{U}{2}(k-p)}{(k+p-2\epsilon_d) + i\frac{U}{2}(k-p)}$$

$$\begin{aligned} S_{ub}(p,\bar{k}) &= \frac{2\bar{k}+p-3\epsilon_d + i\frac{U}{2}((\bar{k}-\epsilon_d)(1-(\frac{U}{2})^{-2}) - (p-\epsilon_d))}{2\bar{k}+p-3\epsilon_d - i\frac{U}{2}((\bar{k}-\epsilon_d)(1-(\frac{U}{2})^{-2}) - (p-\epsilon_d))} \\ &\times \frac{p-\epsilon_d + i\frac{U}{2}((\bar{k}-\epsilon_d)(1+(\frac{U}{2})^{-2}) - (p-\epsilon_d))}{p-\epsilon_d - i\frac{U}{2}((\bar{k}-\epsilon_d)(1+(\frac{U}{2})^{-2}) - (p-\epsilon_d))} \end{aligned}$$

$$\begin{aligned} S_{bu}(\bar{k},p) &= \frac{2\bar{k}+p-3\epsilon_d - i\frac{U}{2}((\bar{k}-\epsilon_d)(1-(\frac{U}{2})^{-2}) - (p-\epsilon_d))}{2\bar{k}+p-3\epsilon_d + i\frac{U}{2}((\bar{k}-\epsilon_d)(1-(\frac{U}{2})^{-2}) - (p-\epsilon_d))} \\ &\times \frac{p-\epsilon_d - i\frac{U}{2}((\bar{k}-\epsilon_d)(1+(\frac{U}{2})^{-2}) - (p-\epsilon_d))}{p-\epsilon_d + i\frac{U}{2}((\bar{k}-\epsilon_d)(1+(\frac{U}{2})^{-2}) - (p-\epsilon_d))} \end{aligned}$$

$$\begin{aligned} S_{bb}(\bar{p},\bar{q}) &= -\frac{2\bar{p}+2\bar{q}-4\epsilon_d - i\frac{u}{2}((\bar{p}-\bar{q})(1-(\frac{U}{2})^{-2}))}{2\bar{p}+2\bar{q}-4\epsilon_d + i\frac{u}{2}((\bar{p}-\bar{q})(1-(\frac{U}{2})^{-2}))} \\ &\times \frac{2\bar{p}-2\epsilon_d - i\frac{U}{2}((\bar{p}-\epsilon_d)(1-(\frac{U}{2})^{-2}) - (\bar{q}-\epsilon_d)(1+(\frac{U}{2})^{-2}))}{2\bar{p}-2\epsilon_d + i\frac{U}{2}((\bar{p}-\epsilon_d)(1-(\frac{U}{2})^{-2}) - (\bar{q}-\epsilon_d)(1+(\frac{U}{2})^{-2}))} \\ &\times \frac{2\bar{q}-2\epsilon_d - i\frac{U}{2}((\bar{p}-\epsilon_d)(1+(\frac{U}{2})^{-2}) - (\bar{q}-\epsilon_d)(1-(\frac{U}{2})^{-2}))}{2\bar{q}-2\epsilon_d + i\frac{U}{2}((\bar{p}-\epsilon_d)(1+(\frac{U}{2})^{-2}) - (\bar{q}-\epsilon_d)(1-(\frac{U}{2})^{-2}))} \end{aligned}$$

The S_{ub}, S_{bu} and S_{bb} represents the Bethe Ansatz S-matrices derived from S_{uu} with the complex solution substituting the real momenta. For example, $S_{bu}(\bar{k},p) = S_{uu}(k_+,p)S_{uu}(k_-,p)$ where $k_\pm = \bar{k}(1 \pm i\frac{2}{U}) \mp i\frac{2}{U}\epsilon_d$. This $k_\pm$ is obtained by letting $S_{uu}(k_+,k_-) = 0$ which corresponds to the bound state solution of Bethe Ansatz.

Next let us rewrite Eq.(5.27) in its differential form. Denote $L\rho_2(p) = \frac{dN}{dp}$ for density of state in lead 2 and $L\rho_1(p) = \frac{dN}{dp}$ for density of state in lead 1 with $p < \epsilon_d$ and $L\sigma_1(\bar{p}) = \frac{d\bar{M}}{d\bar{p}}$ for density of state in lead 1 with $p > \epsilon_d$ and $0 < U < 2$ with $\bar{p}$ as real part of the complex solution $p^\pm$. Denote

$$\mathcal{K}_{ij} = \frac{i}{4\pi}\partial_i \ln S_{ij}.$$

The Bethe Ansatz equations are:

$$\rho_2(p) = \frac{\theta(B_2-p)\Theta(p+D)}{2\pi} - \int_D^{\epsilon_d} \rho_1(k)\mathcal{K}_{uu}(p,k)\ dk - \int_D^{B_2} \rho_2(k)\mathcal{K}_{uu}(p,k)\ dk - \int_{\epsilon_d}^{B_1} \sigma_1(\bar{k})\mathcal{K}_{ub}(p,\bar{k})\ d\bar{k}$$
$$\rho_1(p) = \frac{\theta(\epsilon_d-p)\theta(p+D)}{2\pi} - \int_D^{\epsilon_d} \rho_1(k)\mathcal{K}_{uu}(p,k)\ dk - \int_D^{k_2^0} \rho_2(k)\mathcal{K}_{uu}(p,k)\ dk - \int_{\epsilon_d}^{B_1} \sigma_1(\bar{k})\mathcal{K}_{ub}(p,\bar{k})\ d\bar{k}$$
$$\sigma_1(\bar{p}) = \frac{\theta(B_1-\bar{p})\theta(\bar{p}-\epsilon_d)}{\pi} - \int_D^{\epsilon_d} \rho_1(k)\mathcal{K}_{bu}(\bar{p},k)\ dk - \int_D^{B_2} \rho_2(k)\mathcal{K}_{bu}(\bar{p},k)\ dk - \int_{\epsilon_d}^{B_1} \sigma_1(\bar{k})\mathcal{K}_{bb}(\bar{p},\bar{k})\ d\bar{k}$$

With the integration kernels given by:

$$\mathcal{K}_{uu}(p,k) = \frac{U}{2\pi}\frac{(k-\epsilon_d)}{(p+k-2\epsilon_d)^2+\frac{U^2}{4}(p-k)^2}$$
$$\mathcal{K}_{ub}(p,\bar{k}) = \frac{-\frac{(3U-\frac{4}{U})}{4\pi}(\bar{k}-\epsilon_d)}{(p+2\bar{k}-3\epsilon_d)^2+(\frac{U}{2}(\bar{k}-p)+\frac{2}{U}(\bar{k}-\epsilon_d))^2} - \frac{\frac{(U+\frac{4}{U})}{4\pi}(\bar{k}-\epsilon_d)}{(p-\epsilon_d)^2+(\frac{U}{2}(p-\bar{k})-\frac{2}{U}(\bar{k}-\epsilon_d))^2}$$
$$\mathcal{K}_{bu}(\bar{p},k) = \frac{\frac{(3U-\frac{4}{U})}{4\pi}(k-\epsilon_d)}{(k+2\bar{p}-3\epsilon_d)^2+(\frac{U}{2}(k-\bar{p})+\frac{2}{U}(\bar{p}-\epsilon_d))^2} + \frac{\frac{(U+\frac{4}{U})}{4\pi}(k-\epsilon_d)}{(k-\epsilon_d)^2+(\frac{U}{2}(k-\bar{p})-\frac{2}{U}(\bar{p}-\epsilon_d))^2}$$
$$\mathcal{K}_{bb}(\bar{p},\bar{k}) = \frac{(\bar{k}-\epsilon_d)\frac{(U-\frac{4}{U})}{\pi}}{4(\bar{p}+\bar{k}-2\epsilon_d)^2+(\frac{U}{2}-\frac{2}{U})^2(\bar{p}-\bar{k})^2} + \frac{(\bar{k}-\epsilon_d)\frac{(U+\frac{4}{U})}{2\pi}}{4(\bar{p}-\epsilon_d)^2+\frac{U^2}{4}((\bar{p}-\epsilon_d)(1-\frac{4}{U^2})-(\bar{k}-\epsilon_d)(1+\frac{4}{U^2}))^2}$$
$$+\frac{(\bar{k}-\epsilon_d)\frac{(U+\frac{4}{U})}{2\pi}}{4(\bar{k}-\epsilon_d)^2+\frac{U^2}{4}((\bar{p}-\epsilon_d)(1+\frac{4}{U^2})-(\bar{k}-\epsilon_d)(1-\frac{4}{U^2}))^2}$$

The upper limit B_1 and B_2 are determined by the incoming number of particles N_i from lead i:

$$\frac{N_1}{L} = \int_D^{\mu_1} \frac{1}{2\pi}\ dp = \int_D^{\epsilon_d} \rho_1(p)\ dp + \int_{\epsilon_d}^{B_1} 2\sigma_1(\bar{p})\ d\bar{p}$$
$$\frac{N_2}{L} = \int_D^{\mu_2} \frac{1}{2\pi}\ dp = \int_D^{B_2} \rho_2(p)\ dp$$

μ_i is again connected with B_i by minimizing the free energy $F = \sum_i(E_i - \mu_i N_i)$. To simplify the discussion and avoid the issue of non-steady state, which also occurs for IRLM with complex momenta, we focus on the case of real momenta, or $B_i < \epsilon_d$, in the rest of the numerical results.

5.3 Current and Dot expectation for real momenta case

In this section we compute expectation value of dot occupation, both in and out of equilibrium, and current as a function of voltage. We start with equilibrium dot occupation and check against our

result for one lead limit by taking $t_1 \gg t_2 \to 0$ or equivalently, $t \simeq t_1$, limit. The resulting dot occupation formulation suggests Eq.(5.25) is the correct distribution equation which implies some sort of implicit exclusion for the Bethe momenta.

We also compute dot occupation out of equilibrium and current as a function of voltage numerically at zero temperature. Negative differential conductance is seen for large voltage when the upper bound of Bethe momentum B_1 is close to the impurity level ϵ_d. This non monotonicity in current vs voltage has the physical meaning of Fermi edge singularities and is more apparent as the interaction strength U is stronger.

In numerics the upper bound B_1 is fixed and we lower the other lead's upper bound B_2. This protocol roughly corresponds to fixing μ_1 and lowering μ_2 with μ_1 deviating from its fixed value about few percentage (typically less than five percent) of the fixed value. Same protocol was also adopted in Ref.[16] although they used different equations to solve the density distribution functions.

5.3.1 Equilibrium Bethe momenta density and dot occupation

To discuss the equilibrium dot occupation for two leads IRLM it is useful first to derive the dot occupation for a single lead in IRLM. For a single lead IRLM the Hamiltonian is given by

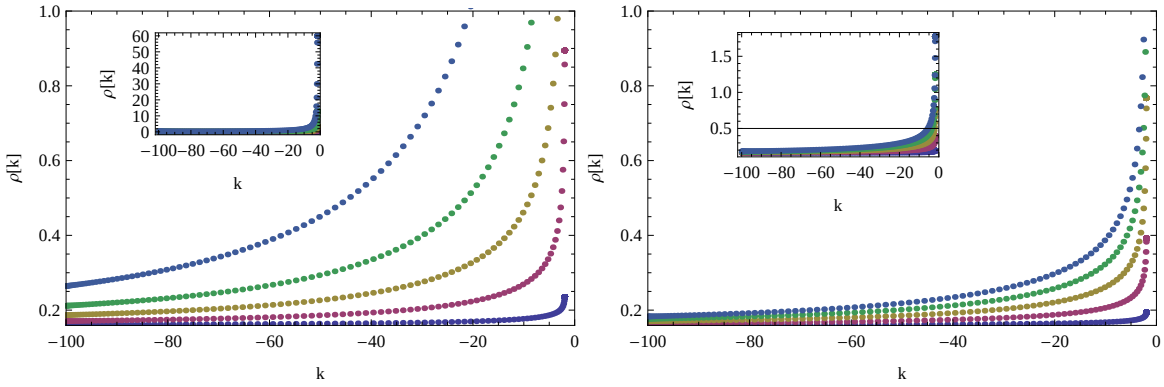

Figure 5.1: Equilibrium Bethe momenta density plots. The color code represents different $\frac{U}{\Gamma}$. $\frac{U}{\Gamma} = 0.1, 0.5, 1, 1.5, 2$ for blue, purple, brown, green, and light blue. The vertical axis starts at $\frac{1}{2\pi}$ which is the density value of $U = 0$ (RLM) case. Left: $\rho(k)$ vs k computed from Eq.(5.33), the published results in Ref.[16] and in P. Mehta's thesis[15] (There is a sign error in the backflow part so the numerical results shown in [15] is for $U < 0$ case). Inset shows the tendency to be divergent at the upper bound when U increases. For U larger than 2.8 the density becomes negative nearby the upper bound. It is not shown in the graph. Right: $\frac{D}{\Gamma} = -100$ in this graph. Right: $\rho(k)$ vs k computed from Eq.(5.26), the one including exclusion in backflow part. Inset shows the well behaved tendency at the upper bound when U increases.

$$H_{IRLM} = -i\int dx\psi^\dagger(x)\partial\psi(x) + \epsilon_d d^\dagger d + t^{(1)}\delta(x)(\psi^\dagger(0)d + h.c.) + U\psi^\dagger(0)\psi(0)d^\dagger d \tag{5.28}$$

We may follow the same procedure as in the two leads case to construct the multi particles eigenstate, starting with a single particle solution with energy eigenvalue $E = p$ as

$$|p\rangle = \int e^{ipx}\{(\theta(-x) + e^{i\delta_p}\theta(x))\psi^\dagger(x) + e_p d^\dagger\delta(x)\}|0\rangle.$$

The single particle phase shift $\delta_p = -2\tan^{-1}\frac{\Gamma^{(1)}}{(p-\epsilon_d)}$ and $e_p = \frac{2\Gamma^{(1)}/t^{(1)}}{(p-\epsilon_d)+i\Gamma^{(1)}}$ with $\Gamma = \frac{(t^{(1)})^2}{2}$. The multi particles eigenstate is constructed with the product form of these single particle eigenstate with two particle S-matrices similar to Eq.(5.24) (with $\alpha_p^\dagger(x)$ replaced by $|p\rangle$ essentially). The dot occupation n_d is then evaluated by

$$\begin{aligned} n_d &= \langle\hat{n}_d\rangle = \frac{\langle p_1, p_2, p_3..., p_N|d^\dagger d|p_1, p_2, p_3..., p_N\rangle}{\langle p_1, p_2, p_3..., p_N|p_1, p_2, p_3..., p_N\rangle} = \frac{1}{L}\sum_p |e_p|^2 \\ &= \int_D^B \rho^{(1)}(p)\frac{2\Gamma^{(1)}}{(p-\epsilon_d)^2 + (\Gamma^{(1)})^2} \end{aligned} \tag{5.29}$$

with the single lead Bethe momenta density $\rho^{(1)}(p)$ given by

$$\rho^{(1)}(p) = \frac{\theta(B-p)}{2\pi} - \int_D^B \frac{U}{\pi}\frac{(k-\epsilon_d)}{(p+k-2\epsilon_d)^2 + \frac{U^2}{4}(p-k)^2}\rho^{(1)}(k)dk \tag{5.30}$$

In Eq.(5.29) we take only $\frac{1}{L}$ terms and neglect $\frac{1}{L^2}$ or smaller terms as we take $L \to \infty$. Similar computation as Eq.(5.29) for two leads case gives the two leads dot occupation

$$\begin{aligned} n_d &= \frac{\langle p_1, p_2, p_3..., p_{N_1}; k_1, k_2, k_3..., k_{N_2}|d^\dagger d|p_1, p_2, p_3..., p_{N_1}; k_1, k_2, k_3..., k_{N_2}\rangle}{\langle p_1, p_2, p_3..., p_{N_1}; k_1, k_2, k_3..., k_{N_2}|p_1, p_2, p_3..., p_{N_1}; k_1, k_2, k_3..., k_{N_2}\rangle} \\ &= \sum_p \frac{1}{L}\frac{\Gamma}{(p-\epsilon_d)^2 + \Gamma^2} = \int_D^B dp(\rho_1(p) + \rho_2(p))\frac{\Gamma}{(p-\epsilon_d)^2 + \Gamma^2} \end{aligned} \tag{5.31}$$

Eq.(5.31) can be checked by comparing with the *exact* result of Resonance Level Model (RLM, $U = 0$ case for IRLM). In RLM the matrix element is the same as this IRLM and $\rho_1(p) = \rho_2(p) = \frac{1}{2\pi}$ for RLM. Thus the limit of $U \to 0$ for IRLM (which renders $\rho_1(p) = \rho_2(p) \simeq \frac{1}{2\pi}$) gives the correct expression for dot occupation both in and out of equilibrium.

If we took $t_1 \gg t_2 \simeq 0$ we would get $t = \sqrt{t_1^2 + t_2^2} \simeq t_1$ or, in another words, $\Gamma \simeq \Gamma^{(1)}$. As lead 2 is essentially decoupled from the dot when $t_2 \to 0$ we can treat this special case as one lead problem.

Thus the formulation of dot occupation for one lead and two leads are the same in this special case. From Eq.(5.29), Eq.(5.30), and Eq.(5.31) we find the equilibrium Bethe momenta density equation for two leads IRLM should take this form

$$\rho(p) = \frac{\theta(B-p)}{2\pi} - \int_D^B \frac{U}{\pi} \frac{(k-\epsilon_d)}{(p+k-2\epsilon_d)^2 + \frac{U^2}{4}(p-k)^2} \rho(k) dk \tag{5.32}$$

with $B_1 = B_2 = B$. This leads us to the assumption that there exists similar exclusion rule for the backflow term as Anderson model in the Bethe Ansatz equation and the out of equilibrium density equation is given by Eq.(5.26). The original Bethe Ansatz equation published in Ref.[**?**] shown in Eq.(5.33)

$$\begin{aligned} \rho_i(p) &= \frac{\theta(B_i-p)}{2\pi} - \int_D^{B_1} K(p,k)\rho_1(k)dk - \int_D^{B_2} K(p,k)\rho_2(k)dk \\ K(p,k) &= \frac{U}{\pi} \frac{(k-\epsilon_d)}{(p+k-2\epsilon_d)^2 + \frac{U^2}{4}(p-k)^2} = \frac{1}{2\pi}\frac{\partial \Phi(p,k)}{\partial p} \end{aligned} \tag{5.33}$$

does not give the correct dot occupation in equilibrium in the limit of $t_1 \gg t_2 \to 0$ (notice the factor of two in the integration kernel). The original derivation [15] does not consider exclusion of equal momenta between different leads which seems to be physically reasonable. So there are both pro and con for this answer and at this moment we do not know in a priori why we need to resort back to some kind of exclusion in the backflow part as shown in Eq.(5.26).

Another issue of Eq.(5.33) is that the density of Bethe momenta obtained numerically has divergence issue nearby the boundary of $B \to \epsilon_d$. The density computed vis Eq.(5.26) is more well behaved at this boundary value. Both are shown in Fig.(5.1).

Now lets come back to the discussion for equilibrium dot occupation in two leads case. We take the Bethe density computed by Eq.(5.26) and compute the dot occupation in equilibrium. As we are confined in real solution we can only investigate the region for Bethe momenta p smaller than impurity level ϵ_d. The numerical results for n_d vs ϵ_d ($\mu_1 = \mu_2 \simeq -2.16$ or $B = -2$ in this case) is plotted in Fig.(5.2). The left figure of Fig.(5.2) shows $U > 0$ case and the right figure shows $U < 0$ case of dot occupation as a function of impurity (dot) level ϵ_d. The equilibrium Fermi surface is fixed at $\mu \simeq -2.16$ which corresponds to upper bound of Bethe momenta $B = -2$. We increase the impurity level ϵ_d from -2.05 to 2. The lower bound $D = -100$. Hybridization strength Γ is fixed at 1 which serves as the unit of U and ϵ_d. Different interaction strengths U are plotted in different

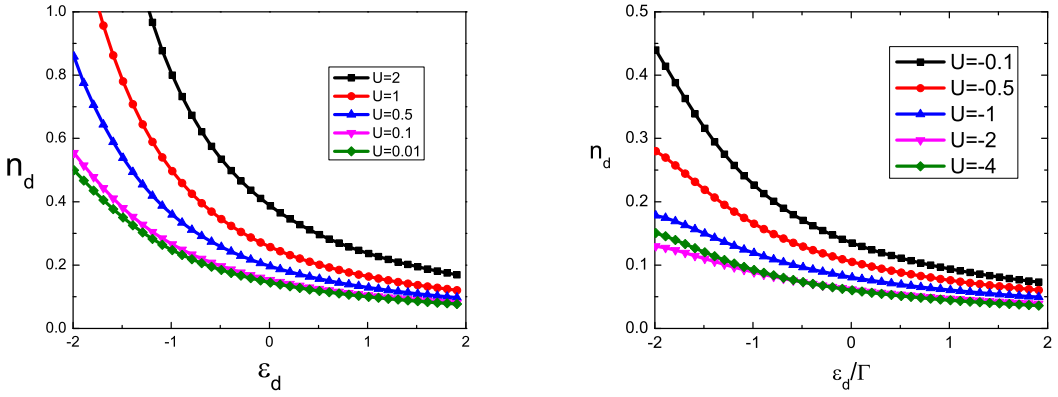

Figure 5.2: Left: n_d vs ϵ_d with $U > 0$ case. Different U are shown in different color lines. Right: n_d vs ϵ_d with $U < 0$ case. Different U are shown in different color lines. Notice the non monotonicity for $U = -4$ in the $U < 0$ case. $B = -2$, $\Gamma = 1$ and $D = -100$ for both figures.

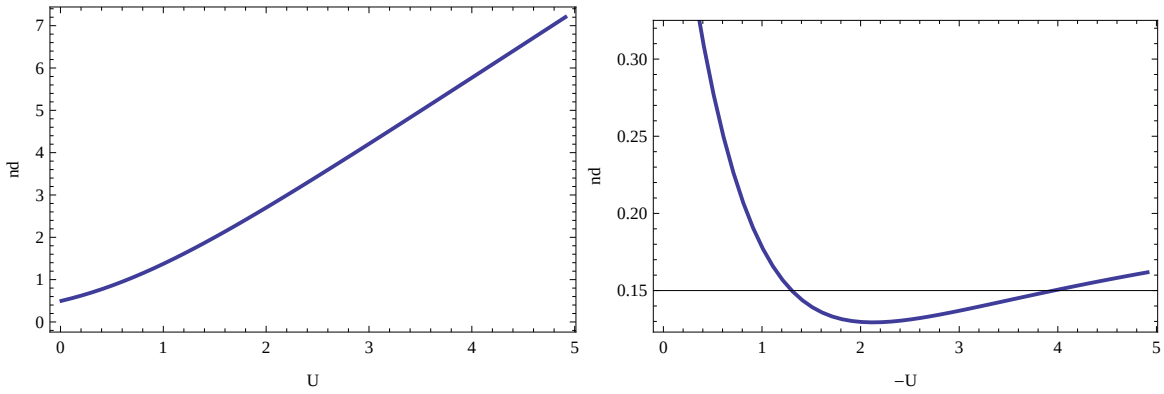

Figure 5.3: Left: n_d vs U with $U > 0$ case. Right: n_d vs $-U$ with $U < 0$ case. $\epsilon_d = -1.99$, $B = -2$, $\Gamma = 1$ and $D = -100$ for both figures in IRLM.

colors. For $U > 0$ case the dot occupation increases monotonically with increasing U at fixed chemical potential and impurity level ϵ_d. For $U \simeq 0.67$ the dot occupation is already approaching 1 as ϵ_d is close to $B = -2$. Thus it seems to be problematic for this formulation as this will eventually violates exclusion principles on the dot.

The figures for dot occupation vs U for fixed boundary B and D and fixed hybridization strength Γ are shown in Fig.(5.3). For the case of $U < 0$ the dot occupation is always less than 0.5 in the range of $B = -2 < \epsilon_d < 2$. We also see non monotonicity in dot occupation number for negative U which is expected from duality in U as suggested by A. Schiller and N. Andrei [37]. For positive U the dot occupation seems to increase monotonically which renders it to be non physical (in the sense that dot occupation higher than one) for $U > 0.67$. As the physical meanings of these discrepancies are not clear at the moment we shall show both $U > 0$ and $U < 0$ results in the following discussion.

Before carrying on the discussion to non equilibrium case let us first investigate the Friedel sum rule in equilibrium in IRLM.

5.3.2 Issue of Friedel sum rule in equilibrium

The idea of Friedel sum rule is to evaluate the change of bulk density of state due to the addition of the impurity. When an impurity is embedded in the metal the itinerant electrons would modify their distributions to screen out the impurity given the thermal fluctuation is lower compared with the energy scale of the onset of the screening. Thus the change in density of state of the bulk electrons is related to the interaction between the bulk electrons and the impurity electrons and the sum of this change must compensate the impurity charge or spin quantity (thus it is named sum rule). Kondo effect is one of the example related to the screening of spin. Here in IRLM the screening part is related to the charge degree of freedom. However as the interaction in IRLM is between the dot and the leads we shall show that Friedel sum rule does *not* apply to this model. In the other words, we show

$$n_{imp} \neq n_d$$

in equilibrium in the following. To simplify the discussion let us take just one lead formulation. As we stated earlier the one lead problem is essentially the same as two leads if the system is in equilibrium.

The equilibrium dot occupation n_d is evaluated in Eq.(5.29). Let us address how to computed the change in bulk density of state which gives n_{imp}. From the traditional Bethe Ansatz (TBA) the change of bulk density due to impurity part is in the order of $\frac{1}{L}$ where L refers to size of the system. By imposing periodic boundary condition including the contribution of the impurity we obtain

$$\rho^{(1)}(p) + \frac{1}{L}\rho^{(1)}_{imp}(p) = \frac{\theta(B-p)}{2\pi} + \frac{\partial\delta_p/\partial p}{2L\pi} - \int_D^B \frac{U}{\pi}\frac{(k-\epsilon_d)}{(p+k-2\epsilon_d)^2 + \frac{U^2}{4}(p-k)^2}(\rho^{(1)}(k) + \frac{1}{L}\rho^{(1)}_{imp}(k))dk$$

or equivalently by taking out the $\frac{1}{L}$ terms only and carrying out the partial differential on single particle phase shift δ_p we get

$$\rho^{(1)}_{imp}(p) = \frac{1}{\pi}\frac{\Gamma}{(p-\epsilon_d)^2+\Gamma^2} - \int_D^B \frac{U}{\pi}\frac{(k-\epsilon_d)}{(p+k-2\epsilon_d)^2 + \frac{U^2}{4}(p-k)^2}\rho^{(1)}_{imp}(k)dk \tag{5.34}$$

The change in the bulk charges is then computed by

$$n_{imp} = \int_D^B \rho_{imp}^{(1)}(p)dp \tag{5.35}$$

By comparing Eq.(5.29) and Eq.(5.35) we can see that these two results are different, showing that Friedel sum rule does *not* apply to this model. Similar proof can also be done by evaluating retarded dot green function. It would also require extra caution when trying to use Landauer Buttiker formula to compute linear response conductance.

5.3.3 Dot occupation vs voltage

Now let us come back to discuss the out of equilibrium case. We start with the discussion on the out of equilibrium dot occupation. The out of equilibrium dot occupation is computed by

$$n_d = \int_D^{B_1} dp\rho_1(p)\frac{\Gamma}{(p-\epsilon_d)^2+\Gamma^2} + \int_D^{B_2} dp\rho_2(p)\frac{\Gamma}{(p-\epsilon_d)^2+\Gamma^2} \tag{5.36}$$

following the evaluation of impurity matrix element computation shown in Eq.(5.31). The voltage

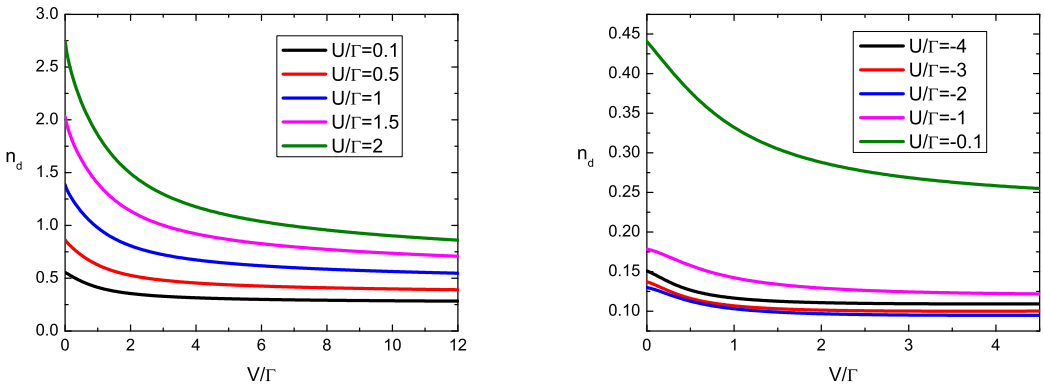

Figure 5.4: Left: n_d vs $\frac{V}{\Gamma}$ with $U > 0$ in IRLM. Right: n_d vs $\frac{V}{\Gamma}$ with $U < 0$ in IRLM.

is given by $\mu_1 - \mu_2$ with μ_i connected with B_i by minimization of *charge free energy*.

$$F = \sum_{p_j}(p_j - \mu_j N_j) = \int_D^{B_1} dp\rho(p)(p-\mu_1) + \int_D^{B_2} dp\rho(p)(p-\mu_2) \tag{5.37}$$

Equivalently we can also obtain the voltage difference by comparing the voltage difference obtained in Fock basis and in Bethe basis:

$$V = \mu_1 - \mu_2 = 2\pi(\int_{\bar{D}}^{\mu_1} dp\frac{1}{2\pi} - \int_{\bar{D}}^{\mu_2} dp\frac{1}{2\pi}) = 2\pi\frac{N_1 - N_2}{L} = 2\pi(\int_{D}^{B_1} dp\rho(p) - \int_{D}^{B_2} dp\rho(p)) \quad (5.38)$$

with $\bar{D}$ representing the Fock space energy lower bound.

This has also been shown in the case of two leads Anderson model. The discrepancy of voltage obtained in this model from Eq.(5.38) and Eq.(5.37) is larger (about ten percentage difference in IRLM compared with one percentage difference in Anderson model at large voltage). It could be due to the fact that we choose the boundary D to be finite and the issue of divergence in Bethe momenta density when B_i is close ϵ_d as shown in Fig.(5.1).

Fig.(5.4) shows the dot occupation as a function of voltage for $U > 0$ case in IRLM. The lower bound of the integral D is fixed at -100. The protocol of driving the system out of equilibrium is fixing the μ_1 close to impurity level ϵ_d and lowering μ_2. In P. Mehta's thesis[15] the plots shown for dot occupation as a function of voltage is in fact for $U < 0$ case due to a mistake in the sign of the integration kernel in the numerical program. From Fig.(5.4) we know that as the voltage increases the dot occupation decreases and eventually reaches a plateau. For $U > 0$ the dot occupation increases monotonically with increasing interaction strength U which again does not show the duality property expected from Ref.[37]. For $U < 0$ we also see the non monotonicity in interaction strength U as has been seen in the equilibrium case.

The common feature for $U > 0$ case compared with two leads Anderson model is that both repulsive interaction increases the value of dot occupation albeit their differences in their interaction form. In the case of Anderson model the reason of this increment in dot occupation is due to the virtual excitations or spin fluctuations at high voltage. For the IRLM the physics behind this increment of dot occupation is related to Fermi Edge singularities. The repulsive interaction between the leads and dot electron depletes the electrons within the leads and therefore the occupation number on the dot increases with increasing U. The effect of removing the electrons from the leads increases the available states for transmission (not to be blockaded by the electrons sitting on those levels) and thus the enhancement of conductance. This can be seen in the following discussion on current vs voltage relation in IRLM.

5.3.4 Current vs voltage

The expectation value for current is obtained by evaluating summation over all momenta in the ground state of the leads in this zero temperature problem. The current is given by

$$\langle \hat{I} \rangle = \int_{B_2}^{B_1} (\rho_1(p) - \rho_2(p)) \frac{\Gamma^2}{(p - \epsilon_d)^2 + \Gamma^2} \tag{5.39}$$

The result of current vs voltage and differential conductance vs voltage are shown in the Fig.(5.5)

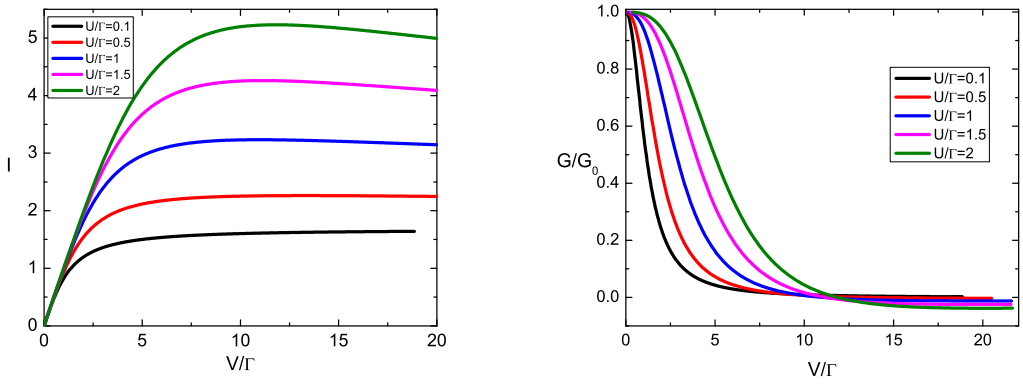

Figure 5.5: Left: Current I vs $\frac{V}{\Gamma}$ in two leads IRLM. Different colors represent different interaction strength U. $\frac{D}{\Gamma} = -100$ and $B_1 = -2.05$, $\epsilon_d = -2$ in this graph. Right: The differential conductance G vs voltage V. G is normalized by conductance at zero voltage G_0. The plot is obtained by taking numerical derivative on the left figure.

for $U > 0$ cases and in the Fig.(5.6) for $U < 0$ cases. The voltage is computed by Eq.(5.38). From Fig.(5.5) we can see that the differential conductance becomes negative at high voltage region for $\frac{U}{\Gamma} > 0.5$. While from Fig.(5.6) there is no such change in the sign of the differential conductance for $U < 0$ in all range of voltage. For $U > 0$ the effect of this repulsive interaction between the leads and the dot pushes away the electrons at the energy level close to the dot level. Therefore for $U > 0$ it would produce more conduction channels and thus increases the conductance. This is also confirmed by the various plots shown in Fig.(5.5).

For $U < 0$ the attractive interaction between the leads and the dot would decrease the available states for transmitting electrons, and therefore the conductance becomes smaller with $U < 0$. This is seen in the Fig.(5.6). In $U < 0$ case we do not see the region of negative conductance but the interesting feature here is there is again non monotonic dependence in interaction strength U. This non monotonicity in U is not seen in the case of $U > 0$ even for $U > 2$. The negative U results could

be non physical as in the case of attractive interaction the lowest energy state is usually formed by bound state or complex momenta. Thus the physically correct feature for $U < 0$ case still needs further numerical work in complex momenta case.

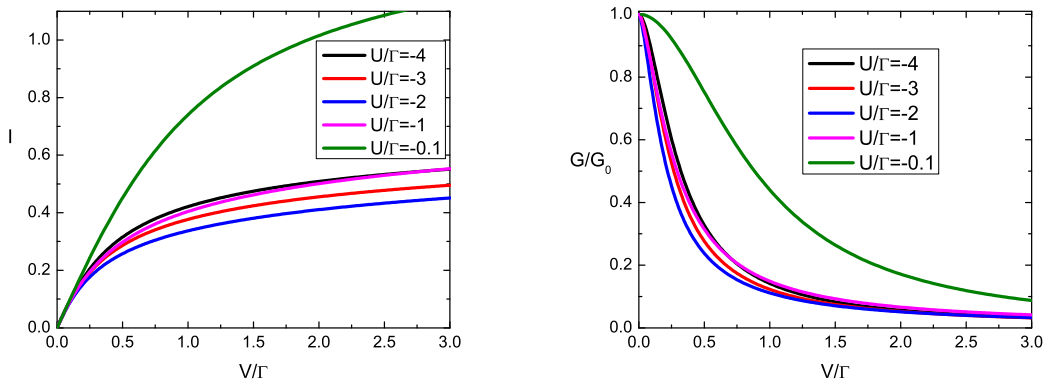

Figure 5.6: Left: Current I vs $\frac{V}{\Gamma}$ in two leads IRLM. Different colors represent different interaction strength U. $\frac{D}{\Gamma} = -100$ and $B_1 = -2.05$, $\epsilon_d = -2$ in this graph. Right: The differential conductance G vs voltage V. G is normalized by conductance at zero voltage G_0. The plot is obtained by taking numerical derivative on the left figure.

For $U > 0$ the negative conductance at large voltage has been observed experimentally in tunneling junctions or larger quantum dot experiments. The physics of this negative conductance is related to the Fermi Edge Singularity[11]. The idea is that the tunneling of electrons between the leads is bound to hole state (or vice versa) of the dot and it produces a power law decay for voltage higher than some threshold voltage. In the case of larger quantum dot the dominant fluctuation in the system is caused by Coulomb repulsion between the electrons in the leads and those in the dot. The spin fluctuation or Kondo effect is less significant in a larger quantum dot or tunneling junctions compared with this electronic interaction. In the following we compare our numerical results with experiments and other theoretical results of IRLM.

5.4 Comparison with other theories and experimental results

Numerous amount of literatures have popped out after the pioneering work by P. Mehta and N. Andrei[16] on this two leads IRLM. Perturbation renormalization group[72], different scattering eigenstates methods by Hershfield Y-operators[73, 74], and exact two particles eigenstates[75] had been proposed. Another exact solutions of this model at the so-called self-dual point[37] by E. Boulat et al. in Refs.[38, 39] uses the conformal field theory and compares with t-DMRG results. Here we

compare the results by L. Borda et al.[72].

To compare with the current vs voltage results in Ref.[72] we rescale the voltage and current axis by the Fock space cutoff $\underline{D}$. In their weak RG results there seems to be no negative conductance region. Thus ths signature of FES is not apparent there. It could be related to their choice of voltage as they use symmetric voltage drive $\pm\frac{V}{2}$ on the leads to take advantage of particle hole symmetry. They saw the non monotonic behavior for $\frac{U}{D} > 0.5$ but the results in that regime are not reliable.

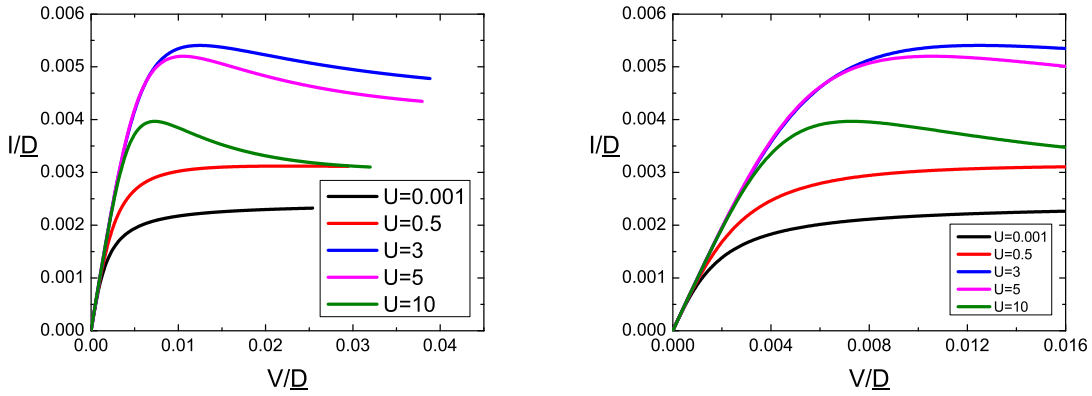

Figure 5.7: Left: Current $\frac{I}{D}$ vs $\frac{V}{D}$ in two leads IRLM. $\Gamma = 1$, $\epsilon_d = 0$ and Bethe lower bound D is fixed at $D = -100$. $\bar{D}$ is the corresponding Fock space energy lower bound. The voltage is driven by fixing $B_1 = -0.005$ and lowering B_2 which corresponds to fixing $\mu_1 \simeq -0.01$ and lowering μ_2. Different colors represent different interaction strength U. Note the non monotonic behavior in $U > 0$ occurs in this rescaled I-V curve. Right: The same plots as left figure with region changed to be the same as in Fig.5.8 from Ref.[72]. The $U = 0.001$ in our plot is used to compare with $U = 0$ in Fig.5.8 and we find that there seems to be a factor of 10 missing in their voltage scale and $\frac{\Delta}{D}$. The correct scale in Fig.5.8 should be from 0 to 0.016 and $\frac{\Delta}{D} = 0.01$.

By rescaling the voltage and current with Fock space cutoff $\underline{D}$ in our results we find that even for $U > 0$ we have non monotonic behavior in the $I - V$ curves for $U > 2$. There are also clear negative conductance for lager U results at voltage $\frac{V}{\underline{D}} \geq 0.005$.

Further comparisons with other theoretical and experimental results are currently underway.

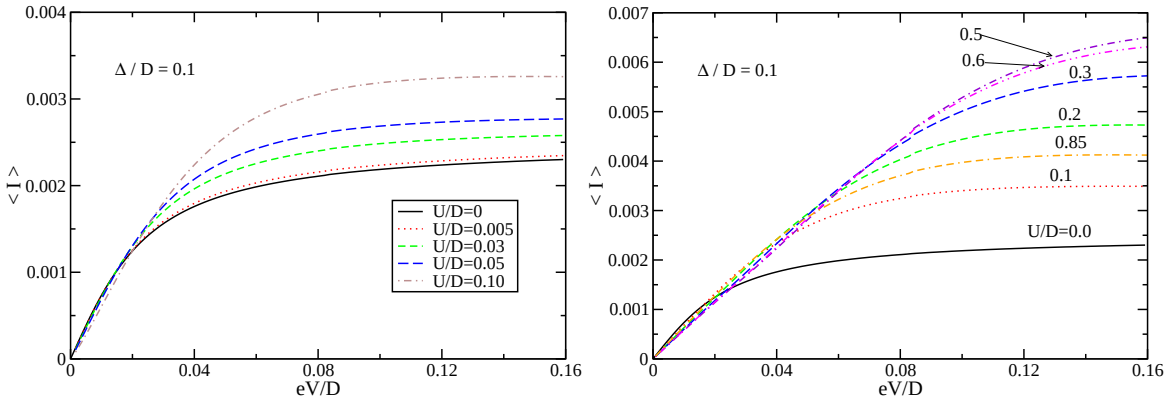

Figure 5.8: Left: (Color online) Current obtained by weak coupling RG for $\frac{\Delta}{D} = 0.1$ and $\frac{U}{D} = 0, 0.005, 0.03, 0.05, 0.10$. For this range of interaction strength the weak-coupling method was reliable in equilibrium. Right: (Color online) Current obtained by the scattering formalism for $\frac{\Delta}{D} = 0.1$ (should be 0.01) and $\frac{U}{D} = 0, 0.10, 0.20, 0.30, 0.50, 0.60, 0.85$. Note that the weak-coupling result is reliable for $\frac{U}{D} < 0.2$ only. Captions and figures taken from Ref.[72]. Notice that Δ in their notation is our Γ. $\frac{\Delta}{D}$ should be 0.01 and their $\langle I \rangle$ is also scaled by D.

Chapter 6

Further extensions of SBA

6.1 Introduction

This chapter is mainly about some extensions of the SBA and most of the work shown here are still in their preliminary stages. It is thus more pedagogical in nature without many concrete results. However this could give an overview of what are the possible questions we can try to tackle with this SBA method as well as providing some ideas how we approach these problems. The order of ths sections follows the sequence of introductions stated below.

As we have mentioned in the introduction of the Scattering Betha Ansatz method, there could be many possible extensions other than evaluating transport property of quantum dot system at zero temperature and zero field. One of the extensions is to describe the quantum dot system at finite temperature and/or at finite magnetic field. This extension is closely connected with the one lead Thermodynamic Bethe Ansatz as we use Bethe basis to construct the multi particles scattering eigenstates. The asymptotic boundary condition we have to solve is thus very similar to the equations we solve in equilibrium system at finite temperature and/or finite magnetic field. We use infinite U Anderson model to illustrate this type of computation in two leads system and show the proof of the ground state configurations are composed of bound state solutions in the Bethe basis.

We can also apply this SBA method to multi leads connect with a dot. Explicit calculations for three leads case, which can be used to measure out of equilibrium dot spectral function when the coupling of the third leads is small, are carried out in the case of three leads IRLM.

Another interesting application of SBA is to apply this method on quantum wire system. In this case we set up the problem by modeling the quantum wire connected with two leads and side coupled to a quantum dot. Transport measurement on this quantum wire system can reveal the information regarding the size of the screening effect related to the interaction between the wire and the dot. We have carried out the Shordinger equations for this problem but we are still working on solving the two particles problem. Thus this work is still in its infant stage.

We give a brief summary in the end of this chapter and comment on the recent work by D. Iyer

and N. Andrie where they applied the scattering formulation to time dependent problem in one lead resonance level model.

6.2 Finite temperature and finite magnetic field

From Chapter 3 to Chapter 5 we have been discussing various models for two leads connected with a quantum dot system at zero temperature and zero field. Often the real experiments are carried out at finite temperature. Magnetic fields are used to determine whether the enhancement of conductance they see in the experiment is really due to the screening effect of magnetic impurity or due to other sources. Thus far the temperature dependence or the change in magnetic field are both well understood in equilibrium system. However in the non equilibrium case, despite numerous theoretical efforts, finite temperature or finite field nonequilibrium quantum dot transport still remains an open question.

Here we give an example of extending this SBA method to finite temperature and finite field by evaluating the free energy in the asymptotic region. We show by explicit calculation that in taking zero temperature and zero field limit the ground state configuration for two leads system is also described by bounded state solution. The main line of the work is done by C. J. Bolech. The modification here is basically put in the correct distribution of states in the two leads case.

We have not yet carried out the computation for matrix element of the physical quantity. Thus the work shown here is just the first step of extending the SBA method to finite temperature and finite field. Further work is required in reaching some results which can really be compared with experimental results and some technical problem not encountered in zero temperature case is also expected. One of the issue is the inability to identify the entropy and magnetization by the lead index.

6.2.1 Free energy of two leads infinite U Anderson model in asymptotic region

Here we write down the main result for finite temperature computation for infinite U Anderson model

$$\begin{aligned}
\frac{N^l}{L} &= \int_k \rho^l(k) + \sum_{l_b,l_{b'}} \int_q (\delta^l_{l_b} + \delta^l_{l_{b'}}) \sigma_b^{l_b l_{b'}}(q) \\
\frac{E}{L} &= \sum_{l_u} \int_k k\rho^l(k) + \sum_{l_b,l_{b'}} \int_q (\delta^l_{l_b} + \delta^l_{l_{b'}}) 2q\sigma_b^{l_b l_{b'}}(q) \\
\frac{S_z}{L} &= \frac{1}{2}\sum_l \int_k \rho^l(k) - \sum_m \int_\lambda m\sigma_{sm}(\lambda)
\end{aligned} \tag{6.1}$$

The free energy of the system is given by

$$F = E - TS - \sum_l \mu_l N^l - 2hS_z \tag{6.2}$$

with S being the entropy of the system expressed by

$$\frac{S\{\rho,\hat{\rho}\}}{L} = (\rho+\hat{\rho})\ln(\rho+\hat{\rho}) - \rho\ln(\rho) - \hat{\rho}\ln(\hat{\rho}) = \rho\ln(1+\eta) + \hat{\rho}\ln(1+\hat{\eta})$$

with $\eta \equiv \frac{\hat{\rho}}{\rho}$ and $\hat{\eta} \equiv \frac{\rho}{\hat{\rho}} = \eta^{-1}$. Notice here that we cannot label S_z nor entropy S by lead indices as the spin rapidities are shared by both leads inherited by quantum inverse scattering method. This casts some doubts on the idea that we are using different basis to describe the same system as in Fock bases the identification has no ambiguity. Let us postpone this issue and continue the discussion for free energy at the moment.

Define $f \equiv \ln(1+\eta)$ and $\hat{f} \equiv \ln(1+\hat{\eta})$ and minimize the free energy by requiring variations of free energy to be zero:

$$\begin{aligned}
\frac{\delta F}{L} &= \sum_l \int_k \{(k - \mu_l - h - T\ln(1+\eta_u^l))\delta\rho_u^l(k) - T\ln(1+\hat{\eta}_u^l)\delta\hat{\rho}_u^l\} \\
&+ \sum_{l,l'} \int_q \{[(2q - \mu_l - \mu_{l'}) - T\ln(1+\eta_b^{ll'})]\delta\sigma_b^{ll'} - T\ln(1+\hat{\eta}_b^{ll'})\delta\hat{\sigma}_b^{ll'}\} \\
&+ \sum_n \int_\lambda \{[2hn - T\ln(1+\eta_{sn})]\delta\sigma_{sn} - T\ln(1+\hat{\eta}_{sn})\delta\hat{\sigma}_{sn}\}
\end{aligned} \tag{6.3}$$

Use the continuous limit of the counting function and the idea of equal distribution in lead indices we have the Bethe Ansatz equation as

$$\rho^l(k)+\hat{\rho}^l(k)=\frac{1}{4\pi}-\frac{1}{2}\sum_{l_a l'_a}\int_{q'}K_1(k-q')\sigma_b^{l_a l'_a}(q')-\frac{1}{2}\sum_{m=1}^{\infty}\int_{\lambda}K_m(k-\lambda')\sigma_{sm}(\lambda') \quad (6.4)$$

$$\sigma_b^{ll'}(q)+\hat{\sigma}_b^{ll'}(q)=\frac{1}{4\pi}-\frac{1}{4}\sum_{l_a}\int_{k}K_1(q-k)\rho^{l_a}(k)-\frac{1}{4}\sum_{l_a l'_a}\int_{q'}K_2(q-q')\sigma_b^{l_a l'_a}(q')$$

$$\sigma_{sn}(\lambda)+\hat{\sigma}_{sn}(\lambda)=\sum_{l}\int_{k}K_n(\lambda-k)\rho^l(k)-\sum_{m}\int_{\lambda'}K_{nm}(\lambda-\lambda')\sigma_{sm}(\lambda')$$

The expression for hole distribution can be obtained from above as:

$$\hat{\rho}^l=\frac{1}{4\pi}-K_0*\rho^l-\frac{1}{2}\sum_{l_a l'_a}K_1*\sigma_b^{l_a l'_a}-\frac{1}{2}\sum_{m}K_m*\sigma_{sm} \quad (6.5)$$

$$\hat{\sigma}_b^{ll'}=\frac{1}{4\pi}-K_0*\sigma_b^{ll'}-\frac{1}{4}\sum_{l_a}K_1*\rho^{l_a}-\frac{1}{4}\sum_{l_a l'_a}K_2*\sigma_b^{l_a l'_a}$$

$$\hat{\sigma}_{sn}=\sum_{l}K_n*\rho^l-\sum_{m}K_{nm}*\sigma_{sm}-K_0*\sigma_{sn}$$

with $*$ indicating the convolution. By substituting hole distribution Eq.(6.5) into Eq.(6.3) we get

$$\begin{aligned}\frac{\delta F}{L}=0 \quad &= \quad \sum_{l}\int_{k}\{(k-\mu_l-h-Tf_u^l)\delta\rho^l+T\hat{f}_u^l(K_0*\delta\rho^l+\frac{1}{2}\sum_{l_a l'_a}K_1*\delta\sigma_b^{l_a l'_a}+\frac{1}{2}\sum_{m}K_m*\delta\sigma_{sm})\}\\
&+ \quad \sum_{ll'}\int_{q}\{(2q-\mu_l-\mu_{l'}-Tf_b^{ll'})\delta\sigma_b^{ll'}+T\hat{f}_b^{ll'}(K_0*\delta\sigma_b^{ll'}+\frac{1}{4}\sum_{l_a l'_a}K_2*\delta\sigma_b^{l_a l'_a}+\frac{1}{4}\sum_{l}K_1*\delta\rho^l)\}\\
&+ \quad \sum_{n}\int_{\lambda}\{(2hn-Tf_{sn})\delta\sigma_{sn}+T\hat{f}_{sn}(-\sum_{l}K_n*\delta\rho^l+\sum_{m}K_{nm}*\sigma_{sm}-\delta\sigma_{sn})\} \quad (6.6)\end{aligned}$$

Use K_n as even function of its argument and divide Eq(6.6) by temperature T and pull out the appropriate varied terms we get

$$\begin{aligned}0 \quad &= \quad \sum_{l}\int_{k}\{[\frac{(k-\mu_l-h)}{T}-f_u^l+K_0*\hat{f}_u^l+\frac{1}{4}\sum_{l_a l'_a}K_1*\hat{f}_b^{l_a l'_a}-\sum_{n}K_n*\hat{f}_{sn}]\delta\rho^l\}\\
&+ \quad \sum_{ll'}\int_{q}\{[\frac{(2q-\mu_l-\mu_{l'})}{T}-f_b^{ll'}+K_0*\hat{f}_b^{ll'}+\frac{1}{4}\sum_{l_a l'_a}K_2*\hat{f}_b^{l_a l'_a}+\frac{1}{2}\sum_{l}K_1*\hat{f}_u^l]\delta\sigma_b^{ll'}\}\\
&+ \quad \sum_{n}\int_{\lambda}\{[\frac{2hn}{T}-f_{sn}+\frac{1}{2}\sum_{l}K_n*\hat{f}_u^l+\sum_{m}K_{nm}*\hat{f}_{sm}-\hat{f}_{sn}]\delta\sigma_{sn}\}\end{aligned}$$

Thus we get

$$\begin{aligned} f_u^l &= \frac{k-\mu_l-h}{T} + K_0 * \hat{f}_u^l + \frac{1}{4}\sum_{l_a l'_a} K_1 * \hat{f}_b^{l_a l'_a} - \sum_n K_n * \hat{f}_{sn} \\ f_b^{ll'} &= \frac{2q-\mu_l-\mu_{l'}}{T} + \frac{1}{2}\sum_l K_1 * \hat{f}_u^l + K_0 * \hat{f}_b^{ll'} + \frac{1}{4}\sum_{l_a l'_a} K_2 * \hat{f}_b^{l_a l'_a} \\ f_{sn} &= \frac{2hn}{T} + \frac{1}{2}\sum_l K_n * \hat{f}_u^l + \sum_m K_{nm} * \hat{f}_{sm} - \hat{f}_{sn} \end{aligned} \tag{6.7}$$

Eq.(6.7) is the general equations for distribution functions in Bethe state. To connect these distribution functions with the density functions we used earlier we may identify

$$\rho_x \equiv s_x \frac{T}{2\pi n_l}\partial_k \hat{f}_x$$
$$\hat{\rho}_x \equiv \bar{s}_x \frac{T}{2\pi n_l}\partial_k f_x$$

with $s_u = s_b = -1$, $s_{sn} = 1$, $n_l = 2$ for unbound state ρ and $n_l = 4$ for bound state distribution σ_b. Using these conventions we have $\rho^l = -\frac{T}{4\pi}\partial \hat{f}_u^l$, $\sigma_b^{ll'} = -\frac{T}{8\pi}\partial \hat{f}_b^{ll'}$, and $\sigma_{sn} = \frac{T}{2\pi}\partial \hat{f}_{sn}$. By using these expression we may rewrite Eq.(6.7) as

$$\begin{aligned} \hat{\rho}^l &= \frac{1}{4\pi} - K_0 * \rho^l - \frac{1}{2}\sum_{l_a l'_a} K_1 * \sigma_b^{l_a l'_a} - \frac{1}{2}\sum_m K_m * \sigma_{sm} \\ \hat{\sigma}_b^{ll'} &= \frac{1}{4\pi} - K_0 * \sigma_b^{ll'} - \frac{1}{4}\sum_l K_1 * \rho^l - \frac{1}{4}\sum_{l_a l'_a} K_2 * \sigma_b^{l_a l'_a} \\ \hat{\sigma}_{sn} &= \sum_l K_n * \rho^l - \sum_m K_{nm} * \sigma_{sm} - \sigma_{sn} \end{aligned} \tag{6.8}$$

This connects the Thermodynamics Bethe Ansatz (TBA) with the Scattering Bethe Ansatz equations. The zero temperature limit of these density equations gives back Eq.(4.20). We may further reformulating the TBA by deriving recursive relations: $\tilde{G}(\omega) \equiv \frac{\tilde{K}_1(\omega)}{\tilde{K}_0(\omega)+\tilde{K}_2(\omega)} = \frac{1}{2\cosh(\frac{\omega c}{2})}$, $G(z) = F^{-1}\{\tilde{G}(\omega)\}(z) = \frac{1}{2c\cosh(\frac{\pi z}{c})}$.

$$\begin{aligned} &K_n - G * (K_{n+1} + \hat{\delta}_{n,1} K_{n-1}) = \delta_{n,1} G \\ &A_{n,m} - G * (A_{n+1,m} + \hat{\delta}_{n,1} A_{n-1,m}) = \delta_{n,m} \\ &K_{n+1} * A_{n,m} - K_n * A_{n+1,m} = -\theta_{m>n}(K_{m-1} + K_{m+1}) \end{aligned} \tag{6.9}$$

with $\hat{\delta}_{n,1} \equiv 1 - \delta_{n,1}$. By using these recursive relation in Eq.(6.9) the spin (n-string) distribution

has the form of $f_{xn} = g_{xn} + A_{nm} * \hat{f}_{xm}$ with $g_{xn} \equiv \frac{2hn}{T} + \frac{1}{2}\sum_l K_n * \hat{f}_u^l$ ($x = s$ in the notation here). Using second line of Eq.(6.9) we get

$$\begin{aligned}\hat{f}_{xn} &= A_{nm} * \hat{f}_{xm} - G * (A_{n+1,m}\hat{f}_{xm} + \hat{\delta}_{n,1}A_{n-1,m} * \hat{f}_{xm}) \\ &= f_{xn} - g_{xn} - G * (f_{x(n+1)} - g_{x(n+1)} + \hat{\delta}_{n,1}(f_{x(n-1)} - g_{x(n-1)}))\end{aligned}$$

Now we define $f - \hat{f} = \ln(1+\eta) - \ln(1+\eta^{-1}) = \ln\eta \equiv \frac{\xi}{T}$. The above expression can be rewritten as

$$f_{xn} - \hat{f}_{xn} = \frac{\xi_{xn}}{T} = g_{xn} + G * (f_{x(n+1)} + \hat{\delta}_{n,1}f_{x,n-1}) - G * (g_{x(n+1)} + \hat{\delta}_{n,1}g_{x,n-1})$$
$$g_{xn} - G * (g_{x(n+1)} + \hat{\delta}_{n,1}g_{x(n-1)}) = \frac{1}{2}\sum_l \delta_{n,1}G * \hat{f}_u^l + \frac{2hn}{T} - G * (\frac{2hn}{T}) \times 2 = \frac{1}{2}\sum_l \delta_{n,1}G * \hat{f}_u^l$$

Thus for spin rapidity:

$$\frac{\xi_{sn}}{T} = \frac{1}{2}\sum_l \delta_{n,1}G * \hat{f}_u^l + G * (f_{s(n+1)} + \hat{\delta}_{n,1}f_{s(n-1)}) \tag{6.10}$$

For unbounded charge rapidity we use the identity: $G * A_{1m} = K_m$ and noting that

$$G * f_{s1} = \frac{h}{T} + \frac{1}{2}\sum_l G * K_1 * \hat{f}_u^l + K_m * \hat{f}_{sm}$$
$$\Rightarrow K_n * \hat{f}_{sn} = -\frac{h}{T} - \frac{1}{2}\sum_l G * K_1 * \hat{f}_u^l + G * f_{s1}$$
$$G * f_b^{ll'} = \frac{q - \frac{\mu_l + \mu_{l'}}{2}}{T} + \frac{1}{2}\sum_l G * K_1 * \hat{f}_u^l + G * \hat{f}_b^{ll'} + \frac{1}{4}\sum_{l_a l'_a} K_1 * \hat{f}_b^{l_a l'_a}$$
$$\Rightarrow \frac{1}{4}\sum_{l_a l'_a} K_1 * \hat{f}_b^{l_a l'_a} = -\frac{q - \bar{\mu}}{T} - \frac{1}{2}\sum_l G * K_1 * \hat{f}_u^l + G * (f_b^{ll'} - \hat{f}_b^{ll'})$$

Rewriting the TBA for unbounded charge rapidity:

$$\begin{aligned} f_u^l &= \frac{k - \mu_l - h}{T} + \hat{f}_u^l + \frac{1}{4}\sum_{l_a l'_a} K_1 * \hat{f}_b^{l_a l'_a} - \sum_n K_n * \hat{f}_{sn} \\ &= \frac{\bar{\mu} - \mu_l}{T} + \hat{f}_u^l - G * f_{s1} + G * (f_b^{ll'} - \hat{f}_b^{ll'}) \\ \Rightarrow f_u^l - \hat{f}_u^l &= \frac{\xi_u}{T} = \frac{\bar{\mu} - \mu_l}{T} + G * (f_b^{ll'} - \hat{f}_b^{ll'}) - G * f_{s1} \end{aligned} \tag{6.11}$$

Similarly for bounded charge rapidity

$$\frac{\xi_b^{ll'}}{T} = \frac{2q - \mu_l - \mu_{l'}}{T} + \frac{1}{2}\sum_l K_1 * \hat{f}_u^l + \frac{1}{4}\sum_{l_a l'_a} K_2 * \hat{f}_b^{l_a l'_a} \tag{6.12}$$

6.3 Three leads coupled to a quantum dot in IRLM

In this section we show the calculation of the three leads connected with a single quantum dot in the Interacting Resonant Level model. From the current in the third probe we may obtain the dot density of state. We show explicit computation of the current through the third lead and comment on the possible issue in the SBA on this problem.

6.3.1 Model Hamiltonian and calculations

The Three-lead interacting resonance level model describes a resonant level, $\epsilon_d d^\dagger d$, coupled to three baths of spinless electrons via tunneling junctions with strength t_i. There is also a Coulomb interaction U between the the level and the baths.

$$\begin{aligned} H_{\rm IRL} &= -i\sum_{i=1,2,3}\int dx\, \psi_i^\dagger(x)\partial\psi_i(x) + \epsilon_d d^\dagger d \\ &+ (\sum_{i=1,2,3} t_i\psi_i^\dagger(0)d + h.c.) + \sum_{i=1,2,3} U_i\psi_i^\dagger(0)\psi_i(0)d^\dagger d. \end{aligned} \tag{6.13}$$

In general the Coulomb interaction and hopping strength can be different for different leads. The simplification can be achieved when we consider all Coulomb interactions are the same. The idea is to write the particle operators in orthogonal bases and decouple the hopping terms. We choose the following bases:

$$\begin{aligned} \psi_e(x) &= \frac{\sum_\alpha t_\alpha\psi_\alpha}{\sqrt{t_1^2+t_2^2+t_3^2}} \\ \psi_{o_1}(x) &= -\frac{t_2\psi_1(x) - t_1\psi_2(x)}{\sqrt{t_1^2+t_2^2}} \\ \psi_{o_2}(x) &= -\frac{t_1t_3\psi_1(x) + t_2t_3\psi_2(x) - (t_1^2+t_2^2)\psi_3(x)}{\sqrt{(t_1^2+t_2^2+t_3^2)(t_1^2+t_2^2)}} \end{aligned} \tag{6.14}$$

This choice is done by observing that the hopping term is related to even combination of the particle operators from each lead. The other two orthogonal bases are chosen by the cross product in the operator bases. These bases obey the similar anti-commutation rule as the Fermion operators

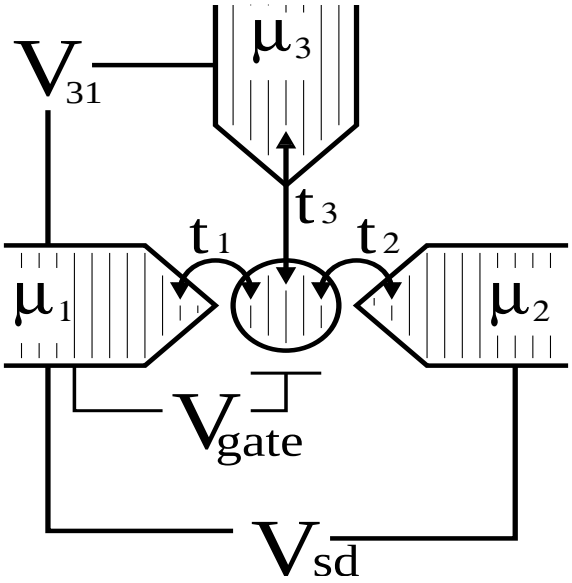

Figure 6.1: A schematic sketch of the proposed apparatus. An ultrasmall quantum dot is coupled by tunneling to three metallic leads, each of which is kept at a separate chemical potential. The corresponding tunneling matrix elements are controlled by varying the potential barriers, while the dot energy level is adjusted by applying a gate voltage. The dot level and the couplings are to be tuned such that the dot is in the Kondo regime, and the coupling to the third lead is much weaker than to the other two leads. Fixing the source-drain voltage bias at $\mu_2 - \mu_1 = eV_{sd}$ and sweeping the chemical potential μ_3 by varying V_{31}, one measures the current $I_3(V_{31})$ between the dot and the third lead. Up to thermal broadening and rescaling, the differential conductance $G_3 = dI_3/dV_{31}$ traces the out-of-equilibrium two-lead dot DOS. Figure and caption taken from Ref.[63]

in different leads. Let us define t and $t^{'}$ as $t = \sqrt{t_1^2 + t_2^2 + t_3^2}$ and $t^{'} = \sqrt{t_1^2 + t_2^2}$. By choosing $U_1 = U_2 = U_3 = U$ we can rewrite the original Hamiltonian in the following form:

$$
\begin{aligned}
H &= H_e + H_{o_1} + H_{o_2} \\
H_e &= -i \int dx\, \psi_e^\dagger(x) \partial \psi_e(x) + \epsilon_d d^\dagger d + t(\psi_e^\dagger(0) d + h.c.) + U \psi_e^\dagger(0) \psi_e(0) d^\dagger d \\
H_{o_i} &= -i \int dx\, \psi_{o_i}^\dagger(x) \partial \psi_{o_i}(x) + U \psi_{o_i}^\dagger(0) \psi_{o_i}(0) d^\dagger d
\end{aligned} \tag{6.15}
$$

We can see that the odd terms are decoupled from the hopping term.

6.3.2 Single particle eigenstate

The single particle eigenstate for Eq.(6.15) is obtained by solving the Shordinger equation. The most general form of single particle eigenstate with eigenvalue p is:

$$
|p\rangle = \int dx\, A[g_p(x)\psi_e^\dagger(x) + e_p d^\dagger] + B h_p(x) \psi_{o_1}^\dagger(x) + C h_p(x) \psi_{o_2}^\dagger(x)
$$

Where A ,B ,and C are arbitrary parameters determined by the boundary condition. We choose our regularization scheme as $\delta(\pm x)\theta(\pm x) = \frac{1}{2}\delta(x)$. The functions $g_p(x)$ and $h_p(x)$ and the parameter e_p are given by:

$$\begin{aligned} g_p(x) &= \frac{2e^{ipx}}{1+e^{i\delta_p}}[\theta(-x) + e^{i\delta_p}\theta(x)] \\ h_p(x) &= \frac{2e^{ipx}}{1+e^{i\delta_p}} \qquad x \neq 0 \\ h_p^{\pm}(0) &= \pm\frac{(p-\epsilon_d)e_p}{t}e^{ipx} = \pm e^{ipx} \qquad x = 0 \\ e_p &= \frac{t}{p-\epsilon_d} \end{aligned} \tag{6.16}$$

with δ_p defined as $\delta_p = -2\arctan[\frac{t^2}{2(p-\epsilon_d)}]$. Again we have introduced a local discontinuity in the odd function the same way as we have done in the two leads case in IRLM.

The boundary condition can be imposed by specifying the origin of incoming particles. The particle coming from lead 1 is described by scattering state with no particles coming from lead 2 or 3. Thus we can get the following equation describing the incoming state from lead 1 as:

$$\begin{aligned} &A\frac{t_2}{t} + B\frac{t_1}{t'} - C\frac{t_2 t_3}{tt'} = 0 \\ &A\frac{t_3}{t} + C\frac{t_1^2 + t_2^2}{tt'} = 0 \\ &\Rightarrow (A,B,C) = C_1(-\frac{t'}{t_3}, \frac{tt_2}{t_1 t_3}, 1) = (-\frac{t_1}{t}, \frac{t_2}{t'}, \frac{t_1 t_3}{tt'}) \end{aligned}$$

Where we choose $C_1 = \frac{t_1 t_3}{tt'}$ as the proper normalization constant. Follow the same procedure we can write down the solution for incoming state from lead 2 and lead 3. The results are:

$$\begin{aligned} (A,B,C) &= C_2(-\frac{t'}{t_3}, -\frac{tt_1}{t_2 t_3}, 1) = (-\frac{t_2}{t}, -\frac{t_1}{t'}, \frac{t_2 t_3}{tt'}) \\ (A,B,C) &= C_3(\frac{t_3}{t'}, 0, 1) = (\frac{t_3}{t}, 0, \frac{t'}{t}) \end{aligned}$$

Thus the particle coming from lead i is written as:

$$|ip\rangle = \int dx\, A_i[g_p(x)\psi_e^\dagger(x) + e_p d^\dagger] + B_i h_p(x)\psi_{o_1}^\dagger(x) + C_i h_p(x)\psi_{o_2}^\dagger(x)|0\rangle$$

6.3.3 Construction of N particle state

From the single particle solution we can try to construct the N-particle solution if a proper two body S-matrix can be found. We begin this construction from finding the solution for two particle state.

Two particle eigenstate

The general two particle eigenfunction $|\Psi\rangle$ can be written as:

$$\begin{aligned}|\Psi\rangle &= \int\int [Ag(x_1,x_2)\psi_e^\dagger(x_1)\psi_e^\dagger(x_2) + C_1 h(x_1,x_2)\psi_{o_1}^\dagger(x_1)\psi_{o_1}^\dagger(x_2) + C_2 h(x_1,x_2)\psi_{o_2}^\dagger(x_1)\psi_{o_2}^\dagger(x_2) \\ &+ C_3 h(x_1,x_2)\psi_{o_1}^\dagger(x_1)\psi_{o_2}^\dagger(x_2) + B_1 j(x_1,x_2)\psi_e^\dagger(x_1)\psi_{o_1}^\dagger(x_2) + B_2 j(x_1,x_2)\psi_e^\dagger(x_1)\psi_{o_2}^\dagger(x_2) \\ &+ Ae(x)\psi_e^\dagger(x)d^\dagger + B_1 f(x)\psi_{o_1}^\dagger(x)d^\dagger + B_2 f(x)\psi_{o_2}^\dagger(x)d^\dagger|0\rangle\end{aligned}$$

Substitute into the Schordinger equation we have:

$$\hat{H}g(x_1,x_2)\psi_e^\dagger(x_1)\psi_e^\dagger(x_2) = -i(\partial_1+\partial_2)g(x_1,x_2)\psi_e^\dagger(x_1)\psi_e^\dagger(x_2) + t[g(0,x_2)d^\dagger\psi_e^\dagger(x_2) - g(x_1,0)d^\dagger\psi_e^\dagger(x_1)]$$

$$\hat{H}h(x_1,x_2)\psi_{o_i}^\dagger(x_1)\psi_{o_j}^\dagger(x_2) = -i(\partial_1+\partial_2)h(x_1,x_2)\psi_{o_i}^\dagger(x_1)\psi_{o_j}^\dagger(x_2)$$

$$\hat{H}j(x_1,x_2)\psi_e^\dagger(x_1)\psi_{o_i}^\dagger(x_2) = -i(\partial_1+\partial_2)j(x_1,x_2)\psi_e^\dagger(x_1)\psi_{o_i}^\dagger(x_2) + tj(0,x_2)d^\dagger\psi_{o_i}^\dagger(x_2)$$

$$\hat{H}e(x)\psi_e^\dagger(x)d^\dagger = -i(\partial_x e(x))\psi_e^\dagger(x)d^\dagger + Ue(0)\psi_e^\dagger(0)d^\dagger - t\psi_e^\dagger(0)e(x)\psi_e^\dagger(x) + \epsilon_d\psi_e^\dagger(x)e(x)d^\dagger$$

$$\hat{H}f(x)\psi_{o_i}^\dagger(x)d^\dagger = -i(\partial_x f(x))\psi_{o_i}^\dagger(x)d^\dagger + Uf(0)\psi_{o_i}^\dagger(0)d^\dagger - t\psi_{o_i}^\dagger(0)f(x)\psi_e^\dagger(x) + \epsilon_d\psi_{o_i}^\dagger(x)e(x)d^\dagger$$

Collecting the same operators term we can get the following equations:

$$(-i\partial_{x_1} - i\partial_{x_2} - E)g(x_1,x_2) - \frac{t}{2}[\delta(x_1)e(x_2) - \delta(x_2)e(x_1)] = 0$$

$$(-i\partial_{x_1} - i\partial_{x_2} - E)h(x_1,x_2) = 0$$

$$(-i\partial_{x_1} - i\partial_{x_2} - E)j(x_1,x_2) - t\delta(x_1)f(x_2) = 0$$

$$(-i\partial_x - E + \epsilon_d)f(x) - tj(0,x) + U\delta(x)f(x) = 0$$

$$(-i\partial_x - E + \epsilon_d)e(x) - 2tg(0,x) + U\delta(x)e(x) = 0$$

From the above work we can see that the two particle S-matrix for three leads is the same as that of two leads. The two particle S-matrix in momentum space ($p+k=E$ for this linear spectrum) in

the asymptotic region is again given by:

$$S(p,k) = e^{i2\phi(p,k)} = \frac{i + \frac{u}{2}\frac{p-k}{p+k-2\epsilon_d}}{i - \frac{u}{2}\frac{p-k}{p+k-2\epsilon_d}} \tag{6.17}$$

The N-particle state can be written as:

$$|\psi\rangle_s = \int dx e^{i\sum p_j x_j} e^{i\sum \phi(p_i,p_j) sgn(x_i - x_j)} \prod \alpha^\dagger_{1p_u}(x_u) \prod \alpha^\dagger_{2p_v}(x_v) \prod \alpha^\dagger_{3p_w}(x_w)|0\rangle \tag{6.18}$$

With $\alpha^\dagger_{ip_u}(x_u) = A_i[g_{p_u}(x_u)\psi^\dagger_e(x_u) + e_{p_u}d^\dagger] + B_i h_{p_u}(x_u)\psi^\dagger_{o_1}(x_u) + C_i h_{p_u}(x_u)\psi^\dagger_{o_2}(x_u)$ given as the single particle state coming from lead i. Notice that the two particle S-matrix is a $U(1)$ phase and it satisfies the Yang-Baxter equation. Thus the generalization to multi particles is valid by Bethe Ansatz method.

6.3.4 Orthogonality of single particle state

Once we have the scattering eigenstate constructed the next thing to do is to evaluate the matrix element of the physical quantity. Again the simplification here is that different Bethe momenta are orthogonal to each other. This is shown in the single particle inner product as following. The inner product of single particle state is quite straightforward:

$$\begin{aligned}\langle ik|jp\rangle = \int dx\ dy\, &[A_i[g_k(y)\psi^\dagger_e(y) + e_k d^\dagger] + B_i h_k(y)\psi^\dagger_{o_1}(y) + C_i h_k(y)\psi^\dagger_{o_2}(y)]^\dagger \\ &[A_j[g_p(x)\psi^\dagger_e(x) + e_p d^\dagger] + B_j h_p(x)\psi^\dagger_{o_1}(x) + C_j h_p(x)\psi^\dagger_{o_2}(x)] \\ = \int dx\ dy\, &\{A_i A_j[g^*_k(y)g_p(x)\delta(x-y) + e_k e_p \delta(x)\delta(y)] + (C_i C_j + B_i B_j)h^*_k(y)h_p(x)\delta(x-y)\}\end{aligned}$$

Note that:

$$\begin{aligned} g^*_k(x)g_p(x) &= \frac{4e^{i(p-k)x}}{(1+e^{i\delta_p})(1+e^{-i\delta_k})}(\theta(-x) + e^{i(\delta_p - \delta_k)}\theta(x)) \\ h^*_k(x)h_p(x) &= \frac{4e^{i(p-k)x}}{(1+e^{i\delta_p})(1+e^{-i\delta_k})} \end{aligned}$$

For the infinite L limit we have:

$$\begin{aligned}\langle ik|jp\rangle &= \delta_{ij}\delta(p-k)\frac{4L|C_i|^2}{(1+e^{i\delta_p})(1+e^{-i\delta_p})} \\ &= \delta_{ij}\delta(p-k)L(1+(\frac{t^2}{2(p-\epsilon_d)})^2)|C_i|^2\end{aligned}$$

In which we neglected the order 1 result. In this infinite L limit we can see that the incoming particle state are orthogonal in lead and momentum index.

6.3.5 Physical quantity calculation

In this section we show the matrix element results of the current and the dot occupation expectation value.

Current calculation

For the current flowing from lead 1 we have:

$$\begin{aligned}\hat{I} &= \frac{-ie}{2\hbar}[\hat{N}_1-\hat{N}_2-\hat{N}_3,\hat{H}] \\ &= \frac{-ie}{\hbar}[t_1(\psi_1^\dagger(0)d-h.c.)-t_2(\psi_2^\dagger(0)d-h.c.)-t_3(\psi_3^\dagger(0)d-h.c.)]\end{aligned}$$

To calculate the steady state current we need to calculate the expectation value for single particle state. The lead 1 current is thus:

$$\langle\hat{I}\rangle = -\frac{2e}{\hbar}\sum(\frac{t_1t_2}{tt'}A_iB_i+\frac{t_1^2t_3}{t^2t'}A_iC_i)\frac{(t^2/2)^2}{|\hat{C}_i|^2[(p-\epsilon_d)^2+(t^2/2)^2]} \tag{6.19}$$

Dot Occupation

The dot occupation value is evaluated by the expectation value of $\hat{n}_d = d^\dagger d$. The result is:

$$\begin{aligned}\langle\hat{n}_d\rangle &= \sum|\frac{A_i}{C_i}|^2\frac{1}{L}\frac{\frac{t^2}{(p-\epsilon_d)^2}}{1+(\frac{t^2}{2(p-\epsilon_d)})^2} \\ &= \int dp(|\frac{A_1}{C_1}|^2\rho_1(p)+|\frac{A_2}{C_2}|^2\rho_2(p)+|\frac{A_3}{C_3}|^2\rho_3(p))\frac{t^2}{(p-\epsilon_d)^2+(\frac{t^2}{2})^2}\end{aligned} \tag{6.20}$$

6.3.6 Current through the 3rd lead and its relation to dot occupation

For the current flowing through the 3rd lead the computation is carried out by first computing the single particle expectation value:

$$\begin{aligned}\langle\hat{I}\rangle_{ij} = \langle[\hat{N}_3,\hat{H}](-\frac{ie}{\hbar})\rangle_{ij} = \langle(-\frac{ie}{\hbar})2t_3[\psi_3^\dagger(0)d - d^\dagger\psi_3(0)]\rangle_{ij} \\ = \langle(-\frac{ie}{\hbar})2t_3[(\frac{t_3}{t}\psi_e(0)+\frac{t'^2}{t't}\psi_{o_2}(0))^\dagger d - d^\dagger(\frac{t_3}{t}\psi_e(0)+\frac{t'^2}{t't}\psi_{o_2}(0))]\rangle_{ij} \\ = -\frac{2ie}{\hbar}(\frac{t_3^2}{t}A_iA_j(g_p^*e_p - h.c.) + \frac{t't_3}{t}(C_iA_jh_p^*e_p - A_iC_je_p^*h_p))\end{aligned}$$

The actual expectation value for the 3rd lead current is thus:

$$\begin{aligned}\langle\hat{I}_3\rangle &= -\frac{2ie}{\hbar}\sum\frac{\frac{t_3^2}{t}|A_i|^2(g_p^*(0)e_p - h.c.) + \frac{t't_3}{t}(A_iC_i)\frac{it^3}{(2(p-\epsilon_d))^2}}{|C_i|^2L(1+(\frac{t^2}{2(p-\epsilon_d)})^2)} \\ &= \frac{2e}{\hbar}\sum\frac{A_i}{C_i}\frac{t't_3}{t^2}\frac{(\frac{t^2}{2(p-\epsilon_d)})^2}{L(1+(\frac{t^2}{2(p-\epsilon_d)})^2)} \qquad (6.21)\end{aligned}$$

If we partial differentiate this 3rd lead current with respect to its chemical potential μ_3 and assume the other two distribution function $\rho_1(p)$ and $\rho_2(p)$ are more or less independent of μ_3 (which is true when the coupling from the 3rd lead is weak, or $t_3 \ll t_1$ or t_2. We can then write down the 3rd lead conductance as:

$$G_3(\mu_3) = \langle\frac{dI_3}{d\mu_3}\rangle = \frac{2e}{\hbar}\int dp\frac{\partial\rho_3(p,\mu_3)}{\partial\mu_3}(\frac{t_3^2}{t^2})\frac{(\frac{t^2}{2})^2}{(p-\epsilon_d)^2+(\frac{t^2}{2})^2} \qquad (6.22)$$

Comparing with Eq.(6.20) we can see that, up to some scaling factor, the differential conductance in the 3rd lead is proportional to the density functional (or more generally, the spectral function) of the dot occupation. The spectral function $A_d(p)$ of the impurity level is obtained by the integrand of the energy integral within the evaluation of $\langle\hat{n}_d\rangle$. We can write down the form of $A_d(p)$ as:

$$\begin{aligned}A_d(p) &= 2(|\frac{A_1}{C_1}|^2\rho_1(p) + |\frac{A_2}{C_2}|^2\rho_2(p) + |\frac{A_3}{C_3}|^2\rho_3(p))\frac{\frac{t^2}{2}}{(p-\epsilon_d)^2+(\frac{t^2}{2})^2} \\ &= 2(\frac{t_1^2+t_2^2}{t_3^2}(\rho_1(p)+\rho_2(p)) + \frac{t_3^2}{t_1^2+t_2^2}\rho_3(p))\frac{\frac{t^2}{2}}{(p-\epsilon_d)^2+(\frac{t^2}{2})^2} \qquad (6.23)\end{aligned}$$

Comparing Eq.(6.22) with Eq.(6.23)we can see that the differential conductance of lead 3 is proportional to the density of state on the impurity level under the assumption that the function $\rho_i(p)$ does

not change much in the regime of interest. This assumption, however, is not quite clear whether it is still true in this Bethe basis. The reason is in the Bethe basis all particles can "sense" the change of other particles through the two particle S-matrices. In the case of IRLM this two particles S-matrix does not depend on the coupling strengths t_i. Thus it casts some doubts whether this assumption is still valid in this basis.

6.4 Quantum wire side coupled with a quantum dot

Quantum wire side coupled with a quantum dot is an interesting proposal for measuring the real space length of the screening cloud in the Kondo effect[76–78]. The Hamiltonian used to describe the leads and the quantum wire coupled with a dot is given by

$$\begin{aligned}
H &= H_0 + H_i \\
H_0 &= -i\sum_j \int \psi_j^\dagger \partial \psi_j - iu \int (\chi_R^\dagger \partial \chi_R - \chi_L^\dagger \partial \chi_L) + V_G \int (\chi_R^\dagger \chi_R + \chi_L^\dagger \chi_L) + \epsilon_d d^\dagger d \\
&+ t_1(\psi_1^\dagger(-\frac{l}{2})(\chi_R + \chi_L)(-\frac{l}{2}) + h.c.) + t_2(\psi_2^\dagger(\frac{l}{2})(\chi_R + \chi_L)(\frac{l}{2}) + h.c.) + t_d((\chi_R + \chi_L)^\dagger(0)d + h.c.) \\
H_i &= U(\chi_R^\dagger \chi_R(0) d^\dagger d + \chi_L^\dagger \chi_L(0) d^\dagger d)
\end{aligned}$$

The single particle solution is expressed as

$$|p\rangle = \{\int (F_1^p(x)\psi_1^\dagger(x) + F_2^p(x)\psi_2^\dagger(x)) + \int_{-\frac{l}{2}}^{\frac{l}{2}} (F_R^p(x)\chi_R^\dagger(x) + F_L^p(x)\chi_L^\dagger(x) + e_p d^\dagger \delta(0))\}|0\rangle$$

The functions $F_i^p(x)$ and e_p are obtained from single particle Schordinger equation $H|p\rangle = p|p\rangle$:

$$\begin{aligned}
&(-i\partial - p)F_1^p(x) + t_1(F_R^p + F_L^p)(-\frac{l}{2}) = 0 \\
&(-i\partial - p)F_2^p(x) + t_2(F_R^p + F_L^p)(\frac{l}{2}) = 0 \\
&(-i\bar{\partial} - p)F_R^p(x) + t_1 F_1^p(-\frac{l}{2}) + t_2 F_2^p(\frac{l}{2}) + t_d e_p \delta(0) = 0 \\
&(i\bar{\partial} - p)F_L^p(x) + t_1 F_1^p(-\frac{l}{2}) + t_2 F_2^p(\frac{l}{2}) + t_d e_p \delta(0) = 0 \\
&t_d(F_R^p + F_L^p)(0) = (p - \epsilon_d)e_p
\end{aligned}$$

Here $\mp i\bar{\partial} \equiv \mp iu\partial + V_G$ is used to simplify the notation and $u\bar{p} + V_G = p$.

$$
\begin{aligned}
F_1^p(x) &= e^{ipx}(A\theta(-x - \frac{l}{2}) + B\theta(x + \frac{l}{2}) \\
F_2^p(x) &= e^{ipx}(C\theta(-x + \frac{l}{2}) + D\theta(x - \frac{l}{2}) \\
F_R^p(x) &= e^{i\bar{p}x}(E\theta(-x) + F\theta(x))\theta(-x + \frac{l}{2})\theta(x + \frac{l}{2}) \\
F_L^p(x) &= e^{-i\bar{p}x}(G\theta(-x) + H\theta(x))\theta(-x + \frac{l}{2})\theta(x + \frac{l}{2})
\end{aligned}
$$

$e_p = \frac{t_d(F_R^p + F_L^p)(0)}{p - \epsilon_d}$ is obtained by the last equation. There are 9 free parameters with 7 constraints from above equations. We may select the remaining two parameters to write the eigenstate as

scattering eigenstate incoming from lead 1 or lead 2. There are 14 terms for two particles equations

$$(-i\partial_1 - i\partial_2 - E)G_{11}(x_1,x_2) + t_1(G_{1R}(x_1,-\frac{l}{2}) + G_{1L}(x_1,-\frac{l}{2}) - G_{1R}(-\frac{l}{2},x_2)$$
$$-G_{1L}(-\frac{l}{2},x_2)) = 0 \tag{6.24}$$
$$(-i\partial_1 - i\partial_2 - E)G_{22}(x_1,x_2) + t_2(G_{2R}(x_1,\frac{l}{2}) + G_{2L}(x_1,\frac{l}{2}) - G_{2R}(\frac{l}{2},x_2) - G_{2L}(\frac{l}{2},x_2)) = 0 \tag{6.25}$$
$$(-i\partial_1 - i\partial_2 - E)G_{12}(x_1,x_2) - t_1(G_{2R}(x_2,-\frac{l}{2}) + G_{2L}(x_2,-\frac{l}{2})) + t_2(G_{1R}(x_1,\frac{l}{2})$$
$$+G_{1L}(x_1,\frac{l}{2})) = 0 \tag{6.26}$$
$$(-i\partial_1 - i\bar{\partial}_2 - E)G_{1R}(x_1,x_2) - t_1(G_{11}(-\frac{l}{2},x_1) - G_{11}(x_1,-\frac{l}{2})) + t_2G_{12}(x_1,\frac{l}{2}))$$
$$+t_dG_{1d}(x_1,0)\delta(x_2) + t_1(G_{RR}(-\frac{l}{2},x_2) - G_{RL}(x_2,-\frac{l}{2}) - G_{RR}(x_2,-\frac{l}{2})) = 0 \tag{6.27}$$
$$(-i\partial_1 + i\bar{\partial}_2 - E)G_{1L}(x_1,x_2) - t_1(G_{11}(-\frac{l}{2},x_1) - G_{11}(x_1,-\frac{l}{2})) + t_2G_{12}(x_1,\frac{l}{2}))$$
$$+t_dG_{1d}(x_1,0)\delta(x_2) + t_1(G_{LL}(-\frac{l}{2},x_2) - G_{RL}(x_2,-\frac{l}{2}) - G_{LL}(x_2,-\frac{l}{2})) = 0 \tag{6.28}$$
$$(-i\partial + \epsilon_d - E)G_{1d}(x,0) + t_d(G_{1L}(x,0) + G_{1R}(x,0)) + t_1G_{Ld}(-\frac{l}{2},0) + t_1G_{Rd}(-\frac{l}{2},0) = 0 \tag{6.29}$$
$$(-i\partial_1 - i\bar{\partial}_2 - E)G_{2R}(x_1,x_2) - t_2(G_{22}(\frac{l}{2},x_1) - G_{22}(x_1,\frac{l}{2})) - t_1G_{12}(-\frac{l}{2},x_1)) \tag{6.30}$$
$$+t_dG_{2d}(x_1,0)\delta(x_2) + t_2(G_{RR}(\frac{l}{2},x_2) - G_{RL}(x_2,\frac{l}{2}) - G_{RR}(x_2,\frac{l}{2})) = 0 \tag{6.31}$$
$$(-i\partial_1 + i\bar{\partial}_2 - E)G_{2L}(x_1,x_2) - t_2(G_{22}(\frac{l}{2},x_1) - G_{22}(x_1,\frac{l}{2})) - t_1G_{12}(-\frac{l}{2},x_1))$$
$$+t_dG_{2d}(x_1,0)\delta(x_2) + t_2(G_{LL}(\frac{l}{2},x_2) + G_{RL}(\frac{l}{2},x_2) - G_{LL}(x_2,\frac{l}{2})) = 0 \tag{6.32}$$
$$(-i\partial + \epsilon_d - E)G_{2d}(x,0) + t_d(G_{2L}(x,0) + G_{2R}(x,0)) + t_2G_{Ld}(\frac{l}{2},0) + t_2G_{Rd}(\frac{l}{2},0) = 0 \tag{6.33}$$
$$(-i\bar{\partial}_1 - i\bar{\partial}_2 - E)G_{RR}(x_1,x_2) + t_1G_{1R}(-\frac{l}{2},x_2) + t_2G_{2R}(\frac{l}{2},x_2) + t_dG_{Rd}(x_1,0) = 0 \tag{6.34}$$
$$(i\bar{\partial}_1 + i\bar{\partial}_2 - E)G_{LL}(x_1,x_2) + t_1G_{1L}(-\frac{l}{2},x_2) + t_2G_{2L}(\frac{l}{2},x_2) + t_dG_{Ld}(x_1,0) = 0 \tag{6.35}$$
$$(-i\bar{\partial}_1 + i\bar{\partial}_2 - E)G_{RL}(x_1,x_2) + t_1G_{1L}(-\frac{l}{2},x_2) + t_2G_{2L}(\frac{l}{2},x_2) - t_1G_{1R}(-\frac{l}{2},x_1)$$
$$-t_2G_{2R}(\frac{l}{2},x_1) + t_dG_{Rd}(x_1,0) + t_dG_{Ld}(x_2,0) = 0 \tag{6.36}$$
$$(-i\bar{\partial} + \epsilon_d - E)G_{Rd}(x,0) - t_d(G_{RR}(0,x) - G_{RR}(x,0)) + t_dG_{RL}(x,0) + UG_{Rd}(0,0) = 0 \tag{6.37}$$
$$(i\bar{\partial} + \epsilon_d - E)G_{Ld}(x,0) - t_d(G_{LL}(0,x) - G_{LL}(x,0)) - t_dG_{RL}(0,x) + UG_{Ld}(0,0) = 0 \tag{6.38}$$

Observing Eq.(6.36,6.37,6.38) we have

$$\begin{aligned} G_{RL}(x_1,x_2) &= (A^{pk}_{RL}\theta(-x_1-x_2)+B^{pk}_{RL}\theta(x_1+x_2))F^p_R(x_1)F^k_L(x_2) \quad (6.39)\\ &- (A^{kp}_{RL}\theta(-x_1-x_2)+B^{kp}_{RL}\theta(x_1+x_2))F^k_R(x_1)F^p_L(x_2)\\ G_{Rd}(x,0) &= (A^{pk}_{Rd}\theta(-x)+B^{pk}_{Rd}\theta(x))F^p_R(x)e_k-(A^{kp}_{Rd}\theta(-x)+B^{kp}_{Rd}\theta(x))F^k_R(x)e_p \quad (6.40)\\ G_{Ld}(x,0) &= (A^{pk}_{Ld}\theta(-x)+B^{pk}_{Ld}\theta(x))F^p_L(x)e_k-(A^{kp}_{Ld}\theta(-x)+B^{kp}_{Ld}\theta(x))F^k_L(x)e_p \quad (6.41) \end{aligned}$$

Similar structure also exists for terms like $G_{RR}(x_1,x_2)$, $G_{LL}(x_1,x_2)$, $G_{12}(x_1,x_2)$, etc. The two particles computation for this quantum wire coupled with a dot is still underway.

6.5 Summary and extension to time dependent problem

This chapter applies the Scattering Bethe-Ansatz to more general description of quantum impurity model. The first extension is to discuss finite temperature and finite field for a two leads single quantum dot system. The second and third parts is basically discussing different physical structure such as multi leads connection and quantum wire. Apart from those we have mentioned this method can also be applied to compute current current correlation functions which gives information of noise measurement. This has been attempted by G. Palacios in the case of two leads IRLM.

Fairly recently computations done by D. Iyer and N. Andrei has brought this method to another exciting level. By performing some special contour integrations they are able to compute time dependent dot occupation in the quench problem (Quench here means the interactions between leads and the dot is turned on suddenly rather than adiabatically.) of RLM by using Bethe Ansatz scattering state. It would be interesting to see if the computation can be extended to two leads system where comparison between the SBA results and perturbative Keldyshi calculations by A. Jahuo[79] et al., which is also *exact* in this non interacting model, is possible.

Chapter 7

Concluding remarks and outlook

We apply the Scattering Bethe Ansatz (SBA) approach on the quantum impurity model to compute steady state transport property of the system. The general ideas of SBA are presented in Chap. 2. The general setups of quantum impurities, ranging from small (with length around 100nm) quantum dots to larger (a few μm) quantum dots or quantum wells, are introduced in Chap. 1. The quantum dot or quantum well is connected with two leads. By using SBA we obtain the steady state current vs voltage and dot occupation vs voltage at zero temperature.

In applying this method to the two leads Anderson impurity model, the standard model to describe Kondo physics in small quantum dot, we encountered some difficulties, which we summarize below, in evaluating the current matrix element. We proposed phenomenological approach, named pSBA, to extract the important physics of the model[64]. In a close analogy to the fundamental excitations in Bethe bases in equilibrium[51] we identify two types of phase shifts, one related to spin fluctuations and the other related to charge fluctuations, related to phase shifts for current transport. We checked pSBA by comparing the dot occupation and Friedel sum rule results in equilibrium and obtain qualitative agreement. The nonequilibrium numerical results for current vs voltage show correct scaling relations in the Kondo regimes as is expected from strong coupling to weak coupling Fermi liquid picture[22].

Other interesting quantities, such as the nonequilibrium charge susceptibility or the usual charge susceptibility, are computed numerically via exact expression for dot occupation as a function of voltage and impurity level. The expression of dot occupation is proved to be exact in equilibrium by comparing with traditional Bethe Ansatz and same expression is valid both in and out of equilibrium. This statement is based on the results of SBA since matrix element computation takes the same form in and out of equilibrium for dot occupation[15].

We believe this is the first report of an exact computation of the dot occupation out-of-equilibrium and it may have interesting application in quantum computing once we understand more about the dephasing mechanism. We have also compared our results with perturbation calculation and experimental measurement of nonlinear differential conductance of a quantum dot. Overall nice

agreements are shown in Chap. 3. Similar applications of pSBA have also been done in infinite U Anderson model. Similar scaling behaviors for voltage $V \ll T_k$ are shown in Chap. 4.

In Chap 5. we reexamine the Interacting Resonant Level Model (IRLM) and extend its formulations to complex momenta case. Detailed analysis on both positive interaction strength and negative interaction strength, assuming Bethe momenta are real, is shown in this chapter. It should be noted that the negative U results may not correspond to the ground state configuration for negative U case (since bound states configurations could exist in this case). We also compare our numerical results with other theories such as weak coupling RG by L. Borda et al [72]. In Chap 6. we mention some possible extensions of the SBA method.

We summarize the major difficulties we have encountered by using SBA approach here. One of the main issues in constructing the many particles scattering eigenstate is that we introduce local discontinuity term of the form $s_{op}\theta(x)\theta(-x)$ in the odd bases of the solutions. By using this term we may transform from even-odd bases back to the lead bases[50] as this choice leads to identical two particle S-matrices in all the channels.

This regularization scheme has two apparent problems. First the criteria $\partial_x s_{op}\theta(x)\theta(-x)$ is zero under two cases: (1) We carried out the spatial integral with s_{op} being even function of x. (2) $\partial_x\theta(\pm x) = \pm\delta(x)$ and $\delta(x)\theta(x) = \frac{1}{2}\delta(x)$. In solving the Schordinger equations we may take case (1) to avoid the issue of a particular regularization scheme. Had we taken case (2) the partial derivative on the theta function needs to be a sharp Dirac delta function[71], otherwise the derivative is nonzero and we cannot say that the eigenstates we have found is truly the eigenstate.

The other problem related to this is that we need to define the current operators away from $x = 0$. Due to the regularization scheme we choose the matrix element of current $\langle\hat{I}\rangle$ would be trivially zero if we insisted on defining

$$\langle\hat{I}_i\rangle \propto \sum_\sigma \langle\psi^\dagger_{i\sigma}(0)d_\sigma - d^\dagger_\sigma\psi_{i\sigma}(0)\rangle \tag{7.1}$$

rather than choosing electron operators defined around $x = 0$. i and σ denote lead and spin index. This problem is the same for all the models we have mentioned, including the IRLM in Ref.[16]. The temporary solution to this problem is to choose the current operator acting around this $x = 0$

and this choice would be consistent with another current operators definition

$$\langle \hat{I}_i \rangle \propto \lim_{\eta \to 0^+} \sum_{i\sigma} \langle \psi^\dagger_{i\sigma}(\eta)\psi_{i\sigma}(\eta) - \psi^\dagger_{i\sigma}(-\eta)\psi_\sigma(-\eta)\rangle \tag{7.2}$$

The third problem in the SBA is the matrix element evaluation in the case of bound state or complex momenta. Although the equilibrium results in the case of finite U Anderson shows the validity of our integrations schemes and orthogonality between different real part of the bound states (see also Appendix B), the computations involving out of equilibrium quantity are far from clear. The major issue is that the time variation of dot expectation value

$$\frac{d\langle n_d \rangle}{dt} \neq 0$$

is nonzero, which violates the steady state assumption. This quantity is indeed zero for real Bethe momenta. So far this problem is still unsolved and we have to use phenomenological ideas to figure out the possible formulation for the current matrix element. One of the reasons leading to this problem could again come from the choice of $\theta(x)\theta(-x)$ term. However given the same choice the real Bethe momenta does not have this issue. So the deeper origin of this problem aside from being complex solutions is not clear.

The last issue is related to the asymptotic boundary conditions. It is not clear a priori which type of bound states solution should describe the free Fermi seas. As we have mentioned in Appendix A the most general choice would be four type of strings solutions. However by performing the computation we find unphysical results. Had we not known the physical properties of the system we could not be able to make this judgment. This also makes SBA less useful in predicting or exploring the physics of the new models.

We have been working on different models to see if we could avoid to use the $s_{op}\theta(x)\theta(-x)$ terms in constructing the scattering eigenstates. So far the likely candidate would be the quantum wire coupled with dot. We also plan to go back to work out the IRLM and make more detailed comparison with other numerical or analytical results in this model. By using proper mapping we can also connect this model with the anisotropic Kondo model[80] and enhance our understanding of both models by this SBA method.

Appendix A

Discussion of 2 strings vs 4 strings

As we have discussed in the main text the bounded pair, formed by $p^{\pm}(\lambda) = x(\lambda) \mp iy(\lambda)$, can be formed by quasi-momenta from lead 1 or lead 2. We have shown the results for two type of strings (bound states). Namely the strings are formed by $\{ij\} = \{11, 22\}$ with i, j denoting incoming lead indices. In this section we discuss the case of 4 type of strings and show their corresponding numerical results in out of equilibrium regime (In equilibrium the 2 strings and 4 strings give the same result for dot occupation).

The density distribution for the Bethe momenta (rapidities) is denoted by $\sigma_{ij}(\lambda)$ with $\{ij\} = \{11, 12, 21, 22\}$ indicating the incoming electrons from lead i and lead j. The $\sigma_{ij}(\lambda)$ is given by

$$4\sigma_{ij}(\lambda) = -\frac{1}{\pi}\frac{\mathrm{d}x(\lambda)}{\mathrm{d}\lambda} - \sum_{i,j=1,2}\int_{B_{ij}}^{\infty}\mathrm{d}\lambda'\ K(\lambda-\lambda')\sigma_{ij}(\lambda') \tag{A.1}$$

The factor of 4 indicates 4 type of possible configurations and the constraint of exclusions in rapidities λ in solving the quantum inverse scattering problem. The idea is that in equilibrium four type of distributions are equally possible for each bound state bare energy $2x(\lambda)$. The B_{ij} play the role of chemical potentials for the Bethe-Ansatz momenta and are determined from the physical chemical potentials of the two leads, μ_i, by minimizing the charge free energy,

$$F = \sum_i (E_i - \mu_i N_i) = \sum_i \int_{B_{ij}}^{\infty}\mathrm{d}\lambda\ (x(\lambda) - \mu_i)\sigma_{(i)}(\lambda)d\lambda$$

with $\sigma_{(1)} \equiv 2\sigma_{11} + \sigma_{12} + \sigma_{21}$ the lead 1 particle density and $\sigma_{(2)} \equiv 2\sigma_{22} + \sigma_{12} + \sigma_{21}$ the lead 2 particle density. In the case of $\mu_1 > \mu_2$ we have $B_{11} < B_{12} = B_{21} < B_{22}$ for this finite U Anderson model but the equation for $\sigma_{ij}(\lambda)$ is the same for different combination of i and j. The reason is we put a quasi-hole state, rather than a quasi-particle, in the integral equation Eq.(A.1) similar to the treatment of Wiener-Hopf approach. For example, for $B_{11} < \lambda < B_{22}$ there could be three type of quasi-particle state $\{ij\} = \{11, 12, 21\}$ and we put $\{ij\} = \{22\}$ state as quasi-hole state. This hole state still count one weight of the probability of 4 distributions and therefore the factor of 4 on the left hand side of Eq.(A.1) retains even out of equilibrium. Similar idea is also applied in two type

of bound state (strings) solution.

Other than their differences in the density distribution the computations for the current and dot occupation expectation value are quite similar to the two strings case. We show their numerical results in the following.

The differential conductance vs voltage as shown in Fig.A.1, obtained by taking numerical derivative on current vs voltage data, essentially gives the same picture as in two strings case, namely a sharp Kondo peak nearby $V = 0$ and a broad side peak corresponding to charge fluctuations. In the case of $\langle n_d \rangle$ vs V, however, there is an additional feature occurring at an energy scale higher than the energy scale of the charge fluctuation side peak (corresponding to the voltage position of 2nd peak shown in the inset) as shown in Fig. A.2. This is especially apparent if we looked at the nonequilibrium charge susceptibility as shown in inset of Fig.A.2.

As we do not expect there should be any further charge fluctuations, we rule out, by physical argument, the possibility of 4 strings configuration.

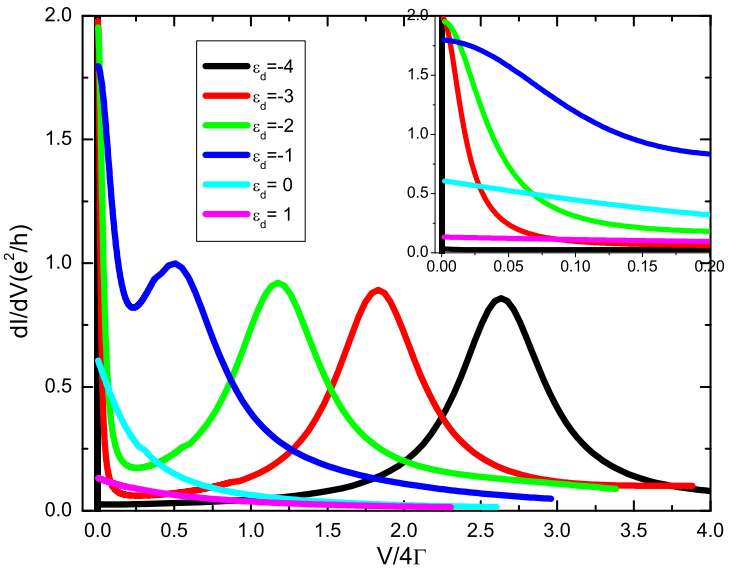

Figure A.1: $\frac{dI}{dV}$ vs $\frac{V}{4\Gamma}$ for $U = 8$, $\Gamma = 0.25$ and various ϵ_d from $\epsilon_d = -\frac{U}{2}$ to $\epsilon_d = 1$. The inset is the enlarged region nearby zero voltage.

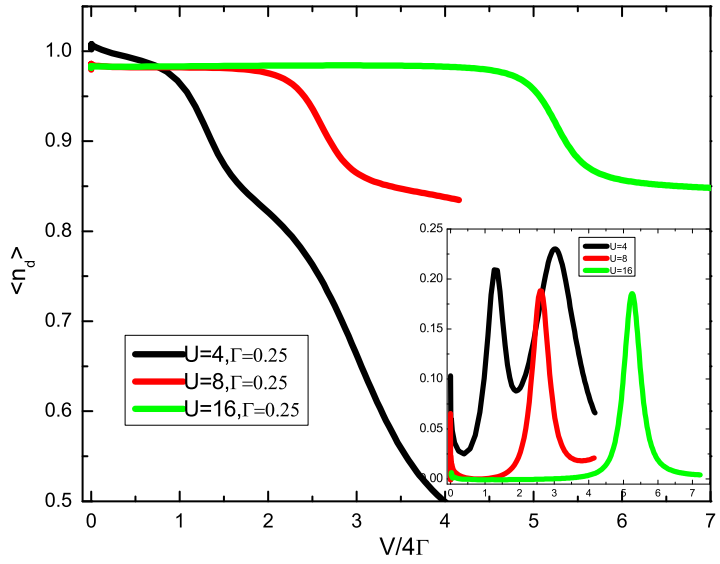

Figure A.2: $\langle n_d \rangle$ vs $\frac{V}{4\Gamma}$ for different U, $\Gamma = 0.25$ and $\epsilon_d = -\frac{U}{2}$. The inset is $-\frac{\partial \langle n_d \rangle}{\partial V}|_{\epsilon_d}$ vs V voltage. A third peak shows up in $U = 4$ case.

Appendix B

Expectation value for IRLM in bound state case

In this section we carry out explicit matrix element computation for complex momenta in the case of IRLM (where imaginary part of Bethe momenta $\xi_p = \frac{2(p-\epsilon_d)}{U}$). The computation for finite U Anderson model is very similar and will not be repeated here. The summary here is that we show the indication of orthogonality for bound state solution. Due to the complexity of different integration regions this is not a solid mathematical proof. However the *exact* results for dot occupation in equilibrium strongly suggests the validity of this orthogonality even in complex momenta case.

B.1 Normalization

We may categorize each term related as "no mixing terms" (preserving channel quantum number) and "one mixing term" and "two mixing terms". Those with no mixing terms have normalization factor as:

$$\begin{aligned}
\langle p^+p^-||p^+p^-\rangle &= \int e^{-2\xi_p(x_1-x_2)}(|R_{p^+}|^2+|T_{p^+}|^2)(|R_{p^-}|^2+|T_{p^-}|^2)\theta_1\theta_2\theta_{12} \\
&+ \int e^{-2\xi_p(x_1-x_2)}\theta_{12}\bar{\theta}_1\bar{\theta}_2 + \int e^{-2\xi_p(x_1-x_2)}(|R_{p^+}|^2+|T_{p^+}|^2)\theta_{12}\theta_1\bar{\theta}_2 \\
&+ \int e^{-2\xi_p(x_1-x_2)}|\frac{\sqrt{2}i}{t}T_{p^+}|^2\delta_1\bar{\theta}_2\theta_{12} + \int e^{-2\xi_p(x_1-x_2)}(|R_{p^+}|^2+|T_{p^+}|^2)|\frac{\sqrt{2}i}{t}T_{p^-}|^2\delta_2\theta_1\theta_{12} \\
&= (\frac{L}{2\xi_p}-\frac{1}{(2\xi_p)^2})(|R_{p^+}|^2+|T_{p^+}|^2)(|R_{p^-}|^2+|T_{p^-}|^2) + (\frac{L}{2\xi_p}-\frac{1}{(2\xi_p)^2}) \\
&+ \frac{2}{(2\xi_p)^2}(|R_{p^+}|^2+|T_{p^+}|^2) + \frac{1}{2\xi_p}|\frac{\sqrt{2}i}{t}T_{p^+}|^2 + \frac{1}{2\xi_p}|\frac{\sqrt{2}i}{t}T_{p^-}|^2(|R_{p^+}|^2+|T_{p^+}|^2)
\end{aligned}$$

Those with one mixing term in p^- region:

$$\begin{aligned}
\langle p^+1p^-||p^+2p^-\rangle &= \int e^{-2\xi_p(x_1-x_2)}(|R_{p^+}|^2+|T_{p^+}|^2)(R_{p^-}T^*_{p^-}+R^*_{p^-}T_{p^-})\theta_1\theta_2\theta_{12} \\
&+ \int e^{-2\xi_p(x_1-x_2)}(|R_{p^+}|^2+|T_{p^+}|^2)|\frac{\sqrt{2}i}{t}T_{p^-}|^2\delta_2\theta_1\theta_{12} \\
&= (\frac{L}{2\xi_p}-\frac{1}{(2\xi_p)^2})(|R_{p^+}|^2+|T_{p^+}|^2)(R_{p^-}T^*_{p^-}+R^*_{p^-}T_{p^-}) + \frac{1}{2\xi_p}(|R_{p^+}|^2+|T_{p^+}|^2)|\frac{\sqrt{2}i}{t}T_{p^-}|^2
\end{aligned}$$

Those with one mixing term in p^+ region:

$$\begin{aligned}
\langle 1p^+p^-||2p^+p^-\rangle &= \int e^{-2\xi_p(x_1-x_2)}(|R_{p^-}|^2+|T_{p^-}|^2)(R_{p^+}T^*_{p^+}+R^*_{p^+}T_{p^+})\theta_1\theta_2\theta_{12} \\
&+ \int e^{-2\xi_p(x_1-x_2)}(R_{p^+}T^*_{p^+}+R^*_{p^+}T_{p^+})\bar{\theta}_2\theta_1\theta_{12}+\int e^{-2\xi_p(x_1-x_2)}|\frac{\sqrt{2}i}{t}T_{p^+}|^2\delta_1\bar{\theta}_2\theta_{12} \\
&+ \int e^{-2\xi_p(x_1-x_2)}(R_{p^+}T^*_{p^+}+R^*_{p^+}T_{p^+})|\frac{\sqrt{2}i}{t}T_{p^-}|^2\theta_1\delta_2\theta_{12} \\
&= (\frac{L}{2\xi_p}-\frac{1}{(2\xi_p)^2})(|R_{p^-}|^2+|T_{p^-}|^2)(R_{p^+}T^*_{p^+}+R^*_{p^+}T_{p^+})+\frac{1}{2\xi_p}|\frac{\sqrt{2}i}{t}T_{p^+}|^2 \\
&+ \frac{2}{(2\xi_p)^2}(R_{p^+}T^*_{p^+}+R^*_{p^+}T_{p^+})+\frac{1}{2\xi_p}|\frac{\sqrt{2}i}{t}T_{p^-}|^2(R_{p^+}T^*_{p^+}+R^*_{p^+}T_{p^+})
\end{aligned}$$

Those with two mixing terms:

$$\begin{aligned}
\langle 1p^+2p^-||2p^+1p^-\rangle &= \int e^{-2\xi_p(x_1-x_2)}(R_{p^+}T^*_{p^+}+R^*_{p^+}T_{p^+})(R_{p^-}T^*_{p^-}+R^*_{p^-}T_{p^-})\theta_1\theta_2\theta_{12} \\
&+ \int e^{-2\xi_p(x_1-x_2)}(R_{p^+}T^*_{p^+}+R^*_{p^+}T_{p^+})|\frac{\sqrt{2}i}{t}T_{p^-}|^2\theta_1\delta_2\theta_{12} \\
&= (\frac{L}{2\xi_p}-\frac{1}{(2\xi_p)^2})(R_{p^+}T^*_{p^+}+R^*_{p^+}T_{p^+})(R_{p^-}T^*_{p^-}+R^*_{p^-}T_{p^-}) \\
&+ \frac{1}{2\xi_p}(R_{p^+}T^*_{p^+}+R^*_{p^+}T_{p^+})|\frac{\sqrt{2}i}{t}T_{p^-}|^2
\end{aligned}$$

B.2 Dot occupation

The general form of dot occupation is given by

$$\langle i'p^+ip^-||\hat{d}^\dagger\hat{d}||j'p^+jp^-\rangle=\int|\frac{\sqrt{2}i}{t}T_{p^+}|^2\langle\alpha^\dagger_{ip^-}|\alpha^\dagger_{jp^-}\rangle\delta_1\theta_{12}+\int|\frac{\sqrt{2}i}{t}T_{p^-}|^2\langle\alpha^\dagger_{i'p^+}|\alpha^\dagger_{j'p^+}\rangle\delta_2\theta_{12}$$

Those with no mixing term has the form:

$$\begin{aligned}
\langle p^+p^-||\hat{d}^\dagger\hat{d}||p^+p^-\rangle &= \int|\frac{\sqrt{2}i}{t}T_{p^+}|^2\delta_1\theta_{12}\bar{\theta}_2e^{-2\xi_p(x_1-x_2)} \\
&+ \int|\frac{\sqrt{2}i}{t}T_{p^-}|^2(|R_{p^+}|^2+|T_{p^+}|^2)\theta_1\delta_2\theta_{12}e^{-2\xi_p(x_1-x_2)} \\
&= \frac{1}{2\xi_p}|\frac{\sqrt{2}i}{t}T_{p^+}|^2+\frac{1}{2\xi_p}|\frac{\sqrt{2}i}{t}T_{p^-}|^2(|R_{p^+}|^2+|T_{p^+}|^2)
\end{aligned}$$

Those with one mixing term in p^- sector:

$$\begin{aligned}\langle p^+2p^-||\hat{d}^\dagger\hat{d}||p^+1p^-\rangle &= \int|\frac{\sqrt{2}i}{t}T_{p^-}|^2(|R_{p^+}|^2+|T_{p^+}|^2)\theta_1\delta_2\theta_{12}e^{-2\xi_p(x_1-x_2)}\\ &= \frac{1}{2\xi_p}|\frac{\sqrt{2}i}{t}T_{p^-}|^2(|R_{p^+}|^2+|T_{p^+}|^2)\end{aligned}$$

Those with one mixing term in p^+ sector:

$$\begin{aligned}\langle 1p^+p^-||\hat{d}^\dagger\hat{d}||2p^+p^-\rangle &= \int|\frac{\sqrt{2}i}{t}T_{p^+}|^2\delta_1\theta_{12}\bar{\theta}_2e^{-2\xi_p(x_1-x_2)}\\ &+ \int|\frac{\sqrt{2}i}{t}T_{p^-}|^2(|R_{p^+}|^2+|T_{p^+}|^2)\theta_1\delta_2\theta_{12}e^{-2\xi_p(x_1-x_2)}\\ &= \frac{1}{2\xi_p}(|\frac{\sqrt{2}i}{t}T_{p^+}|^2+|\frac{\sqrt{2}i}{t}T_{p^-}|^2(R_{p^+}T^*_{p^+}+R^*_{p^+}T_{p^+})\end{aligned}$$

Those with two mixing terms:

$$\begin{aligned}\langle 1p^+2p^-||\hat{d}^\dagger\hat{d}||2p^+1p^-\rangle &= \int|\frac{\sqrt{2}i}{t}T_{p^-}|^2(R_{p^+}T^*_{p^+}+R^*_{p^+}T_{p^+})\theta_1\delta_2\theta_{12}e^{-2\xi_p(x_1-x_2)}\\ &= \frac{1}{2\xi_p}|\frac{\sqrt{2}i}{t}T_{p^-}|^2(R_{p^+}T^*_{p^+}+R^*_{p^+}T_{p^+})\end{aligned}$$

The general expressions after divided out by the normalization factors are categorized as following:

$$\begin{aligned}\langle\hat{d}^\dagger\hat{d}\rangle_{rr} &= \frac{\frac{1}{\Gamma}(|T_{p^+}|^2+|T_{p^-}|^2(|R_{p^+}|^2+|T_{p^+}|^2))}{((|R_{p^+}|^2+|T_{p^+}|^2)(|R_{p^-}|^2+|T_{p^-}|^2)+1)}\\ &= \frac{\frac{1}{\Gamma}(\frac{\Gamma^2}{(p-\epsilon_d)^2+(\Gamma+\xi_p)^2}+\frac{\Gamma^2}{(p-\epsilon_d)^2+(\Gamma-\xi_p)^2}\frac{(p-\epsilon_d)^2+\xi_p^2+\Gamma^2}{(p-\epsilon_d)^2+(\Gamma+\xi_p)^2})}{\frac{(p-\epsilon_d)^2+\xi_p^2+\Gamma^2}{(p-\epsilon_d)^2+(\Gamma+\xi_p)^2}\frac{(p-\epsilon_d)^2+\xi_p^2+\Gamma^2}{(p-\epsilon_d)^2+(\Gamma-\xi_p)^2}+1}\\ \langle\hat{d}^\dagger\hat{d}\rangle_{rt} &= \frac{\frac{1}{\Gamma}|T_{p^-}|^2}{R_{p^-}T^*_{p^-}+R^*_{p^-}T_{p^-}}=\frac{\frac{\Gamma}{(p-\epsilon_d)^2+(\Gamma-\xi_p)^2}}{\frac{2\xi_p\Gamma}{(p-\epsilon_d)^2+(\Gamma-\xi_p)^2}}\\ \langle\hat{d}^\dagger\hat{d}\rangle_{tr} &= \frac{\frac{1}{\Gamma}(|T_{p^-}|^2(R_{p^+}T^*_{p^+}+R^*_{p^+}T_{p^+})+|T_{p^+}|^2)}{(R_{p^+}T^*_{p^+}+R^*_{p^+}T_{p^+})(|R_{p^-}|^2+|T_{p^-}|^2)}\\ &= \frac{\frac{1}{\Gamma}(\frac{\Gamma^2}{(p-\epsilon_d)^2+(\Gamma+\xi_p)^2}+\frac{\Gamma^2}{(p-\epsilon_d)^2+(\Gamma-\xi_p)^2}\frac{-2\xi_p\Gamma}{(p-\epsilon_d)^2+(\Gamma+\xi_p)^2})}{\frac{-2\xi_p\Gamma}{(p-\epsilon_d)^2+(\Gamma+\xi_p)^2}\frac{(p-\epsilon_d)^2+\xi_p^2+\Gamma^2}{(p-\epsilon_d)^2+(\Gamma-\xi_p)^2}}\\ \langle\hat{d}^\dagger\hat{d}\rangle_{tt} &= \frac{\frac{1}{\Gamma}|T_{p^-}|^2}{R_{p^-}T^*_{p^-}+R^*_{p^-}T_{p^-}}=\frac{\frac{\Gamma}{(p-\epsilon_d)^2+(\Gamma-\xi_p)^2}}{\frac{2\xi_p\Gamma}{(p-\epsilon_d)^2+(\Gamma-\xi_p)^2}}\end{aligned} \tag{B.1}$$

A common factor $\frac{1}{L}$ is implied in the expression above. Some useful identities are listed below:

$$\begin{aligned}
R_{p\pm} &= \frac{(p-\epsilon_d) \pm i\xi_p}{(p-\epsilon_d)+i(\Gamma \pm \xi_p)} \\
T_{p\pm} &= \frac{-i\Gamma}{(p-\epsilon_d)+i(\Gamma \pm \xi_p)} \\
R_{p^+}T^*_{p^+} + R^*_{p^+}T_{p^+} &= \frac{-2\xi_p\Gamma}{(p-\epsilon_d)^2+(\xi_p+\Gamma)^2} \\
R_{p^-}T^*_{p^-} + R^*_{p^-}T_{p^-} &= \frac{2\xi_p\Gamma}{(p-\epsilon_d)^2+(\Gamma-\xi_p)^2} \\
|R_{p^+}T_{p^+}|^2 &= \frac{((p-\epsilon_d)^2+\xi_p^2)\Gamma^2}{((p-\epsilon_d)^2+(\xi_p+\Gamma)^2)^2} \\
|R_{p^-}T_{p^-}|^2 &= \frac{((p-\epsilon_d)^2+\xi_p^2)\Gamma^2}{((p-\epsilon_d)^2+(\Gamma-\xi_p)^2)^2} \\
|R_{p^+}|^2 + |T_{p^+}|^2 &= \frac{(p-\epsilon_d)^2+\xi_p^2+\Gamma^2}{(p-\epsilon_d)^2+(\xi_p+\Gamma)^2} \\
|R_{p^-}|^2 + |T_{p^-}|^2 &= \frac{(p-\epsilon_d)^2+\xi_p^2+\Gamma^2}{(p-\epsilon_d)^2+(\Gamma-\xi_p)^2}
\end{aligned} \tag{B.2}$$

Eq.(B.2) will be handy for the computation of physical quantity in this section.

B.3 Expectation value of current

The expectation value of current for one bound state is given by

$$\frac{\langle ij||\hat{I}||i'j'\rangle}{\langle ij||i'j'\rangle} = \frac{it}{\sqrt{2}}\frac{\langle ij||(\hat{\psi}_1^\dagger(0)-\hat{\psi}_2^\dagger(0))\hat{d}-\hat{d}^\dagger(\hat{\psi}_1(0)-\hat{\psi}_2(0)))||i'j'\rangle}{\langle ij||i'j'\rangle} \equiv \frac{\langle ij||\hat{o}-\hat{o}^\dagger||i'j'\rangle}{\langle ij||i'j'\rangle} \tag{B.3}$$

The expressions involving no mixing term have the following property: $\langle 11||\hat{o}||11\rangle = \langle 12||\hat{o}||12\rangle = -\langle 21||\hat{o}||21\rangle = -\langle 22||\hat{o}||22\rangle$ with $\langle 11||\hat{o}||11\rangle$ given by

$$\langle 11||\hat{o}||11\rangle = \frac{-1}{\xi_p}\Re(T_{p^+}+T_{p^-}(|R_{p^+}|^2+|T_{p^+}|^2))$$

Those with one mixing term in p^- sector have the following property: $\langle 11||\hat{o}||12\rangle = -\langle 12||\hat{o}||11\rangle = -\langle 21||\hat{o}||22\rangle = \langle 22||\hat{o}||21\rangle$ with $\langle 11||\hat{o}||12\rangle$ given by

$$\langle 11||\hat{o}||12\rangle = \frac{-1}{\xi_p}\Re(T_{p^-}(\frac{1+R_{p^-}-T_{p^-}}{2})^*(|R_{p^+}|^2+|T_{p^+}|^2))$$

Those with one mixing term in p^+ sector have the following property: $\langle 21||\hat{o}||11\rangle = -\langle 12||\hat{o}||22\rangle$ and $\langle 11||\hat{o}||21\rangle = -\langle 22||\hat{o}||12\rangle$ with $\langle 11||\hat{o}||21\rangle$ and $\langle 21||\hat{o}||11\rangle$ given as

$$\langle 11||\hat{o}||21\rangle = \frac{-1}{\xi_p}\Re(T_{p^+}(\frac{1+R_{p^+}-T_{p^+}}{2})^* + T_{p^-}(\frac{1+R_{p^-}-T_{p^-}}{2})^*(R_{p^+}T^*_{p^+} + R^*_{p^+}T_{p^+}))$$
$$\langle 21||\hat{o}||11\rangle = \frac{-1}{\xi_p}\Re(T_{p^+}(\frac{T_{p^+}-R_{p^+}-1}{2})^* + T_{p^-}(\frac{1+R_{p^-}-T_{p^-}}{2})^*(R_{p^+}T^*_{p^+} + R^*_{p^+}T_{p^+}))$$

Those with two mixing terms $\langle 11||\hat{o}||22\rangle = -\langle 22||\hat{o}||11\rangle = \langle 21||\hat{o}||12\rangle = -\langle 12||\hat{o}||21\rangle$ with $\langle 11||\hat{o}||22\rangle$ given by

$$\langle 11||\hat{o}||22\rangle = \frac{-1}{\xi_p}\Re(T_{p^-}(\frac{1+R_{p^-}-T_{p^-}}{2})^*(R_{p^+}T^*_{p^+} + R^*_{p^+}T_{p^+}))$$

The general expressions after divided out by the normalization factors and timed by the appropriate pre factor are categorized as following:

$$\begin{aligned}
\langle\hat{I}\rangle_{rr} &= 2\frac{\frac{\Gamma(\Gamma-\xi_p)\left((p-\epsilon_d)^2+\Gamma^2+\xi_p^2\right)}{((p-\epsilon_d)^2+(\Gamma-\xi_p)^2)((p-\epsilon_d)^2+(\Gamma+\xi_p)^2)} + \frac{\Gamma(\Gamma+\xi_p)}{(p-\epsilon_d)^2+(\Gamma+\xi_p)^2}}{\frac{(p-\epsilon_d)^2+\xi_p^2+\Gamma^2}{(p-\epsilon_d)^2+(\Gamma+\xi_p)^2}\frac{(p-\epsilon_d)^2+\xi_p^2+\Gamma^2}{(p-\epsilon_d)^2+(\Gamma-\xi_p)^2}+1} \\
\langle\hat{I}\rangle_{rt} &= 2\frac{\frac{\Gamma(\Gamma-\xi_p)\left((p-\epsilon_d)^2+\Gamma^2+\xi_p^2\right)}{((p-\epsilon_d)^2+(\Gamma-\xi_p)^2)((p-\epsilon_d)^2+(\Gamma+\xi_p)^2)}}{\frac{(p-\epsilon_d)^2+\xi_p^2+\Gamma^2}{(p-\epsilon_d)^2+(\Gamma-\xi_p)^2}\frac{-2\xi_p\Gamma}{(p-\epsilon_d)^2+(\Gamma+\xi_p)^2}} \\
\langle\hat{I}\rangle_{tt} &= 2\frac{\frac{\Gamma(\Gamma+\xi_p)}{(p-\epsilon_d)^2+(\Gamma+\xi_p)^2} - \frac{2\Gamma^2\xi(\Gamma-\xi_p)}{((p-\epsilon_d)^2+(\Gamma-\xi_p)^2)((p-\epsilon_d)^2+(\Gamma+\xi_p)^2)}}{\frac{2\xi_p\Gamma}{(p-\epsilon_d)^2+(\Gamma-\xi_p)^2}\frac{-2\xi_p\Gamma}{(p-\epsilon_d)^2+(\Gamma+\xi_p)^2}}
\end{aligned}$$

The common feature of $\langle\hat{I}\rangle_{rr}$ from Fig.(B.1) is that the expectation value for current is zero at $p = \epsilon_d$.

In the case of real momenta there exist another equivalent definition for current:

$$\langle\hat{I}\rangle = e\langle\psi_1^\dagger(-\infty)\psi_1(-\infty) - \psi_1^\dagger(\infty)\psi_1(\infty)\rangle \tag{B.4}$$

To compute this quantity let us take $\pm\infty$ at some finite value (say $\epsilon_1 < 0$, $\epsilon_2 > 0$) and then take

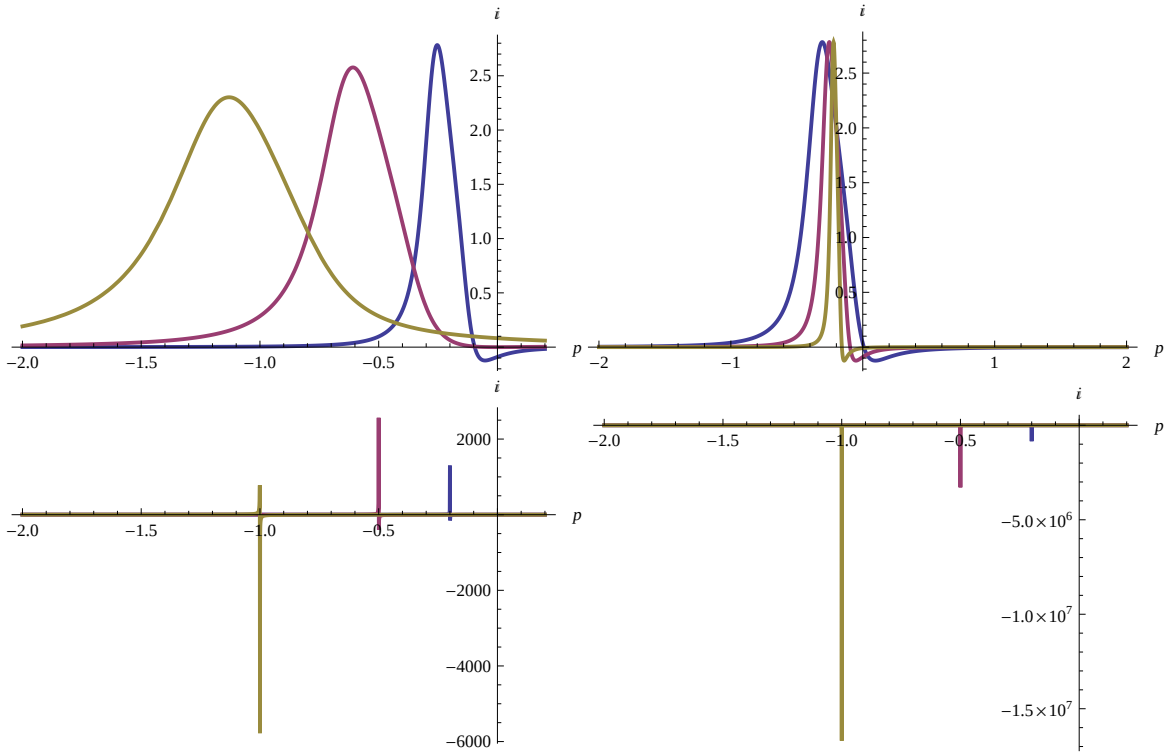

Figure B.1: $\langle \hat{I} \rangle$ vs p for different U or Γ in Interacting Resonance Level Model. Top left: $\langle \hat{I} \rangle_{rr}$ vs p for U=0.4 (blue), 1(purple), 2(brown) with $\epsilon_d = -\frac{U}{2}$, $\Gamma = 0.5$. Top right: $\langle \hat{I}_{rr} \rangle$ vs p for Γ=1 (blue), 0.5(purple), 0.2(brown) with $\epsilon_d = -0.2$, $U = 0.4$. Bottom left: $\langle \hat{I} \rangle_{rt}$ vs p for U=0.4 (blue), 1(purple), 2(brown) with $\epsilon_d = -\frac{U}{2}$. Bottom right: $\langle \hat{I} \rangle_{tt}$ vs p for U=0.4 (blue), 1(purple), 2(brown) with $\epsilon_d = -\frac{U}{2}$

the limit. We then get:

$$
\begin{aligned}
&\langle 1p^+ 1p^- | \psi_1^\dagger(\epsilon_1)\psi_1(\epsilon_1) - \psi_1^\dagger(\epsilon_2)\psi_1(\epsilon_2) | 1p^+ 1p^- \rangle \\
&= \int \langle \alpha_{1p^-} | \alpha_{1p^-} \rangle \theta_{\epsilon_1,2} e^{-2\xi_p(\epsilon_1 - x_2)} - |R_{p^+}|^2 \langle \alpha_{1p^-} | \alpha_{1p^-} \rangle \theta_{\epsilon_2,2} e^{-2\xi_p(\epsilon_2 - x_2)} \\
&+ \int \langle \alpha_{1p^+} | \alpha_{1p^+} \rangle \theta_{1,\epsilon_1} e^{-2\xi_p(x_1 - \epsilon_1)} - |R_{p^+}|^2 \langle \alpha_{1p^+} | \alpha_{1p^+} \rangle \theta_{1,\epsilon_2} e^{-2\xi_p(x_1 - \epsilon_2)} \\
&= \frac{1}{2\xi_p} - |R_{p^+}|^2 \left(\frac{e^{-2\xi_p \epsilon_2}}{2\xi_p} + (|R_{p^-}|^2 + |T_{p^-}|^2) \frac{1 - e^{-2\xi_p \epsilon_2}}{2\xi_p} + \frac{|T_{p^-}|^2}{\Gamma} e^{-2\xi_p \epsilon_2} \right) \\
&+ (|R_{p^+}|^2 + |T_{p^+}|^2) \frac{e^{2\xi_p \epsilon_1}}{2\xi_p} + \frac{|T_{p^+}|^2}{\Gamma} e^{2\xi_p \epsilon_1} + \frac{1 - e^{2\xi_p \epsilon_1}}{2\xi_p} - |R_{p^-}|^2 (|R_{p^+}|^2 + |T_{p^+}|^2) \frac{1}{2\xi_p}
\end{aligned}
$$

B.4 Orthogonality for bound state solution in IRLM

Here we show the orthogonality between different value of real part of Bethe momenta is still valid. The proof is not complete in all possible regions but it shows strong indications that the orthogonality

is still correct.

B.4.1 Normalization and impurity computation

The normalization factor can be expressed as

$$\int_{x_i}\int_{y_j}\theta^x_{12}\theta^x_{34}e^{i[p(x_1+x_2)+k(x_3+x_4)]-\xi_p(x_1-x_2)-\xi_k(x_3-x_4)}Z_{p^+k^+}(x_1-x_3)Z_{p^+k^-}(x_1-x_4)$$
$$Z_{p^-k^+}(x_2-x_3)Z_{p^-k^-}(x_2-x_4)\alpha^\dagger_{p^+}(x_1)\alpha^\dagger_{p^-}(x_2)\alpha^\dagger_{k^+}(x_3)\alpha^\dagger_{k^-}(x_4)(\theta^y_{12}\theta^y_{34}$$
$$e^{i[p(y_1+y_2)+k(y_3+y_4)]-\xi_p(y_1-y_2)-\xi_k(y_3-y_4)}Z_{p^+k^+}(y_1-y_3)Z_{p^+k^-}(y_1-y_4)$$
$$Z_{p^-k^+}(y_2-y_3)Z_{p^-k^-}(y_2-y_4)\alpha^\dagger_{p^+}(y_1)\alpha^\dagger_{p^-}(y_2)\alpha^\dagger_{k^+}(y_3)\alpha^\dagger_{k^-}(y_4))^\dagger$$
$$=\int\int e^{-2\xi_p(x_1-x_2)-2\xi_k(x_3-x_4)}\delta(x_1-y_1)\delta(x_2-y_2)\delta(x_3-y_3)\delta(x_4-y_4)\theta_{12}\theta_{34}$$
$$|Z_{p^+k^+}(x_1-x_3)|^2|Z_{p^+k^-}(x_1-x_4)|^2|Z_{p^-k^+}(x_2-x_3)|^2|Z_{p^-k^-}(x_2-x_4)|^2$$
$$\langle\bar\alpha_{p^+}|\bar\alpha_{p^+}\rangle(x_1)\langle\bar\alpha_{p^-}|\bar\alpha_{p^-}\rangle(x_2)\langle\bar\alpha_{k^+}|\bar\alpha_{k^+}\rangle(x_3)\langle\bar\alpha_{k^-}|\bar\alpha_{k^-}\rangle(x_4)$$
$$-e^{ip(x_1-x_3)+ik(x_3-x_1)-\xi_p(x_1+x_3-2x_2)-\xi_k(x_1+x_3-2x_4)}\delta(x_1-y_3)\delta(x_2-y_2)$$
$$\delta(x_3-y_1)\delta(x_4-y_4)\theta_{12}\theta_{34}\theta_{32}\theta_{14}Z_{p^+k^+}(x_1-x_3)Z_{p^+k^-}(x_1-x_4)$$
$$Z_{p^-k^+}(x_2-x_3)Z_{p^-k^-}(x_2-x_4)(Z_{p^+k^+}(x_3-x_1)Z_{p^+k^-}(x_3-x_4)$$
$$Z_{p^-k^+}(x_2-x_1)Z_{p^-k^-}(x_2-x_4))^\dagger\langle\bar\alpha_{k^+}|\bar\alpha_{p^+}\rangle(x_1)\langle\bar\alpha_{p^-}|\bar\alpha_{p^-}\rangle(x_2)$$
$$\langle\bar\alpha_{p^+}|\bar\alpha_{k^+}\rangle(x_3)\langle\bar\alpha_{k^-}|\bar\alpha_{k^-}\rangle(x_4)$$
$$-e^{ip(x_1-x_4)+ik(x_4-x_1)-\xi_p(x_1+x_4-2x_2)-\xi_k(2x_3-x_1-x_4)}\delta(x_1-y_4)\delta(x_2-y_2)$$
$$\delta(x_3-y_3)\delta(x_4-y_1)\theta_{12}\theta_{34}\theta_{42}\theta_{31}Z_{p^+k^+}(x_1-x_3)Z_{p^+k^-}(x_1-x_4)$$
$$Z_{p^-k^+}(x_2-x_3)Z_{p^-k^-}(x_2-x_4)(Z_{p^+k^+}(x_4-x_1)Z_{p^+k^-}(x_4-x_1)$$
$$Z_{p^-k^+}(x_2-x_3)Z_{p^-k^-}(x_2-x_1))^\dagger\langle\bar\alpha_{k^-}|\bar\alpha_{p^+}\rangle(x_1)\langle\bar\alpha_{p^-}|\bar\alpha_{p^-}\rangle(x_2)$$
$$\langle\bar\alpha_{k^+}|\bar\alpha_{k^+}\rangle(x_3)\langle\bar\alpha_{p^+}|\bar\alpha_{k^-}\rangle(x_4)+\textit{15 other nonzero terms..}$$

The 18 nonzero terms can be understood as following. There are 4! = 24 possible combinations in (x_i, y_j) while the convergence constraints coming from two particle S matrix $\theta^x_{12}\theta^x_{34}$ and $\theta^y_{12}\theta^y_{34}$ exclude the combinations such as $\delta(x_1-y_4)\delta(x_2-y_3)$ etc. These combinations take $2\times 2+2\times 1=6$ possible combinations out of the 4! and leave 18 nonzero terms. Note that there exist oscillating term in position coordinates except for $x_i = y_i$. In what follows we shall show a few terms related to normalization and impurity computation explicitly. Lets first compute normalization

factor contributed by first term:

$$\int_{x_i}\int_{y_j} e^{-2\xi_p(x_1-x_2)-2\xi_k(x_3-x_4)}\delta(x_1-y_1)\delta(x_2-y_2)\delta(x_3-y_3)\delta(x_4-y_4)\theta_{12}\theta_{34}$$
$$(\theta_{13}+|S_{k^+p^+}|^2\theta_{31})(\theta_{14}+|S_{k^-p^+}|^2\theta_{41})(\theta_{23}+|S_{k^+p^-}|^2\theta_{32})(\theta_{24}+|S_{k^-p^-}|^2\theta_{42})$$
$$\langle\bar{\alpha}_{p^+}|\bar{\alpha}_{p^+}\rangle(x_1)\langle\bar{\alpha}_{p^-}|\bar{\alpha}_{p^-}\rangle(x_2)\langle\bar{\alpha}_{k^+}|\bar{\alpha}_{k^+}\rangle(x_3)\langle\bar{\alpha}_{k^-}|\bar{\alpha}_{k^-}\rangle(x_4)$$
$$=\int_{x_i} e^{-2\xi_p(x_1-x_2)-2\xi_k(x_3-x_4)}\langle\bar{\alpha}_{p^+}|\bar{\alpha}_{p^+}\rangle(x_1)\langle\bar{\alpha}_{p^-}|\bar{\alpha}_{p^-}\rangle(x_2)\langle\bar{\alpha}_{k^+}|\bar{\alpha}_{k^+}\rangle(x_3)\langle\bar{\alpha}_{k^-}|\bar{\alpha}_{k^-}\rangle(x_4)$$
$$\{\theta_{1234}+\theta_{12}\theta_{34}\theta_{31}\theta_{14}\theta_{23}\theta_{24}|S_{k^+p^+}|^2+\theta_{12}\theta_{34}\theta_{13}|S_{k^-p^+}|^2\theta_{41}\theta_{23}\theta_{24}+\ldots\}$$
$$=\int_{x_i} e^{-2\xi_p(x_1-x_2)-2\xi_k(x_3-x_4)}\langle\bar{\alpha}_{p^+}|\bar{\alpha}_{p^+}\rangle(x_1)\langle\bar{\alpha}_{p^-}|\bar{\alpha}_{p^-}\rangle(x_2)\langle\bar{\alpha}_{k^+}|\bar{\alpha}_{k^+}\rangle(x_3)\langle\bar{\alpha}_{k^-}|\bar{\alpha}_{k^-}\rangle(x_4)$$
$$\{\theta_{1234}+|S_{k^+p^-}|^2\theta_{1324}+|S_{k^+p^+}|^2|S_{k^+p^-}|^2\theta_{3124}+|S_{k^-p^-}|^2|S_{k^+p^-}|^2\theta_{1342}$$
$$+|S_{k^+p^+}|^2|S_{k^+p^-}|^2|S_{k^-p^-}|^2\theta_{3142}+|S_{k^+p^-}|^2|S_{k^+p^+}|^2|S_{k^-p^+}|^2|S_{k^-p^-}|^2\theta_{3412}\}$$

In general there are $4\times 4=16$ terms and at most $C_2^4=\frac{4!}{2!2!}=6$ nonzero combinations and at least 1 nonzero term. These nonzero term give specific ordering in position space of the form θ_{ijkl} which means $x_i>x_j>x_k>x_l$. In turn they are also multiplied by θ_i, θ_j, θ_k, θ_l etc. coming from $\langle\bar{\alpha}_p|\bar{\alpha}_p\rangle(x_i)$. We write down each term explicitly as following

$$\int dx_i dx_j dx_k dx_l \theta_{ijkl}\{a\theta_i\theta_j\theta_k\theta_l+b\theta_i\theta_j\theta_k\bar{\theta}_l+c\theta_i\theta_j\bar{\theta}_k\bar{\theta}_l+d\theta_i\bar{\theta}_j\bar{\theta}_k\bar{\theta}_l+e\bar{\theta}_i\bar{\theta}_j\bar{\theta}_k\bar{\theta}_l\}$$

with a,b,c,d,e referring to T_p, R_p, Γ etc. $\theta_i=\theta(x_i)$ and $\bar{\theta}_i=\theta(-x_i)$. Thus we see that there are 5 nonzero terms associated with each θ_{ijkl}. The integrals we need to carry out in order to get the full expression for normalization or impurity related quantity is therefor ranged between $18\times 1\times 5=90$ and $18\times 6\times 5=540$ terms.

Let us evaluate some spatial integrals explicitly in the following.

$$\int dx_1dx_2dx_3dx_4\theta_{1234}\theta_1\theta_2\theta_3\theta_4 e^{-2\xi_p(x_1-x_2)-2\xi_k(x_3-x_4)} \tag{B.5}$$
$$=\int dx_1dx_2dx_3 e^{-2\xi_p(x_1-x_2)-2\xi_k x_3}\frac{e^{2\xi_k x_3}-1}{2\xi_k}=\int dx_1dx_2 e^{-2\xi_p(x_1-x_2)}(\frac{x_2}{2\xi_k}+\frac{e^{-2\xi_k x_2}-1}{(2\xi_k)^2})$$
$$=\int_0^L dx_1\{\frac{x_1e^{2\xi_p x_1}}{(2\xi_p)(2\xi_k)}-\frac{e^{2\xi_p x_1}-1}{(2\xi_p)^2(2\xi_k)}+\frac{e^{2(\xi_p-\xi_k)x_1}-1}{(2(\xi_p-\xi_k))(2\xi_k)^2}-\frac{e^{2\xi_p x_1}-1}{(2\xi_p)(2\xi_k)^2}\}e^{-2\xi_p x_1}$$
$$=\frac{L^2}{8\xi_k\xi_p}-\frac{L}{8\xi_k\xi_p^2}+\frac{1}{16\xi_k\xi_p^3}+\frac{1}{16\xi_k^3(\xi_p-\xi_k)}-\frac{1}{16\xi_k^2(\xi_p-\xi_k)\xi_p}-\frac{L}{8\xi_k^2(\xi_p)}+\frac{1}{16\xi_k^2\xi_p^2}$$

The $L \to \infty$ limit picks up L^2 term in Eq.($B.5$). Now let us evaluate another nonzero term contributing to normalization which contains the oscillating term.

$$\int dx_1 dx_2 dx_3 dx_4 e^{ip(x_1-x_4)+ik(x_4-x_1)-\xi_p(x_1+x_4-2x_2)-\xi_k(2x_3-x_1-x_4)}\theta_{3412}\theta_3\theta_4\theta_1\theta_2$$
$$= \int dx_3 dx_4 dx_1 e^{ip(x_1-x_4)+ik(x_4-x_1)-\xi_p(x_1+x_4)-\xi_k(2x_3-x_1-x_4)}(\frac{e^{2\xi_p x_1}-1}{2\xi_p}) \tag{B.6}$$

$$= \int dx_3 dx_4 dx_1 e^{i(k-p)x_4-\xi_p x_4-\xi_k(2x_3-x_4)} e^{i(p-k)x_1-(\xi_p-\xi_k)x_1}(\frac{e^{2\xi_p x_1}-1}{2\xi_p})$$
$$= \int dx_3 dx_4 e^{i(k-p)x_4-\xi_p x_4-\xi_k(2x_3-x_4)}\{\frac{e^{i(p-k)x_4+(\xi_p+\xi_k)x_4}-1}{(i(p-k)+(\xi_p+\xi_k))(2\xi_p)} - \frac{e^{i(p-k)x_4-(\xi_p-\xi_k)x_4}-1}{(i(p-k)-(\xi_p-\xi_k))(2\xi_p)}\}$$
$$= \int_0^L dx_3 e^{-2\xi_k x_3}\{\frac{(e^{2\xi_k x_3}-1)}{(i(p-k)+(\xi_p+\xi_k))(2\xi_p)(2\xi_k)} - \frac{(e^{(i(k-p)-(\xi_p-\xi_k))x_3}-1)}{(i(p-k)-(\xi_p-\xi_k))(i(p-k)+(\xi_p+\xi_k))(2\xi_p)}$$
$$-\frac{(e^{-2(\xi_p-\xi_k)x_3}-1)}{(i(p-k)-(\xi_k-\xi_p))(2\xi_p)(2(\xi_k-\xi_p))} + \frac{(e^{(i(k-p)-(\xi_p-\xi_k))x_3}-1)}{(i(p-k)-(\xi_p-\xi_k))(i(p-k)-(\xi_p-\xi_k))(2\xi_p)}\}$$
$$= \{\frac{L}{(i(p-k)+(\xi_p+\xi_k))(2\xi_p)(2\xi_k)} + \frac{-1}{(i(p-k)+(\xi_p+\xi_k))(2\xi_p)(2\xi_k)^2}$$
$$-\frac{e^{(i(k-p)-(\xi_p+\xi_k))L}-1}{(i(p-k)+(\xi_p+\xi_k))(i(k-p)-(\xi_p-\xi_k))(i(k-p)-(\xi_p+\xi_k))(2\xi_p)}$$
$$+\frac{1}{(i(p-k)+(\xi_p+\xi_k))(i(k-p)-(\xi_p-\xi_k))(4\xi_p\xi_k)} + \frac{1}{(i(p-k)-(\xi_k-\xi_p))(2(\xi_k-\xi_p))(2\xi_p)^2}$$
$$-\frac{1}{(i(p-k)-(\xi_k-\xi_p))(8\xi_p\xi_k(\xi_p-\xi_k))} - \frac{1}{(i(k-p)-(\xi_p-\xi_k))(i(p-k)-(\xi_p-\xi_k))(4\xi_p\xi_k)}$$
$$+\frac{e^{(i(k-p)-(\xi_p+\xi_k))L}-1}{(i(p-k)-(\xi_p-\xi_k))(i(k-p)-(\xi_p-\xi_k))(i(k-p)-(\xi_p+\xi_k))(2\xi_p)}\}$$

The $L \to \infty$ limit picks up order L term in Eq.(B.6). Note that this expression should also be multiplied by $S_{k^-p^+}|S_{k^+p^+}|^2|S_{k^+p^-}|^2|S_{k^-p^-}|^2$ in comparing with Eq.(B.5). By using the convention $Z_{p^+p^-}(x_1,x_2) = \theta_{12}+S_{p^-p^+}\theta_{21} = \theta_{12}$ we have $S_{k^+p^+} = \frac{(p+k-2\epsilon+\frac{U}{2}(\xi_k-\xi_p))+i(\xi_k+\xi_p-\frac{U}{2}(k-p))}{(p+k-2\epsilon-\frac{U}{2}(\xi_k-\xi_p))+i(\xi_k+\xi_p+\frac{U}{2}(k-p))}$, $S_{k^+p^-} = \frac{(p+k-2\epsilon+\frac{U}{2}(\xi_k+\xi_p))+i(\xi_k-\xi_p-\frac{U}{2}(k-p))}{(p+k-2\epsilon-\frac{U}{2}(\xi_k+\xi_p))+i(\xi_k-\xi_p+\frac{U}{2}(k-p))}$, $S_{k^-p^-} = \frac{(p+k-2\epsilon-\frac{U}{2}(\xi_k-\xi_p))-i(\xi_k+\xi_p+\frac{U}{2}(k-p))}{(p+k-2\epsilon+\frac{U}{2}(\xi_k-\xi_p))-i(\xi_k+\xi_p-\frac{U}{2}(k-p))}$, and $S_{k^-p^+} = \frac{(p+k-2\epsilon-\frac{U}{2}(\xi_k+\xi_p))+i(-$
$\frac{U}{2}(\xi_k+\xi_p))+i(\xi_k-\xi_p+\frac{U}{2}(k-p))}$
The factor $S_{k^-p^+}|S_{k^+p^+}|^2|S_{k^+p^-}|^2|S_{k^-p^-}|^2$ approaches to zero for $p \to k$ and does not diverge in all range of (p,k). Thus Eq.(B.6) is smaller by an order L than Eq.(B.5). Also note that the limit $p \to k$ does not change the order of magnitude in both Eq.(B.5) and Eq.(B.6) as can be observed in both expressions there are counter terms to cancel this possible divergence.

Now let us compute the impurity related term by putting one of the position coordinate to be

zero. For the first term (no oscillating term in position coordinate) we take $x_4 = 0$ and we get

$$\begin{aligned}
&\int dx_1 dx_2 dx_3 e^{-2\xi_p(x_1-x_2)} e^{-2\xi_k x_3} \theta_{1234}\theta_1\theta_2\theta_3\delta_4 \qquad \text{(B.7)}\\
&= \int dx_1 dx_2 e^{-2\xi_p(x_1-x_2)} \frac{e^{-2\xi_k x_2}-1}{-2\xi_k}\\
&= \frac{-1}{(2\xi_k)^2(2(\xi_p-\xi_k))} + \frac{1}{(2\xi_k)(2\xi_p)(2(\xi_p-\xi_k))} + \frac{L}{(2\xi_k)(2\xi_p)} - \frac{1}{(2\xi_k)(2\xi_p)^2}
\end{aligned}$$

For those come with oscillating term we choose $x_2 = 0$ in Eq.(B.6) and compute impurity related term. The integral we need to carry out is of the form:

$$\begin{aligned}
&\int dx_3 dx_4 dx_1 e^{ip(x_1-x_4)+ik(x_4-x_1)-\xi_p(x_1+x_4)-\xi_k(2x_3-x_1-x_4)}\theta_{3412}\theta_3\theta_4\theta_1\delta_2 \qquad \text{(B.8)}\\
&= \frac{1}{(i(p-k)-(\xi_p-\xi_k))(-2(\xi_p-\xi_k))(2\xi_p)} - \frac{1}{(i(p-k)-(\xi_p-\xi_k))(-2(\xi_p-\xi_k))(2\xi_k)}\\
&-\frac{e^{(i(k-p)-(\xi_p+\xi_k))L}-1}{(i(p-k)-(\xi_p-\xi_k))(i(k-p)-(\xi_p-\xi_k))(i(k-p)-(\xi_p+\xi_k))}\\
&+\frac{1}{(i(p-k)-(\xi_p-\xi_k))(i(k-p)-(\xi_p-\xi_k))2\xi_k}
\end{aligned}$$

Thus we see that the oscillating terms is smaller by an order L in impurity related computation. It is therefore consistent with the normalization results that those with oscillating term in position coordinates contribute less than order L compared with non oscillating term.

The above results can be analyzed in the general case as following. Let us discuss normalization factor first and ignore the regional separations coming from inner product of $\alpha_p^\dagger(x_i)$ terms. The results we get thus will be overestimated as we integrate out larger phase space.

$$\int_{x_i-x_j}\int_{x_i+x_j}\int_{x_k-x_l}\int_{x_k+x_l} e^{-2\xi_p(x_i-x_j)}e^{-2\xi_k(x_k-x_l)}\theta_{ijkl} = \frac{L^2}{2\xi_p\xi_k}$$

$$\begin{aligned}
&\int_{x_i-x_l}\int_{x_i+x_l}\int_{x_j}\int_{x_k} e^{i(p-k)(x_i-x_l)-\xi_p(x_i+x_l-2x_j)-\xi_k(2x_k-(x_i+x_l))}\theta_{klij}\\
&= \int_{-L}^{0} d(x_i-x_l)\int_{-L}^{L} dx_k \int_{-L}^{x_k} d(x_i+x_l)\int_{-L}^{x_i+x_l} dx_j e^{i(p-k)(x_i-x_l)-\xi_p(x_i+x_l-2x_j)-\xi_k(2x_k-(x_i+x_l))}\\
&= \frac{1-e^{-i(p-k)L}}{i(p-k)}\frac{L}{2\xi_k\xi_p}
\end{aligned}$$

$$\int_{x_i}\int_{x_j}\int_{x_k}\int_{x_l} e^{ip(x_j-x_l)+ik(x_l-x_j)-\xi_p(2x_i-x_j-x_l)-\xi_k(x_j-x_l)}\theta_{ijkl}$$
$$= \frac{L}{\xi_p(i(k-p)+(\xi_p+\xi_k))^2} + \frac{e^{-4\xi_p L}-1}{(2\xi_p)^2(i(k-p)+(\xi_p+\xi_k))^2}$$
$$-\frac{e^{-2(\xi_p+\xi_k)L}-1}{(i(p-k)+(\xi_p-\xi_k))(i(k-p)+(\xi_p+\xi_k))^2(i(p-k)-(\xi_p+\xi_k))}$$
$$-\frac{e^{-4\xi_p L}-1}{2\xi_p(i(p-k)+(\xi_p-\xi_k))(i(k-p)+(\xi_p+\xi_k))^2} + \frac{Le^{2(i(p-k)-(\xi_p+\xi_k))L}+L}{(i(p-k)+(\xi_p-\xi_k))(i(p-k)-(\xi_p+\xi_k))^2}$$
$$-\frac{e^{2(i(p-k)-(\xi_p+\xi_k))L}-1}{(i(p-k)+(\xi_p-\xi_k))(i(p-k)-(\xi_p+\xi_k))^3} - \frac{Le^{-4\xi_p L}-L}{2\xi_p(i(p-k)+(\xi_p-\xi_k))(i(k-p)+(\xi_p+\xi_k))}$$
$$+\frac{e^{2(i(p-k)-(\xi_p+\xi_k))L}-1}{(i(p-k)+(\xi_p-\xi_k))^2(i(p-k)-(\xi_p+\xi_k))^2} - \frac{e^{-4\xi_p L}-1}{2\xi_p(i(p-k)+(\xi_p-\xi_k))^2(i(k-p)+(\xi_p+\xi_k))}$$
$$+\frac{Le^{2(i(p-k)-(\xi_p+\xi_k))L}-L}{(i(p-k)+(\xi_p-\xi_k))(i(p-k)-(\xi_p+\xi_k))^2} - \frac{Le^{-4\xi_p L}-L}{2\xi_p(i(p-k)+(\xi_p-\xi_k))(i(k-p)+(\xi_p+\xi_k))}$$

$$\int_{x_i}\int_{x_j}\int_{x_k}\int_{x_l} e^{i(p-k)(x_i+x_j-x_k-x_l)}e^{-(\xi_p+\xi_k)(x_i-x_j+x_k-x_l)}\theta_{ijkl}$$
$$= \frac{e^{4i(p-k)L}-1}{2i(p-k)(i(p-k)+(\xi_p+\xi_k))^2(i(p-k)-(\xi_p+\xi_k))} - \frac{e^{2(i(p-k)-(\xi_p+\xi_k))L}-1}{(i(p-k)+(\xi_p+\xi_k))^2(i(p-k)-(\xi_p+\xi_k))^2}$$
$$-\frac{2Le^{2(i(p-k)-(\xi_p+\xi_k))L}}{(i(p-k)+(\xi_p+\xi_k))(i(p-k)-(\xi_p+\xi_k))^2} + \frac{e^{2(i(p-k)-(\xi_p+\xi_k))L}-1}{(i(p-k)+(\xi_p+\xi_k))(i(p-k)-(\xi_p+\xi_k))^3}$$
$$+\frac{e^{4i(p-k)L}-1}{(2i(p-k))^2((p-k)^2+(\xi_p+\xi_k)^2)} - \frac{e^{2(i(p-k)-(\xi_p+\xi_k))L}-1}{2i(p-k)(i(p-k)+(\xi_p+\xi_k))((p-k)^2+(\xi_p+\xi_k)^2)}$$
$$+\frac{L}{i(p-k)(i(p-k)-(\xi_p+\xi_k))^2} - \frac{e^{2(i(p-k)-(\xi_p+\xi_k))L}-1}{2i(p-k)(i(p-k)-(\xi_p+\xi_k))(i(p-k)-(\xi_p+\xi_k))^2}$$

B.4.2 summary

In above we have shown explicit results in 2 bound state computation both in normalization factor and impurity related term. By taking the $L \to \infty$ limit the present results suggest the orthogonality in real part of the bound state is valid. Further investigation into other cases (regions of integrals) is underway and to compute complete results a further simplification is required to reduce the number of integrals being carried out.

Bibliography

[1] M. Grobis, I. G. Rau, R. M. Potok, and D. Goldhaber-Gordon, Handbook of Magnetism and Advanced Magnetic Materials, Vol. 5, Wiley. See also cond-mat/0611480.

[2] M. Pustilnik and L. Glazman, J. Phys. Condens. Matter **16**, R153 (2004)

[3] L. Kouwenhoven and L. Glazman, Physics World **14**, 33 (2001). See also cond-mat/0104100.

[4] T. Inoshita, Science **281**, 526 (1998)

[5] D. Goldhaber-Gordon, H. Strickman, D. Mahalu, D. Abusch-Magder, U. Meirav and M. A. Kastner, Nature **391**, 156 (1998) M. Grobis, I. G. Rau, R. M. Potok, H. Shtrikman, and D. Goldhaber-Gordon, Phys. Rev. Lett. **100**, 246601 (2008)

[6] J. Schmid, J. Weis, K. Eberl, and K. Von Klitzing, Physica **B258**, 182 (1998)

[7] S. M. Cronenwett, T. H. Oosterkamp and L. P. Kouwenhoven, Science **281**, 540 (1998)

[8] S. M. Cronenwett, H. J. Lynch, D. Goldhaber-Gordon, L. P. Kouwenhoven, C. M. Marcus, K. Hirose, N. S. Wingreen, and V. Umansky, Phys. Rev. Lett. **88**, 226805 (2002)

[9] W. G. van der Wiel, S. De Franceschi, T. Fujisawa, J. M. Elzerman, S. Tarucha, L. P. Kouwenhoven, Science **289** 2105 (2000)

[10] J. Park, A. N. Pasupathy, J. I. Goldsmith, C. Chang, Y. Yaish, J. R. Petta, M. Rinkoski, J. P. Sethna, H. D. Abruna, P. L. McEuen, and D. C. Ralph, Nature **417**, 722 (2002)

[11] K. A. Matveev and A. I. Larkin, Phys. Rev. **B 46**, 15337 (1992)

[12] A. K. Geim, P. C. Main, N. La Scala, Jr., L. Eaves, T. J. Foster, P. H. Beton, J. W. Sakai, F. W. Sheard, M. Henini, G. Hill, and M. A. Pate, Phys. Rev. Lett. **72**, 2061 (1994)

[13] H. Frahm, C. v. Zobeltitz, N. Maire, and R. J. Haug, Phys. Rev. **B 74**, 035329 (2006)

[14] M. Ruth, T. Slobodskyy, C. Gould, G. Schmidt, and L.W. Molenkamp, Appl. Phys. Lett.**93**, 182104 (2008)

[15] P. Mehta, Ph.D. thesis (2007)

[16] P. Mehta and N. Andrei, Phys. Rev. Lett. **96**, 216802 (2006) ibid. **100**, 086804 (2008). See also cond-mat/0702612 for more detailed discussion of techniques of Scattering Bethe Ansatz and cond-mat/0703426 by P. Mehta ,S. P. Chao, and N. Andrei for erratum.

[17] T. K. Ng and P. A. Lee, Phys. Rev. Lett. **61**, 1768 (1988)

[18] Glazman, L. I. and Raikh, M. E., JETP Letters,**47**, 452 (1988)

[19] Y. Meir and N. Wingreen, Phys. Rev. **B 49**, 11040 (1994)

[20] M. Pustilnik and L. I. Glazman, Phys. Rev. Lett. **87**, 216601 (2001)

[21] M H. Hettler and H. Schoeller, Phys. Rev. Lett. **74**, 4907 (1995)

[22] A. Oguri, Phys. Rev. **B 64**, 153305 (2001)

[23] A. Oguri, J. Phys. Soc. Jpn. **74**, 110 (2005)

[24] Z. Ratiani and A. Mitra, Phys. Rev. **B 79**, 245111 (2009)

[25] A. Rosch, J. Kroha, and P. Wölfle, Phys. Rev. Lett. **87**, 156802 (2001)

[26] J. Eckel, F. Heidrich-Meisner, S. G. Jakobs, M. Thorwart, M. Pletyukhov and R. Egger, cond-mat/1001.3773 (2010)

[27] F. Heidrich-Meisner, A. E. Feiguin, and E. Dagotto, Phys. Rev. **B 79**, 235336 (2009)

[28] R. V. Roermund, S-Y Shiau and M. Lavagna, cond-mat/1001.3873 (2010)

[29] D. Matsumoto, J. Phys. Soc. Jpn. **69** , 1449 (2000)

[30] C. D. Spataru, M. S. Hybertsen, S. G. Louie, and A. J. Millis , Phys. Rev. **B 79**, 155110 (2009)

[31] Luis G. G. V. Dias da Silva, F. Heidrich-Meisner, A. E. Feiguin, C. A. Busser, G. B. Martins, E. V. Anda, and E. Dagotto ,Phys. Rev. **B 78**, 195317 (2008)

[32] A. Schiller and S. Hershfield, Phys. Rev. **B 51** (R), 12896 (1995).

[33] S. Kehrein, Phys. Rev. Lett. **95**, 056602 (2005)

[34] A. Kaminski, Yu.V. Nazarov, L.I. Glazman, Phys. Rev. **B 62**, 8154 (2000)

[35] T. Fujisawa, Y. Tokura, and Yoshiro Hirayama, Phys. Rev. **B 63**, 081304(R) (2001)

[36] B. Doyon and N. Andrei, Phys. Rev. **B 73**, 245326 (2006)

[37] A. Schiller and N. Andrei, cond-mat/0710.0249 (2007).

[38] E. Boulat and H. Saleur, Phys. Rev. **B 77**, 033409 (2008)

[39] E. Boulat, H. Saleur and P. Schmitteckert, Phys. Rev. Lett. **101**, 140601 (2008)

[40] J. S. Langer and V. Ambegaokar, Phys. Rev. **121**, 1090 (1961)

[41] D. C. Langreth, Phys. Rev. **150**, 516 (1966)

[42] R. M. Konik, H. Saleur, and A. Ludwig, Phys. Rev. Lett. **87**, 236801 (2001)

[43] R. M. Konik, H. Saleur, and A. Ludwig, Phys. Rev. **B 66**, 125304 (2002)

[44] P. Fendley, A.W.W. Ludwig, H. Saleur, Phys. Rev. **B 52**, 8934 (1995)

[45] P. Fendley, A.W.W. Ludwig, H. Saleur, Phys. Rev. Lett. **74**, 3005 (1995)

[46] P. B. Wiegman and A. M. Tsvelik, J. Phys. **C. 16**, 2281(1983); P. B. Wiegman and A. M. Tsvelik, Adv. in Phys. **32**, 453 (1983)

[47] N. Kawakami and A. Okiji, J. Phys. Soc. Jap. 51, 1145 (1982); N. Kawakami and A. Okiji, Solid State Commun. 43, 365 (1982)

[48] The thermodynamic Bethe Ansatz proof of ground state configuration for two leads case was done by C. J. Bolech and then by myself, the proof done by me is shown in Chap 6.

[49] A renormalizable Hamiltonian such as the Anderson model requires regularization and a cut-off scheme to define it. The results are universal once the cut-off is removed. In intermediate stages as the cut off is finite it is important to adopt a scheme that does not break integrabilty. The scheme adopted here satisfies this requirement. N.Andrei, K. Furuya and J. H. Lowenstein, Rev. Mod. Phys. **56**, 331 (1984), section VI. In our regularization scheme the locally discontinuous function $s(x) \equiv \theta(x)\theta(-x)$ satisfies $\partial_x s(x) = 0$.

[50] Without the regularization factor in the odd sector the model is still integrable. However, it is not possible to identify the fixed number of incoming particles by this choice, A. Nishino and N. Hatano in J. Phys. Soc. Jpn. **76**, 063002 (2007).

[51] N. Kawakami and A. Okiji, Phys. Rev. **B 42**, 2383 (1990)

[52] D. K.K. Lee and P. A. Lee, Physica **B 259-261** , 481 (1999)

[53] This dressed energy is the sum of the dressed energy of spinon and that of antiholon nearby equilibrium Fermi surface.

[54] N. Andrei, Phys. Lett. **A 87**, 299 (1982).

[55] The equality can be proved analytically in linear response. In numerics we also see very good agreement, especially for large voltage, with voltage computed by $\mu_1 - \mu_2$ given by free energy and voltage computed by difference in particle number.

[56] R. Feynman, Phys. Rev. **56**, 340 (1939)

[57] Numerical Recipes in C: The Art of Scientific Computing, Cambridge University Press (1992)

[58] F. D. M. Haldane, Phys. Rev. Lett. **40**, 416 (1978)

[59] A.C. Hewson, A. Oguri, and D. Meyer, Eur. Phys. J. **B 40**, 177 (2004)

[60] J. Paaske and K. Flensberg, Phys. Rev. Lett. **94**, 176801 (2005)

[61] A. C. Hewson, *The Kondo Problem to Heavy Fermions*, Cambridge Studies in Magnetism (1993).

[62] Here we adopted the Kondo scale as in the article by N. S. Wingreen and Y. Meir, Phys. Rev. **B 49**, 11040 (1994). We put a factor of $\sqrt{10}$ to increase this scale so the Kondo peak can be observed more easily in numerics.

[63] E. Lebanon and A. Schiller, Phys. Rev. **B 65**, 035308 (2001)

[64] S. P. Chao and G. Palacios, arXiv:1003.5395

[65] P. Schlottmann, Phys. Rev. Lett. **50**, 1697 (1983)

[66] N. Andrei and A. Jerez, Phys. Rev. Lett. **74**, 4507 (1995)

[67] N. Andrei and C. Destri, Phys. Rev. Lett. **52**, 364 (1984)

[68] G. Palacios, note on numerical computation of dot occupation for Anderson model, private commumications.

[69] C. J. Bolech, note on quantum impurity model related to one lead IRLM, private communications.

[70] M. Takahashi, Thermodynamics of one-dimensional solvable models, Cambridge University Press (1999).

[71] K. Wagh, note on Interacting resonance level model, private communications.

[72] L. Borda, K. Vladar, and A. Zawadowski, Phys. Rev. **B 75**, 125107 (2007)

[73] S. Hershfield, Phys. Rev. Lett. **70**, 2134 (1993)

[74] B. Doyon, Phys. Rev. Lett. **99**, 076806 (2007)

[75] A. Nishino, T. Imamura, and N. Hatano, Phys. Rev. Lett. **102**, 146803 (2009)

[76] S. Eggert and I. Affleck, Phys. Rev. **B 46**, 10866 (1992)

[77] Y. L. Liu and T. K. Ng, Phys. Rev. **B 61**, 2911 (2000)

[78] A. C. Seridonio, M. Yoshida, and L. N. Oliveira1, Phys. Rev. **B 80**, 235318 (2009)

[79] A. Jauho, N. S. Wingreen, and Y. Meir, Phys. Rev. **B 50**, 5528 (1994)

[80] P. Schlottmann , Phys. Rev. **B 25**, 4815 (1982)

Curriculum Vita

Sung-Po Chao

2010 Ph.D. in Physics, Rutgers University, NJ, USA.

2001 MS in Physics, National Tsing Hua University, Hsinchu, Taiwan (R.O.C).

1999 BS in Physics, National Tsing Hua University, Hsinchu, Taiwan (R.O.C).

2007-2009 Graduate Assistant, Department of Physics and Astronomy, Rutgers University, NJ.

2003-2007, 2009-2010 Teaching Assistant, Department of Physics and Astronomy, Rutgers University, NJ.

Publications

Sung-Po Chao and Guillaume Palacios, "Non-equilibrium Transport in the Anderson model of a biased Quantum Dot: Scattering Bethe Ansatz Phenomenology", arXiV:1003.5395

Pankaj Mehta, Sung-Po Chao, and Natan Andrei, "Erratum: Nonequilibrium Transport in Quantum Impurity Models (Bethe-Ansatz for open systems)." arXiv:cond-mat/0703426

Sung-Po Chao, "Current transport in a superconducting superlattice system", Masters Thesis, June 2001, National Tsing Hua University, Taiwan.